TUM School of Engineering and Design

FOCUS AREA
BIOPOLYMER
MATERIALS

Controlling the Adhesive Properties of Polymeric Materials by Surface Functionalizations

a thesis presented by

Maria G. Bauer

Technische Universität München

Technische Universität München
TUM School of Engineering and Design

Controlling the Adhesive Properties of Polymeric Materials by Surface Functionalizations

Maria Gabriela Bauer

Vollständiger Abdruck der von der

TUM School of Engineering and Design der Technischen Universität München

zur Erlangung einer Doktorin der Ingenieurwissenschaften (Dr.-Ing.)

genehmigten Dissertation.

Vorsitz: Prof. Dr. Jan Torgersen

Prüfende der Dissertation:

1. Prof. Dr. rer. nat. Oliver Lieleg
2. Prof. Martin Browne

Die Dissertation wurde am 20.11.2023 bei der Technischen Universität München eingereicht und durch die TUM School of Engineering and Design am 04.03.2024 angenommen.

Summary

Based on the diverse structures and configurations of polymers, their range of properties and functionalities, and thus the conceivable applications of polymeric materials, are basically unlimited. However, it is also this diverse structure and configuration, based on long chains of monomeric units, which makes understanding and predicting the behavior of polymeric materials so complex – especially on a microscopic to molecular scale. In particular the adhesive behaviors of polymeric materials, *i.e.*, their interactions with other materials, are frequently of interest: here, the properties are predominantly dictated by the surfaces of and interfaces between the assessed materials.
Thus, in this thesis, the interactions of polymeric materials, based on synthetic and/or natural polymers, with each other and with their surrounding environment are assessed, and the surface and interface related mechanisms underlying those interactions are discussed. The gained understanding can help broaden the knowledge about polymer-polymer interactions and can support the development of polymeric materials and devices employing specific functionalities.
Therefore, different synthetic polymer materials (*e.g.*, poly(vinyl alcohol), polydimethylsiloxane, or polyurethane) were compounded with different natural polymers (*e.g.*, mucin, hyaluronic acid, or dextran) *via* different coupling routes (*e.g.*, glutaraldehyde crosslinking, carbodiimide-medicated coupling, dopamine-based coupling, or physical interactions). The adhesive, mechanical, and tribological properties of the resulting constructs were assessed in different environments, *i.e.*, atmospheric, or aqueous. Furthermore, the constructs were exposed to various challenging treatments, such as long-term usages, storage, or sterilization procedures. Afterwards, the performance and functionality of the treated constructs was evaluated.
The observed behaviors of the established compounds are interpreted, based on relevant theoretical fundamentals, such as the concepts of surface energy, of adhesion, and of (bio-)tribological systems (which are also explained in this thesis). Therefore, first the establishment and feasibility of a thin bilayer construct with (anti-)adhesive properties on either side of the construct are discussed. Then, the effects of different surface activation strategies on synthetic polymeric materials are explained. Afterwards, these surface activations were employed to establish surface coatings with biopolymers as top-layer. The successful establishment of the desired surface properties and the avoidance of undesired influences on the bulk of the substrate material are assessed. Moreover, the good lubrication between two strongly autohesive, elastomeric foils (achieved by substrate-adjusted surface modifications combined with suitable lubricants) is rationalized. Additionally, the resilience and performance of the differently compounded materials are compared: different coating strategies (*i.e.*, dopamine-based and carbodiimide-mediated) as well as different bio-macromolecules employed as top-layers (*i.e.*, mucins and dextrans) are evaluated.
Overall, in this thesis, surface modifications of polymeric materials by (mainly) biopolymers are assessed and the suitability of the achieved functionalizations to influence the adhesive behavior, of the compounded materials, in specific manners is confirmed and explained.

Zusammenfassung

Aufgrund der vielfältigen Strukturen und Konfigurationen von Polymeren sind die Bandbreite ihrer Eigenschaften und Funktionalitäten und damit der denkbaren Anwendungen von Polymer-basierten Materialien im Grunde unbegrenzt. Jedoch, genau diese vielfältige Struktur (die auf langen Ketten von Monomereinheiten beruht) ist es, die das Verständnis und die Vorhersage des Verhaltens von Polymer-basierten Materialien so komplex macht - insbesondere auf mikroskopischer bis molekularer Ebene. Speziell das Adhäsionsverhalten von Polymer-basierten Werkstoffen, d.h. ihre Wechselwirkungen mit anderen Materialien, ist häufig von Interesse: Hier werden die Eigenschaften überwiegend von den Oberflächen der und Grenzflächen zwischen den untersuchten Materialien bestimmt.

In dieser Arbeit werden daher die Wechselwirkungen Polymer-basierter Materialien, hergestellt aus synthetischen und/oder natürlichen Polymeren, untereinander sowie mit ihrer Umgebung untersucht und die Oberflächen- und Grenzflächenmechanismen, die diesen Wechselwirkungen zugrunde liegen, diskutiert. Das gewonnene Verständnis kann dazu beitragen, das Wissen über Polymer-Polymer-Wechselwirkungen zu erweitern und die Entwicklung von Polymer-basierten Materialien und Geräten mit spezifischen Funktionalitäten zu unterstützen.

Daher wurden verschiedene synthetische Polymerwerkstoffe (z.B. Polyvinylalkohol, Polydimethylsiloxan oder Polyurethan) mit verschiedenen natürlichen Polymeren (z.B. Mucin, Hyaluronsäure oder Dextran) über unterschiedliche Kopplungswege (z.B. Glutaraldehyd-Vernetzung, Carbodiimid-vermittelte Kopplung, Dopamin-basierte Kopplung oder physikalische Wechselwirkungen) verbunden. Die adhäsiven, mechanischen und tribologischen Eigenschaften der entstandenen Konstrukte wurden in verschiedenen Umgebungen, d.h. atmosphärisch oder wässrig, bewertet. Darüber hinaus wurden die Konstrukte verschiedenen kritischen Behandlungen ausgesetzt, z.B. Daueranwendung, Lagerung oder Sterilisationsverfahren. Anschließend wurde die Funktionalität der behandelten Konstrukte bewertet.

Die beobachteten Verhaltensweisen der hergestellten Verbundmaterialien werden auf der Grundlage relevanter theoretischer Grundlagen, wie den Konzepten der Oberflächenenergie, der Adhäsion und von (bio-)tribologischen Systeme (die in dieser Arbeit ebenfalls erläutert werden), interpretiert. Daher wird zunächst die Entstehung und Umsetzbarkeit eines dünnen Doppelschichtkonstrukts mit (anti-)adhäsiven Eigenschaften auf den gegenüberliegenden Seiten des Konstrukts diskutiert. Anschließend werden die Auswirkungen verschiedener Oberflächenaktivierungsstrategien auf synthetische, polymer-basierte Materialien erläutert. Ferner wurden diese Oberflächenaktivierungen eingesetzt, um Oberflächenbeschichtungen mit Biopolymeren als Deckschicht herzustellen. Die erfolgreiche Erzeugung der gewünschten Oberflächeneigenschaften und die Vermeidung von unerwünschten Einflüssen auf den Kern des Trägermaterials werden beurteilt. Darüber hinaus wird die gute Schmierung zwischen zwei stark an sich selbsthaftenden, Elastomerfolien (erreicht durch an das Trägermaterial angepasste Oberflächenmodifikationen in Kombination mit geeigneten Schmiermitteln) erörtert. Darüber hinaus werden die Belastbarkeit und die Leistungsfähigkeit der entstandenen Verbundmaterialien verglichen: verschiedene Beschichtungsstrategien (z.B. Dopamin-basiert und Carbodiimid-vermittelt) sowie verschiedene Bio-Makromoleküle, die als Deckschicht verwendet werden (z.B. Mucine und Dextrane) werden bewertet.

Insgesamt werden in dieser Arbeit die Oberflächenmodifikationen von Polymer-basierten Werkstoffen durch (hauptsächlich) Biopolymere bewertet und die Eignung der generierten Funktionalisierungen zur spezifischen Beeinflussung des Adhäsionsverhaltens der Verbundwerkstoffe wird bestätigt und erläutert.

Table of Contents

This project has received funding from the European Union's Horizon 2020 research and innovation programme under grant agreement No 863183. This publication represents the views of the author(s) only. The European Commission is not responsible for any use that may be made of the information it contains.

1 Introduction

Due to their property-wise exceptionally broad diversity and adaptability, the utilization of polymeric materials is ubiquitous in our modern world. Especially in the biomedical, life sciences, and the cosmetic fields, the employment of polymers, whether of synthetic or of natural origin, has become substantial.

Polymers are macromolecules constituted of long chains of repeating units, so-called monomers, which typically are organic molecules or include organic groups, *i.e.*, they are composed to a high degree of carbon and hydrogen atoms. In general, there are homopolymers, which are established by a single identical monomer, and heteropolymers, which are established by at least two different monomers. Additionally, depending on the available linking options between the monomers, linear and branched polymers can be distinguished. Similar to the linking options of monomers, there are also different crosslinking and interaction behaviors of polymer chains. Here, mainly the formation of physical entanglements, transient interactions, and covalent bonds establish slightly or highly crosslinked polymer networks, which arrange into amorphous or (semi-)crystalline structures.[1,2]

Whereas synthetic polymers are mainly categorized according to their degree of crosslinking and thermal behavior, the type of monomer is used as the main distinctive feature of natural polymers. Thus, for the latter, polynucleotides (*e.g.*, RNA, DNA) based on nucleotides (each constituted of a nucleobase, a pentose sugar, and a phosphate group), polypeptides (*e.g.,* polyglutamate, serum albumin) based on amino acids, and polysaccharides (*e.g.*, starch, cellulose, alginic acid, hyaluronic acid, dextrans) based on simple sugars are differentiated. Additionally, sometimes the source of the natural polymers, *i.e.*, animal origin, plant origin, or microbial/algae origin, is distinguished. In contrast, synthetic polymers are commonly categorized into thermosetting, thermoplastic, or elastomeric polymers.[3–5]

Thermosetting polymers are formed in an irreversible curing process establishing an extensively crosslinked, permanent network. Such thermosets differ from thermoplastic polymers regarding the type of crosslinks and from elastomeric polymers regarding the density of crosslinks. The networks of thermoplastic materials are established by transient interactions which weaken at increased temperatures, thus enabling their name giving thermo-softening behavior. This characteristic behavior enables reshaping of such materials at elevated temperatures by specialized processing techniques such as injection molding, extrusion, or thermoforming. In contrast, thermosetting polymers disintegrate and decompose at elevated temperatures. Elastomeric polymers are formed by only slightly crosslinked networks; however, these networks can be established predominantly by transient or by permanent crosslinks alike. Thus, elastomers are available as thermosetting variants (*e.g.,* polydimethylsiloxane, PDMS) and as thermoplastic variants (*e.g.,* thermoplastic polyurethanes). Owing to the low density of crosslinks, the mobility of the polymer chains is less restricted. This enables the characteristic abilities of elastomeric polymers to reversibly stretch and to deform to a considerable degree, as the polymer chains can slide along each other and reconfigure themselves. Consequently, elastomers can be compliant and resilient at the same time. [2] This constitutes an extraordinary property combination, which makes them suitable for challenging applications, which require a flexible but also durable material.

The most prominent everyday use of such elastomeric materials is in balloons, but they are also found in tights or rubber bands. Life sciences and healthcare applications include single-use gloves or condoms; in the (bio-)medical field, they are used in medical tubings, urethral catheters, as inflatable balloons of stents or of intubation tubes, and in implants and prosthetics. Even though implants from elastomers were initially mainly used for reconstructive and cosmetic reasons, e.g., as breast implants, they have also been used for highly functional applications as artificial skin, vascular grafts, or even as artificial tendons or heart valves. All those examples make use of the capability of elastomers to maintain their flexibility and robustness even as considerably thin structures. Thus, more recently, further applications of such thin and flexible implants have been envisioned, e.g., as flexible retinal implants, flexible biosensing implants, or as components for cushion-like implants aiming at separating damaged articular surfaces in small joints or replacing intervertebral disks. [6–12]

Over the last four years, an example for such a thin flexible joint implant has been envisioned and developed in the course of the APRICOT project (a European Union founded Horizon 2020 FET Open project, grant number: 863183) in a joint effort of seven trans-European partners. The aim of this project was to develop a radically new type of implant for the treatment of osteoarthritis of small joints in the hand, as displayed in ***Figure 1.1***.

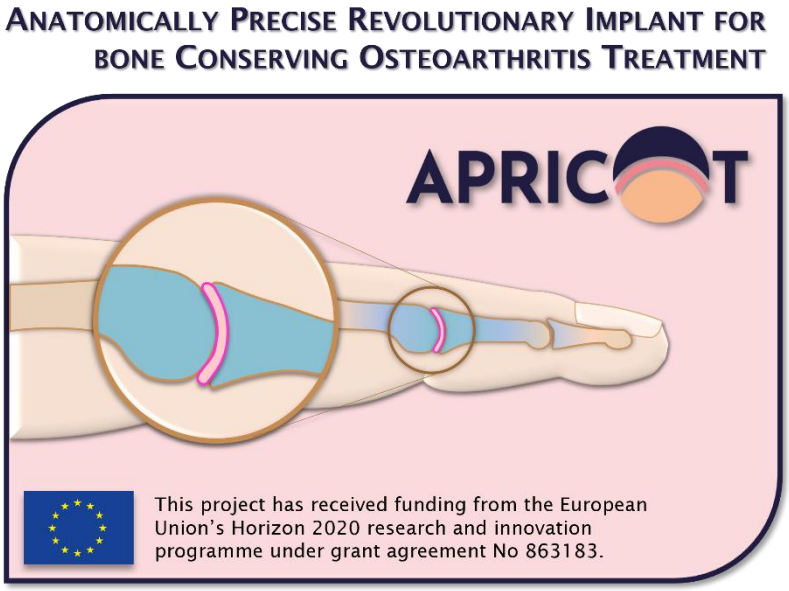

Figure 1.1: *Schematic representation of the APRICOT implant:* For the treatment of osteoarthritis in finger joints, the APRICOT implant (pink) is intended to be placed into the joint gap to restore the natural mobility of the joint.

The therefore developed novel polymer-based technique should not require invasive surgery and enable the preservation of healthy bone and tissue. Consequently, among other objectives, it was required to design an extremely thin, compliant implant with an integrated lubrication system fulfilling the identified mechanical, geometric, biological, and regulatory implant design requirements. By the employment of an integrated lubrication system, which reduces friction and wear inside of the implant, the APRICOT implant should be able to restore smooth and natural movement of the respective joint. [13] Thus, a material which is well shapeable into specific thin structures, repetitively deformable, durable, and suitable for the employment in the body (*i.e.*, biocompatible) was required. Here, elastomeric materials such

as PDMS and polyurethane-based materials, which are also available as medical-grade materials, appeared to be an obvious choice.

However, elastomeric materials have been reported to behave considerably adhesive which can interfere with intended applications. When implanted into the body, unspecific protein adsorption could promote pathogen adhesion which might trigger further bio-fouling events and, potentially, infections.[14–16] Furthermore, in the case of e.g., a vascular graft or a heart valve, the establishment of a biofouling layer would partially block the available diameter and thus reduce the achieved flow volume. Moreover, the reported strong propensity of some elastomeric materials to adhere to themselves, the so-called autohesive behavior[17,18], can further impair the intended functionality of the implants. Such autohesive behavior is typically associated with reptation and entanglements of polymer chains across the interface of both materials.[1,19,20] For the described medical devices, such autohesive behavior could increase the resistance of an artificial heart valve to reopen or reduce the smoothness and range of motion of replaced joints or intervertebral discs. Yet, suitable alternative materials with appropriate bulk properties are scarce. Thus, coating such polymeric materials to specifically adjust their surface properties is the currently preferred method to render them suitable for the intended (medical) applications. [21–25]

However, efficiently applying surface modifications onto polymeric materials is not trivial as synthetic polymers typically behave chemically rather unreactive to inert and often are intrinsically uncharged.[26] Consequently, their propensity to interact with other materials to establish (chemical) intermolecular interactions is rather limited. Moreover, synthetic polymers tend to be considerably hydrophobic and/or insoluble in water [27,28] which particularly restricts their interaction with biopolymers (which commonly are hydrophilic and/or soluble in water, as they occur (and were evolutionary developed) in aqueous environments). Additionally, biopolymers are often found to be charged polymers carrying various functional groups, which form the base for their rather reactive behavior.[3,4] Consequently, synthetic polymers and biopolymers generally show no high affinity to (permanently and strongly) bind to each other as charge-wise, wettability-wise, or from a chemical reactivity point of view, they rarely possess similar properties which would promote molecular interactions between them.

However, there is a range of biopolymers which carry hydrophobic groups at least on parts of the molecules (*i.e.*, amphiphilic molecules), such as lipids, or some amino acids and thus proteins. Accordingly, such amphiphiles can, due to hydrophobic effects, to some degree interact with synthetic polymers.[29] One of these amphiphilic biopolymers is mucin, a very large, bottlebrush-like structured glycoprotein. Even though, for the largest part, it is constituted of hydrophilic glycan sidechains, the termini (which do not carry any side chains) behave hydrophobic.[30–32] Thus, hydrophobic interactions [33–35] of the termini of mucin with synthetic polymers are feasible. This enables passive adsorption of mucins to the surfaces of synthetic polymer substrates in aqueous environment. Such an adsorbed layer can already be understood as a coating; and such passive mucin layers have frequently been reported to restrain cell integration with surfaces and adsorption of proteins or lipids and thus biofouling. Furthermore, it was shown that such mucin layers can reduce friction as well as the generation of wear. [36–41] However, as the layer is only formed transiently, it will not be very resistant to different kinds of stresses, e.g., mechanical, chemical, or thermal stresses. Consequently, to establish stable biopolymer coatings on synthetic polymer substrates, a

connecting aid is required; and such an aid is typically provided by a tailored surface coating strategy.

Such coatings strategies are typically only suitable for specific functional groups (which they connect) and must be selected explicitly for a certain combination of substrate and top layer. To ensure an efficient coupling, the exact coupling procedure, and its parameters (e.g., treatment times, temperatures, or concentrations) must be optimized for the individual application. In this thesis, mainly two prominent coupling strategies are assessed to support the compounding of synthetic and natural polymers: carbodiimide-mediated (carbo) coupling and dopamine-based (dopa) coupling.[42–44]

Especially in the bioconjugation field, carbodiimide-mediated coupling is a frequently employed strategy, as it permanently connects carboxyl groups with amine groups. Therefore, the carboxyl groups are activated *via* the introduction of a carbodiimide, which eventually will be replaced by a primary amine group available on the target molecule. Thus, the carbodiimide only mediates the conjugation but is not actually a part of the final product.[44] Whereas carboxyl- and/or amine groups are commonly found on a broad range of biomolecules, they are typically not available on synthetic polymers. Consequently, a pretreatment of the synthetic polymers to introduce either carboxyl or amine groups is required. Especially for the pretreatment of surfaces, a frequently employed technique is plasma activation followed by a silanization.[20] Here, the employed silane is selected such that the desired functional group is introduced onto the material surface.

Thus, the carbodiimide-mediated conjugation is established by a comparably complex multi-step process of specific chemical reactions. In contrast, dopamine-based coupling is rather unspecific, as it can employ a combination of various secondary interactions (e.g., hydrogen bridges, π-stacking, van der Waals interactions) and has also been reported to establish primary bonds with specific functional groups.[45,46] Consequently, in a simplified manner, it can be understood as a molecular multipurpose glue connecting two entities. To modify a surface *via* dopamine, a simple dip-coating process is sufficient. [47–50] Nonetheless, differences in the interaction efficiency and behavior of dopamine treated materials have been observed.[51–53] Thus, the suitability of a coupling strategy to be employed on a given material must be verified.

In addition to, coupling a (bio-)polymer to a (synthetic) material surface (which will be mostly discussed in this thesis), the carbodiimide-mediated coupling strategy is also suitable for a direct conjugation of molecules, to e.g., achieve a special functionalization of a polymer. This approach is frequently used to attach fluorescent labels to (macro-)molecules but can also be employed to attach individual dopamine molecules *via* their amine group to biomacromolecules such as hyaluronic acids or mucins.[54,55] In contrast, a simple dopamine coincubation with another (macro-)molecule (which has been used to establish a single step coating process [56]) is not suitable for such a specific conjugation as the diverse interaction possibilities of dopamine would lead to oligomeric clusters. Thus, instead of specifically attaching individual molecules to a target molecule, the formation of large agglomerates of a random mixture of both molecules can be triggered.

So far, mainly mucins have been introduced as biopolymeric candidates suitable for modifications of synthetic polymer materials. However, even though the broad range of beneficial functionalities provided by mucins have been examined and reported in the literature for more than half a century [57–59], actual industrial applications or clinical usages (either in trials or in real clinical applications) are still scarce. [60–63]

Here several potential reasons can be found explaining this limited usage of such a promising, multi-functional biopolymer. First of all, mucins are typically animal-sourced (commonly from pigs or cows). These animals have to be raised, and the mucins must be harvested and purified. [64,65] Overall, this is a very time- and work-consuming production route. However, owing to the animal source, considerable biological variation between separately purified mucin batches can be observed, making it difficult to reliably obtain fully functional, high-quality mucins. Moreover, it has been reported that the aggressive purification process employed for (some) commercially available mucins has compromised their functionality.[66] Thus, it remains a challenge to obtain high amounts of mucins with a reproducible purification quality that qualify for medical grade applications. Furthermore, the animal-source in general, and the porcine origin in particular, can be problematic for the acceptance among vegetarian or vegan people and among Jewish or Muslim populations, respectively. Even though there a several approaches capable of (to some degree) creating mucin-inspired structures, up to now, no efficient synthesis route has been reported for mucins.[67,68] An alternative approach would be to use the knowledge gathered about (the origin of) the functionalities of mucins in various research fields (such as biological, medical, material, and polymer research) and try to mimic certain mucin functionalities by polymers that are less complex (to obtain).

Here, dextrans are suggested and evaluated as potential alternative polymers. Like mucins, dextrans are biopolymers but of microbial origin. They are linear polysaccharides constituted solely of glucose monomers; thus, dextrans are structurally much simpler than mucins. Accordingly, their industrial production in bioreactors employing bacterial strains, as well as their purification, sorting by molecular weight, and modification with a broad range of functional groups is well established. Furthermore, several clinical applications of dextrans, such as volume expanding, blood flow improving, and antithrombogenic usages, have been employed for decades. More recently, the employment of dextrans for the formation of hydrogels and as drug delivery carrier has been discussed. [69–74]

In this thesis, two different dextran variants are employed to establish dextran coatings on synthetic materials, *via* the above introduced coupling strategies. Moreover, such dextran coatings are compared to mucin coated materials. Their influences on the wettability and adhesive properties of the coated synthetic materials are evaluated; in a further step, those dextran coatings are combined with different macromolecular lubricants to evaluate the achievable lubrication performance. Such combinations were chosen as it has been reported that the combination of a suitable macromolecular lubricant with a macromolecular coating can improve the lubrication behavior. [75]

Similar to most reported bio-macromolecular surface functionalizations, also those discussed in this thesis mainly aim at a biomedical application. For a safe biomedical application, effective sterilization of the employed medical devices is crucial. To obtain a sterilized, coated medical device, two strategies are feasible: either an individual sterilization of the components with a subsequent application of the coating or a sterilization of a previously coated medical device. However, owing to the limiting necessity of a complex sterile clean room environment, the latter approach appears more practical. Consequently, it was assessed whether mucin- or dextran coatings maintain their functionality if exposed to commonly used sterilization procedures. Furthermore, for the less established dextran-coatings, the most suitable storage conditions were evaluated.

In this thesis, the development, manufacturing, and characterization of bio-functionalized material compounds is discussed. The employed functionlizations aim at controlling specific surface properties of the compounds and the resulting interactions with the surrounding environment. Especially those properties and interactions influencing the adhesion behavior (or influenced by it) are analyzed.

To confirm the suitability of the designed constructs for the desired applications:

1. the successful establishment of the construct based on the employed e.g., conjugation-, compounding-, or coating-techniques must be verified,
2. it must be ensured that the employed materials do not have any undesired or unintended influences on other materials/properties of the construct,
3. the desired functionalities of the constructs must be demonstrated, and
4. for certain applications, further treatments such as storage or sterilization might be required; consequently, it must be shown that the introduced functionalities are maintained after exposure to such treatments.

Based on this list of requirements, the results presented in the publications summarized by this thesis will be discussed, starting with the mainly bio-based bi-layer construct introduced by Kimna et al. 2022[76]. Here, primarily the establishment of pro-adhesive and anti-adhesive properties on either layer of the thin construct is assessed. Afterwards, the effects of different surface activation strategies on different synthetic polymer materials as described in Bauer et al. 2021[77] and in Bauer and Lieleg 2023[78] are evaluated to ensure the applicability of the intended carbo- and dopa-coating strategies. Based on Bauer and Lieleg 2023[78], the influences of such coatings employing either mucins or dextrans on the wettability and the autohesive behavior of elastomeric polymer foils are compared. Further, the effects enabling efficient lubrication by the dextran coatings in combination with macromolecular lubricants as presented in Bauer et al. 2023[79] are assessed. Lastly, the application-relevant behavior of sterilized, mucin-coated and of sterilized, dextran-coated materials, as presented in Rickert et al. 2021[80] and Bauer et al. 2023[79], respectively, is discussed.

2 Materials & Methods

In this section an overview of the predominately used materials, surface modifications, treatments, and examination methods is given.

2.1 Materials

In general, two different main groups of materials, used in the scope of this thesis, can be differentiated. First, synthetic polymers, which were primarily used as substrate materials to which the different surface modifications were applied, and second, natural polymers, which were mainly used to modify or functionalize a substrate material.

2.1.1 Synthetic Polymers

Synthetic polymers are a broad range of typically petrol-based materials, which are ubiquitous in our everyday lives. The here used material types, *i.e.*, polyurethane (***Figure 2.1 a)*** and polydimethylsiloxane (*Figure 2.1 b)*, are polymers which are also used in (bio-)medical applications.

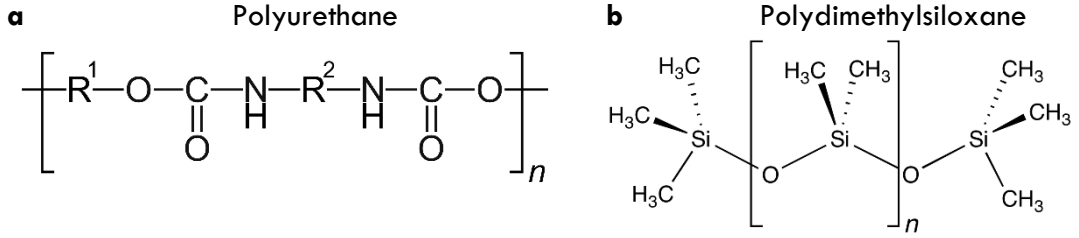

Figure 2.1: *Chemical structures of the repetitive units of PU and PDMS:* a) R1 and R2 are substitutes for various potential residual groups, the mutually shared and name-giving part of PUs are the connecting urethane groups (–NH–CO–O–); b) PDMS is constituted of a siloxane backbone alternating silicon atoms and oxygen atoms, with methyl groups (–CH3) attached to the silicon atoms.

2.1.1.1 Polyurethane

The term polyurethane summarizes a large range of versatile and structurally diverse materials, which typically show extraordinary mechanical, physical, and chemical behaviors. PUs can even combine competing properties such as high robustness and good flexibility. They are synthesized *via* polyaddition of isocyanate groups (–N=C=O) found on polyisocyanates with hydroxy groups (–OH) available on polyhydric alcohols. Thus, resulting in the chemical feature that all PU materials share, a urethane group (–NH–CO–O–), the general structure of PU materials is displayed in *Figure 2.1 a*. To fit different requirements, PU-based materials can be tailored in terms of chemistry, by varying either monomers or the type (linear or branched) and degree of cross-linking. Furthermore, their appearance and physical state can be adapted: they can be manufactured into *e.g.*, solid materials, soft/hard foams, foils, accordingly, the range of applications that PU materials can be used for is vast.[7,81–83]

For the studies discussed in this thesis only solid PU materials were examined, in particular the aromatic, polycarbonate-based polyurethane Carbothane™ AC-4085A (Lubrizol Life Science, Cleveland, USA) was assessed, which is a clear, medical-grade, thermoplastic elastomer.[84] Therefore, thin extruded sheets (thicknesses of ~ 100 – 200 µm) were

obtained either as material samples from the manufacturer directly or from Gerlinger Industries GmbH (Netzschkau, Germany). Trimming those sheets into the test-specific, desired shape and dimensions was conducted manually.

2.1.1.2 Polydimethylsiloxane

Polydimethylsiloxane (chemical formula: $CH_3[Si(CH_3)_2O]_nSi(CH_3)_3$) is a clear and elastomeric silicone polymer, frequently used in cosmetics, life-sciences products and (bio-)medical devices, as it is non-toxic and inert, especially for the first two use cases it is also referred to as dimethicone. Typically, PDMS is synthesized *via* a polymerization reaction which additionally produces an acidic component, *i.e.*, hydrochloric acid or acetic acid. The structure of the final polymer is displayed in *Figure 2.1 b,* based on the number of repetitive monomer units (indicated by *n*) the mechanical properties of the material can be influenced. [8,85,86]

In the scope of this thesis, mainly a two-part PDMS curing kit (SYLGARD™ 184 Silicone Elastomer Kit, Dow Corning, Midland, USA) was employed, therefore the PDMS oil was mixed with the curing initiator in a ratio of 10:1, cast in bespoke molds, cured at 70°C, and tempered at 110°C. Any further trimming, required to achieve the test-specific shapes and dimensions was conducted manually.

2.1.2 Natural Polymers

In contrast, to synthetic polymers natural polymers are produced by biological organisms and only must be harvested, purified, and - if desired - modified (*e.g.*, with functional groups or fluorescent dyes) to obtain the wanted product. For this thesis, mostly three different types of biomacromolecules, *i.e.*, mucins, dextrans, and hyaluronic acids, were used ***(Figure 2.2)***.

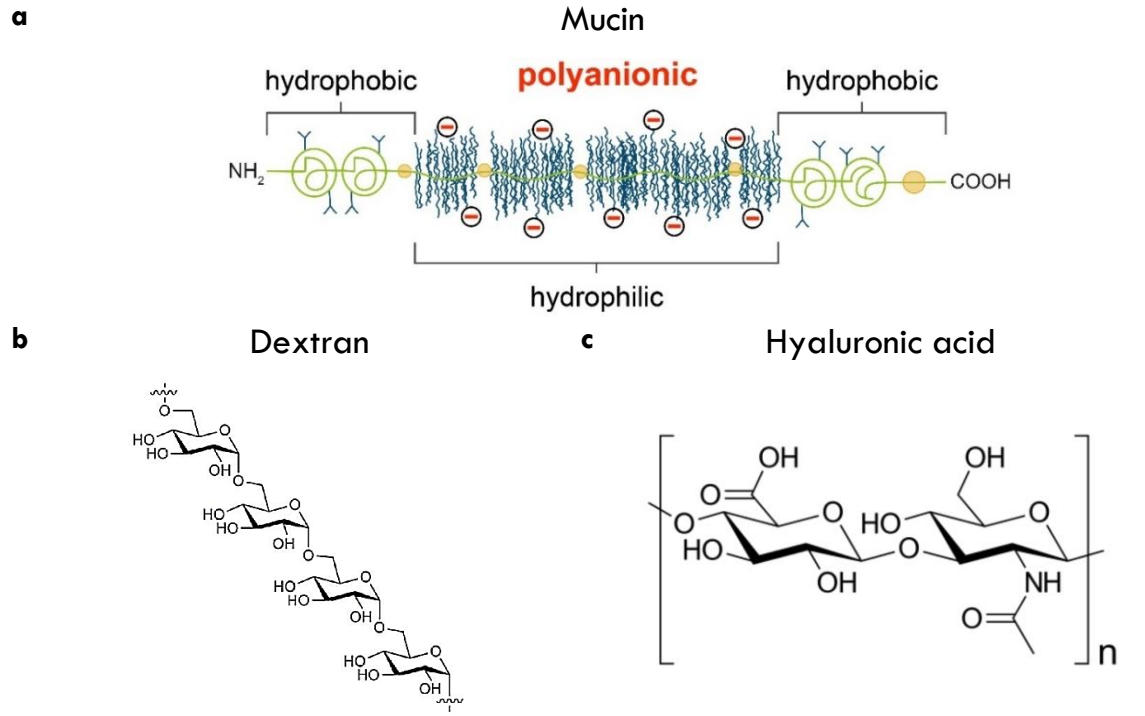

Figure 2.2*: Chemical structures of mucins, dextrans and HA:* a) schematic representation of a mucin molecule with a protein backbone (green), a hydrophilic, glycosylated (blue) and anionic (red) central region, and hydrophobic non-glycosylated termini. B) dextrans are constituted of glucose monomer units and c) HA is constituted of disaccharide subunits.

2.1.2.1 Mucins

Mucins are a group of endogenous, elongated glycoproteins and constitute the main macromolecular component found in the mucus layer which typically covers wet mucosal tissues in mammals, e.g., the oral tract, the gastrointestinal tract, or the eyes. Since this mucus layer functions as initial barrier between the external environment and the internal tissues and body systems, it must fulfill a broad range of functions, such as good lubrication, avoidance of tissue damage, protection from pathogens, and uptake of nutrients. Consequently, this multifunctionality has made mucins a promising candidate for many biomedical applications, and their suitability for such applications has been shown in a multitude of scientific publications in the last few decades. Mucins achieve their beneficial properties mainly due to their specific structure, which is established by a protein backbone carrying a polyanionic, highly glycosylated and hydratable bottlebrush-like central region and barely glycosylated, hydrophobic termini at either end of the molecule, carrying a higher degree of cationic groups as well as cysteine knots.[30,31] Whereas the central region allows for the formation of a hydration shell around the macromolecule, which has previously been found to be crucial for the lubrication and anti-adhesive properties of mucins, the termini enable hydrophobic interactions with e.g., hydrophobic surfaces, oligomerization of the several mucin molecules, and are well accessible for modifications to e.g., conjugate them with other molecules or to attach them to surfaces.[22,39–41,87,88] As it was reported previously that the structure of commercially available mucins is compromised, diminishing their functionality, the mucins employed in the scope of this thesis were lab-purified porcine gastric mucins.[66] They were harvested and purified as described in detail by *Marczynski et al. 2022*.[65] In brief, the mucosal layer was manually harvested from pig stomachs, diluted, homogenized and treated with a bactericide agent. Subsequently, the obtained solution was either ultracentrifuged or filtrated *via* several filters prior to running them over a size exclusion chromatography column, exposing the collected eluent to a high salt treatment and employing a diafiltration against ultrapure water. Finally, the gained mucins solution was frozen and lyophilized to obtain a white, cotton candy-like material.

2.1.2.2 Dextrans

Dextrans are bio-macromolecules based on glucose units connected *via* α-1,6 and/or α-1,4 glycosidic bonds. Glucose is known as the main energy source of the body and is stored in the liver as glycogen. In contrast to the branched glycogen molecules, dextrans are mostly linearly linked and not endogenous to humans but can be elaborated by different bacteria stems such as *Leuconostoc mesenteroides*. Nevertheless, owing to the very high structural similarity of dextran to glycogen, dextran molecules are highly biocompatible. Additionally, dextrans are commercially available at a high degree of purity, different molecular weights (ranging from a few kDA to about a MDa), and with different functional modifications and/or fluorescent labeling.[69–71,89,90]

In the scope of the thesis the mainly employed dextran derivates were lysine-dextran (LDex, TdBLabs, Uppsala, Sweden)[91], Q-dextran (QDex, TdBLabs)[92], and carboxymethyl-dextran (CMDex, TdBLabs)[93] were used. As its name says, LDex is modified by attaching the zwitterionic amino acid lysine *via* either of its two amine groups to the dextran backbone (achieving a degree of substitution between 0.005 - 0.03 (mol lysine/mol glucose)). QDex is a polycationic derivate functionalized with a quaternary ammonium group at about each

fourth glucose unit. For the polyanionic CMDex, a carboxymethyl group was attached to about every fifth glucose unit (which is equivalent to a carboxyl content of about 5%).

2.1.2.3 Hyaluronic Acids

The glycosaminoglycan hyaluronic acid is a polyanionic, linear macromolecule comprising disaccharide subunits, namely D-glucuronic acid, and the N-acetyl-D-glucosamine, which are ß-glycosidically linked via 1,3 or 1,4 bonds. Since the incorporated carboxyl- and N-acetyl groups can form hydrogen bonds HA, like mucins, establishes a hydration shell in aqueous solution due to its high water-binding capacity.[94–96] Physiologically, hyaluronic acid is present in joint fluids contributing to their good lubricity but also in the extracellular matrix of connective tissues, here it is known to support cell proliferation and -migration.[45,97–99] Accordingly, hyaluronic acids and their beneficial properties have frequently been employed for tissue engineering approaches.[100,101] Similar to dextrans hyaluronic acids can be produced using bacteria stems such as *Streptococcus equi* and HAs are commercially available at high purity and with different ranges of size. These are typically categorized into low MW (< 50 kDA), medium MW (hundreds of kDA) and high MW (>700 kDA). In the scope of this thesis predominantly the latter two size ranges were used.

2.2 Methods

The relevant methods for this thesis have been summarized into three main categories, first surface modifications which typically aim at attaching the above-described natural polymers to either of the substrate materials manufactured from the synthetic polymers. Second, treatments, which describe conditions and procedures such coated materials were exposed to, *e.g.*, to examine the coatings' performance, durability, or resilience. And third, the examination methods which were used to characterize the coatings and their properties and performance.

2.2.1 Surface Modifications

2.2.1.1 Surface Activation & Pre-Treatments

Various surface treatment procedures to activate or hydrophilize polymeric materials have been presented in the literature, previously; here, some of the most prominent strategies, *i.e.*, plasma treatment and dopamine treatment were employed.

Plasma Treatment

The term "plasma treatment" summarizes numerous methods/processes that generate (partially) ionized gas and/or radicals, which are frequently applied to various materials for different purposes, *e.g.,* cleaning, sterilization, surface modification, or etching. Mostly, plasma processes require either low ambient pressure (or even vacuum)[102] or high treatment temperatures (greater than or equal to several hundred degrees Celsius),[103] which in addition to the desired treatment can have negative influences on the properties of the treated materials. Consequently, for each material and desired aim of the treatment, a suitable plasma process and specific treatment conditions (*i.e.,* type of gas, treatment time, employed power, *etc.*) must be chosen. For plasma treatments of the different materials

discussed here, commercial plasma generators, operating at low pressure (p_{abs} = 0.4 mbar) and ambient temperature, were used. Therefore, clean and dry samples were inserted into the plasma chamber and either oxygen or atmospheric air was employed as ignition gas, using power ranges from 30 W to 60 W with exposure times of 1.5 to 25 min. To maintain enough unreacted plasma in the chamber, the used plasma/gas was removed by the vacuum system and unused gas was provided and ionized alternately during the treatment. To avoid hydrophobic recovery, the treated samples were used directly once the plasma treatment process had finished. Since plasma can only reach uncovered surfaces, to mainly convert nonpolar methyl groups into hydroxy groups, only the upwards facing sample surfaces were used for any further modifications or investigations.

Dopamine Treatment

In contrast to the first surface activation strategy, typically no adaptation of the process type or conditions is required for dopamine treatments as the employed conditions are comparably mild. Additionally, the multitude of adhesion processes putatively combined by dopamine molecules achieves an almost material unspecific applicability. This solution-based, additive process was first introduced in 2007[47] and mimics marine mussels producing adhesive proteins, which contain a specific amino acid called L-3,4-Dihydroxyphenylalanin (L-DOPA). Like L-DOPA dopamine hydrochloride (which was used to prepare the dopamine solutions) contains an amino group as well as a catechol group (a benzene ring to which two hydroxy groups are attached at neighboring C-atoms). This combination of functional groups enables (non-)covalent binding interactions of the dopamine molecules with each other and with a broad range of surfaces enabling dopamine layer deposition. Even though the detailed mechanisms driving this layer formation are not fully understood yet (despite extensive studies),[50,104,105] it was agreed that the process is initialized by oxidative reactions leading to o-quinones. Many options of how dopamine can interact with other molecules/objects have been observed/suggested. Dopamine has been found capable of forming covalent bonds with *e.g.*, the amino acid side chains of lysine, cysteine and histidine, furthermore at basic pH it can auto-polymerize into poly-dopamine strands. However, interactions with surfaces are typically established by non-covalent interactions such as hydrogen bonding, π-π electron stacking, cation-π interactions and interactions with metal oxides.[52,106–109] Previously, it was shown that this strategy can be successfully applied to a broad range of materials including metals, glass, ceramics, and different polymeric materials.[47]

Here, a thin layer of (poly)dopamine was established on the surfaces of materials exposed to basic dopamine solutions (pH ~8.5), by oxidatively initiating dopamine polymerization and surface adhesion through exposure to atmospheric oxygen.

2.2.1.2 Macromolecular Coatings

Carbodiimide-Mediated Coatings

Carbodiimide crosslinker chemistry is a frequently used technique to activate carboxyl-groups (-COOH) of a substance and conjugate them to primary amine-groups (-NH_2). Since carbodiimides such as 1-ethyl-3-(3-dimethylaminopropyl) carbodiimide hydrochloride (EDC) only establish a crosslink during the coupling reaction but are not actually a part of the final

product, they belong to the class of zero-length crosslinkers and allow for a direct conjugation of amine-groups to carboxyl-groups.
To initiate the coupling reaction, the carboxyl groups designated to be crosslinked are exposed to EDC dissolved in acidic buffer (the highest efficiency of this step is obtained at pH 4.5) devoid of any further carboxylic acid residues. However, since the created intermediate *o*-acylisourea is unstable and very prone to hydrolysis (which would lead to the regeneration of chemically inactivated carboxyl-groups), N-hydroxysuccinimide (sulfo-NHS) is added to the solution; this molecule temporarily stabilizes the activation until the final conjugation partner (containing a primary amine-group) is introduced. This second step, where the actual conjugation process takes place, has its highest efficiency at physiological pH 7.[44]
Previously, based on this chemical conjugation process, a covalent coupling procedure to bind macromolecules containing primary amines onto synthetic polymer materials has been presented.[75] There, the coupling process was optimized to efficiently function on PDMS, for the application on PU process parameters of the different coating process steps such as exposure/incubation time, temperature, reagent concentrations or washing solutions, had to be adjusted. In brief, the process step are as follows:

Surface Activation: As most synthetic polymer materials are rather unreactive, a pre-treatment of the surfaces is required. Therefore, the samples are exposed to a plasma activation as described above. This plasma treatment introduces mostly hydroxyl groups and, to a smaller extent, carboxyl groups to the material surface. Once the plasma treatment has finished, the activated samples were directly placed into the silane solution to avoid hydrophobic recovery, which would re-establish an unreactive surface.

Silanization: To establish carboxylated surfaces, suitable for the final macromolecular coupling, silane molecules were covalently bound to the activated surface. Here, a silane solution containing the coupling agent N-[(3-trimethoxysilyl)propyl]ethylenediamine triacetic acid trisodium salt (TMS-EDTA, abcr GmbH, Karlsruhe, Germany) diluted in an acidic buffer (pH 4.5) was employed. To allow the silanes to react with the activated surfaces, the samples were incubated in the silane solution at 37 – 60°C for 5 – 8h. Afterwards, the silanization was stabilized by either exposing the samples to increased temperature or to low pressure and unbound silanes were removed by washing the samples in ethanol.

Macromolecular Coupling: To activate the carboxyl groups of the silane layer, the precoated samples were incubated in an acidic solution (pH 5) containing 5 mM EDC and 5 mM sulfo-NHS at room temperature (RT) for 30 min. Afterwards, the EDC–NHS solution was exchanged by Dulbecco's phosphate buffered saline (DPBS) solution (pH 7.4) containing the desired macromolecule at a concentration of 0.05 % w/v. The reaction was allowed to take place for at least 12 h and eventually all samples were washed in ethanol and stored in DPBS until further use.

Furthermore, carbodiimide chemistry was also used to conjugate dopamine molecules to hyaluronic acids. Here, the carboxy groups of HA were activated via incubation with EDC and sulfo-NHS, and subsequently the HA solution was mixed with a freshly prepared dopamine solution, avoiding dopamine polymerization.

Dopamine-Based Coatings

As indicated by the name this surface coating process is based on the above-described dopamine treatment. Instead of only applying a dopamine layer, its capability of interacting with a broad range of different materials is used to additionally attach a macromolecular top-layer. Therefore, a simple dip-coating process was employed, in which the "sticky" properties of dopamine were used first to form a (poly-)dopamine base layer on the material surface and second to further bind macromolecules to this layer and hence to the surface. Therefore, the samples were first immersed into a freshly prepared basic solution (pH 8.5) containing 0.4 % (w/v) dopamine hydrochloride for 3h. To achieve a homogenous dopamine layer and avoid sedimentation of big dopamine agglomerates onto the sample surface, the samples were placed into the solution such, that the surface intended to be coated was oriented vertically. After the removement of unbound dopamine molecules, the samples were further incubated in a solution (pH 7) containing 0.1 % (w/v) of the designated macromolecule for at least 12h.

2.2.2 Treatments

To assess the resilience of the different (pre-)coatings, (un-)coated samples were exposed to different application-relevant treatments to evaluate and compare the influence of those treatments on the functionality of the coatings.

2.2.2.1 Storage

Almost any product will undergo some period of storage within its lifetime, consequently, to assess the durability of the (pre-)coatings, coated samples were stored in different dry and wet conditions for time periods of up to 200 days. In detail, samples were either stored immersed in PBS at different temperatures ranging from 7°C to 37°C or stored dehydrated at a room temperature of about 21°C.

2.2.2.2 Disinfection & Sterilization

Especially, for (bio-)medical products, surfaces void of pathogens are crucial, therefore those products typically undergo disinfection or sterilization procedures. Thus, to be used in biomedical applications a surface coating must maintain its functionality when exposed to such disinfection or sterilization. The procedures examined here, were exposure to UV-irradiation or to γ-irradiation, autoclavation, or fumigation with ethylene oxide gas. Whereas the autoclavation as well as the treatment with UV-irradiation could be conducted in the chair's laboratory, procedures involving γ-irradiation or ethylene oxide gas were performed by an external company specialized in sterilization procedures.

2.2.2.3 Mechanical Treatments

These treatments typically aim at generating structural changes and/or wear on a material and on evaluating the capability of different modifications to avoid such undesired influences. Short-term (several minutes) and long-term (up to 9h) mechanical treatments were used on different materials, always employing the linear tribology setup, in detail described in section 2.2.3.3. In brief, a measuring head, applying a specific load, is moved over the sample fixated on a bottom plate, in an oscillating manner.

2.2.3 Examination Methods

The following examinations methods were used predominately to evaluate the influence of coatings on the substrate material as well as the influence of the treatments on the coatings.

2.2.3.1 Contact Angle Measurements

A material's wettability by a liquid is dictated by the surface energy of both or, in detail, the proportion of cohesive forces to adhesive forces. Cohesive forces hold the molecules of the liquid material together, adhesive forces are established between the liquid and the solid material when they come close to each other. The sum of attractive forces in the area between the solid phase and the liquid phase is also referred to as interfacial tension. If this interfacial tension is higher than the surface tension of the liquid, *i.e.*, if the attractive forces of the solid phase towards the liquid phase are higher than the attractive forces inside the liquid phase, the liquid will wet the solid. Typically, high energy surfaces can establish high interfacial tensions. Thus, if the surface energy of the solid phase is higher than the surface energy of the liquid phase, the liquid will spread on the surface.
To determine these wetting properties of the differently coated and treated materials, contact angle measurements were conducted. Therefore, a droplet of 4 – 10 µL of deionized water was placed onto a dry and clean sample and a transversal image of the liquid–solid interface was captured using a high-resolution, high-speed camera. The contact angle (CA) is defined at the contact point of solid and liquid phase with the surrounding gas phase. Here, the angle between the tangent aligned along the droplet surface and the solid surface is determined inside of the droplet. If the CA is smaller than 90° the surface exhibits good wettability by the liquid, if the CA is above 90°, the wettability is low. In the context of water as liquid phase, surfaces showing such wetting properties are referred to as hydrophilic and hydrophobic, respectively (***Figure 2.3***).

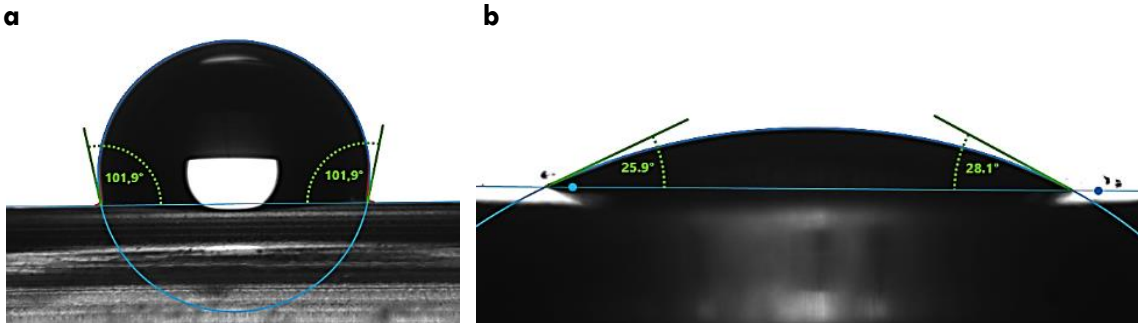

Figure 2.3: *Exemplary images obtained for contact angle measurements*: a) depicts a droplet on a hydrophobic surface and b) a droplet on a hydrophilic surface. The detected droplet contours are fitted in blue and the determined contact angles are displayed in green.

2.2.3.2 Confocal Laser Scanning Microscopy

Confocal laser scanning microscopy (CLSM) is an advanced light/laser microscopy technique which creates quantitative 3D-images of surfaces with enhanced contrast and optical resolution without requiring special preparation (e.g., gold sputtering) of the samples prior to imaging. Therefore, a special beam path configuration (confocal principle, displayed in ***Figure 2.4 a***), cover discs with tiny holes (so-called pinholes) to block out-of-focus light, and optical sectioning, *i.e.*, the stacking of multiple 2D-images captured at different depths are

employed. Two beam paths are called "confocal" if they share the same focal point. Thus, a CLSM is configured such that the beam path from the light source to the sample surface and the beam path reflected from the sample surface to the detector have the same focal point. Additionally, the pinholes limit the light reaching the detector to light reflected from a region adjacent to the focal plane only. For each location in the X-Y-plane, the Z-coordinate is identified as the z-position that achieved the highest light intensity on the detector. By using several pinholes to scan the surfaces and examine several locations at the same time, and by stacking the slices detected at different depths, an image of the surface metrology can be obtained (exemplary image depicted in *Figure 2.4 b*). From such images, quantitative surface roughness parameters can be derived to compare the roughness and surface structure of different samples.

Here, images of dry and clean samples were captured employing a VK-X1000 laser scanning microscope (Keyence, Oberhausen, Germany) equipped with objectives either with a 20x magnification (numeric aperture $NA = 0.46$) or a with 50x magnification ($NA = 0.95$). Subsequently, those images were postprocessed by removing a macroscopic tilt and/or waviness from the images. Finally, based on ISO 25178-2 the following surface roughness parameters were determined:

S_q, the root-mean-square-height:

$$S_q = \sqrt{\frac{1}{A}\iint_A z^2(x,y)dxdy} \qquad \textit{(Equation 2.1)}$$

The resulting value of this height parameter is equivalent to the standard deviation of the height profile of the analyzed sample area A.

S_{dr}, the developed interfacial area ratio:

$$S_{dr} = \frac{1}{A}\left[\iint_A \left(\sqrt{\left[1 + \left(\frac{\partial z(x,y)}{\partial x}\right)^2 + \left(\frac{\partial z(x,y)}{\partial y}\right)^2\right]} - 1\right)dxdy\right] \qquad \textit{(Equation 2.2)}$$

The S_{dr} value quantifies the percentage of additional surface area contributed by the texture as compared to an ideal plane. It is zero if the surface is completely flat and perpendicular to the orientation of the height. As a hybrid parameter, the S_{dr} value is sensitive towards both feature amplitude and wavelength.

S_{pc}, the arithmetic mean peak curvature:

$$S_{pc} = -\frac{1}{2}\frac{1}{n}\sum_{k=1}^{n}\left(\frac{\partial^2 z(x,y)}{\partial x^2} + \frac{\partial^2 z(x,y)}{\partial y^2}\right) \qquad \textit{(Equation 2.3)}$$

This is a feature parameter examining the average curvature of all peaks detected on the surface. A large value indicates pointy peaks, whereas a low value is determined for rounded peaks.

S_{xp}, the peak extreme height:

This functional parameter represents the difference in height between the peaks and the central plane of the surface. Therefore, based on the areal material ratio distribution, the height value at 50% is subtracted from the height value at 2.5% (excluding outliers and extremely high peaks).

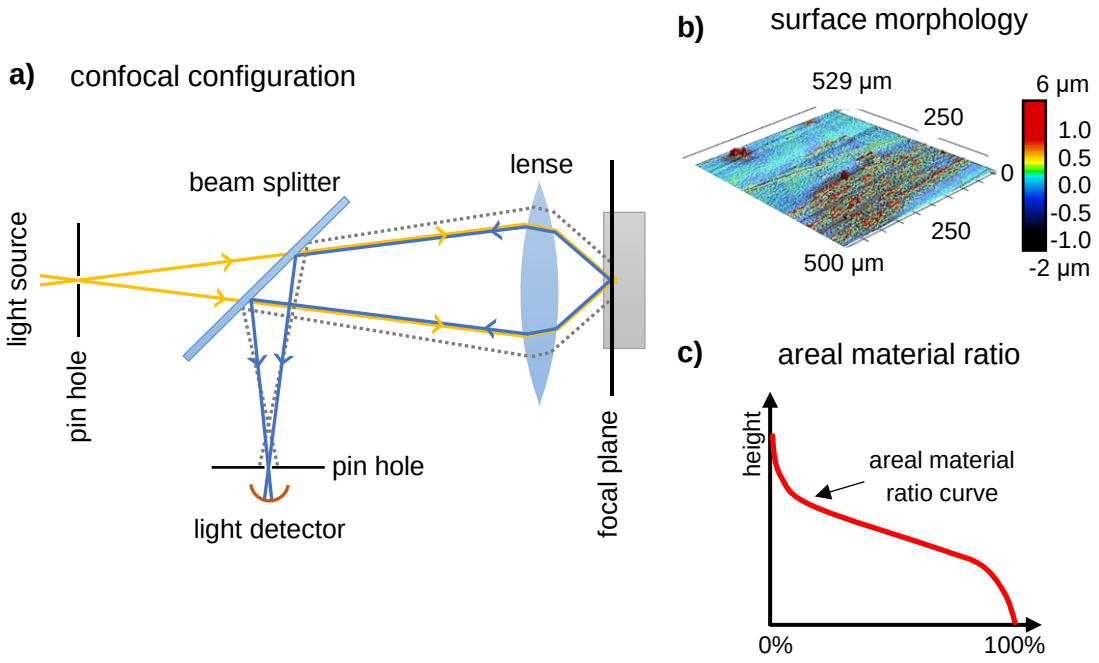

Figure 2.4: *Relevant aspects of confocal laser scanning microscopy:* a) displays a beam path (yellow and blue lines) in a confocal configuration; b) depicts an exemplary representation of a surface morphology and c) shows a areal material ratio distribution.

2.2.3.3 Examinations on a Modular Shear Rheometer

As rheometers are intended to determine rheological parameters such as viscosity or viscoelasticity, they are designed to very precisely set and determine the torque, the deflection angle, and the number of revolutions by employing a highly precise rotational engine, an optical encoder, and air bearings very precisely. Additionally, the temperature and the normal force can be influenced and traced. Generally, a rheometer is set up of a temperature-controlled bottom plate unit (onto which the sample is applied) and a maneuverable measuring head, which induces the movement and a normal force. However, due to the modular concept of the used rheometer a broad range of different units can be inserted. Owing to the multitude of detectable parameters (from which even more can be calculated) and the modular construction of the employed rheometer (a MCR302 from Anton Paar, Graz Austria), several different modifications were applied here to enable rotational and linear tribology measurements as well as tests examining the lap shear, detachment, and flexibility behavior of different samples (***Figure 2.5***).

Rotational Tribology

Rotational tribology examines the friction behavior of two material partners in static contact. For all examinations conducted here, a lubricant was applied to the system. However, dry friction behavior could also be determined. Rotational tribology examinations were conducted in a ball-on-three-pins or ball-on-three-plates setup, always employing a stainless-steel sphere ($\varnothing$ = 12.7 mm) and a fixed normal force and temperature (the exact setup is described in *Boettcher et al. 2014*[110]). The examined (coated) material was inserted as pins or plates, depending on the availability of the material in those shapes. During the measurement, the sliding velocity was varied ranging from 0.01 – 1000 mm*s^{-1}. Based on the Sommerfeld number S, which is defined as:

$$S = \frac{sliding\ velocity * lubricant\ viscosity}{normal\ contact\ pressure} \qquad \textit{(Equation 2.4)}$$

And Hertzian pressure theory[111], due to which the average contact pressure is defined by the geometric contact type (here, always a sphere on a plane), the applied normal force (which was selected to be always the same) and the Young's modulus as well as the Poisson's ratio of the employed contact partners (of which one was always steel), the remaining parameters influencing the friction behavior are the viscosity of the lubricant and the material properties of the examined material. Mostly elastomers with mechanical properties and lubricants with viscosities in a similar range (see ***Appendix A1.1***) were used. The determined coefficient of friction μ is defined as:

$$\mu = \frac{F_f}{F_n} \qquad \textit{(Equation 2.5)}$$

Where F_f is the detected friction force and F_n the applied normal force. In this thesis, μ is displayed directly over the used sliding velocity instead of the Sommerfeld number.

Lap Shear Tests

In lap shear tests, the normal force applied to detach the samples is oriented parallel to the contact interface of two samples. Such tests were performed by employing two in-house made clamps (first presented in [76]) which can be attached to the rheometer bottom plate as well as to the measuring shaft.
To prepare the measurements, two foil samples were partially pressed on top of each other thus generating an overlap region of ≈ 10 mm². The non-overlapping part of either sample was inserted into one clamp each and they were pulled apart by lifting the measuring head. Since the required normal force to separate the samples as well as the z-position of the measuring head were traced during the measurement, it was possible to determine the lap shear resistance. Such tests were employed to examine the influence of applied coatings on the autohesive behavior of the substrate foils.

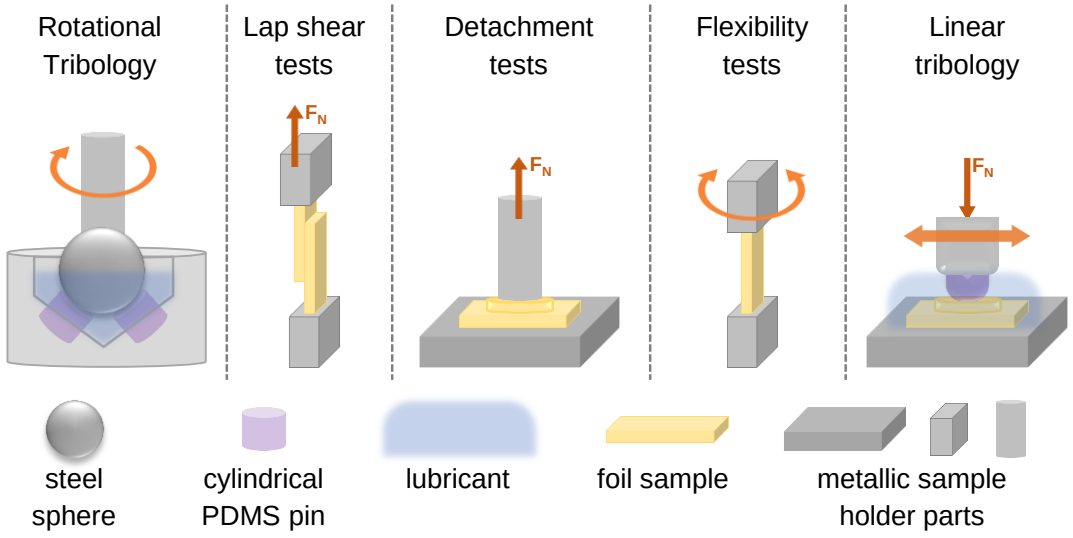

Figure 2.5: *Schematic representations of the setups employed in a modular shear rheometer:* By employing several different modifications to the same rheometer, it was feasible to enable rotational and linear tribology measurements as well as tests examining the lap shear, detachment, and flexibility behavior of different samples. Schematics are not to scale.

Detachment Tests

For detachment tests, the normal force applied to detach the samples was oriented perpendicular to the contact interface of two samples. These tests were conducted by attaching a sample each to the planar bottom plate and to the planar measuring head. Then, load was applied to the samples in contact before lifting the measuring head to initiate the detachment. Once more, the necessary normal force and the z-position of the measuring head were traced during this process to evaluate the detachment resistance of the samples. Like laps shear tests, these tests aim at examining the influence of the surface coatings on the autohesive properties of the materials.
In addition, detachment tests of samples in contact with different porcine tissues were conducted. Therefore, the same clamp as for lap shear tests was inserted into the measuring head and a bespoke sample holder designed to fixate tissue samples was connected to the bottom plate. The samples were inserted into the clamp, brought into contact with the tissues, and the energy required to detach them from the wet surface was determined.

Flexibility Tests

For flexibility tests, the same two clamps as for lap shear tests were employed but only one sample was inserted into both clamps, which were positioned 10 mm apart from each other. Then, the top clamp was moved in an oscillating manner to bend the sample back and forth several hundred times. Here, the required torque was compared for differently coated samples to assess any influence of the coatings on the flexibility of the thin foils. Subsequently, CLSM was employed to examine the effects of the repetitive deformation on the surface structure of the material.

Linear Tribology

Friction measurements in a migrating contact, so called linear tribology measurements, were conducted by employing a setup based on the one described by Winkeljann et al 2018[112]. In brief, this setup works as follows: a sample holder made from stainless steel, providing a planar surface, was connected to the bottom plate. The opposing, maneuverable measuring head was equipped with three custom-made PDMS pins (cylinders, $\varnothing = 7$ mm) having rounded edges on the down-facing side (radius = 3 mm); as, those dedicated PDMS pins provide a planar surface with a diameter of 3 mm, this combination allows for conducting plane-on-plane friction measurements while avoiding undesired edge artefacts.
For each measurement run, three rectangular samples were attached to the stainless-steel bottom plate, and a round foil sample was attached to each of the three PDMS pins in the measuring head. For each measurement run, only identical samples (*i*.e., same coating and same treatment) were used. The designated lubricant was applied before the samples were brought into contact; to avoid evaporation of this lubricant a moisture trap was installed around the setup. As the employed migrating movement of the top samples leads to alternatingly loaded and unloaded periods on different locations of the bottom samples the such employed load is typically assumed to resemble a physiological loading situation (e.*g.*, in a joint) more closely than the static loading during rotational tribology measurements.
The described setup was also used to tribologically stress constructs fabricated from mainly natural polymers. Therefore, the constructs were applied onto a PDMS based bottom plate and the above-described PDMS pins were directly moved over the constructs.

2.2.3.4 Zeta Potential Analysis

If a charged object, which might be a macroscopic sample, a nanoparticle, or even a macromolecule, is immersed into an electrolyte solution, an electrical double layer (EDL) is established at the interface between the object and the surrounding fluid. Here, the first layer, the so-called Stern layer, is constituted of counterions that are rather firmly adsorbed to the object surface. The second layer is formed by loosely bound ions, mainly attracted to the surface by Coulomb forces. Driven by electrostatic interactions as well as thermal fluctuations, these ions move around the object in close proximity. Thus, this layer is called the diffusive layer. The EDL forms a stationary fluid layer around the dispersed object and screens the initial surface charge of the object from the bulk medium. The interface between the object associated EDL and the mobile bulk medium is called the slipping plane. The zeta potential is defined as the electrokinetic potential at this slipping plane. Since it accounts for all charges bound in the slipping plane, it represents an electrical net charge. Even though the zeta potential is not equal to the electric surface potential of an object, it is often the only readily detectable potential of an object dispersed in a medium. Nonetheless, the zeta potential indicates the magnitude of electrostatic repulsion such charged objects would experience in this medium if they came next to each other.

For this thesis, mainly the zeta potentials of macroscopic solids were determined by employing a SurPASS Eco 3 device (Anton Paar). Here, two identically coated and treated samples were placed into the sample chamber with a gap of ~ 100 µm between them. An electrolyte solution flushed through this gap leads to a pressure difference Δp before and after the samples and induces a streaming potential U_{str} due to movements of the surface associated charges at the solid/fluid interface in the sample chamber. By varying the pressure difference and detecting the resulting streaming potential, a linear relation can be found between those two parameters. The zeta potential of the examined surface is proportional to the slope $^{dU_{str}}/_{d\Delta p}$.

Such surface analyses were conducted to comprehend the influence of the different surface coatings and their intermediate steps on the sample surface, as well as to evaluate the influence of different treatments on the surface coatings.

2.2.3.5 UV/Vis Spectroscopy

This technique was used for different purposes, e.g., to confirm the successful conjugation of dopamine to HA, to assess the influence of the surface coatings on the transparency of the materials, or to determine the drug release from different layers.
Generally, this method works by sending a laser beam at specific wavelengths in the spectral range of ultraviolet and visible light (~ 190 – 800 nm) through a sample and detecting the light after transmission of the sample.

3 Relevant Theoretical Fundamentals

3.1 Surface Tension

In an ideal liquid, the molecules in the bulk of the liquid establish an isotropic, dynamic equilibrium, where each molecule is constantly exposed to attractive and repulsive forces caused by its surrounding molecules. However, for long time periods, those differently directed forces compensate each other and the net force a molecule experiences will on average be zero.[113] Nonetheless, these intermolecular interactions with adjacent molecules are thermodynamically beneficial, as they reduce the potential energy of a molecule and thus stabilize the system.[114] Since repulsive forces generally have a short range (and typically only become relevant at extremely high external pressures), the intermolecular interactions are governed by attractive forces leading to cohesion of the molecules of the liquid.[115]

When including a surrounding gaseous phase with a density distinctively lower than the density of the liquid into the considerations, the molecules close to the surface have less available neighbor molecules than the molecules in the bulk of the liquid and show anisotropic behavior. As the molecules at the interface of liquid and gas cannot establish the same number of interactions, they experience a higher potential energy.[116] This higher potential energy of the surface molecules, also referred to as interface potential energy, induces a shear stress parallel to the interface (due to deviant tangential pressures close to the surface of the liquid) which establishes the surface tension of a fluid.[117] This surface tension can also be defined as the interface potential energy per interface area. As lower energy potentials are always preferred, the surface molecules aim at integrating into the bulk of the liquid, generating a pulling force into the liquid normal to the surface. As the molecules try to escape the disadvantageous position at the surface of the liquid, the surface area is decreased until the geometry with the smallest surface/volume ratio, *i.e.*, a sphere, is reached.[116] This movement of molecules from the surface inward of the liquid leads to a reduced concentration of molecules close to the surface, which creates a concentration gradient decreasing from the bulk towards the surface creating an opposing, outward force, which traps the surface bound molecules at the undesired state of a high energy potential, maintaining the surface tension.[116] Eventually, the inward bound densifying process will draw the molecules in such close proximity that the repulsive forces between the molecules become relevant, and this avoids a full collapse of the fluid sphere.[118]

Upon adding an ideal, solid surface to the system, such that the solid comes in contact with the liquid and with the gas, the predominantly relevant interacting forces are expanded: now, there are cohesive forces in the liquid, adhesive forces between the liquid and the gas, as well as adhesive forces between the liquid and the solid.[119,120] At the contact line, the location where the liquid surface meets the solid surface, a balance of the interacting forces is established. The equations associated with this mechanical equilibrium, set up for the components parallel to the solid surface, became famous as Young's equation:[121]

$$\gamma_{LV} cos\theta = \gamma_{SV} - \gamma_{SL} \qquad \text{(Equation 3.1)}$$

Here, γ_{LV} is the above-described surface tension between the liquid and the gaseous phase (denoted as V for 'vapor'). Accordingly, γ_{SV} describes the surface tension for the solid-vapor

interface, and γ_{SL} the surface tension for the solid-liquid interface. θ is the contact angle, *i.e.*, the angle between the liquid surface and the solid surface measured at the contact line and inside of the liquid (***Figure 3.1***); this intersection is also referred to as the three-phase-point. As mentioned above this equation assumes an ideal solid phase, *i*.e., a smooth, flat, rigid, chemically homogenous, insoluble, and non-reactive phase.

For real (non-ideal) solid phases, surface irregularities such as roughness, chemical variations, as well as reactions with the gas phase or with the liquid phase can influence the resulting contact angle.[122,123] Furthermore, the surface tensions on the right-hand side of the equation, which are associated with the solid phase, are frequently regarded as (free) surface energies of the solid, corresponding to the tangential stresses induced by the solid on the interface with the respective fluid.[124] Thus, the terms "surface tension" and "surface energy" are often used interchangeably; however, mostly "surface tension" is used with fluids and "surface energy" with solids.

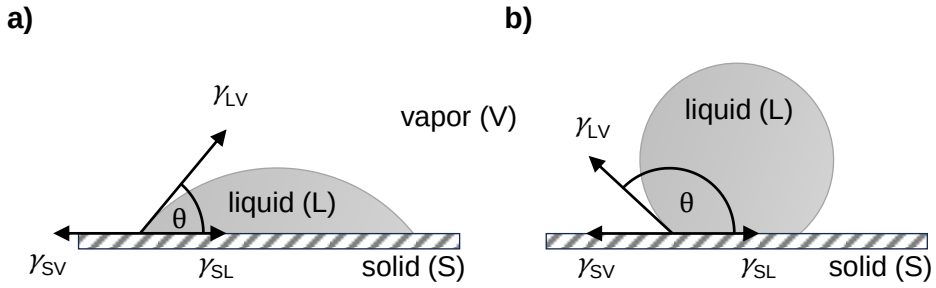

Figure 3.1: *Typical wetting situations and the corresponding surface tensions at the 3-phase-point*: Schematics of a liquid (L) phase in contact with a vapour (V) phase, and a solid (S) phase. Wetting situatuins are displayed with a) a contact angle $\theta < 90°$, and with b) a contact angle $\theta > 90°$ on a planar solid surface. Surface/interfacial tensions γ are directed tangential to the corresponding interface and are indexed according to the contacting phases.

3.2 Fundamentals of Adhesion

Already for Aristotle, Galileo, and Sir Isaac Newton, adhesion was a fascinating topic which asked for further investigations. Whereas the macroscopic, practical outcome of adhesion is simple to identify and has been extensively optimized experimentally, understanding the underlying microscopic and molecular fundamentals behind the adhesion between two phases is not trivial.[19] At the interface of the material phases, effects and processes from different scientific fields such as macromolecular science, physical chemistry of surfaces and interfaces, materials science, mechanics and micromechanics of fracture, and rheology interact and interfere, making fundamental adhesion a highly complex topic.[20] Thus, only in the early 20th century, scientific theories (*e.g.,* the adsorption theory, the mechanical theory, and the electrostatic theory) about those adhesion fundamentals started to be proposed and were controversially discussed; in fact, those theories were mainly understood as mutually exclusive and contrary.[19] Nowadays, having access to examination, analysis, and modeling techniques with much higher resolution, sensitivity, and capacity, it is mainly assumed that a complex interplay of the processes proposed in the theories almost 100 years ago establishes the adhesive bond between two phases. However, the degree of contribution of each effect is highly dependent on the parameters, conditions, and application of the adhesive bonding, *e.g.,* the types of materials, the environment, and the bonding time.[19,20,125,126] Instead of explaining the historic theories individually, a symbiotic approach will be followed to explain the processes and fundamentals of adhesion in the following paragraphs.

The first and obvious requirement for adhesion is that two phases must be brought into close contact with each other to enable interactions between both. Here, good wettability, *i.e.*, compatible surface energies of the phases, supports the efficient approximation of both surfaces.[127] This, enables adsorption interactions between molecules of both phases at the interface, due to (at least) London dispersion forces (a type of van-der-Vaals forces formed between two transient dipoles). Furthermore, also all other types of bonds and forces enabling physical (*e.g.*, hydrogen bonds, van-der-Vaals forces, polar and electrostatic interactions) and chemical (*i.e.,* covalent, ionic, and metallic bonds) adsorption are assumed to participate in adhesion processes; however, the specific types of interacting bonds and forces and their degree of contribution are highly dependent on the employed material pairing.[19,126] Here, not only the strength of the individual types of bonds is relevant for the resulting adhesive strength, but especially a high amount and density of interactions is crucial to achieve a strong bonding between the phases. Consequently, to increase the amount of available bonding partners and thus the number of interactions, a large interface area is beneficial. Accordingly, a pronounced surface roughness, often established at a nanoscopic, microscopic, and macroscopic scale, leading to an accessible surface area much larger than the projected area of the bond, is helpful to achieve high adhesive strength. However, this effect requires good wetting properties between both phases; otherwise, generating a multiscale rough surface can lead to the opposite effect. Here, insufficient wetting interactions can be further promoted by rough surfaces, as the points of contact are reduced to mainly the peaks of the surfaces. This enables that air cushions are maintained (in the cavities between the phases), which minimize the contact between the phases and thus the accessible interaction partners.[19,128] Furthermore, high surface roughnesses, under the perquisite of good wetting interactions, can promote mechanical interlocking, which

physically promote the resultant adhesion strength. Thus, adhesion can be promoted by symbiotic interactions of good wettability, enabling molecular contact between the phases, surface roughness, majorly increasing the accessible interface area and the initial surface energy, and the availability of suitable molecular interaction partners leading to form a high number of physical and chemical adsorption interactions. Thus, the effects behind the general fundamentals of adhesion can be understood as a joint effort between mechano-physical, molecular-chemical, and thermodynamic effects.[129]

However, in this thesis, mainly polymers and their interactions are examined. Thus, in the following paragraphs, polymer specific adhesion effects arising from polymer intrinsic properties and behaviors are discussed in more detail.

Polymer materials have intrinsic properties specific to their constitution from mainly flexible polymer chains. Especially elastomers and thermoplastics – above their glass transition temperature T_g – contain mobile polymers with only a low number of (permanent) inter-polymer crosslinks, leading to their amorphous and viscoelastic behavior. In addition to permanent, covalent crosslinks, such polymer materials can also be held together *e.g.,* by physical entanglements of different flexible polymer chains (*i.e.,* polymers with chain lengths much larger than the polymer specific persistence length) or by secondary bonding forces such as van-der-Vaals forces or hydrogen bonds between the polymer chains. Thus, overall, the polymer chains are only loosely bound within the polymer material and can rotate and migrate within the surrounding polymer network.[1] This migrating movement of an individual polymer embedded in the network is also referred to as "reptation", a model developed based on the work on molecular dynamics by de Gennes[130], and by Doi and Edwards[131]. Here, a polymer chain is imagined to be enclosed within an initial tube (defined by obstacles caused by the surrounding polymers), from which the polymer gradually migrates by thermal fluctuations, establishing a snake-like, creeping movement.[19]

At an interface between two polymer phases (amorphous, and $T > T_g$), such reptation movements of polymer chains can establish interdiffusion of (parts of) polymer chains from either phase into the other. Considerable interpenetration depths in the range of the radius of gyration of a polymer chain can be achieved.[19] However, the toughness and efficiency of such interdiffusion processes highly depend on the contact parameters (*e.g.,* time, temperature, pressure) and polymer properties (*e.g.,* molecular weight, polarity, and type & degree of crosslinking).[20,132] Especially the lack of mutual solubility of two different polymers is often seen as a limiting factor for the establishment of interdiffusion. From a thermodynamic perspective, most polymers exhibit low compatibility with other polymers: mixing of different, long polymer chains typically leads to an increase in Gibb's free energy of the system (based on the second law of thermodynamics). However, if two phases of the same polymer are brought into contact (so-called autohesion), interdiffusion is not expected to be limited by a lack of mutual solubility.[19,20] Instead, given enough time, the interactions between the polymer surfaces could theoretically develop so far that the interface is disintegrated and one cohesive phase is formed.[126] Depending on the contact time as well as the molecular weight, *i.e.*, the available chain length, of the polymer chains, different dominant interaction behaviors of interdiffused polymers have been reported. Typically, interdiffusion will be initiated by the penetration of the tails of the polymers into the other phase, comparable to nails. Progressing further, prolonged reptation will enable entanglements with the polymer chains of the penetrated phase. Eventually, bonds between the polymer chains of both phases would be established.[19]

However, the aforementioned lack of mutual solubility between different polymers also applies to additives, impurities, or low-molecular fractions found in most of the polymer materials. With time, dissolution of the mixed sub-phases will lead to an accumulation of the smaller components close to the surface of the polymer material. This typically reduces the strength of the cohesive forces in that area, *e.g.*, due to less entanglements feasible with shorter polymer chains.[20,133] Often, failure of adhesion of polymer materials is found to happen in this layer close to the surface of either phase, rather than at the interface.[126,134,135]

Different from synthetic polymers, which are mostly uncharged, natural polymers frequently are charged molecules. They are typically encountered in the context of physiological solutions (aqueous solutions containing considerable amounts of ions). Consequently, interactions between natural polymers can additionally include, *e.g.*, electrostatic attraction or repulsion,[136] interactions with water molecules such as hydrolysis [137] or hydrophobic effects,[33–35] or complexation with multivalent metal ions.[138–140]

3.3 Basics of Tribology

Tribology is the science and engineering of two surfaces in relative motion. It investigates phenomena regarding friction, lubrication, and wear of tribological systems. Consequently, the resulting findings are always associated with a specific combination of materials and the employed parameters and conditions. In addition to the two tribological material partners, *i.e.,* the two surfaces in relative motion, the type of lubricant (if applied) and its viscosity, the applied normal pressure, the sliding velocity, the temperature, and mode of contact (either static or migrating contact) are of high relevance.[141,142]

Friction is the resistance which any body experiences when moving over another body. Typically, static and kinetic/sliding friction are distinguished. As tribology examines systems in relative motion, only the sliding friction is of interest here. For the rest of the thesis, if not stated differently, the term "friction" refers to sliding friction. Furthermore, different types of friction are known, of which tribology mainly investigates dry friction and lubricated friction. In addition, at very high sliding velocities, fluid friction can become relevant. As in this thesis no dry friction is regarded, the following explanations will mainly focus on lubricated friction. Even though friction is present and employed ubiquitously in our everyday lives (e.g., when matches are lit, when a rolling ball comes to a hold, or in the shower, where the ground becomes slippery once wetted with soapy water - an effect caused by a lack of friction due to lubrication) understanding the phenomena behind friction is not trivial: In addition to the already mentioned system parameters, friction is also influenced by other factors such as adhesive/repulsive interactions between the surfaces, surface roughness, surface deformations, geometric properties of the surface contact (e.g., point, line or areal contact), and (if a lubricant is employed) interactions with the lubricant.[143] Consequently, it is a very complex system, which is typically examined empirically. Therefore, the friction behavior of a system is examined and interpreted by the empirical, dimensionless parameter named "coefficient of friction" (CoF) (also known as friction factor) μ which is defined as:[144]

$$\mu = {F_f}/{F_N} \qquad \text{(Equation 3.2)}$$

Here, F_n is the applied normal force pressing the surfaces together, and F_f is the force of friction (also Coulomb's force) between the surfaces (directed parallel to the surface and opposite to the moving direction), which impairs movement.[145] The kinetic energy required to overcome the friction resistance is (at least partially) converted into thermal energy; consequently, a tribological system can heat up during applications. μ can take any value between 0 (the absence of friction) and above 1 (e.g., steel on silicone can reach values above 1). However, for most applications and examinations, the value range between 0 and 1 is observed; values above 1 are associated with very high friction and insufficient lubrication.

Lubrication is the utilization of a lubricant, *i.e.,* a fluid which makes motion or action smooth or reduces friction, in the contact between both surfaces. A lubricant works by interacting with both surfaces and thus modifying the contact, it carries (parts of) the applied load and dissipates the introduced energy. Since the tribological movement constantly shears the lubricant from the contact, it is typically provided abundantly such that the lubricant can

constantly be replaced. A good lubricant does not only reduce friction but also avoids the generation of wear and abrasion on the surfaces.
Wear is the process or condition of a material being worn or gradually reduced in bulk or impaired in quality by continued use, friction, attrition. Thus, it describes the deterioration of the surfaces occurring during tribology measurements, typically caused by mechanical or chemical processes (*e.g.,* an unsuitable material pairing, or lubricant can lead to corrosion). Wear residues, e.g., abraded material, can influence the tribological system if they remain in the contact area and/or lubricant and damage to the surfaces can impede their functionality as it influences material properties such as ductility and surface roughness (which, in turn, can influence the resulting friction). In the worst case, wear can lead to failure of one component and thus to failure of the tribological system.
However, counterintuitively, wear and friction do not necessarily correlate with each other. Typical technical material pairings, where this becomes obvious, is the comparison of steel moving on silicone to steel moving on polytetrafluorethylene (PTFE). Here, the resulting friction generally will be high for the first pairing and low for the second pairing; however, the wear observed on either material of the first pairing will be close to negligible, whereas, for the second pairing clear signs of wear on the PTFE material will be observed.[88] Similar effects have also been observed for biological tissues. Here, even though the determined CoF are in a similar range, wear detected on corneas after tribological contact with coated contact lenses was much less pronounced than for uncoated contact lenses.[37,146]
Owing to the many components, parameters, conditions, and phenomena influencing a tribological system, evaluating and comparing results is not trivial. Therefore, the CoF is frequently evaluated over the so-called Sommerfeld number S,[147] sometimes also referred to as Hersey number,[148] or Stribeck number.[149,150] This is a dimensionless number relating some of the relevant parameters, *i.e.,* the viscosity η of the lubricant, the employed sliding velocity v and the applied normal pressure p. Accordingly, the Sommerfeld number is defined as:

$$S = \frac{\eta * v}{p} \qquad \text{(Equation 3.3)}$$

Evaluating traditional tribological (e.g., steel on PDMS with an aqueous buffer) systems results in a characteristic graph shape as displayed in ***Figure 3.2***, which is referred to as "Stribeck curve".

Based on Stribeck's theory,[149,150] which applies for a standard, technical tribological system (*i.e.,* two surfaces in relative motion, employing a fluid lubricant a lubricant) this curve can be subdivided into three different lubrication regimes, which are associated with specific contact states between the surfaces and distribution behaviors of the lubricant (going from left to right in *Figure 3.2*):
(a) the boundary lubrication regime: Here, the two surfaces are in full contact and most of the lubricant is displaced from the contact area; only very little remains in asperities *e.g.,* dents or cavities, between the two surfaces, resulting in high CoFs,[151,152]
(b) the mixed lubrication regime: this is the intermediate regime, the two surfaces start to slightly separate thus giving way for the lubricant to creep into the established gap and fill the asperities, leading to gradually decreasing CoFs,[153] and

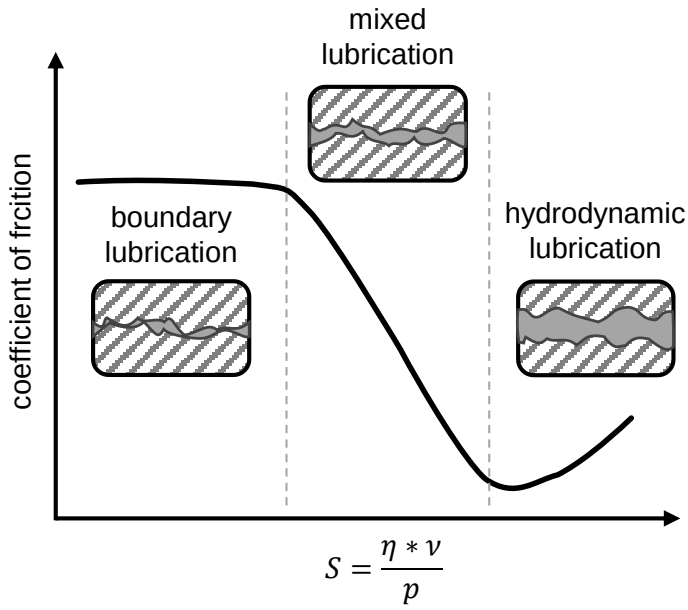

Figure 3.2: *Typical shape of a Stribeck curve:* The CoF is displayed on the y-axis and the Sommerfeld number *S* is displayed at the x-axis. From left to right a) the boundary lubrication regime, b) the mixed lubrication regime, and c) the hydrodynamic lubrication regime with each a corresponding schematic of the interfacial contact are displayed.

(c) the hydrodynamic lubrication regime: here, a continuous lubrication film has formed between the two surfaces with a thickness in the range of the size of the surface roughnesses. This limits the direct contact of the two surfaces thus resulting in especially low CoFs.[154–156]
Further increasing the Stribeck number (*e.g.*, by increasing the sliding velocities) can lead to rising CoFs as at very high sliding velocities. Thus, fluid friction, turbulences and fluid film ruptures become relevant.[141]
To reduce potential influences from the vast number of parameters and to facilitate comparison and interpretation, the viscosity of the lubricant as well as the applied normal pressure are often maintained during a set of measurements. The friction behavior can then be directly evaluated as a function of to the employed sliding velocities. Consequently, in a system with fixed viscosity and normal pressure, the three characteristic regimes can be associated with (a) low, (b) medium, and (c) high sliding velocities.
So far, the principles of technical tribology systems were discussed, in the next section, mechanism typically associated with biotribology will be discussed.

3.4 Hydration Lubrication and Sacrificial Layer Formation

Lubrication is a substantial process in most complex living organisms. In the human body, efficient lubrication is crucial for e.g., swallowing, blinking, joint movement, or blood flow in (small) arteries and veins. Accordingly, over millions of years, nature has developed highly efficient lubrication systems. In the scope of biotribology, such sophisticated systems are identified and analyzed to understand their functionality and reveal the underlying mechanisms. Furthermore, it is aimed at transferring the functionality of bio-lubrication systems to technical systems, especially for biomedical applications such as artificial joints or invasive procedures like intubation or catheterization. Typically, this involves employing specific biomolecules in the technical systems or by trying to mimic the identified mechanisms with technical/synthesized molecules.[157–160]

Two of those specific mechanisms promoting bio-lubrication are sacrificial layer formation and hydration lubrication (***Figure 3.3***).

The basic concept behind hydration lubrication is, that water molecules associate around hydrophilic/charged molecules in a confined way, forming densely hydrated hydration shells around the molecules. Then they can withstand high normal pressures, for which the water molecules still behave fluid-like. At the same time the relaxation times of the water molecules under shear are still very low such that rapid exchange of confined water molecules with free water molecules from the bulk fluid is feasible.[161–163]

The formation of hydration shells around charges originates in the strong dipole of water molecules, which enables them to interact with cationic as well as anionic charges.[164] As the association of the water molecules with the charges, leads to a strong reduction of the self-energy of the charges, permanent removal of water molecules from the hydration shell turns out to be rather difficult.[161] As the water molecules associated with a charge will mainly be oriented such that their counter-charged pole faces the central charge, this leads to the formation of the outer shell area by the other pole of the water molecules. This uniform association (which should be understood as a simplified model of highly dynamic scenario depicting the most likely state averaged over time) leads to a strong, short-range repulsion of steric origin between the hydration shells surrounding the central charges, referred to as hydration repulsion.[165–170] At the same time, the replacement of associated water molecules with 'free' water molecules from the surrounding bulk fluid can still take place rapidly: relaxation times found for of water molecules bound to specific ions were only about 100 times longer than for water molecules in the bulk (yet, also much higher relaxation times can apply for the association with other ions), and maintaining a rapid exchange mechanism has been identified as an important contribution to hydration lubrication.[171,172] Additionally, another beneficial property very specific to water, has been identified, as it is capable of maintaining its bulk-like fluidity even at very high normal pressures and for ultra-thin layers with a thickness in the range of monolayers (~ 3nm).[173] This is in contrast to other frequently used lubricants based on organics or oils, which behave like solid layers at such conditions.[174–176] The explanation for this exceptional behavior is found in the density abnormality of water, a property basically unique to water: the liquid phase of water can obtain higher densities than the solid phase, which suppresses the tendency to solidify at high pressures.[177]

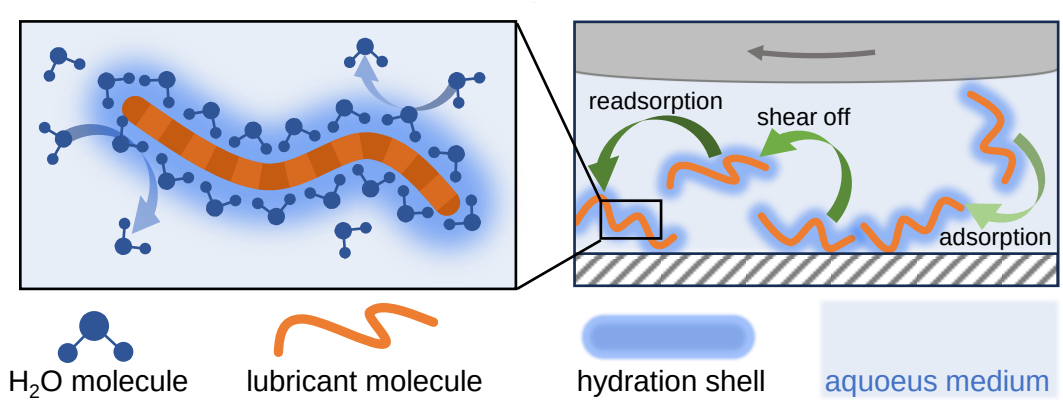

Figure 3.3: *Lubrication mechanism and friction response of mucins:* schematics showing lubrication mechanisms typical of biomolecules, hydration lubrication (left) and sacrificial layer mechanism (right).

Consequently, the attachment of a charged polymer to a surface in an aqueous environment leads to the formation of a hydration layer on the surface, which is highly hydrated and can be interpreted as a permanent fluid film established on the surface (*Figure 3.3, left*). For a broad range of challenging conditions, such hydration layers are capable of avoiding compression due to hydration repulsion between the hydration shells associated with the individual charges, of enabling energy dissipation even at low shear forces due to the rapid exchange of confined water molecules with free water molecules, and of maintaining the bulk-like fluidity of water due to the fact that water reaches its highest density in the liquid phase. Therefore, these extraordinary properties of hydration layers can enable good lubrication even at boundary lubrication conditions.[161,171]
The sacrificial layer formation mechanisms (*Figure 3.3., right*) on the other hand, involves the establishment of a thin and transiently bound layer as the most superficial zone on a substrate surface. In case of external stresses or shear forces, e.g., induced by sliding motions, such a sacrificial layer (SL), as indicated by the name, is sacrificed instead of the underlying substrate surface. This dissipates the externally introduced energy thus reducing friction and avoiding wear of the substrate surface. To be efficient, an SL must be constantly renewed with attachment rates higher than the detachment rates. Therefore, the surface affinity of the molecules establishing the SL must be high and such molecules must be available at high redundancy.[178–180]
A bio-macromolecule capable of employing both mechanisms simultaneously is mucin. In contact with a hydrophobic surface, the hydrophobic termini of the mucin can transiently bind to the surface via hydrophobic interactions and the hydrophilic, bottlebrush-like structured central region allows for the establishment of a hydration layer. Thus, if mucins in an aqueous solution are used as a lubricant in a suitable tribological system, e.g., steel on PDMS, the resulting friction is very low and almost independent of the used sliding velocities, *i.e.*, of the lubrication regime.[36,40,41,66,87]

Here, Stribeck's theory[149,150] does no longer apply. This can be explained as Stribeck's theory assumes two solid, intrinsically static surfaces employed in the tribological system. However, the introduction of a hydration layer and/or a sacrificial layer establishes a new, intrinsically dynamic, and much more complex layered surface.

4 Summaries of the Publications

4.1 Summary of "Multifunctional "Janus-Type" Bilayer Films Combine Broad-Range Tissue Adhesion with Guided Drug Release"

A research article published by Ceren Kimna, Maria G. Bauer, Theresa M. Lutz, Salma Mansi, Enes Akyuz, Zuleyha Doganyigit, Percin Karakol, Petra Mela, and Oliver Lieleg in "Advanced Functional Materials" in April 2022.[76]

In this study, an asymmetrically designed bilayer construct was introduced, which was engineered such that the opposing sides were distinctively functionalized with specific bio-macromolecules, *i.e.*, dopamine-conjugated hyaluronic acid (dHA) and lab-purified porcine gastric mucin (MUC). These bio-macromolecules were selected to promote good wet tissue adhesion and accelerated wound healing on one side and to avoid inflammatory reactions, mechanical abrasion, or unspecific protein or tissue adhesion on the other side, respectively (***Figure 4.1 a***). Such a complex construct is necessary as tissue healing is a challenging process which requires managing conflicting issues simultaneously: The handling of the construct in a dry state should be convenient, the application to a wound should not require any aids or sophisticated training (like for sutures), unidirectional drug release (of *e.g.,* antibiotics for the treatment of infected wounds), from the dHA layer would be desirable, and the compound should fully decompose in wet environments, leaving no residues or alterations on the treated tissue, so no consecutive removal step is required.
To confirm the suitability of the bilayer concept for efficient wound healing applications and to prove the above-described, desired multi-functionality of the construct, multi-faceted examinations were conducted in this study. First, the successful production route for the bilayer films, employing casting for the carbodiimide-coupled dHA layer and electro-spraying for the generation of a homogenous, fibrous MUC layer, was confirmed *via* UV-spectroscopy, SEM imaging (*Figure 4.1 b*), and contact angle analysis. In a next step, the mechanical superiority of the bilayer film compared to single layer films was shown by stretching tests investigating the normal force at break and by mechanically challenging the films in a linear tribology setup followed by surface morphology evaluations (*Figure 4.1* c&d). Subsequently, by spectroscopically analyzing the eluents of the films incubated in buffer and by high-speed imaging of the films' swelling behavior, the time dependent degradation behavior and the uni-directional drug-release capability in different simulated body fluids (*Figure 4.1* e) as well as the hydrogel-forming behavior of a dry film encountering a wet surface were demonstrated. The desired interactions of either side of the films with different types of cells and proteins was verified *in vitro* by detecting the amount of adhered proteins, epithelial HeLa cells, or prokaryotic cells (*S. aureus*, *E. coli*) on either side of the films *via* (fluorescent) microscopy and colony forming unit counts. Moreover, the immune response to the construct was examined by comparing the cytokine expression levels of monocyte-derived macrophages after cultivation on either side of the films. Lastly, the time dependent recovery behavior of a damaged HeLa cell monolayer covered by a bilayer film was traced by employing microscopy imaging. To confirm the beneficial influence of the bilayer film *in vivo,* its wound healing performance was investigated by the application of bilayer films to wounds created on the back of Sprague-Dawley rats.

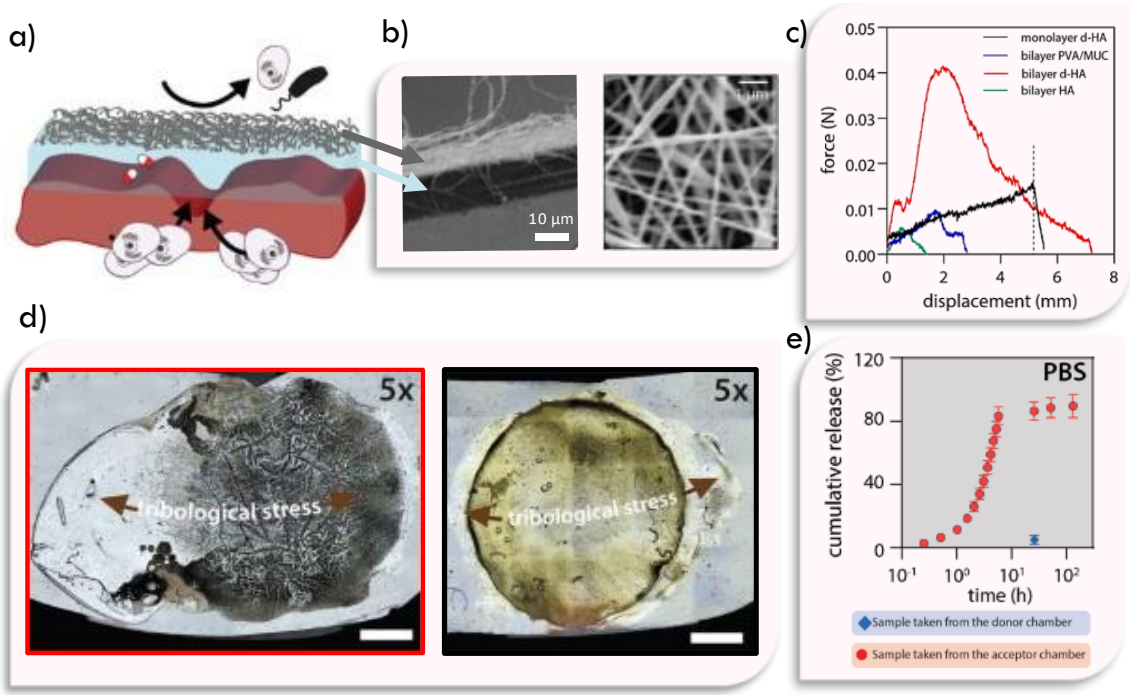

Figure 4.1: *Schematic overview of the study and exemplary data sets*: a) depicts a schematic representation of the bilayer patch intended for wound healing applications, presented in this study. *b*) depicts SEM images of the bilayer patch (left) and the PVA/MUC fibers (right). c) shows exemplary force-displacement curves determined in stretching tests. d) images of a d-HA monolayer (left) and a crosslinked bilayer patch (right) acquired after exposure to tribological stress are displayed. e) unidirectional drug release from the bilayer patch. Error bars denote the standard error of the mean as obtained from at least n = 3 measurements. If no error bars are visible, their size is on the order of the symbol size.

The wound healing behavior of untreated wounds, wounds treated with a bilayer film, and wounds treated with a drug-loaded bilayer film was traced for up to 14 postoperative days. Therefore, tissue sections were taken from the wounds and compared to healthy skin sections *via* hematoxylin and eosin as well as Masson's trichrome stainings from which the epidermis thickness, the number of hair follicles, and the collagen index were derived. In a last set of tests, the strong attachment behavior of bilayer films to different porcine tissue samples was determined *ex vivo* and topographical imaging was employed to demonstrate that, after the disintegration of the bilayer films, no residues of the film or tissue alterations could be observed.

<u>The candidate's contributions:</u> I conducted the tribology and swelling experiments, for which I also participated in the design of the graphics and writing of the associated paragraphs in the manuscript. I participated in conducting the shearing tests and drug release studies. I critically revised the original manuscript draft.

4.2 Summary of "Wetting Behavior and Stability of Surface-Modified Polyurethane Materials"

A research article published by Maria G. Bauer, Rosa Reithmeir, Theresa M. Lutz, and Oliver Lieleg in "Plasma Processes and Polymers" in September 2021.[77]

In this study, seven different surface modification approaches (*i.e.*, an oxygen plasma treatment, two dopamine layer deposition methods and four wet chemical etching solutions) were tested for their suitability to enhance the wettability of three different polyurethane (PU) materials - in detail two medical-grade materials, *i.e.*, the aromatic 'AC' and the aliphatic 'PC', and a technical-grade material 'PUR'. However, at the same time, the surface morphologies and structures of the materials should remain unchanged.
Such surface modifications are often desired for synthetic polymer materials, which typically behave hydrophobic, but are intended for applications in biological environments or for applications which require enhanced interactions with aqueous solutions, *e.g.,* for tribological applications.
In this publication, first the efficiencies to render the surfaces of the different polyurethane materials hydrophilic without influencing their surface morphologies were compared for all seven treatment approaches. Therefore, contact angle measurements and confocal laser microscopy images (*Figure 4.2 a*) as well as surface roughness parameters derived from those images were evaluated before and after either treatment applied to the different PU materials. Subsequently, the durability of the efficient treatments (*i.e.,* plasma treatment and the two dopamine layer depositions) was demonstrated - by examining the wettability of the treated samples at various time points - for up to a month (*Figure 4.2 b*): in particular, when exposed to wet storing conditions, in contrast to dry storing.
In the next step the robustness of the surface modifications to UV irradiation for up to 30 min was shown. Such a treatment was required to obtain disinfected samples, which were necessary to reliably confirm the noncytotoxic behavior of and good cell attachment onto the modified medical-grade PU variants (*i.e.*, AC and PC). For the technical material PUR, rotational tribology assessments were conducted as an application-oriented test instead. Here, especially for the oxygen plasma treated samples, a friction reducing effect was detected (*Figure 4.2 c*), as the treatment improved the interaction of the surface with the aqueous lubricant without introducing a sticky layer as observed for the dopamine layer.
Overall, this study showed that with a suitable treatment it is possible to modify the surface properties of PU materials for extended time periods. Furthermore, the results emphasized the importance of selecting a designated surface treatment, specifically, for the exact material variant as even within the same family of materials each modification can have different effects. Moreover, the results of this study can be used to optimize surface modifications, like (multi-) functional surface coatings, and their process steps for the application onto PU materials which could further broaden the field of applications of PU materials consequently.

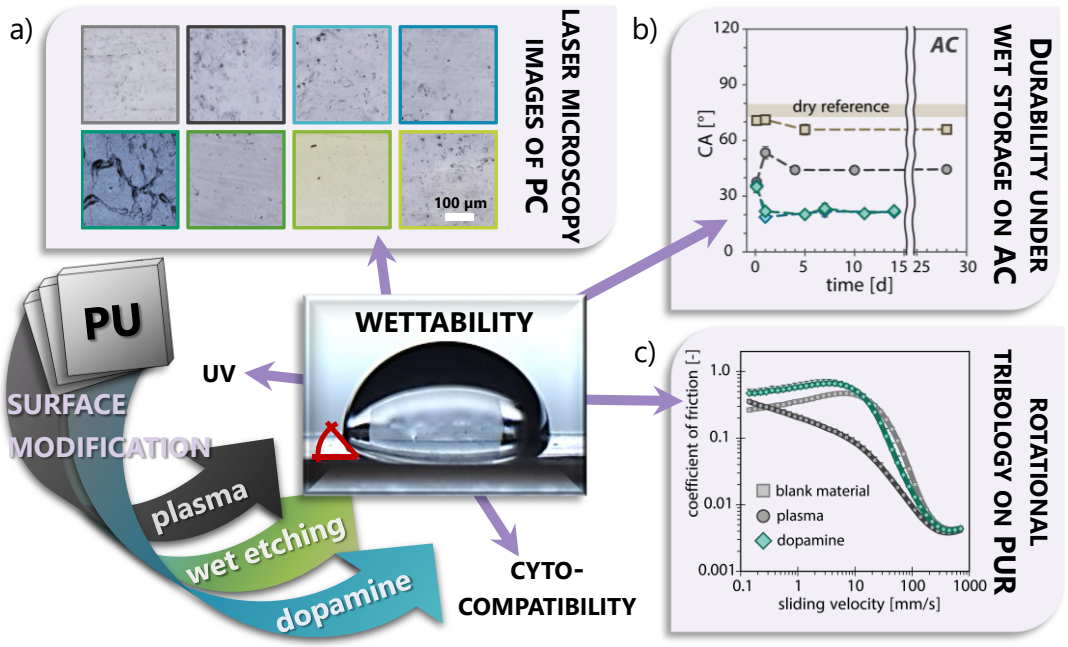

Figure 4.2: *Schematic overview of the study and exemplary data sets:* As depicted in the schematic at the bottom left of the figure the surfaces of the PU samples were modified employing three different treatment strategies and their influences on the sample wettability were assessed. Data were obtained before (beige/gray) and after the implementation of the designated surface activation strategies, *i.e.*, plasma activation (dark gray/circles), two types of dopamine treatments (light blue and dark blue/diamonds), and four chemical etching approaches (different shades of green). Surface morphologies were examined by confocal laser scanning microscopy, exemplary images acquired on PC samples are depicted in (a). Contact angle measurements were conducted over a period of 2–4 weeks as shown in (b) for AC samples stored in PBS at 37°C. (c) The technical-grade PUR samples were assessed *via* a tribological examination in a rotational ball-on-three-plates setup. The scale bar in (a) represents 100 µm and applies to all microscopy images in (a). Error bars denote the standard error of the mean as obtained from at least n = 3 measurements. If no error bars are visible, their size is on the order of the symbol size.

<u>The candidate's contributions:</u> I participated in the conceptualization of the study and design of experiments. I performed all experiments involving samples exposed to chemical etching, all light profilometry analyses, and tribological examinations and participated in the contact angle measurements. I evaluated and interpreted all acquired results (except for the data regarding tests with eukaryotic cells) and designed all included graphics. I participated in writing the article by drafting the manuscript.

4.3 Summary of "Bio-Macromolecular Surface Coatings for Autohesive, Transparent, Elastomeric Foils"

A research article published by Maria G. Bauer and Oliver Lieleg in "Macromolecular Materials and Engineering" in February 2023.[78]

This study investigated the impact of two different coating strategies (carbodiimide-mediated coatings (carbo) and dopamine-based coatings (dopa)), their intermediate layers, and the different top-layer molecules (overall anionically charged mucins vs. dextrans comprising cationic groups) on the resulting (surface) properties when applied to two different polymeric substrate materials (polydimethylsiloxane (PDMS) and polycarbonate-based polyurethane (PCU)). Such elastomeric, thermoplastics combine a broad range of beneficial properties like mechanical robustness, transparency, and flexibility; however, their application is often limited by their adhesive behavior, especially their propensity to stick to themselves, which is referred to as autohesive behavior. This property not only impedes handling and processing but can also interfere with the designated applications. To overcome this undesired behavior, bio-macromolecular coatings were applied in this study and their influence on the autohesive behavior of the foils was examined, while ensuring that those coatings did not negatively influence the flexibility, transparency, or surface roughness of the substrate materials. First, contact angle measurements were conducted and confirmed the successful application of either coating onto the substrates as the wettability of the coated materials was improved for all variants. The influence on the autohesive behavior of the materials was examined by employing lap shear tests and detachment tests (***Figure 4.3 a&b***). Overall, the influence of the coatings on the PCU samples, which initially showed the stronger autohesive behavior, was more pronounced, and especially the carbo-coatings achieved clearly reduced resistances in either test. For the dopa coatings on both materials, the sticky behavior of the dopamine layer used to apply the designated macromolecules appeared to influence the overall results, as the reduction of either resistance was comparably low. Even though both materials initially showed similar, strongly negative surface potentials, surface zeta potential analyses showed that the surface properties of PDMS are more dominant as, once again, the effects of the coatings on the PCU samples were more pronounced. Here, the dopa-coating employing dextrans even resulted in positive surface potentials *(Figure 4.3* c). Using UV/Vis spectroscopy, no influence of any coating/macromolecule combination on the transparency of either substrate material was detected. Additionally, confocal laser scanning microscopy revealed similarly low surface roughness parameters for uncoated and coated samples alike. Lastly, the foil flexibility was assessed by repeatedly twisting the samples in a reciprocating manner. Here, only the carbo-mucin coating slightly softened the material response of the PCU. When conducting a post-examination of the samples, no narrowing of the samples or any influences on the surface structure due to the flexibility tests was detected.

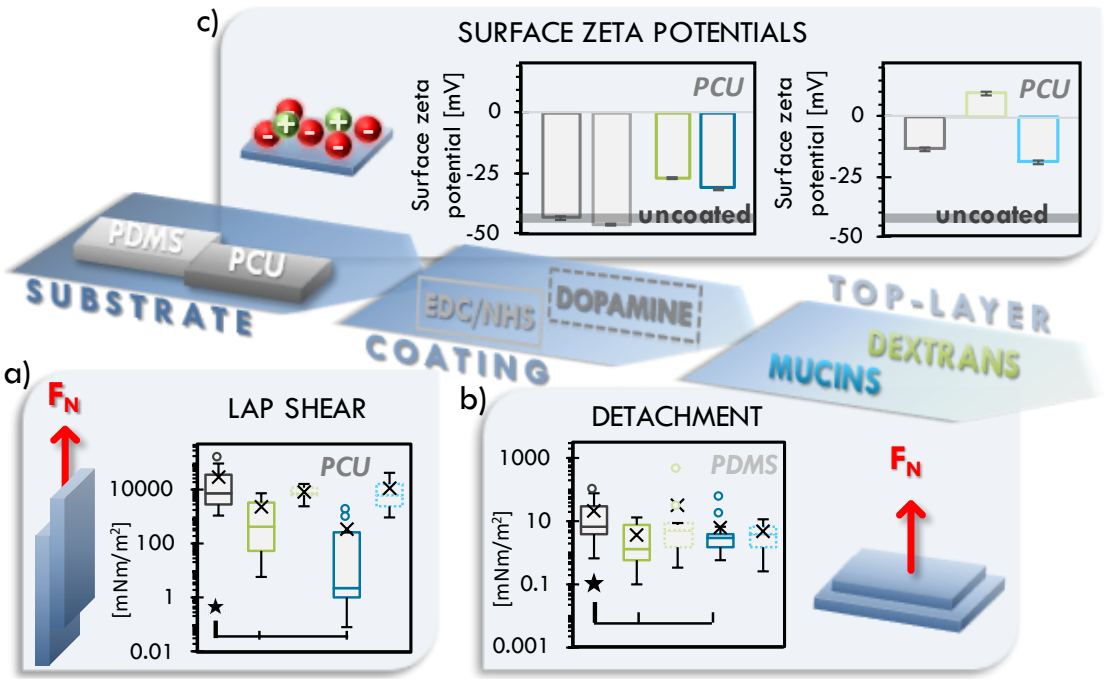

Figure 4.3: *Schematic overview of the study and exemplary data sets:* Resistance of (surface modified) foils against a) lap shear and b) detachment. c) Zeta potentials of bare and coated substrate materials. The grey bar labeled with uncoated indicates results obtained for the uncoated substrate. Results for uncoated (dark grey lines), carbo-LDex coated (intense green lines), dopa-Qdex coated (dashed, light green lines), carbo-mucin coated (intense blue lines), and dopa-mucin coated (dashed, light blue lines) are depicted. Error bars denote the standard error of the mean as obtained from at least n = 3 measurements. If no error bars are visible, their size is on the order of the symbol size. Asterisks denote statistically significant differences between samples (based on a *p*-value of 0.05).

Overall, it was demonstrated that the final surface properties of coated polymeric foils were not purely dictated by the properties of the applied top layer-molecules but could still be strongly impacted by the substrate as well as the specific coating strategy. Thus, especially the following aspects should be considered for future coating applications: First, the facile and broad range application of dopamine-based coatings appears to come at the price of a comparably dominant, sticky intermediate dopamine layer. Second, to achieve a desired behavior tailor-made for the intended usage, it is important to choose a substrate- and application-specific coating strategy in combination with a suitable top-layer molecule.

<u>Candidate's contribution:</u> I participated in the conceptualization of the study as well as the design of the experiments. I performed and evaluated all experiments and designed all included graphics. I contributed to the writing of the manuscript by writing the draft of the text.

4.4 Summary of "Comparing the Resilience of Macromolecular Coatings on Medical-Grade Polyurethane Foils"

A research article published by Maria G. Bauer, Kjetil Baglo, Luca Reichert, Jan Torgersen, and Oliver Lieleg in "Surfaces and Interfaces" in August 2023.[79]

In this study, the functionality of two different coatings, obtained *via* a carbodiimide-mediated (carbo) and a dopamine-based (dopa) coating process, employing dextrans with cationic groups as top-layers applied to polyurethane (PU) foils was compared after those coated foils were exposed to different application-oriented treatments (including long-term usage, storage, and sterilization procedures).
As elastomeric, thermoplastic materials such as the here examined PCU often show autohesive properties they are often deemed unsuitable for tribological applications which demand a smooth relative motion between two samples. However, in this study the feasibility of obtaining efficient gliding motions between two PCU foils was demonstrated in a linear tribology setup. This was achieved by altering the surface properties of the foils *via* combining either hydrophilic surface coating with a suitable macromolecular lubricant to utilize hydration lubrication and (potentially) sacrificial layer formation between both coated foils. Both coatings were found to be about or even less than 1 µm thick. To assess the resilience of the examined coatings, first, long-term tribological measurements running for 9 h were conducted. Here, even though the determined coefficients of friction were rather similar, the carbo-coated samples were the most reliable, steady, and reproducible; for uncoated and dopa-coated samples, the detected friction traces showed lots of variability. Furthermore, for the latter two sample types, the autohesive behavior of the PCU material induced a full inhibition of the movement at several occasions; thus, restarts during most of the measurements were necessary. Confocal laser scanning microscopy was conducted to assess the surface morphology of the samples after long-term usage and further emphasized the tribological superiority of the carbo-coating as no signs of wear were visible. This observation was confirmed by surface roughness parameters derived from those surface morphology images. In a second set of tests, the durability of coatings exposed to different storing conditions was examined (***Figure 4.4***). Here, in addition to the CoFs, the effective runtime (*i.e.*, the time the samples were freely gliding over each other) was recorded. Generally, for both coatings hydrated storage appeared more beneficial than dry storage, and the carbo-coated samples were found capable of maintaining their functionality for up to 200 days (under certain conditions). Lastly, the effects of commonly used sterilization methods (*i.e.*, ethylene oxide fumigation (ETO) and gamma-irradiation (gamma)) were assessed. Once again, the carbo-coated samples were least affected and especially the ETO treatment had barely any influence on the performance of the coatings. For the dopa-coating, the long duration of the sterilization treatments already affected their performance to such a degree that the influence of the sterilization procedures themselves was difficult to reliably identify. Furthermore, both coatings seemed to shield the substrate material from the negative influences of the sterilization treatments as only little to no change in FTIR scans was observed for coated and sterilized samples compared to uncoated and sterilized samples.

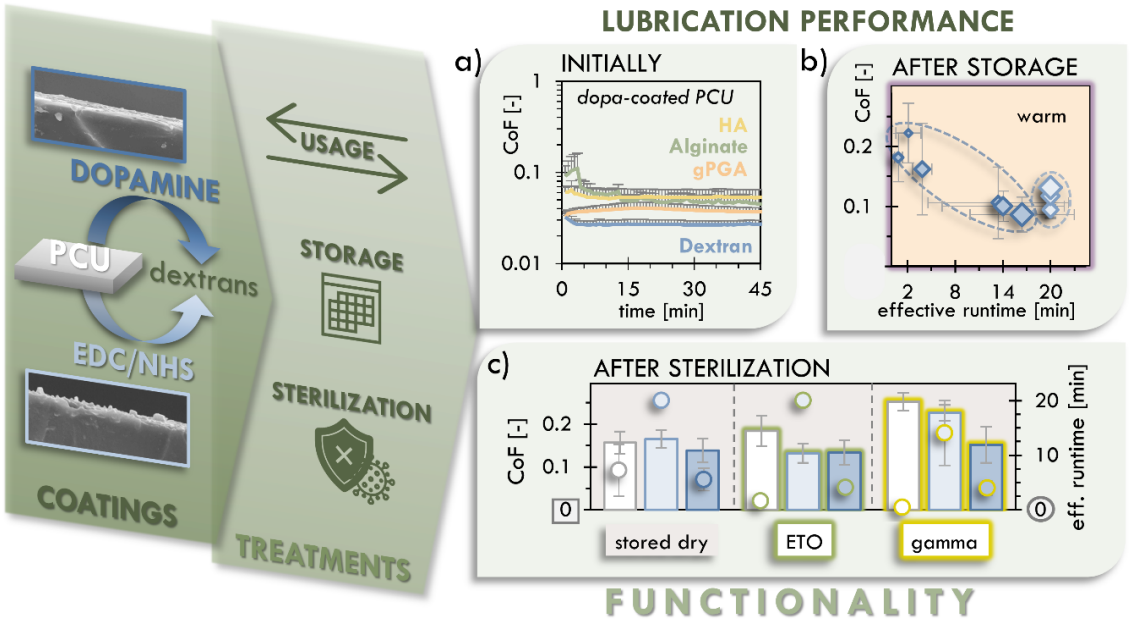

Figure 4.4: *Schematic overview of the study and exemplary data sets:* In this study the resilience of fucntionality of dopa-Qdex coatings and carbo-LDex coatings was compared. a) depicts the friction response determined initalliy for dopa-QDex coated PCU. b) displays the lubrication performance of stored carbo-LDex coated PCU samples. c) gives a comparison of the lubrucaiton perfomrance obtained for uncoated (white), carbo-LDex coated (light blue), or dopa-QDex coated samples, either stored, or exposed to sterilizatiion treatments with ethylene oxide (green) or with gamma-irradiation (yellow). Error bars denote the standard error of the mean as obtained from at least n = 3 measurements. If no error bars are visible, their size is on the order of the symbol size.

This study showed that either coating is suitable to overcome the autohesive behavior of the PCU foils and enable efficient gliding; however, especially for long-term applications, wear avoidance, and applications requiring sterilization, the carbo coatings outperform the dopa coatings.

The candidate's contributions: I participated in the conceptualization of the study and the design of the experiments. I performed and evaluated all experiments except for the curation and interpretation of the dynamic scanning calorimetry measurements, the interpretation of the FTIR scans, as well as the acquisition of the scanning electron microscopy images. I designed all included graphics and contributed to the manuscript by writing the draft of the text.

4.5 *Summary of "Effects of Sterilization Methods on the Integrity and Functionality of Covalent Mucin Coatings on Medical Devices"*

A research article published by Carolin A. Rickert, Maria G. Bauer, Julia C. Hoffmeister, and Oliver Lieleg in "Advanced Materials Interfaces" in December 2021.[80]

In this study the influence of commonly used sterilization methods (*i.e.*, autoclavation (AC), ethylene oxide fumigation (EO), γ-irradiation (γ), and UV-irradiation (UV)) on the structural integrity and functionality of covalently coupled mucin coatings applied onto three medical devices (urethral catheters, intubation tubes, and contact lenses) made from different polymeric materials (*i.e.*, polyurethane (PU), polyvinylchloride (PVC), or polydimethylsiloxane (PDMS) was investigated. Previously, such covalent mucin coatings – established with lab-purified MUC5AC - had been found to exhibit beneficial properties with great potential to improve different surface characteristics of the substrates, such as their wettability, lubricity, and anti-biofouling behavior. However, to be employed as part of a medical device, effective sterilization is indispensable. However, sterilization processes typically are aggressive treatments and require harsh conditions, which might unintentionally impede the structural integrity and functionality of the applied coatings. Thus, to assess the structural integrity of the mucins - coated onto either medical device and treated with any of the sterilization procedures - two specific detection methods (*i.e.*, ELISA and a lectin depletion assay) were employed (***Figure 4.5 a***). Here, it was found that the bottlebrush-like glycosylation found in the central part of the mucin molecules appears to shield the protein backbone of the molecule from the influence of the physico-chemical challenges: the glycosylated part of the mucins demonstrated to be more resilient than the un-glycosylated, hydrophobic termini of the mucin molecules.

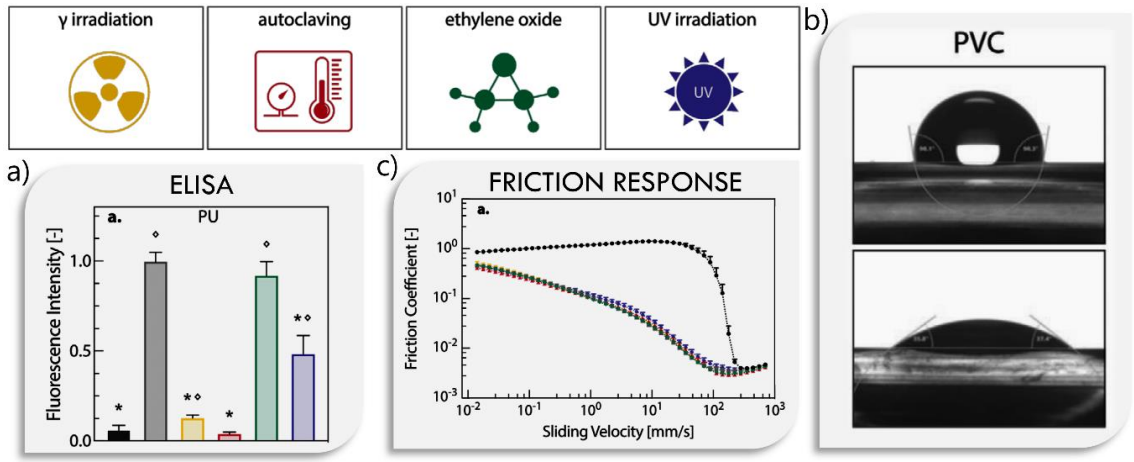

Figure 4.5: *Schematic overview of the study and exemplary data sets:*
Sterilization of the coated devices was conducted *via* γ-irradiation (yellow), autoclaving (red), ethylene oxide fumigation (green), or UV irradiation (purple). The normalized fluorescence intensities obtained with an ELISA on mucin-coated PU samples are shown in (a). b) Exemplary contact angle images of a PVC based medical device surface and the same set of surfaces carrying a mucin coating (prior to any sterilization process). In c) the Stribeck curves obtained for mucin coated and sterilized PDMS samples are displayed. Additionally, a) and c) show results for uncoated (black) and coated but untreated (grey) samples. The error bars denote the standard error of the mean as obtained from $n \geq 4$ samples. Asterisks and rhombi denote statistically significant differences between a treated sample and the untreated reference or the blank sample, respectively (based on a *p*-value of 0.05).

Assessing the wettability *via* contact angle measurements (*Figure 4.5 b*) showed that the hydrophilic characteristics of the mucin surface coatings were maintained for almost all examined treatments. Moreover, for neither of the sterilization procedures, any influence on the lubricity provided by the mucin coatings, was detected by rotational tribology examinations (*Figure 4.5 c*). Furthermore, lipid adsorption tests (evaluating the anti-biofouling potential of the coating) emphasized the overall finding that coatings exposed to ethylene oxide outperformed the coatings subjected to any of the other techniques in maintaining the integrity and functionality of the mucin coatings.

Generally, the results of this study further promote the suitability of mucin coatings for medical devices, as the various beneficial properties established by such mucin coatings were demonstrated to be robust towards commonly used sterilization processes (to different extents), which represents a crucial advancement in the development of mucin coated medical devices to qualify for usage in a clinical context.

The candidate's contributions: I participated in the conceptualization of the study as well as in the design and the analysis of the experiments. I critically revised the original manuscript draft.

5 Discussion

In this thesis, different approaches to achieve specific adhesive properties of polymeric materials are discussed. Depending on the chosen material and intended application, the desired adhesive properties can range from strongly adhesive bonds, over reservable physical interactions, to anti-adhesive, repellent behavior. To successfully develop a material employing specific adhesive properties (required for the envisioned application), it is necessary to assess and understand the potential chemical, physical, and biological interactions, which the polymers can establish with each other and with their surrounding environment.

The mainly bio-based construct presented by Kimna et al. 2022[76], was a thin bi-layer patch employing specific functionalizations in either layer aiming at an optimized wound healing management provided by the construct. From a material engineering point of view, achieving the desired (anti-)adhesive behavior of both layers and, at the same time, good interconnection of those layers is not trivial. Additionally, sufficient mechanical stability of the patch was required to ensure good manageability and resistance against external mechanical stresses. Here, for the tissue facing layer, good wet tissue adhesion was achieved by conjugating dopamine to hyaluronic acid thus forming d-HA. In contrast, the anti-adhesive properties of the environment facing layer were established by the incorporation of mucin molecules into the poly(vinyl alcohol) (PVA) network as schematically depicted in ***Figure 5.1***. This network was established by long, randomly oriented, electro-spun PVA/MUC fibers and mechanically reinforced by glutaraldehyde (GTA) crosslinks. GTA is a short organic molecule with a carbonyl group at either terminus, and GTA is frequently used to permanently crosslink proteins and to fixate biological tissues.[181,182] It has been reported that GTA interacts predominantly with amine, but crosslinking of PVA has been reported, too. For the latter, it has been suggested that the connection is formed between two neighboring hydroxy groups of the PVA with a carbonyl group of GTA.[183–185] Thus, for the PVA/MUC network, a high degree of crosslinking between the polymers inside a fiber as well as between different fibers should be established.

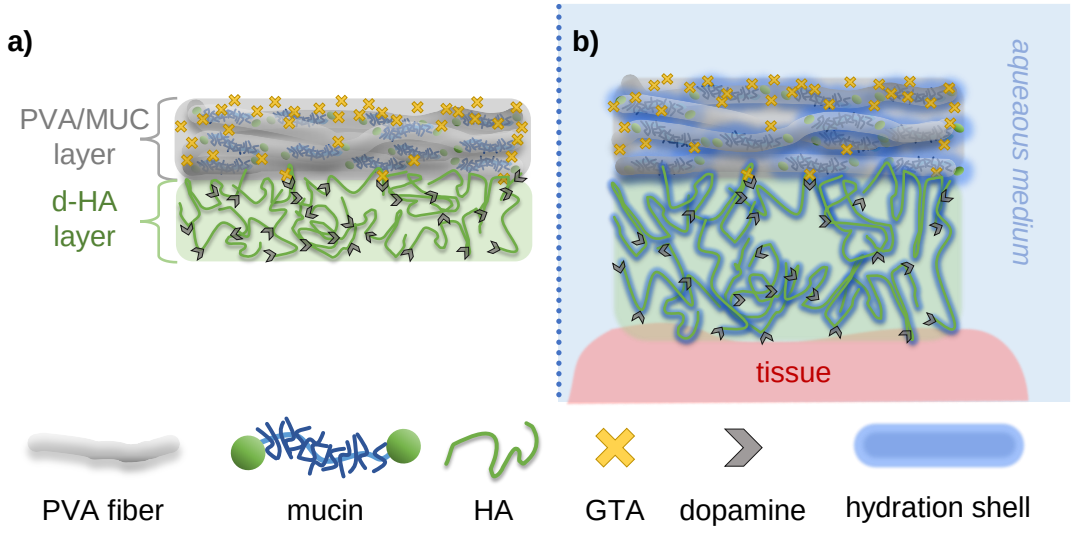

Figure 5.1: *Schematic representation of polymer interactions of the bilayer patch:* the predominate polymer interactions of a) the PVA/MUC layer (grey) and the d-HA layer (green) in a dry state and of b) the swollen d-HA layer in contact with biological tissue (pink) and the hydrated PVA/MUC layer in aqueous environment. The schematics are not to scale.

Here, the effectiveness of the crosslinks was confirmed practically by detecting a maximum rupture force for the crosslinked bilayer constructs that was higher than the sum of rupture forces obtained for both single layers. Additionally, the absence of distinctive spreading observed for the bilayer patch after exposure to tribological load confirmed that the crosslinked fiber network resists deformation and that the fibers do not align in the movement direction in a pronounced manner. This indicates good stability of the crosslinks as the patch behaved as one entity rather than a conglomeration of many individual chains.
Furthermore, the good interconnection between both layers was assessed by lap shear tests of partially overlapping bilayer constructs. As the locus of failure was always found in a monolayer rather than between both layers, considerable adhesion between both layers must have been achieved. However, GTA driven crosslinks of the d-HA layer are unlikely, as crosslinking of HA via GTA requires an acidic medium as catalyst [100,186], and the amine group of the dopamine has already been employed in the conjugation process with HA. Based on the mode of crosslinking discussed above for PVA, it is speculated that bonding of GTA with the two neighboring hydroxy groups of the catechol groups of the dopamine molecules could be conceivable. Other than that, the adhesive interactions between both layers are presumably formed mainly by hydrogen bridges, entanglements of the involved polymers, and interactions of the catechol groups with the PVA/MUC layer. Indeed, a good interaction of dopamine with mucins has already been reported.[88,187,188] Furthermore, the limited crosslinking of d-HA by GTA is underscored by the behavior observed for hydrated d-HA layers and bilayer patches: Here, distinctive swelling of the d-HA layer was observed, and strong limitations of swelling have been reported for GTA crosslinked materials.[185,189,190] Additionally, as basically the same viscoelastic behavior was determined for d-HA monolayers and for crosslinked bilayer patches, an entirely GTA crosslinked construct appears doubtable. Still, the d-HA layer showed storage-modulus dominated, and therefore gel-like, elastic behavior in those rheological assessments. This indicates good intermolecular interactions in the d-HA network. This points towards a transiently crosslinked network (established by the incorporation of dopamine molecules) rather than a mainly physically entangled solution as typical for pure HA in an aqueous medium.[96,191] Additionally, the catechol groups introduced by the dopamine molecules clearly promote tissue adhesion: about 10 times as much energy was required to detach a d-HA layer from wet tissues than for an HA layer. As putative interactions, hydrogen bonds, oxidations, and Schiff base reactions with amines, carboxyl groups, hydroxy groups, or thiols available on the tissue surface have been reported for adhesion of dopamine materials to biological tissues; and the reported detachment energies were in a similar range.[45,192,193] For the anti-adhesive properties of the PVA/MUC layer, the desired behavior was confirmed by detachment tests from tissues, as well as incubation tests performed with proteins, eukaryotic cells, and prokaryotic cells. This indicates, that neither the low content of mucins (< 5 weight-%) in the PVA/MUC layer nor the reported, negative influences of GTA crosslinking on the functionality of some proteins[182] could inhibit the anti-adhesive properties brought about by the mucins. For the former, the restriction of swelling introduced by GTA crosslinking might be beneficial, as it maintains a high density of mucins even in a hydrated state. For the latter, as the anti-adhesive properties of mucins are mainly associated with hydration shells formed around the glycosylated part of the protein[39,55,194,195], any changes potentially introduced to the structure of the folded termini appear negligible. Lastly, the reported reduced solubility of GTA crosslinked materials might contribute to the delayed degradation

observed for the PVA/MUC layer.[186,196] Overall, even though the specific functionalities of the bilayer patches were introduced by the incorporation of certain (macro-)molecules, the coexistence of partially contrary properties was achieved by spatially compartmentalizing the functionalized polymers by a consecutive preparation of the full construct in two layers. Additionally, the bespoke behavior of either layer was maintained even in an aqueous environment by carefully chosen suitable crosslinking agents.

In the next section, the attachment of biopolymers to the surfaces of synthetic polymer-based materials is discussed. As explained in the introduction, to establish such an attachment, the low reactivity of synthetic polymer materials must be overcome. Therefore, in Bauer et al 2021[77], different surface activation strategies were examined on PU materials. For the identified, effective activation strategies, *i.e.,* strategies that achieved distinctively enhanced wettability without negatively influencing the surface morphology, the durability of the achieved modifications in atmospheric and in aqueous environment was assessed.

As expected, dry storage had adverse effects on the plasma activated samples, which were attributed to hydrophobic recovery. This effect is associated with the re-establishment of the un-reactive material surface, and it is caused by polymer chain reptation and rotation transporting activated polymer chain segments into the bulk of the material. [197,198] In contrast, a preservation of the activated surface was achieved in an aqueous environment as polar interactions temporarily stabilized the activated polymer chain segments on the material surface. Qualitatively, dopamine treated samples stored in atmospheric environment showed a similar behavior as plasma activated samples. However, it is important to consider that dopamine layer deposition does not establish a continuous, monomolecular layer but rather forms a supramolecular aggregate constituted of diversly interacting oligomeric and polymeric dopamine snippets.[199] If these snippets do not establish any permanent bonds with the material surface, they can be gradually detached. Moreover, some oligomeric snippets might still be small enough to be affected by the effects of hydrophobic recovery, and thus can be transferred into the material. For dopamine treated surfaces stored in aqueous medium, the wettability was even further enhanced within the first days of storage. Even though water uptake of the substrate material might have also contributed to this effect, rearrangements of the dopamine molecules and of the interactions between them would be conceivable, which could have enabled the establishment of an energetically more advantageous structure of the dopamine layer. Thus, higher surface energy and consequently enhanced wettability would have been achieved.

As it is reversible by hydrophobic recovery, the plasma treatment would have been too instable in an atmospheric environment to reliably conduct more complex examinations. Thus, to avoid such activation reversing effects, silane precursors were attached to the surfaces directly after the plasma activation. In an acidic, aqueous medium, the silanes hydrolyzed to form silanols (-Si-OH), which readily reacted with the plasma induced, hydroxylated surfaces by forming a strong connection *via* hydrogen bridges, van der Waals interactions, as well as covalent bonds through hydrolytic condensation. For the latter, strong siloxane bonds (Si-O-SI) are established, if silicone atoms were accessible in the polymer backbone, such as for PDMS. Otherwise, the formation of silyl derivates (e.g., silyl ester Si-O-C) between the silane precursor and hydroxylated or carboxylated materials was reported. Through bonding with sufficiently large silane precursor molecules, the free movement of the polymer chains was restrained and thus a permanent surface layer was created. [200–203]

On PCU samples, such silane pretreatments achieved a significantly reduced resistance against lap shear as well as against detachment movements compared to uncoated samples (which behaved strongly autohesive). In contrast, on PDMS, such a reduction of resistance against either movement was not observed. In fact, the resistance against lap shear motion was even increased for silane treated PDMS. This was surprising as, on both materials, the silane treatment should have induced a reduction of interdiffusion, owing to the restrained movability of the silane modified polymer chains, as well as to the barrier formed by the silane precursors, which the polymers would have needed to overcome to interact. Furthermore, the high number of carboxyl groups available on the silane precursors should have locally induced electrostatic repulsion. However, a difference can be found in the chemical groups established by the hydroxylation induced by the plasma treatment: on PDMS, reactive silanol groups were generated, whereas, on PCU (putatively) mainly simple C-OH bonds were introduced. If not all silanol groups on the PDMS surface were occupied by the precursors, the remaining silanol groups on the opposing samples could have interacted and thus formed siloxane bonds (by the same reaction as described above for the bonding of the silane precursor to the PDMS surface above). In fact, to produce microfluidic setups, the formation of siloxane bonds between plasma activated PDMS and plasma activated glass is commonly employed to permanently bond both materials to each other; and this process has also been reported for the bonding of two PDMS samples.[204–208] In contrast, on both materials, dopamine treatments assessed in either setup showed a slight tendency towards higher resistances against the movements (only for lap shear tests of dopamine coated PDMS, a significant difference compared to the respective uncoated samples was observed). Since the effects of limited polymer chain moveability and barrier layer formation described above should apply for the dopamine treatment as well, this observed tendency underscores the strongly adhesive behavior of dopamine layers.

In the next section, the influences of mucin and dextran coatings (applied *via* either coating strategy) on the surface properties of the materials is discussed. Here, some fundamental differences in the manner of surface attachments can be anticipated, and those are depicted schematically in ***Figure 5.2***. Owing to the terminal, well accessible amine group available on mucins, an attachment employing the carbo-coating is assumed to predominantly establish a polymerbrush-like coating.[209,210] However, since amine groups might also be accessible in the glycosylated region, attached mucins with alternative orientations could also be present. Enabled by the diverse interaction modes of dopamine molecules, the attachment *via* dopa-coatings is expected to be rather unspecific establishing random orientations of the macromolecules. However, owing to their densely glycosylated central region, the mucins should always maintain a mainly elongated state.[30,31]
In contrast, simply linearly built, flexible polymers such as the employed dextrans tend to condense and form ball-like structures ('Gaussian ball').[211–213] However, attached charges have been reported to limit the degree of condensation due to electrostatic repulsion.[161,214] For the employed dextrans, the influence of electrostatic repulsion in Q-Dextran is expected to be stronger, as the incorporated quaternary ammonium groups are of strong cationic charcter.[92] Furthermore, on L-dextrans, amine groups as well as carboxyl groups are available: thus, repulsive, and attractive electrostatic forces could be possible.[91] This zwitterionic structure putatively reduces the resistance against condensation compared to the solely cationic charged Q-dextrans.

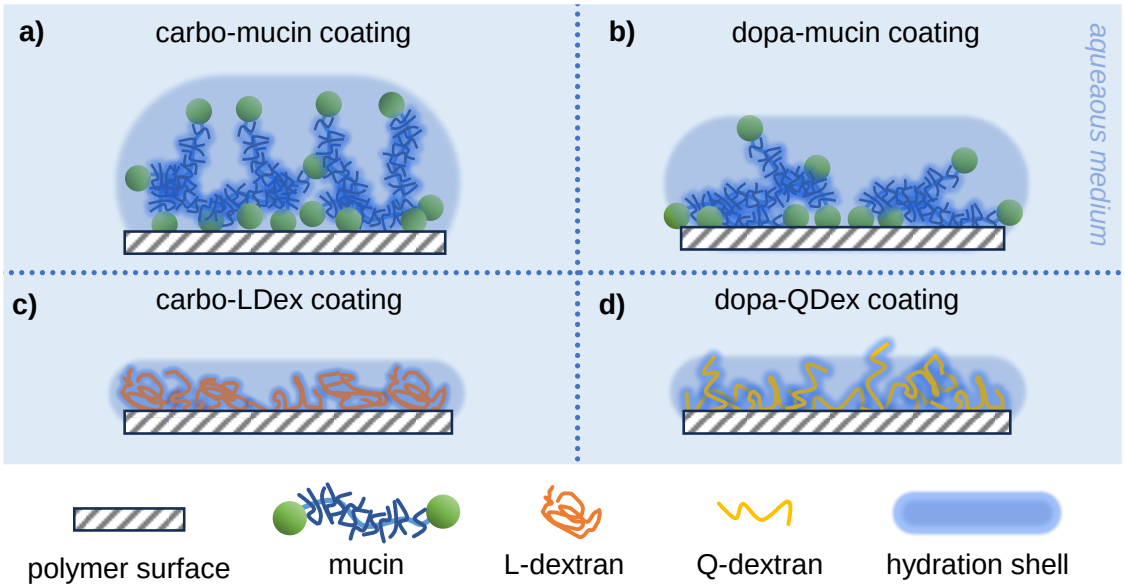

Figure 5.2: *Schematic representations of the putative attachment modes of different macromolecular surface modifications:* Hydration layers established by a, b) mucins, c) L-dextrans, and d) Q-dextrans attached to the polymeric surfaces via a, c) carbo-coatings or b, d) dopa-coatings in aqueous medium. The intermediate layers of the coatings are not depict. The schematics are purely qualitative respresentations and not to scale.

Moreover, as the functional groups are distributed over the entire polymer chain, the attachment of the dextrans would not predominantly be executed *via* a terminal group as for mucins. Instead, it might occur anywhere on the polymer chain and, potentially, at several locations for the same polymer. Thus, overall, the mode of attachment of both dextran types, even though different coating processes are employed, can be expected to be fairly comparable.

For all four coating variants, a successful application was confirmed by detailed examinations of the wettability as well as zeta potentials as reported in Bauer and Lieleg 2023[78]. For the latter, by the application of either surface coating, a clear shift from the zeta potentials detected on the uncoated polymer materials towards the corresponding zeta potentials determined for each macromolecule in solution was observed. However, as depicted in *Figure 5.2* the attachment modes and behaviors of the mucins and dextrans discussed so far, were described for an aqueous environment (as it was present during both macromolecular coupling processes). Yet, for several assessments, such as detachment tests, lap shear tests, and contact angle measurements, dry samples were examined. Accordingly, the influence of dehydration on the coating properties must be considered, too. Here, for short periods of dehydration, it is assumed that the surface coupling should be maintained, and any alterations should mainly occur in the structure of the attached macromolecules. All assessed macromolecules are expected to collapse and condense (at least partially) in the course of dehydration, as the hydration shells surrounding the macromolecules are disintegrated and the number of associated counterions decreases.[212,215] However, caused by steric hindrance and electrostatic repulsion between the densely attached glycan chains, the mucins are expected to resist a full collapse and to maintain their brushy structure (at least to some degree). In contrast, both dextrans are expected to collapse distinctively. Here, the anticipated, more condensed structure and zwitterionic nature of the L-dextrans might be beneficial to maintain and promote the intra- and intermolecular associations during dehydration, which might eventually enable a more

homogenous surface coverage. This assumption is based on studies examining the conformational changes of intrinsically disordered proteins (IDP), which reported that, during the dehydration of surface bound IDPs, solvent-protein interactions tend to be replaced by intra-protein interactions. They further suggested that the observed promotion of intra-molecular interactions might also be relevant for inter-molecular interactions.[216,217] Even though those studies regarded proteins, they were intrinsically disordered ones, *i*.e., they lacked quaternary, tertiary, and, to a high degree, also secondary structures.[218] In other words, those proteins were simple, unstructured polypeptide chains. Thus, their conformational behavior might be transferable to the polysaccharides discussed here.

For the reported detachment tests and lap shear tests, two main tendencies were observed: the anti-adhesive effects of the coating appeared more pronounced on the initially more intensively autohesive PCU material; and in most tested situations, the application of either macromolecule decreased the autohesive behavior compared to the pre-coated samples (independent of the employed coating strategy). The difference in reduction of autohesive behavior between PDMS and the PCU is assumed to be mainly attributed to the fact that PDMS is a thermosetting elastomer whereas PCU is a thermoplastic elastomer. Since the crosslinks between the PDMS polymers are predominantly covalent ones, the initial free mobility of the polymer chains is already considerably restrained. Consequently, the effect of additional restriction of the chain mobility was not as pronounced as for the initially highly mobile, transiently crosslinked PCU chains.

For the second observed tendency, the application of the top-layer molecules is expected to enhance the barrier formation (discussed above regarding the silane treatment) mainly spatially but also electrostatically (especially for the strongly charged mucins and Q-dextrans). Furthermore, for the dopa-coated samples, the degree of coverage of the sticky dopamine layer by the applied macromolecules is assumed to contribute distinctively. Additionally, the observed effect of the applied macromolecules might be attributed (to some degree) to a locally limited alteration of the effective glass transition temperature at the interface. Both discussed materials have glass transition temperatures in the subzero range. For PCU, a T_g of -10°C [84] is stated by the manufacturer; and for PDMS materials T_g values ranging from - 60°C to - 150°C were reported.[86,219,220] For PCU, a T_g clearly below 0°C was further confirmed experimentally by measurements of the heat flow as reported in Bauer et al 2023: Those measurements also showed that there was no global influence on the T_g of the full compound by either dextran coating. Based on the glass transition temperatures reported by Imamura et al.[221] for dextrans with different molecular weights and by employing a logarithmic fit, the glass transition temperature for dextrans with a molecular weight of 150 kDa can be approximated. At a relative humidity of 0 % a T_g of ~ 215°C is estimated, decreasing to ~ 128 °C at 33 % relative humidity. For mucins, many different T_g values have been reported in the literature ranging from -15°C[222] to 130°C[223]; however, most values range between 25°C and 65°C.[224–226] Thus, the T_g of the top-layer molecules can be assumed to be not only clearly above those of the substrate materials but mostly also above the employed examination temperatures of 20°C to 30°C. Therefore, the propensity of the attached top-layer molecules to interdiffuse should be comparably small. Additionally, neither of the discussed coatings showed any influence on the transparency of the substrate materials. Whereas, for carbo-coatings, this has been reported previously[146], this was not so obvious for dopa-coatings. Dopamine polymerization, which contributed to dopamine layer deposition, is typically associated with the formation of a characteristic

brown to black color.[199,227] However, for the dopa-coatings examined in Bauer and Lieleg2023[78] and in Bauer et al. 2023[79], the formation, sedimentation, and attachment of large polydopamine agglomerates was limited by vertically placing the samples into a freshly prepared dopamine solution for a restricted time only and by removing any not fully attached molecules and larger agglomerates after the incubation. Consequently, a thin and homogenous dopamine layer was formed on the material avoiding the development of an intense dark color. The homogeneity of the layer and absence of large agglomerates was further confirmed by surface roughness examinations.

As reported in Bauer et al. 2023, by combining either dextran coating with a suitable lubricant (*e.g.,* 12 % CM-Dex), good lubrication performance was achieved for the strongly autohesive material pairing of two PCU foils. Here, friction responses similarly low as those observed for carbo-mucin coated PCU foils lubricated with poly ethylene oxide (which previously has been identified as a suitable lubricant for coatings comprising the polyanionic mucins[75]) were detected (see **Appendix A.1.2**). Furthermore, it was shown that such coating/lubricant combinations could avoid wear formation even after prolonged tribological treatments of 9h. Here, the carbo-LDex coating performed particularly well as it reliably enabled smooth and continuous relative movement between both foils.
By combining the theoretical fundamentals described in this thesis with the discussed results, it is now attempted to explain the complex interplay of the different mechanisms which potentially enabled this extraordinary lubrication of the autohesive PCU material (***Figure 5.3***):
As explained in the section 3.2, if two layers of PCU, (at $T > T_G$) come in direct contact, an interplay of, *e.g.,* thermodynamic polymer chain movements, van-der-Waals forces, and polar interactions between the polar regions of the PCU can be expected to entail interdiffusion of the two layers (putatively caused by – partial - reptation of individual polymer chains from one layer into the other and entanglements between the polymer chains of both layers). This can establish strong autohesive behavior between the foils.[17,19,228,229]
In contrast, the application of either coating (indicated in yellow in *Figure 5.3*) would basically introduce a new surface acting as a barrier, thus restricting direct contact between both PCU surfaces. Here, several examinations presented in Bauer and Lieleg 2023 and Bauer et al. 2023 demonstrated that, even though the applied coatings altered the surface properties compared to the initial substrate surface, the coatings had only little (to no) influence on the bulk properties of the PCU. Nonetheless, on the surface of the coated material, the coatings can locally dominate the behavior of the material.
Here, the chemical coupling employed for the coatings would limit the mobility of the polymer chains at the surface of the PCU. Considering the charges introduced to the surface by the coatings, electrostatic repulsion forces may contribute, too. Additionally, the effective glass transition temperature at the interface might be influenced by a comparably high T_g approximated for the dextrans (with values clearly above the testing temperature of 28 °C employed for the tribological examinations). Thus, compared to the bare PCU surfaces, little interdiffusion between the applied dextran layers would be expected.
When uncoated PCU foils are immersed into an aqueous medium, all the above-described, autohesion-promoting effects still apply; in addition, hydrophobic interactions may now contribute as well.[29,230] Here, the hydrophilizing nature of the coatings should mitigate such hydrophobic effects.

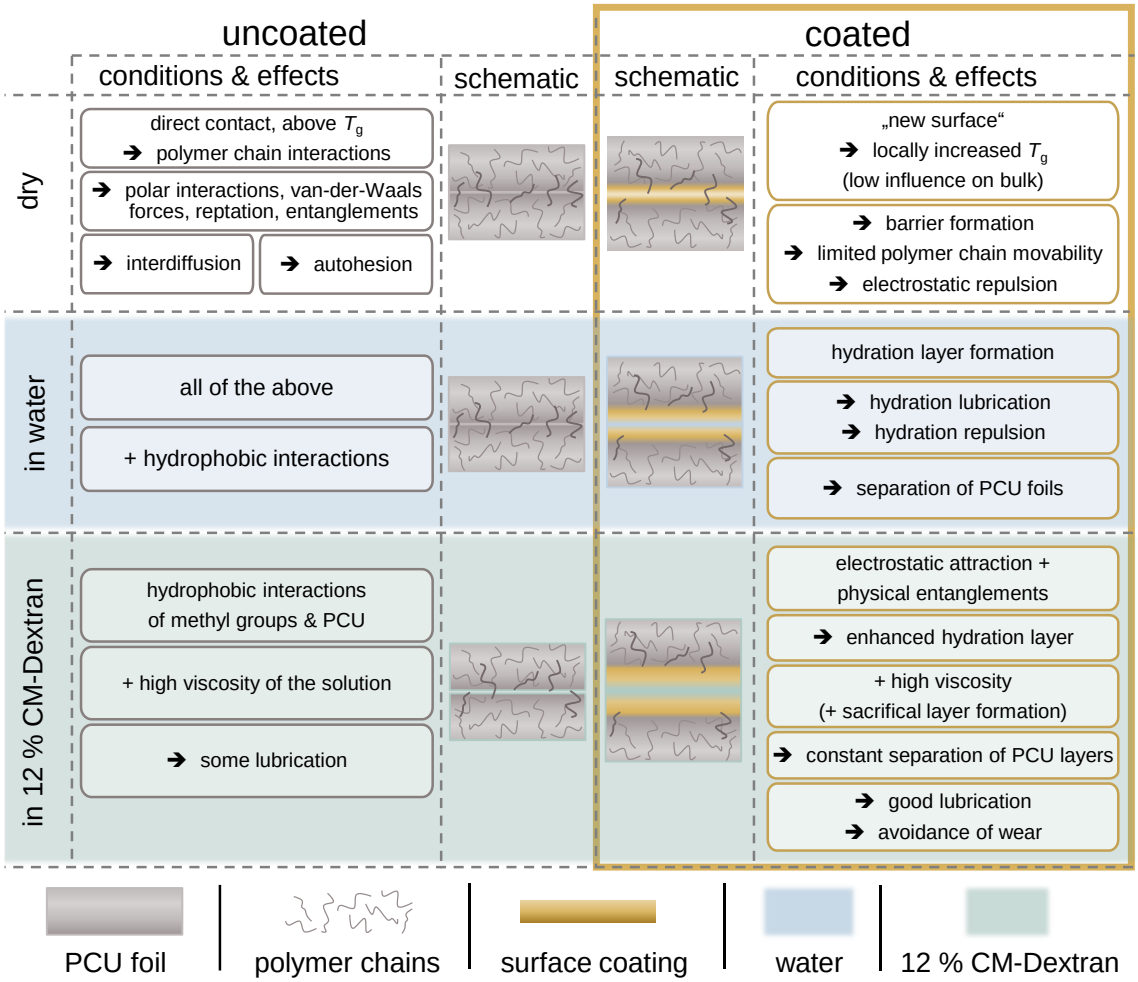

Figure 5.3: *Possible conditions and effects influencing the behavior of PCU foils:* overview of different conditions and effects that may influence the autohesive properties and tribological behaviour of (un-)coated PCU foils in dry or aqueous eviroments or when surrounded by a macromolecular solution. The schematics are not to scale.

Furthermore, the hydrophilic coatings lead to the formation of a hydration layer on the sample surface, which helps to keep the PCU layers separated owing to hydration repulsion[165,167,170] and enables hydration lubrication.[36,41,161,231]
In case the uncoated samples are submerged into 12 % CM-Dex, *i.e.*, a macromolecular lubricant solution, the hydrophobic methyl groups available on the dextrans should (at least to some degree) allow for hydrophobic interactions between the dextran macromolecules and the hydrophobic surface of the uncoated material. In combination with the high viscosity of the dextran solution, this should be beneficial for lubrication. For coated samples, electrostatic attractions between the charged functional groups of the surface-bound macromolecules and the anionic CM-Dex macromolecules in solution as well as physical entanglements between both polymers could improve (the density and thickness of) the hydration layer. Additionally, those interactions between both dextran types could enable the formation of a sacrificial layer. [36,75,178] Consequently, efficient separation of both PCU foils should be achieved, which would enable good lubrication and avoidance of wear.

However, to be employed in biomedical applications, such surface coatings must maintain their functionalities even after exposure to sterilization procedures. Consequently, the

influences of sterilization methods on carbo-mucin coated polymeric medical devices and on carbo-LDex or dopa-QDex coated PCU foils were assessed in Rickert et al 2021[80] and Bauer et al. 2023[79], respectively.

Both assessed functionalities for sterilized carbo-mucin coated medical devices, *i.e.*, lubrication and anti-adhesive properties, are typically attributed to the glycosylated central region of the mucins.[36,39–41,55,87,194] The glycosylation was found to be less affected by most of the examined sterilization methods than the non-glycosylated termini. This was attributed to the accessible protein-backbone at the termini, which, as characteristic for most proteins, contains hierarchically folded structures.[232,233] However, since secondary and tertiary protein structures are mainly induced by transient interactions, they are frequently denatured by aggressive treatments.[234–236] In contrast, the glycosylated part of the mucins lacks such a hierarchical structure; thus, it cannot be denatured but the intramolecular covalent bonds must be cleaved to affect the polypeptide backbone of the glycans: Consequently, this section is more resilient. Nonetheless, especially a treatment with γ-irradiation or autoclavation affected the glycosylation to some degree - putatively by radical attack and thermal hydrolysis, respectively.[237–239] A consequence of this sterilization-induced damage was clearly observed for the anti-adhesive properties of the respective sterilized samples. In contrast, none of the sterilization procedures had any effect on the lubrication behavior. Indeed, this was in line with previously reported findings, which demonstrated that, even though the glycosylation is essential for the lubrication properties of mucins, specific glycan side chains can be removed without influencing the friction response.[36]

Accordingly, the glucose-based dextrans were also expected to be considerably resilient towards the examined sterilization methods. This was the case for the carbo-LDex coated samples, which maintained their functionality especially after treatment with ethylene oxide; however, they were somewhat affected by a treatment with γ-irradiation just like the carbo-mucin coated medical devices discussed above. In contrast, the functionality of dopa-QDex coated samples was clearly impaired for either sterilization procedure. This reduced functionality appeared to be mainly due to the prolonged dry storage of the coated samples required to apply the sterilization treatments: already the functionality of the stored reference was clearly reduced for dopa-QDex coated samples. This observation was confirmed not only for prolonged dry storage, but also for hydrated storage of dopa-QDex coated samples independent of the storage temperature. However, rather than a degradation of the applied dextran, a deterioration of the employed coupling is assumed in this case. Whereas, for hydrated storage, especially at a temperature of 30°C, some degradation of the dextrans caused by thermal hydrolysis would be conceivable, such dry storage should actually be favorable for the structural integrity of the dextrans. Indeed, dry and dark storage is recommended by the manufacturer of the dextrans and a shelf life of at least three years is suggested.[91,92]

To avoid microbial contaminations the coated samples were exposed to UV irradiation and 80 % ethanol. Afterwards, the samples were placed into fresh and clean containers for dehydration and subsequent airtight storage amid light. As shown in Bauer et al 2023[79], the coated samples remained functional after this pretreatment. Thus, influences of microbial attacks or of the pretreatment should have been considerably little. Consequently, it is assumed that the observed, impaired functionality must have been caused by detachments

of either the dextrans from the dopamine layer, of the dopamine layer from the PCU substrate, or by a combination of both.
It is assumed that the detachments predominantly originated between the Q-dextrans and the dopamine layer as, here, mainly transient interactions are expected. Indeed, hydrogen bonds have been suggested as the dominant interaction mode between dextrans and dopamine.[240] Additionally, these interactions are expected to be supported by electrostatic attraction between the cationic quaternary ammonium group and anionic, deprotonated catechol groups available in the dopamine layer.[241] In contrast, interactions between the dopamine layer and the PCU might involve interactions of the aromatic structures (e.g., hydrophobic interactions or π-π stacking)[242], interactions with the highly reactive carbonyl compounds[243] available in the urethane groups as well as in the carbonate groups (e.g., Schiff base reactions with the amine group of dopamine), or interactions with the secondary amine of the urethane groups. Moreover, there might be additional interactions with functional motifs found in the PCU backbone; however, as the exact structure of the polymer of which the PCU material is constituted, is unknown, these interactions cannot be identified.
The assumption that mainly the dextrans detached was further underscored by the low effective run times as well es high friction responses observed for stored dopa-QDex coated samples. As this lubrication behavior was even worse than that obtained on uncoated PCU, it points towards an impairment of the lubrication and relative movement by the adhesive attraction between the dopamine layers on both foils. Such a negative influence on the friction response of a dopamine layer applied to a polyurethane material was also observed in the tribological assessments presented in Bauer et al 2021[77]. Additionally, for the samples stored hydrated at 30°C, the initial impairment of the lubrication performance was followed by an improvement of the lubrication performance for even longer storage periods. This might indicate a sequential detachment: first, the dextrans were removed, subsequently, the dopamine layer was disintegrated. For the second step, thermal hydrolysis putatively contributed. Additionally, effects associated with the detachment of dopamine agglomerates and hydrophobic recovery (as discussed above for a deposited dopamine layer only) might have affected parts of the dopamine layer.
Lastly, it is suggested that the required rehydration of the stored samples participated in the disintegration of the coating. Here, the instantaneous exposure to an abundancy of aqueous medium might have triggered highly dynamic dissolution and flushing effects affecting only weakly bound or entangled dextrans (and potentially also dopamine molecules). However, the probability of reattachment, though feasible, is expected to be low, as the degree of dissolution was high. Such dissolution and flushing effects, especially of entangled dextrans, might also have been the origin of the adverse effects of dry storage on carbo-LDex coated PCU. Additionally, even though restrained by the application of the coating, hydrophobic recovery might have occurred locally for extended periods of storage.
Overall, the importance of an appropriate selection of the coating strategy and a top-layer molecule for a specific material to establish an efficient and functional surface modification was demonstrated. Furthermore, especially regarding potential applications, the resilience of the applied surface modification must be considered to ensure a successful employment of the developed compound material.

6 Conclusions & Outlook

In this thesis, it was shown that it is necessary to carefully select a suitable combination of substrate material, coupling strategy, and functionalizing molecules to successfully adjust the adhesive properties of the established compound specifically to the requirements of the envisioned application. To be able to control the resulting adhesive properties of a construct during its development, it is required to understand and consider the diverse and complex potential interaction modes of the employed materials on a macroscopic, microscopic as well as molecular scale. Here, the behavior of polymeric materials can be especially complex: in addition to the factors commonly associated with the adhesive behavior between two phases, *i.e.,* the feasible interaction modes enabled by primary and secondary bonds, the wettability dictated by the surface energies of both phases, and the surface roughness influencing the available contact area, factors resulting from the polymer chain mobility must be considered, too. Such factors include polymer chain rotations, reptations, and entanglements. Here, the interactions and adhesive behaviors of various synthetic and natural polymers were assessed and the influences of surface modifications, mainly established by incorporating functional biopolymers into the surfaces of synthetic polymer materials, were evaluated. The gained understanding of the putative interaction mechanisms can help to broaden the knowledge about polymer-polymer interactions - especially for such material compounds, which are established by more than one type of polymer.
In this thesis, it was discussed how a constructs with (anti-)adhesive properties on either side (as presented by Kimna et al. 2022[76]) can be established. Moreover, it was shown that the controlled combination of such contrary adhesive properties is not only feasible but often required to achieve the desired final behavior. To establish the above-mentioned construct, in addition to introducing the desired functionalities to either side, it was necessary to achieve sufficient interaction between the strongly adhesive side and the anti-adhesive side. Furthermore, for a surface modification of the discussed elastomeric materials, it was required to overcome their chemically unreactive behavior (as strong interactions with a coupling agent were desired) and to limit the autohesive behavior of the materials, which is mainly enabled by physical polymer chain interactions. The coupling agent was further required to establish good interactions with the functionalizing polymers to eventually achieve anti-autohesive properties. However, to promote good lubrication behavior of the functionalized compound, the applied polymers intended to limit interactions between two functionalized surfaces had to interact with the macromolecules introduced by the employed lubricant. Such good lubrication performance of elastomeric materials is required for a thin and compliant implant as envisioned by the APRICOT project (already addressed in the introduction). To achieve the desired re-establishment of smooth, natural movability of the treated joint, not only low friction responses are of interest, more importantly enabling reliable, uninterrupted movement is essential. Furthermore, the avoidance of wear is substantial to the integrated lubrication system of the APRICOT implant; here, abraded residues cannot be removed, and thus would potentially interfere with the friction response and mode of movement of the implant. Moreover, extensive wear could lead to a rupture of the thin structure of the APRICOT implant. Similarly, a failure of the implant could also be induced by a restrained flexibility of the surface modified material. All these aspects relevant for the successful employment of the APRICOT implant can be targeted by the

application of a suitable surface modification to control the surface interactions in the desired manner.

Accordingly, in this thesis, the impacts of surface modifications, employing different coupling strategies, and applying various biopolymers to establish the top-layer, on the properties associated with the adhesive behavior of elastomeric materials were discussed. In detail, the influences of different surface activation strategies on elastomeric materials, as reported in Bauer et. al 2021[77] and Bauer and Lieleg 2023[78] were assessed. Furthermore, the effects enabling the desired alterations of the surface properties while, at the same time, avoiding undesired influences on the bulk of the substrate material were elucidated. Additionally, the mechanisms and interactions introduced by the applied surface functionalizations, which limit the autohesive behavior of an elastomeric material and enable good lubrication behavior with a macromolecular lubricant (as reported in Bauer et al. 2023[79]) were discussed. Moreover, differences in the resilience and the durability of the established couplings and attached top-layer molecules, as reported in Rickert et al 2021[80] and Bauer et al. 2023[79], were described.

Overall, it could be shown that dopamine-based coatings and carbodiimide-mediated coatings are suitable to attach various biopolymers onto the surfaces of elastomeric PDMS- and PU-based materials. Regardless of the applied top-layer molecules, the dopa-coatings performed particularly well in terms of enhancing wettability and enabling short-term lubrication. However, they were somewhat outperformed by the carbo-coatings regarding the reduction of the autohesive properties, the reliability of enabling lubrication in long-term assessments, the avoidance of wear, and the durability of the coatings. Consequently, whereas the facile dopa-coatings are a decent option to rapidly establish a surface modification intended for prompt and short usage, the carbo-coatings should be preferred if resilience and reliability are required. Furthermore, it was confirmed that dextran coatings are overall suitable to mimic the anti-adhesive and lubricating properties of the mucin-coatings. The attachment of either biopolymer led to similarly enhanced wettability and to similarly decreased friction responses. For the latter, the QDex coatings performed especially well. Additionally, the LDex coatings achieved a reduction of the autohesive properties, avoidance of wear, and resilience against certain sterilization procedures similar to the mucin-coatings. Thus, several combinations of coating strategy, attached top-layer molecule, and macromolecular lubricant suitable for e.g., the integrated lubrication system envisioned in the APRICOT implant, were discussed. To identify the coating/lubricant combination most favorable for the APRICOT implant, further examinations would be required. Here, the transferability of the coating process onto a 3D-structure would be required to ensure the manufacturability of the implant. Furthermore, comparing the lubrication performance of the different coatings/lubricants incorporated in a prototype of the implant would be interesting and could reveal unpredicted interferences. Eventually, the biocompatibility of the APRICOT implant would need to be assessed, to be able to apply for a medical device permission.

Also, in Kimna et al 2022[76] and in Rickert et al 2021[80], the developed materials were intended as medical devices. Both had an advanced level of development and, as both employed lab-purified mucins (as already addressed in the introduction), it must be considered that the effort to obtain fully functional mucins with reproducible purification quality is high. However, an improved purification process with higher yields was introduced recently.[65] This filtration-based process should be more easily scalable, which would increase

the feasible throughput and, putatively, reduce the batch variability. Furthermore, the *in vitro* and *in vivo* examinations included in Kimna et al 2022[76] reported good biocompatibility of the bilayer patch, and thus of the incorporated lab-purified mucins. These promising developments regarding the mucin purification process and biocompatibility could enable the establishment of an industrial-scale production line and a detailed clinical evaluation (which is an essential part to obtain a medical device approval in the EU), respectively.

Furthermore, the manufacturing process of the bilayer patch and the mucin coated medical devices could be optimized. Here, the patch could be adjusted to suit the requirements of specific wound healing applications, such as an application onto aphtha in the oral cavity or as suture replacements to close surgical cuts. Not only different shapes and dimensions would be required for such applications, but they would also expose the patches to specific challenges. Conceivable required alterations could be an enhanced adhesive behavior, preservation of the adhesiveness in acidic environments, or further mechanical reinforcement. To enable stronger adhesion, the incorporation of a higher amount of dopamine might be suitable; and this could be achieved by improving the coupling efficiency during the production of d-HA. The exposure to acidic environments appears especially challenging as an impairment of the adhesive properties of dopamine molecules was reported for acidic environments.[51,108,244] Such an exposure could occur, for example, in the oral cavity if acidic drinks (such as many sodas or juices) are ingested. Dissolving d-HA in a suitable buffer (instead of pure water) during the manufacturing of the d-HA layer might enable a local regulation of a surrounding acidic solution; then, a neutral pH milieu could be maintained for the contact area of the patch. A mechanical reinforcement of the patch might be achievable by applying a thicker PVA/MUC layer (which is subsequently crosslinked) or by establishing a more densely crosslinked PVA/MUC layer. The latter could be accomplished by alternatingly applying a PVA/MUC layer and the GTA crosslinking step several times.

For the mucin-coated medical devices, the attached number of mucins could, putatively, be optimized. Therefore, it would be necessary to identify the mucin density required on the device surfaces to maintain the desired lubricating and anti-adhesive properties. Consequently, the concentration of the mucin solution employed during the coating process could be adjusted. Furthermore, the coating process could also be altered by e.g., employing the more facile dopamine-based coating strategy. Such an approach was recently presented by Miller Naranjo et al. 2023[187] for endotracheal tubes: there, replacing the carbo-mucin coating with a dopa-mucin coating performed comparable, especially lubrication-wise.

Based on the anti-autohesive effects of carbo-dextran coatings observed in the macroscopic lap shear and detachment examinations, it would be very interesting to test the adhesive behavior of such coatings on a microscopic scale, e.g., in incubation tests with proteins, or with eukaryotic or prokaryotic cells (similar to the tests presented in Kimna et al 2023[76]). In contrast to the mucin coatings, the lysine modification of the dextrans, would be expected to promote the attachment of eukaryotic cells: a (poly-)lysine pretreatment is often applied for cell culture containers to facilitate the attachment of cells. However, antibacterial properties of (poly-)lysine motifs have been reported.[245–247] Such a combination of behaviors could be particularly beneficial for permanent implants, for which a eukaryotic cell attachment and ingrowth would be desired to e.g., lock the implant in position. However, for an effective anti-adhesive behavior of a hydrophilic coating, it must form a particularly

dense and sufficiently thick hydration layer to efficiently avoid adsorption of any biofouling-associated polymers and cells; here, even the attachment of individual polymers onto the surface could serve as a hook for the attachment of further bio-fouling entities. Thus, it might be required to increase the thickness and density of the applied L-Dex layer to achieve the desired anti-adhesive properties. On the one hand, this could be achieved my attaching dextrans with a higher molecular weight; on the other hand, the establishment of a multi-layer system should be feasible by a layer-by-layer approach (employing the same carbodiimide chemistry as used to create the monolayer coating). Owing to the primary amine and carboxy-groups available on LDex, this would be feasible without introducing any additional crosslinkers. Here, the layers could be established of always the same L-Dex variant or by combining L-Dex variants with different molecular weights. Indeed, for similar approaches employing dopamine-assisted multilayer deposition, influences on structural and functional properties of the surface coatings were reported recently.[107,248,249] Here, even for a combination of dopamine deposition with layers of poly-lysine (for both components, cell attracting properties were reported [88,249,250]), a reduction in cell attachment was observed if at least two layers each were applied.

For the dopa-coatings, the second main difference (in addition to the adhesive behavior) compared to carbo-coating was their lack of durability. To prolong this durability, the incubation in the dopamine solution could be prolonged to achieve a denser dopamine layer; however, this would putatively come at the expense of transparency. Alternatively, the substrate and/or top-layer molecules could be changed into variants with, *e.g.,* primary amine and/or thiol groups. Then, the formation of covalent bonds with the dopamine layer would be feasible. Whereas this might be comparably facile for the employed top-layer molecules (as biopolymers frequently contain the respective functional groups), for the substrate material, this would be not so trivial, at least not without requiring an additional modification step. Alternatively, an initial plasma activation of the substrate material could enhance the interactions with the dopamine layer - in particular for silicone containing materials, as the formation of silyl ester bonds should be enabled here. However, the reversibility of the dopa-coatings can also be an advantage. For example, a membrane employed in wastewater treatment could be dopamine coated to efficiently bind the residues; then, a subsequent exposure to an acidic solution would detach the dopamine coating and the residues. Thus, the cleaned membrane could be reused.

Furthermore, tracing the effective runtime in addition to the CoF, as introduced in Bauer et al. 2023[79], allowed for comparing the friction response in a manner that was very sensitive to any lubrication impairing effects, even for very similar coating/lubricant combinations. Such evaluations might also be useful for other lubrication promoting systems. For example, the influence of varying the number of coating layers and/or the MW of the employed macromolecules on the tribological behavior could be assessed. Furthermore, it would be interesting to perform measurements, for which no difference could be detected in the rotational tribology setup, e.g., with the carbo-mucin coated and sterilized samples, examined in Rickert et al. 2021[80]. To facilitate the data interpretation and to avoid the (so far necessary) parallel evaluation of the CoF and the eRT, a new coefficient could prove useful. Here, a coefficient evaluating friction over runtime (FoRT-coefficient) defined as:

$$FoRT \equiv \frac{CoF}{eRT/_{maxRT}} \qquad \textit{Equation 6.1}$$

would be possible. This coefficient would be equivalent to the *CoF* as long as the predefined full runtime (*maxRT*) was achieved. The *FoRT* coefficient would return higher values for either high *CoFs* or low *eRTs*, *i.e.,* for bad lubrication behavior. Furthermore, by the normalization to the predefined *maxRT*, a comparison between data sets collected for different full runtimes would be enabled. This coefficient could not only support the identification of the minimal required number of applied layers or of the minimal density of a coating but could as well help to assess and to compare the functionality of tribological systems after the exposure to mechanical, thermal, temporal, or chemical challenges. Overall, this could improve the optimization of surfaces towards the multi-faceted problem, which they face in (bio-)tribological applications.

A Appendix

A.1 Supporting Information

A.1.1 Viscosities of Different Macromolecular Lubricants

Rheological measurements were conducted on a commercial shear rheometer (MCR 102, Anton Paar, Graz, Austria) using a plate/plate measuring setup (PP25, Anton Paar). For each measurement, a sample volume of 220 µL was required. The designated macromolecule was dissolved in PBS (pH 7.4). The viscosities of the different lubricants were determined for shear rates between $\dot{\gamma} = 1\ s^{-1}$ and $\dot{\gamma} = 1000\ s^{-1}$ at 28 °C. A solvent trap was installed to avoid dehydration of the samples during the measurement.

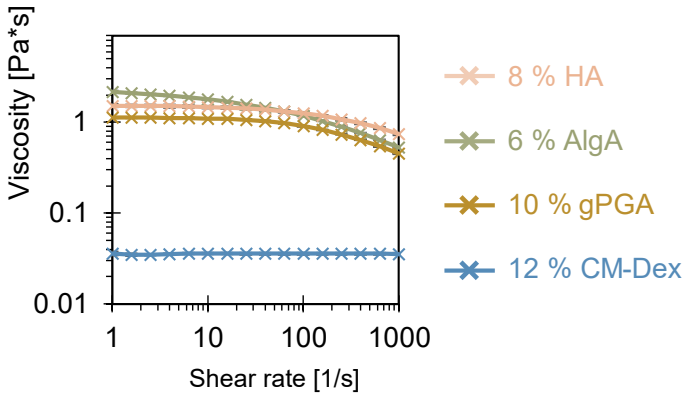

Figure A1.1: *Viscosities of different macromolecular lubricants:* Viscosities determined for solutions contiang 8% hyaluronic acid (beige), 6% alginic acid (green), 10% γ-polyglutamic acid (yellow), or 12% carboxymehtyl-dextran.

A.1.2 Linear Tribology Examinations on Carbo-Mucin Coated PCU

The linear tribology measurements were conducted exactly as described in detail in Bauer et al. 2023[79]. However, here carbo-mucin coated PCU samples were employed and lubricated with an aqueous solution containing 3% (w/v) polyethylene oxide (PEO) with a MW of 1MDa, as PEO has previously been identified as a suitable lubricant for coatings comprising the polyanionic mucins[75]

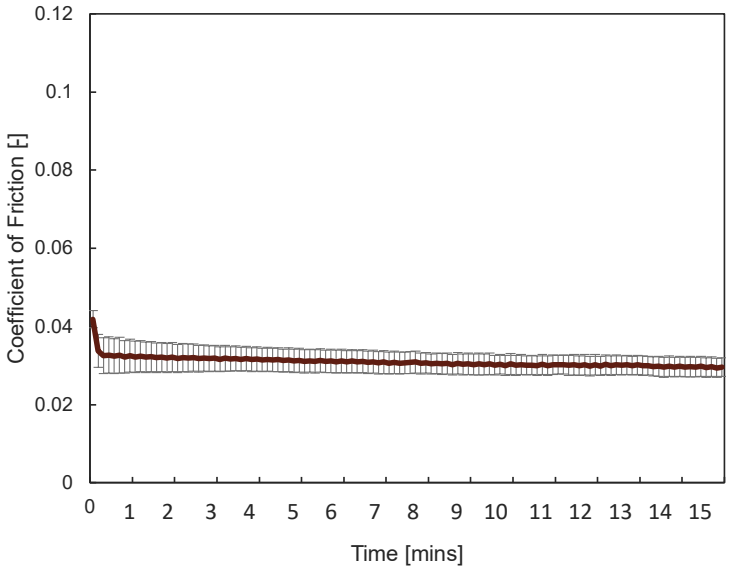

Figure A.1.2: *Linear tribology examinations on carbo-mucin coated PCU:* Foil-on-foil tribology was conducted with carbo-mucin coated PCU foils lubricated with 3% polyethylene oxide.

A.2 Full Texts of the Presented Publications

A.2.1 "Multifunctional "Janus-Type" Bilayer Films Combine Broad-Range Tissue Adhesion with Guided Drug Release"

A.2.1.1 Full Research Article

RESEARCH ARTICLE

ADVANCED FUNCTIONAL MATERIALS
www.afm-journal.de

Multifunctional "Janus-Type" Bilayer Films Combine Broad-Range Tissue Adhesion with Guided Drug Release

*Ceren Kimna, Maria G. Bauer, Theresa M. Lutz, Salma Mansi, Enes Akyuz, Zuleyha Doganyigit, Percin Karakol, Petra Mela, and Oliver Lieleg**

Tissue healing is a challenging process that requires the successful and simultaneous management of conflicting priorities. While promoting wound closure, a battle must be won against different external factors that may adversely affect the healing process. Here this problem is approached by creating asymmetrically designed double-layer Janus-type bilayer films where distinct functions are implemented into the two sides of the film. Once deployed, those Janus-type films exhibit strong adhesion to a wide variety of wet tissues and canalize the release of integrated therapeutics toward the tissue side. At the same time, the outer surface of the films acts as a shield against tribological stress, pathogens, and cellular immune recognition. Moreover, when compared to untreated wounds, Janus-treated skin lesions show accelerated wound closure as well as fast formation of new, intact tissue. Having performed their tasks, Janus-type films degrade without leaving any traces on the tissues, which makes it possible to apply them to sensitive body surfaces. Thus, it is expected that the Janus-type bilayer films designed here can be used in a variety of medical applications where conflicting demands must be met at the same time.

1. Introduction

There are several examples where nature has found a way to combine apparently contradicting properties into the same material to achieve a specific function. For instance, the desert beetle *Stenocara gracilipes* employs a combination of both, hydrophilic and superhydrophobic areas on its head to efficiently collect water.[1] Similar to biological examples, also many problems in materials science benefit from the possibility to combine orthogonal properties into one and the same object. Macroscopically, this can be achieved relatively easily: for instance, the two opposing surfaces of a table tennis racket are designed to interact differently with the ball, e.g., to accelerate or slow down its motion. Microscopically, this is more difficult even though there are biomolecules such as lipids that combine antagonistic properties such as hydrophilic and hydrophobic regions. Nevertheless, the development of Janus-like objects was successful for selected applications such as separation processes, catalysis, electronic displays, and electrical/magnetic actuators.[2–4] Yet, in other areas, such as the management of wet tissue wounds, the simultaneous accomplishment of conflicting tasks remains a tremendous challenge: here, strong adhesion to the (wet) point-of-care is required while uncontrolled adhesion to neighboring tissues needs to be prevented.[5] These conflicting tasks are especially critical when wet-adhesive materials are applied to sensitive areas such as buccal, ocular, or intraintestinal tissue.

C. Kimna, M. G. Bauer, T. M. Lutz, O. Lieleg
School of Engineering and Design
Department of Materials Engineering
Technical University of Munich
Boltzmannstraße 15, 85748 Garching, Germany
E-mail: oliver.lieleg@tum.de
C. Kimna, M. G. Bauer, T. M. Lutz, O. Lieleg
Center for Protein Assemblies (CPA)
Technical University of Munich
Ernst-Otto-Fischer Straße 8, 85748 Garching, Germany

The ORCID identification number(s) for the author(s) of this article can be found under https://doi.org/10.1002/adfm.202105721.

DOI: 10.1002/adfm.202105721

S. Mansi, P. Mela
Medical Materials and Implants
Department of Mechanical Engineering and Munich Institute of Biomedical Engineering
TUM School of Engineering and Design
Technical University of Munich
Boltzmannstr. 15, 85748 Garching, Germany
E. Akyuz
Faculty of Medicine
Department of Biophysics
University of Health Sciences
Istanbul 34668, Turkey
Z. Doganyigit
Faculty of Medicine
Department of Histology and Embryology
Yozgat Bozok University
Yozgat 66900, Turkey
P. Karakol
Sisli Hamidiye Etfal Research and Training Hospital
Department of Plastic Reconstructive and Aesthetic Surgery
University of Healthy Sciences
Istanbul 34371, Turkey

ADVANCED SCIENCE NEWS
www.advancedsciencenews.com

ADVANCED FUNCTIONAL MATERIALS
www.afm-journal.de

In the field of wound management, asymmetric functionality often goes beyond macromechanical aspects: although good microscopic interaction of a material with proteins is required for good tissue adhesion, this property is undesired on the other side facing away from the tissue: there, protein-based conditioning films often trigger cellular biofouling events and can provoke unfavorable immune responses.[6] Similarly, drug transport from the therapeutic material to the wound site is required to promote the healing process; however, the diffusive liberation of drugs into surrounding body fluids (e.g., blood, mucus, and interstitial fluids) would strongly reduce the efficiency of the treatment and could cause unwanted side effects.

To date, many different adhesive formulations—mostly in the form of hydrogels—have been introduced to achieve better mechanical properties than those provided by commercial adhesives used in clinical applications.[7–12] To tackle the problems associated with using surgical sutures (e.g., requiring expert skills and a suture removal appointment), very promising materials with strong adhesion properties were developed in the last years. Recent examples include a polyethylenimine-poly(acrylic acid) powder for closing gastrointestinal perforations,[13] poly(vinyl alcohol)–dihydroxyphenylalanine (DOPA) films for the delivery of drugs to wet buccal tissue,[14] and macroporous carboxymethyl/agarose hydrogels for the delivery of Ag^+ ions.[15] These materials all exhibit strong tissue adhesion in combination with promising biological performance. Furthermore, materials for wet tissue adhesion can be equipped with important additional features such as controlled cell engraftment,[16,17] self-healing,[18,19] and hemorrhage control.[20,21] However, one clinical problem that remains is the postsurgical adhesion of such materials to other, undesired tissue areas.

To cope with this problem, medical materials with asymmetric functionalities were recently introduced, and they were indeed successful in promoting tissue repair in vivo.[22–25] For example, Cui et al.[22] presented a Janus structure with oppositely charged surfaces, which enables the overall material to seal tissue perforations and—at the same time—prevents undesired adhesions to its exterior part. Very recently, a three-layered Janus adhesive with asymmetric wetting properties developed by Xu et al.[23] was found to be successful in keeping the wound area dry while absorbing the wound exudate. Other very recent and highly promising examples from this area are peritoneum-inspired porous poly(vinyl alcohol) (PVA) hydrogels for canalizing cellular growth at the desired site,[26] and double-layered (ionically and covalently cross-linked) alginate/chitosan films for advanced tendon healing.[25] These asymmetric materials provide a set of distinct functions for the wound-healthy tissue interface. However, these materials exhibit a long lifetime, which limits their use to specific applications that are strictly controlled under medical care. Thus, multifunctional "all-in-one" solutions that synergistically manage different, and—indeed—often somewhat conflicting tasks, that are easy to use and rapidly make way for new, healed tissue by decomposing autonomously are scarce.

Here, we present asymmetrically designed Janus-type bilayer films to address all the problems listed above simultaneously. These bilayer films were engineered such that they provide distinct functionalities on their opposing surfaces to fulfill multiple tasks relevant for the treatment of epithelial wounds (Figure 1a). The bilayer material combines a sticky, hydrogel-forming bottom layer based on dopamine-conjugated hyaluronic acid with a lubricating, nonadhesive top layer based on mucin glycoproteins. Materials comprising multifunctional mucins were introduced earlier, e.g., as anti-biofouling coatings, smart drug delivery materials, selective filters, and lubricating agents.[27] In our Janus-type bilayer films, the mucin-containing surface can protect the wet wound tissue of interest from biological and mechanical challenges such as nonspecific protein adsorption, bacterial colonization, and undesired tissue adhesions. The sticky layer, on the other hand, provides strong adhesion to various types of tissues (e.g., eye, tongue, intestine, and cartilage) and releases incorporated therapeutics into the desired direction only. Overall, they are easy to handle and can be effortlessly applied onto complex surfaces without requiring a supporting material for fixation. Furthermore, the Janus-type films readily adhere to wounds and accelerate the tissue regeneration process in vivo without causing any unwanted reactions. Finally, when their tasks are completed, the Janus-type bilayer films decompose on the applied surface and neither leave any traces nor induce alterations on the tissue microtopography. Thus, they do not require any professional (removal) step.

2. Results and Discussion

We here develop a hybrid material based on two layers with distinct functionalities: the bottom layer comprises dopamine conjugated hyaluronic acid (d-HA) biopolymers. This modified biomacromolecule was selected for two reasons: first, hyaluronic acid (HA) is known to condition intracellular signals responsible for cell proliferation and migration thus promoting wound healing;[28] second, catechol-type molecules can engage in unspecific, noncovalent interactions that enable adhesion to a broad range of materials including wet tissues.[29,30] Here, the successful conjugation of HA with dopamine is verified spectroscopically (Figure 1b), and the conjugation efficiency is calculated as 27%.

To ensure that adhesive properties are only present on one side of the film, the d-HA layer is coated with a nonadhesive polymer mesh. As a coating material, we select a PVA/mucin mixture which is electrospun onto the adhesive d-HA layer (Figure 1c,d). This mixture is chosen since PVA can be easily processed into fibers, thus serving as a structural reinforcement. Mucin glycoproteins are incorporated since mucin coatings have been shown to suppress biofouling events.[31] In fact, mucin-rich biomass obtained from different sources such as jellyfish and snails have been previously included in polymer mixtures to fabricate wound dressing materials.[32,33] Here, we purify porcine gastric mucins to obtain a well-defined macromolecular component for our bilayer film to harness the rich chemistry of mucins[34] as well as their important biological features such as prokaryotic and eukaryotic cell repellence[31,35,36] and immunomodulation ability.[37] In detail, when integrated into a nanofibrous network, we expect the mucins to establish two beneficial effects: first, due to the bacteria-repellent properties of mucins, their presence should protect epithelial cells covered with the bilayer film from infection; second, they can

ADVANCED SCIENCE NEWS
www.advancedsciencenews.com

ADVANCED FUNCTIONAL MATERIALS
www.afm-journal.de

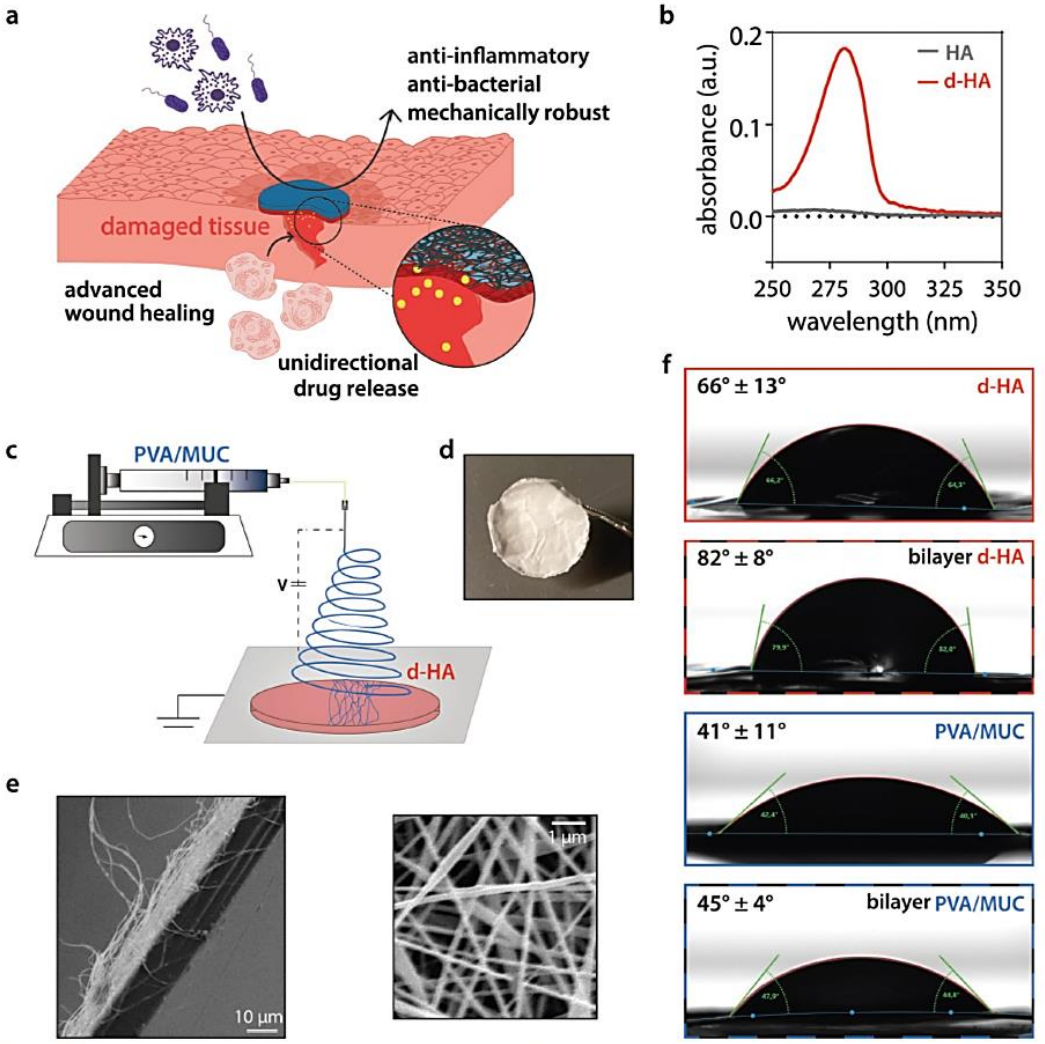

Figure 1. Production process and morphology of Janus-type bilayer films. a) Schematic representation of the multifunctional properties of the Janus-type bilayer films. b) Absorbance spectra of HA and -HA, respectively. The peak at 280 nm indicates successful catechol functionalization of HA as expected for d-HA. c) Schematic representation of the bilayer film formation procedure. d) Photograph of the top side of the bilayer film. e) A cross-sectional SEM image of the bilayer film (left) visualizes the nanofibers covering the top surface (right). f) Wettability of monolayers and each surface of the bilayer film. The value at the upper left corner of each photograph represents the contact angle calculated from $n = 10$ independent samples.

help avoiding inflammatory reactions.[37] The fibers located in the top-layer of this two-component film have a random orientation and create a network with sub-micrometer mesh sizes in the range of (480 ± 200) nm (Figure 1e; Figure S1, Supporting Information). Furthermore, a quantitative analysis of the surface roughness of the film demonstrates a homogeneous topography devoid of irregular bead formation (Figure S1, Supporting Information).

Another advantage brought about by the bilayer structure of the film is an improvement in mechanical properties. A film fabricated from d-HA alone exhibits a rather low stretching resistance (≈2-fold lower rupture forces compared to the bilayer film, Figure 2a,b) and weak overall integrity: the ensuing hydration of the biopolymer layer triggers rapid swelling, which turns this d-HA layer into a viscoelastic gel (Figure S2, Supporting Information). This can complicate the applicability of

ADVANCED SCIENCE NEWS
www.advancedsciencenews.com

ADVANCED FUNCTIONAL MATERIALS
www.afm-journal.de

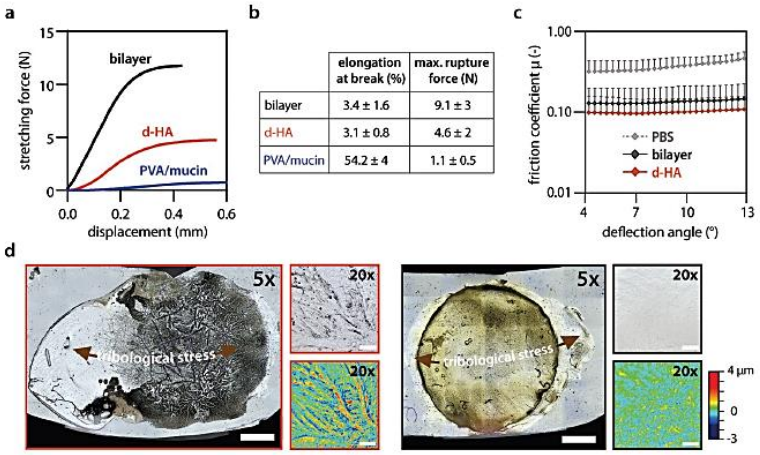

	elongation at break (%)	max. rupture force (N)
bilayer	3.4 ± 1.6	9.1 ± 3
d-HA	3.1 ± 0.8	4.6 ± 2
PVA/mucin	54.2 ± 4	1.1 ± 0.5

Figure 2. Mechanical properties of bilayer films. a) Representative stretching force–displacement curves of monolayer (d-HA and PVA/mucin, respectively) and bilayer films and b) the corresponding mechanical properties. c) Friction response and d) morphology of d-HA monolayers (left) and bilayer films (right) upon exposure to tribological stress. Images in gray scales represent combined laser confocal/light microscopy pictures; colored images represent topographical images (the color code on the right applies to both). Scale bars in 5× images depict 2 mm and scale bars in 20× images depict 0.1 mm. Data shown represent mean values, error bars denote the standard deviation as obtained from $n \geq 3$ independent samples.

the film in a physiological setting. Yet, with the fibrous mucin/PVA layer added and cross-linked to the d-HA layer via glutaraldehyde vapor exposure, this issue is remedied. Furthermore, measurements performed with bilayer samples that contain monolayer extensions at either end showed that the bonding strength between the two layers of the film is higher than the tensile strength of individual monolayers (Figure S7, Supporting Information); thus, the integrity of the bilayer film under mechanical load should be sufficient for the application envisioned here. Similar to the results of the stretching tests, we also find enhanced robustness of the bilayer film toward tribological stress: when probed in an oscillatory tribology setup, both films show good friction behavior with low friction coefficients around $\mu = 0.1$ (Figure 2c). This result was expected as both, HA and mucins, are highly hydrated macromolecules and thus enable hydration lubrication.[38,39] However, when both film variants are optically evaluated after the tribological test, clear differences are detected (Figure 2d): d-HA monolayers are spread out by (43 ± 8)%, whereas the bilayer films keep their circular shape and show only little spreading of (10 ± 8)% (Table S1, Supporting Information). Moreover, topographical images (Figure 2d, small images) indicate that the bilayer films maintain their homogenous surface structure even after tribological treatment; by contrast, d-HA monolayers exhibit wrinkles on their surface which indicates irreversible mechanical deformation. Owing to the added top layer, the film construct becomes sturdier and can be handled very well; it can be manually stretched (e.g., with a tweezer) and conveniently placed onto a complex surface such as a tongue or buccal mucosa (Video S1, Supporting Information) without being damaged.

In its dry state, the bilayer construct behaves as a thin, flexible film; upon contact with a wet surface, the bottom layer becomes a sticky, soft hydrogel. Importantly, we also selected hydrophilic polymers for creating the nonadhesive top layer of the bilayer film.[31,40] Also, the surface of this nonadhesive side has hydrophilic properties; here, we measure contact angles of (41 ± 11)° (Figure 1f). Such a hydrophilic, well-hydrated film is well suited to keep a covered tissue layer moist and to prevent crust formation (e.g., when placed onto wounded tissues). To fulfill its function, the bilayer film should maintain its structural integrity until its main task, i.e., releasing the incorporated drugs while allowing for closure of damaged tissue, is completed. However, the material is not designed to remain on tissues for extended time periods: instead, the sticky, drug-loaded layer is engineered such that it degrades over a finite lifetime to be helpful for achieving the efficient release of its payload. Accordingly, in the next step, we spectrophotometrically determine the degradation profiles of each layer of the bilayer film (**Figure 3**a).

For those degradation tests, we incubate the bilayer film in different physiologically relevant fluids (i.e., phosphate-buffered saline (PBS), simulated tear fluid (STF), human saliva mimetic (HSM), and simulated intestinal fluid (SIF)); those fluids are selected to mimic the different liquid environments the film can encounter when placed onto a wet tissue in the human body. In all those tested conditions, the d-HA layer disintegrates more quickly, i.e., it reaches the maximum of its degradation profile within ≈12 h; by contrast, the mucin/PVA layer reaches its degradation peak after ≈2 days. From an application point of view, this delayed degradation behavior of the fibrous layer is very helpful: its presence protects the drug-loaded, sticky layer from undesired mechanical challenges and facilitates a controlled removal of the film once its task is completed. It is noteworthy to mention that, since the material developed here is mainly composed of biological polymers, their degradation products can be expected to be nontoxic. Additionally, it was shown that, owing to its high flexibility, PVA can be excreted through the

ADVANCED SCIENCE NEWS
www.advancedsciencenews.com

ADVANCED FUNCTIONAL MATERIALS
www.afm-journal.de

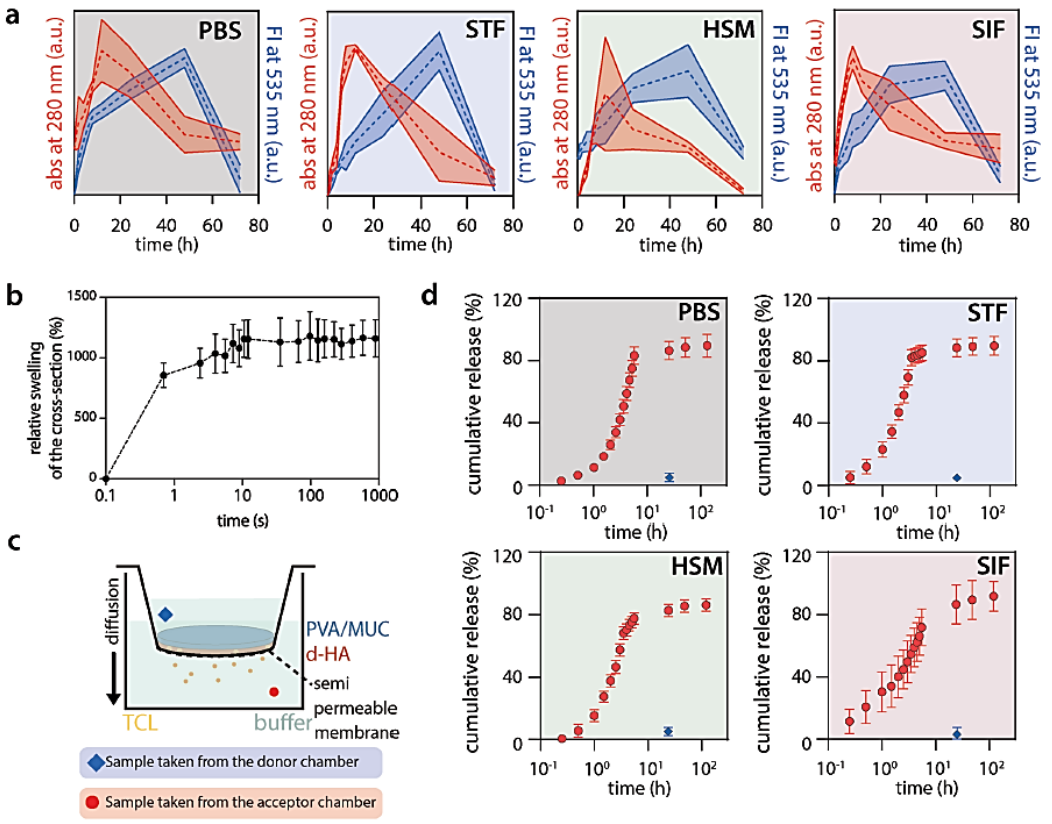

Figure 3. Degradation and drug release profiles of bilayer films. a) Degradation profiles of the two individual film layers when placed into physiologically relevant aqueous solutons (i.e., PBS, STF, HSM, and SIF, respectively). Blue and red lines correspond to PVA/mucin and d-HA layers, respectively. b) Relative swelling profile of the cross-section of the bilayer films (n = 7). The error bars denote the standard error of the mean. c) Schematic representation of the experimental setup used for determining in vitro drug release profiles. d) Cumulative drug release from bilayer films immersed in PBS, STF, HSM, and SIF, respectively. Diamond symbols (blue) denote the percentage of drug released into the donor chamber after 24 h. Data shown represents mean values, error zones denote the standard deviation as obtained from n = 5 independent samples.

kidneys without causing any damage to renal glomeruli;[41–44] moreover, PVA does not permanently accumulate in body tissues and it does not cause any toxic effects to cells.[45,46] Thus, the rapid and complete degradation behavior of the bilayer film construct under biological conditions is expected to be non-harmful to the body.

Next, the swelling profile of the bilayer films is determined by measuring the relative increase in their cross-sectional area. As shown in Figure 3b, the bilayer films start to swell rapidly after they get in contact with water. The swelling profile reaches a plateau level at ≈1100% after ≈10 s. This finding agrees very well with the strong hygroscopic nature of hyaluronic acid reported in the literature.[47] The fast and strong swelling behavior we here obtain for the bilayer films can also be beneficial when the material is applied to wounds: here, the film can immediately soak up the wound exudate, which otherwise can promote bacterial infection and thus hamper the wound healing process.[48]

The efficiency of the main task, i.e., guided (= unidirectional), the diffusive release of drugs toward the "tissue" side, is assessed in the next set of experiments. Here, we load the adhesive layer of the film with a model broad-spectrum antibiotic (tetracycline hydrochloride, TCL) and conduct drug release tests (Figure 3c). For all the model fluids the bilayer films are tested with, a highly efficient (>87%) and unidirectional drug liberation toward the attached surface is achieved. In detail, the drug release profiles enter a plateau around ≈6 h, and the release process is completed within 24 h. This result is consistent with the degradation profiles of the drug-containing d-HA layer of the film. Importantly, only a minor portion of the loaded drug (<8%, diamond symbols in Figure 3d) is detected in the upper surface of the bilayer film. Thus, in a potential application, the fibrous surface not only provides mechanical stability but also acts as a gatekeeper during the therapeutic action by preventing a dilution of the incorporated drug molecules. Furthermore,

ADVANCED SCIENCE NEWS
www.advancedsciencenews.com

ADVANCED FUNCTIONAL MATERIALS
www.afm-journal.de

control experiments where the PVA/mucin layer was facing the semipermeable membrane showed that drug leakage to this side was minimal (<2% for the first 6 h), and the cumulative drug release after 3 days of incubation (when film degradation has already started to set in) was (13 ± 8) % only (Figure S3, Supporting Information).

When a wound dressing material is placed onto a damaged tissue, protein adsorption onto the surface of the material can strongly affect its fate: whereas such adsorption of proteins from wound exudates can be beneficial for cellular adhesion (which improves the performance of such dressings[49]), nonspecific protein adsorption may initiate an immune response by activating immune cells.[50] To investigate such unspecific protein–material interactions, we expose both sides of the bilayer film to fluorescently labeled bovine serum albumin (BSA, which is selected as a model protein since albumin is the most abundant protein in blood[51]) and quantify the fraction of protein adsorbed on either side of the film. In full agreement with the asymmetric properties of the bilayer film, we observe that the two sides of the construct exhibit significantly different BSA adsorption characteristics (**Figure 4a**). Whereas the d-HA-based layer binds ≈25% of the offered BSA molecules, only ≈16% of

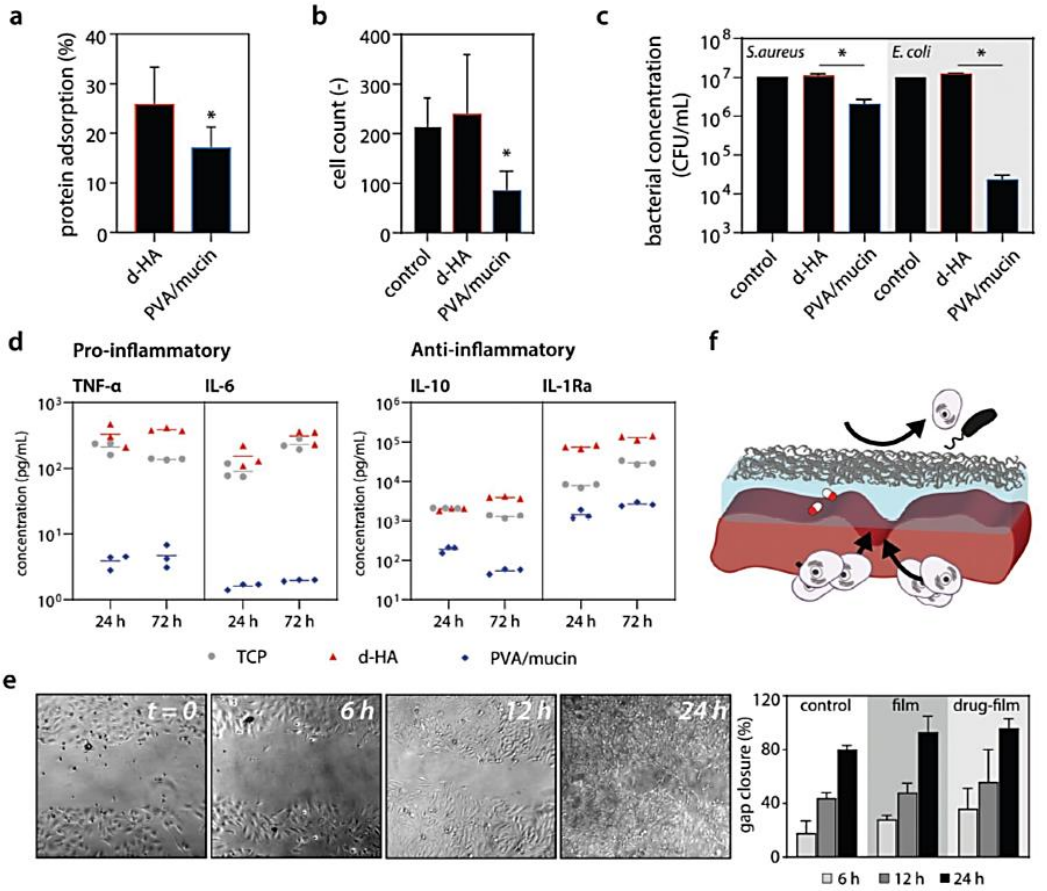

Figure 4. Interaction of proteins, prokaryotic, and eukaryotic cells with the bilayer films. a) Protein adsorption onto d-HA and PVA/mucin layers. An unpaired *t*-test was used to detect the statistical significances between the groups. b) HeLa cells counted after cultivation on the two different layers of the Janus-type film. c) *S.aureus* and *E.coli* adhesion to the d-HA and PVA/mucin surfaces of the bilayer film. For data shown in (b) and (c), a Welch's *t*-test was conducted to compare each group with the control. d) Cytokine expression levels in monocyte-derived macrophages after cultivation on tissue culture polystyrene (TCP, gray), d-HA layers (red), and PVA/mucin layers (blue). The data points denote the cytokine concentration per well, the vertical lines denote the average. e) Time-lapse microscopy images of HeLa cells covered with a bilayer film (left). The closure of the gap (right) was calculated as the average determined from $n = 5$ independent samples per each group (right). f) Schematic representation of the distinct biological functions installed into the two surfaces of the bilayer film. Data in (a–d) represent mean values, and error bars denote the standard deviation as obtained from $n = 5$ independent samples. Asterisks mark statistically significant differences based on a *p*-value of 0.05.

ADVANCED SCIENCE NEWS
www.advancedsciencenews.com

ADVANCED FUNCTIONAL MATERIALS
www.afm-journal.de

the BSA feed adsorb to the PVA/mucin layer. We speculate that this reduced amount of unspecific protein adsorption is probably brought about by the presence of mucins.[31]

Motivated by the outcome of the protein adsorption test, we next quantify cellular attachment to either side of the bilayer film using epithelial HeLa cells as a model cell line. As an in vivo application of the bilayer film has epithelial tissues as one likely target (see the wound healing tests described below), selecting an epithelial cell line for cytotoxicity and attachment tests was a natural choice.

As fluorescent images obtained after live/dead staining show (Figure S4a, Supporting Information), none of the two sides of the bilayer film elicits a perceivable cytotoxic effect—and neither do degradation products generated from the bilayer film (Figure S4b, Supporting Information). In terms of cell colonization efficiency, the d-HA surface of the bilayer film exhibits a similar density of adherent cells as the control, i.e., the wells of cell culture plates (Figure 4b). By contrast, we detect a significantly lower number of cells on the PVA/mucin surface. Additionally, the few adherent cells attached to this side of the bilayer film tend to show a round morphology, which suggests that they are only weakly attached. This observation agrees with previous findings that attributed a good cell-repellency of mucin-coated surfaces to a high density of strongly hydrated glycans provided by the mucin glycoproteins.[52–54] Thus, the mucin-containing top layer of the film can contribute to the protection of a wounded tissue area from uncontrolled cellular overgrowth. Moreover, we hypothesize that the presence of cysteines located in the polypeptide backbone of mucins might promote binding of collagen digesting enzymes (e.g., neutrophil elastase or metalloproteinases) thus potentially influencing the propensity of the bilayer film to become prematurely degraded by enzymatic attack.[55]

Although HA coatings have been shown to contribute to bacterial inhibition at the early stages,[56,57] the dopamine conjugation is likely to counter this effect. Indeed, both, *Staphylococcus aureus* and *Escherichia coli* bacteria adhere equally well to d-HA films as to control surfaces (Figure 4c). From an application point of view, this can be advantageous as it suggests that the bilayer films might also adhere well to infected wounds. In contrast, the PVA/mucin side significantly reduces bacterial adhesion. This effect is moderate for *S. aureus* but strong for *E. coli*. This is an important finding as bacterial colonization of the film (and subsequent biofilm formation) could drastically complicate wound treatment. Here, the PVA/mucin layer reduces such risks and can protect both the wound and bottom layer by repelling bacteria.

However, also in the absence of bacterial colonization, any artificial object may trigger a foreign body response by its interaction with immune cells. If this were to occur, the ensuing inflammation reaction would slow down the healing process. To evaluate a key aspect of the cellular immune response toward each surface of the bilayer film, the secretion of typical pro- and anti-inflammatory cytokines by macrophages incubated with either layer of the construct is assessed. As the results demonstrate (Figure 4d), also here, the asymmetric design of the bilayer film becomes evident: when seeded onto the d-HA layer, macrophages produce proinflammatory markers (expression of tumor necrosis factor-α/TNF-α and interleukin-6/IL-6) at similar levels as when directly seeded onto tissue culture plates (TCP). Furthermore, anti-inflammatory cytokines—particularly the interleukin-1 receptor antagonist (IL-1Ra)—are expressed more strongly on d-HA than on TCP. This observation can be explained by previous findings, which reported hyaluronic acid-rich materials to promote the transformation of macrophages from a proinflammatory (M1) to a reparative (M2) phenotype.[58–60] When the macrophages are incubated on the PVA/mucin layer, we find remarkably low cytokine expression levels that are up to two orders of magnitude smaller than those obtained on both, TCP and d-HA surfaces. This outcome is in line with previous results on the short- and long-term response of macrophages seeded onto mucin-based materials: there, mucin-based gels were shown to have a broad dampening effect on the cytokine expression in macrophages, both in vitro and in vivo.[37,61] Thus, the upper PVA/mucin layer of our film could generate a stealth effect to avoid immune recognition and thus should help preventing acute inflammation reactions. Taken together, the different cytokine expression patterns we find on the opposing surfaces of the Janus-type film suggest that the bilayer construct can support wound repair processes by initiating a desirable immune response—but only where required.

Having analyzed different aspects of how both, eukaryotic and prokaryotic cells, interact with the two sides of the bilayer film, we now ask if the adhesive properties of the sticky layer might interfere with the ability of a damaged tissue layer to regenerate. To test this, we evaluate the ability of an artificially damaged cellular monolayer to "heal" itself when covered with a sticky bilayer film. As our results show, within 24 h, a combination of cell proliferation and migration effects efficiently close the gap in such a cellular monolayer (Figure 4e); the result only slightly depends on whether or not the cell layer is covered with a (drug-loaded or drug-free) bilayer film. Interestingly, film-treated groups show a slightly higher gap closure rate than the control group. Possibly, the hyaluronic acid molecules constituting the sticky layer matrix are responsible for this: HA has been found to be an important regulator of the re-epithelization process of tissues by affecting various intracellular pathways that control proliferation and migration.[62–64] Thus, both biomacromolecules constituting the film (HA and mucin) contribute to the properties of the construct by adding distinctive features to the respective surface of the bilayer material: while the fibrous PVA/mucin layer reduces protein adsorption, bacterial attachment, and uncontrolled cell adhesion, the d-HA side of the film promotes wound healing—at least in an in vitro model setting (Figure 4f).

Thus, in the next step, we investigate the wound healing performance of the Janus-type bilayer films in vivo by applying them to skin wounds that were created on the backs of rats. Here, we test full bilayer constructs to prevent unwanted adhesions to covering bandages that are applied around the created wounds (to prevent the rats from interfering with the wound healing process by scratching) while guaranteeing successful adhesion to the wound tissue. To allow for a better comparison of untreated and film-assisted wound healing processes, we generate two circular wounds (with a diameter of 1 cm each) on the dorsal side of each animal and cover one of those defects with a Janus-type film (either with an unloaded or antibiotic-loaded variant, $N = 7$ wounds each) while leaving the other one uncovered (Figure 5a, left; see Figure S10 of the Supporting Information for an exemplary documentation of the

ADVANCED SCIENCE NEWS
www.advancedsciencenews.com

ADVANCED FUNCTIONAL MATERIALS
www.afm-journal.de

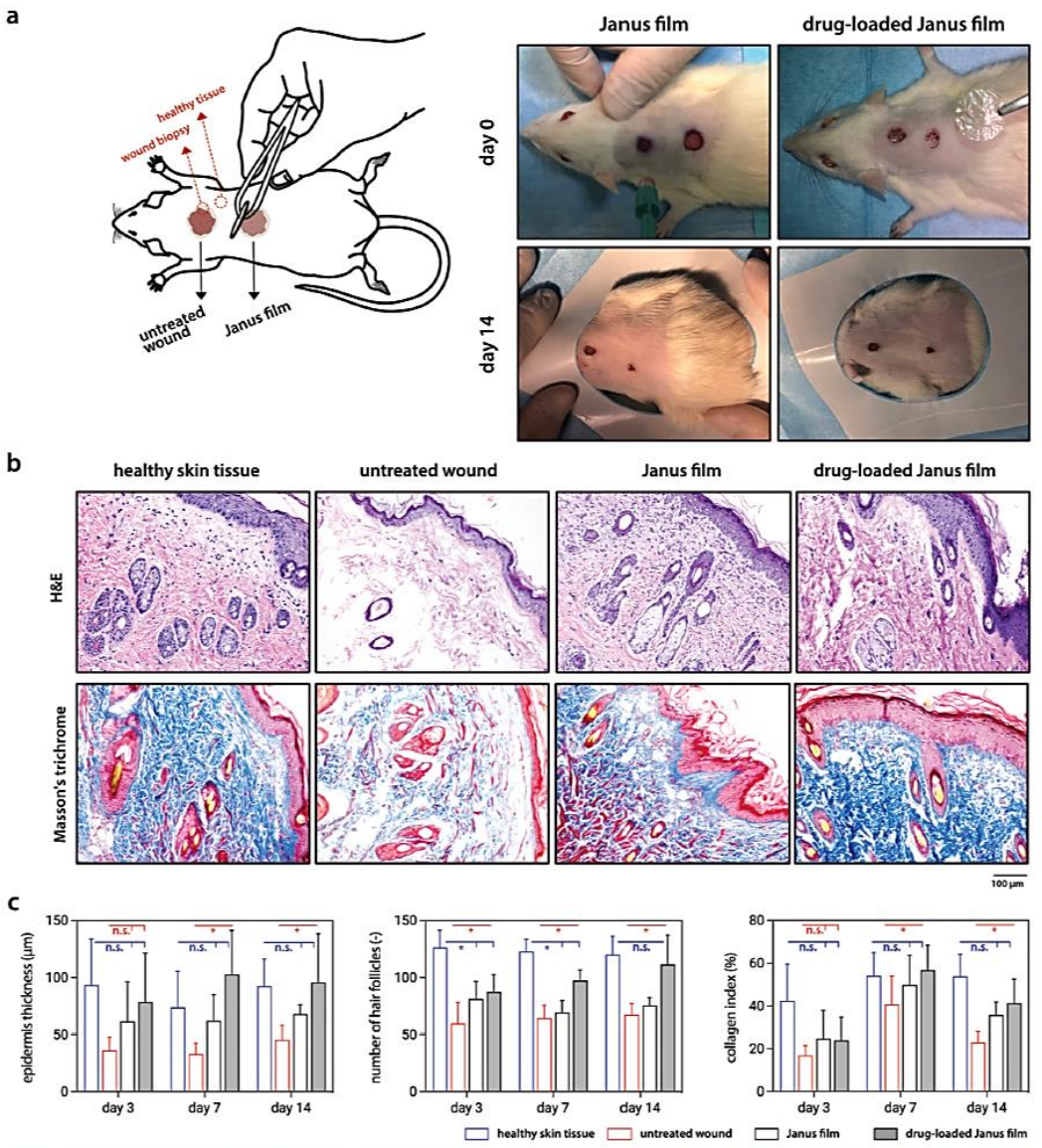

Figure 5. In vivo wound healing performance as observed by the application of Janus-type bilayer films to Sprague-Dawley rats. a) Schematic representation of untreated and film-treated wounds on the back of rats; representative images acquired on different postoperation (day 0 and 14) days images visualize the direct comparison of healing process of untreated wounds (left lesion) and film treated wounds (right lesion). b) Results of hematoxyline and eosin (H&E, top line) as well as Masson's trichrome stainings (bottom line) of different skin samples taken on the 14th day. The scale bar denotes 100 µm and applies to all histology images. c) Quantitative assessments (epidermis thickness, number of hair follicles, and the collagen index) of H&E and Masson's trichrome stained tissue sections. Red lines indicate a statistical significance compared to the untreated wound; blue lines indicate a comparison with the healthy skin tissue. Data shown in the histograms represents mean values of parameters determined from $N = 6$ animals per group (from each animal, ten histological images were analyzed); error bars denote the standard deviation. For each observation day, mean values obtained for Janus-type or drug-loaded Janus-type films were compared to values obtained for healthy skin tissue and untreated wound tissue by using Tukey's multiple comparisons test. Asterisks mark statistically significant differences based on a p-value of 0.05.

ADVANCED SCIENCE NEWS
www.advancedsciencenews.com

ADVANCED FUNCTIONAL MATERIALS
www.afm-journal.de

individual steps). As expected, when brought into contact with the wound tissue, the Janus-type bilayer films are able to adhere tightly without requiring additional fixation (see Video S3, Supporting Information). Our observations over a time span of 14 days reveal that Janus-type bilayer film treatment accelerates the healing process, which is in line with the results obtained from the in vitro tests: when wounds treated with films are compared to those of the untreated group, an improvement of the wound healing process is observed on the 14th postoperative day (Figure 5a, right). Compared to other materials tested for wet tissue adhesive applications,[16,65–67] the wound healing performance of the Janus-type bilayer films presented here is quite promising since the material itself promotes wound closure without the need of adding a stimulating agent such as growth factors.

To analyze the efficiency of the wound healing progress in more detail, biopsies are taken from the wounds at several stages of the healing process. Those tissue sections are stained with hematoxylin and eosin (H&E) and Masson's trichrome and then subjected to a histological evaluation (Figure 5b; Figure S11, Supporting Information); here, samples obtained from film-treated wounds are compared to both, untreated wound areas, and healthy skin tissue sections. For all groups, H&E staining indicates the presence of healthy corpuscles, hair follicles and blood vessels. Of course, as expected, the number of hair follicles in the wound zone is significantly smaller than in the healthy skin tissue. Notably, at day 14 of healing, wounds treated with films do not significantly differ anymore from healthy skin tissue in terms of epidermis thickness, number of hair follicles, and collagen index (Figure 5c). The observed wound healing performance is very similar for both, antibiotic loaded and antibiotic-free film variants. However, in a scenario where the tissue defect might already be challenged by a bacterial attack (i.e., under infection conditions), the application of an antibiotic-loaded Janus-type bilayer film should be beneficial to combat such existing wound infections, i.e., by canalizing the delivery of antibiotics to the wound site and by preventing bacterial adhesion on the opposing site.

These observations strongly underscore the excellent biocompatibility of the Janus-type bilayer films. In addition, at the 14th day after treatment, we observe successful hair regeneration in the healed area without any visible scar formation; we would like to emphasize that the applied Janus-type films were not removed manually—they degraded on their own thus making way for new tissue to grow (Figure S11, Supporting Information). Of course, depending on the application site, the degradation period of the films can vary. However, based on the findings shown here, it can be expected that the degradation products of the film do not impair tissue regrowth.

Having confirmed the ability of our films to promote wound healing in vivo, we next quantify the adhesive properties of the bilayer film when brought into contact with different tissues. In detail, we test porcine cornea, tongue, intestine, and cartilage samples, all of which exhibit a (geometrically) complex surface. Porcine tissue samples are selected due to their size and geometric similarity to human tissues. In those adhesion tests, we bring the bilayer film in contact with the selected tissue sample, allow the film to remain attached for a few seconds without applying any pulling force, and then retract the film at a constant pulling rate. Although the mechanical sensitivity of adhesives is typically highest in this particular loading direction, we prefer this technique over the more commonly used lap shear tests: the lap shear tests are typically employed when two tissue samples are glued to each other (e.g., skin on skin, or muscle tissue on muscle tissue)[9,10,65,68]—and this requires the tissue samples to be properly fixated in the testing setup. Whereas easily possible for flat samples, this is trickier for tissues having complex geometries (such as eyeballs and tongues).

When we subject different variants/subcomponents of the bilayer film to the detachment test, we observe the following behavior: a d-HA monolayer has good adhesive properties; however, it ruptures during the detachment tests before any peeling sets in (Figure S5, Supporting Information). This behavior is not surprising since the d-HA layer forms an unstable gel when brought into contact with a wet tissue. Thus, it cannot withstand the stretching forces it is exposed to during the detachment test. Different from an adhesive that is supposed to connect two tissue samples, this would be problematic for the application envisioned here: the film would stick to fingers or tools during its application, which renders handling complicated. In contrast, the bilayer films are both, sticky and robust, i.e., they adhere well to tissues (even to those with complex topologies, see Figure 6a and Video S2, Supporting Information) but do not rupture as easily as simple d-HA films. Overall, we observe a good adhesion behavior. The adhesion energies we calculated from the detachment curves are highest for the tongue samples ($\approx 4 \times 10^{-3}$ mJ mm^{-2}), and a bit lower for intestine and eye samples ($\approx 2.4 \times 10^{-3}$ and $\approx 1.7 \times 10^{-3}$ mJ mm^{-2}, respectively). Also, the detachment forces at which the bilayer films are removed from the tissues are very similar; this underscores the versatility of catechol-based adhesives as we use them here (Figure 6b). Additionally, control experiments performed with bilayer films containing a bottom layer of pristine, unmodified HA showed that catechol conjugation to HA is essential to obtain good adhesive behavior (Figure S4, Supporting Information).

Interestingly, the application of the bilayer film is not limited to tissues covered with wet epithelia: additional tests performed with cartilage samples show that the same bilayer construct can adhere to this particular tissue as well. For this group, we determine adhesion energy of $\approx 1.3 \times 10^{-3}$ mJ mm^{-2}. Indeed, an adhesive bilayer film could be applied to lateral areas of, e.g., knee joints, after osteochondral cylinders were transplanted into osteoarthritic areas of joints (i.e., when mosaicplasty with autografts is conducted). Moreover, it could be applied to other (nonarticular) cartilage surfaces located in, e.g., the face region. Here, such a bilayer film could protect implanted cartilage grafts from postoperation infections after reconstructive surgeries.

On a molecular scale, the strong and broad-range adhesion properties of the film are brought about by different interactions taking place between the catechol groups of dopamine and different chemical motifs present on the respective tissues. Those interactions include covalent, chemical bonds with $-NH_2$ and $-SH$ groups (as established by, e.g., Michael addition and Schiff base reactions[69]). In addition, dopamine can also engage in physical interactions with nucleophile groups (e.g., amines, thiol, imidazole) on the tissue surfaces.[70] Owing to the presence of the stabilizing PVA/mucin layer, the complete bilayer

ADVANCED SCIENCE NEWS
www.advancedsciencenews.com

ADVANCED FUNCTIONAL MATERIALS
www.afm-journal.de

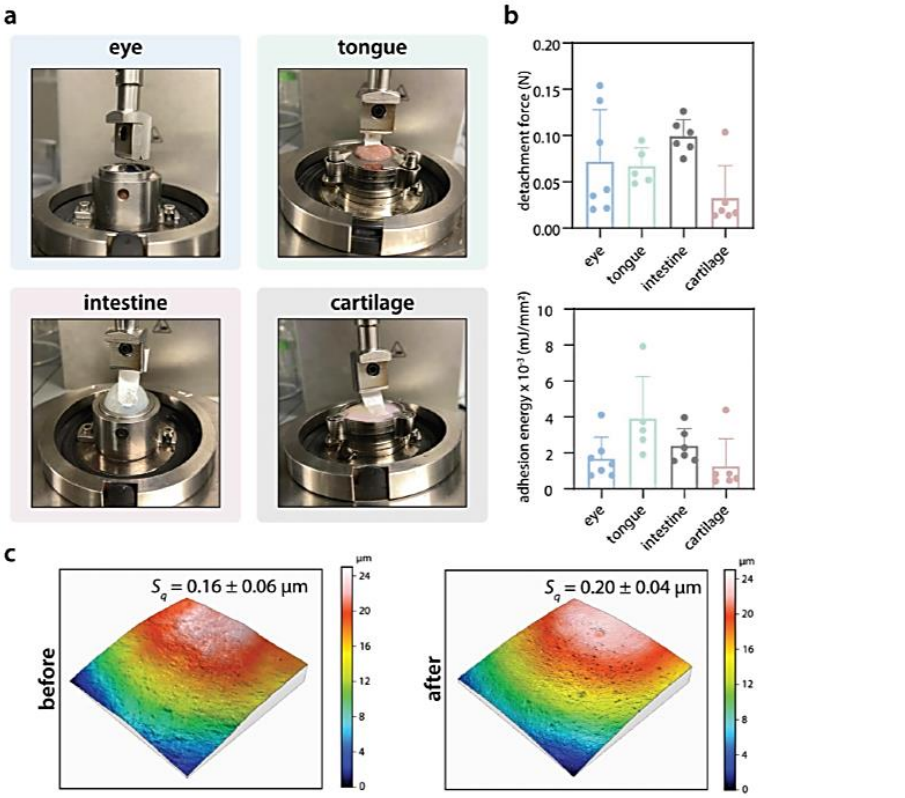

Figure 6. Detachment behavior of bilayer films from tissues. a) Ex vivo tissue detachment tests performed with porcine eye, tongue, intestine, and cartilage samples. The humidity chamber used for the measurements was removed for imaging. b) Detachment forces and adhesion energies as obtained for bilayer films (sticky side facing the tissue) when applied to and detached from different tissue samples. The data points denote individual measurements ($n \geq 5$), vertical lines denote the standard deviation. c) Topographical 3D image of a representative cornea tissue sample before and after 3 days of treatment with a bilayer film (adhesive side facing the tissue). The numbers above the images denote average S_q values as determined from the images after the sample waviness was mathematically removed. Calculations are based on $n = 5$ independent cornea samples, and error bars denote the standard deviation.

construct can be fully detached from the tissues without rupturing or leaving visible traces. When the detachment energy values from those peeling tests are calculated, we obtain comparable results for all tissues tested here, i.e., values in the range of 0.001–0.002 mJ mm^{-2}. Those values agree well with previous results using a similar strategy to achieve tissue adhesion.[16] Moreover, adhesion energies with a similar order of magnitude were recently reported for bulk hydrogels employing polydopamine for adhesion promotion.[71] Other studies exploring bulk hydrogels as tissue adhesives were able to achieve even higher adhesion strengths,[72,73] but aimed at the long-term fixation of mechanically highly stressed tissues such as tendons[25] rather than short-term wound healing. Importantly, with the nonadhesive fibrous layer degrading slower than the adhesive d-HA layer (Figure 3a), it is reasonable to assume that this upper mucin-based layer prevents other tissues (e.g., the eyelid, when the film is applied to the ocular cornea) from adhering to any film-treated tissue area while the bilayer film is present.

In practice, adhesive films are widely applied to tissues with quick healing abilities such as buccal mucosa or skin. Here, slight alterations in the surface structure of the tissue after wound healing are not a big issue, and any residues of the adhesive can easily be removed by the natural regeneration of the mucus layer or by manual rubbing. However, delicate tissues such as the ocular cornea are more sensitive, and any traces of material residues must be avoided. Even microscopic surface alterations would be detrimental for the optical function of the eye. Thus, in a final step, we analyze the microtopography of porcine cornea surfaces that were treated with a bilayer film for 3 days. This treatment time corresponds to the time span the bilayer film requires for efficient degradation in full immersion conditions. Probably, this degradation time can

ADVANCED SCIENCE NEWS
www.advancedsciencenews.com

ADVANCED FUNCTIONAL MATERIALS
www.afm-journal.de

be accelerated under dynamic conditions (e.g., when the film is exposed to continuous mechanical challenge such as blinking) that the film would encounter in vivo. However, in case a particular application calls for an extended lifetime, the supporting nonadhesive layer can be reinforced by incorporating other, more durable polymers into the mucin matrix, e.g., polycaprolactone instead of PVA.

To assess any alterations in the topography of the corneal tissue samples, we quantify 3D images obtained via light profilometry using established metrological parameters. This analysis shows that indeed, a bilayer film treatment (as well as its degradation products generated during film decomposition) does not induce a microtopographical change on the porcine cornea. This is demonstrated by very similar values calculated for the roughness parameter S_q (Figure 6c) and confirmed by a set of additional surface parameters that can define small pits and very fine scratches[74,75] (e.g., the surface area development, the isotropy of the surface, Table S2, Figure S6, Supporting Information). Together, these results show that—when autonomously degrading on the ocular cornea tissue—the bilayer film does not damage the tissue surface. The findings suggest that the material developed here is a very promising candidate for local drug delivery on sensitive body areas, where patient discomfort would severely limit the applicability of such a drug-loaded film.

3. Conclusion

In this work, we introduce a bilayer film that tackles core paradigms of wound management in a simple, yet, effective way. Owing to its asymmetric design, the bilayer film can fulfill distinct and indeed, contradictory physical and biological tasks even on complex and sensitive tissue surfaces.

With the macromolecular architecture and the bilayer design of the Janus-type films, it is not only possible to tailor the properties of the film to enable material adhesion; cellular migration, and drug release on the bottom side of the film, i.e., where wounded tissues would be treated, are possible. By contrast, the top layer of the film is here designed to achieve a stealth effect to minimize cellular immune response and to canalize the therapeutic and adhesive properties of the material to the desired area. Importantly, the mucin macromolecules present in this top layer would also allow for integrating a dynamic response into this top layer to meet additional, specific demands. For example, conformational changes of such mucin glycoproteins in combination with transiently stabilizing agents can be employed to encapsulate a wide variety of substances (hydrophilic, hydrophobic, charged, uncharged) into mucin films and to release them into surrounding tissues upon exposure to a trigger molecule.[76] The ability of these films to accelerate wound healing combined with their bacteria repellent surface properties makes them ideal candidates to prevent postoperative infections and to boost the tissue healing process. Additionally, as an alternative to a postinjury application, multifunctional Janus-type films could also be considered as interface materials mediating between wet tissues and artificial objects that are placed into the human body for extended time periods, e.g., wearable electronics such as glucose monitoring devices. In conclusion, Janus-type bilayer films as we describe them here can be a promising alternative for patients or caregivers alike.

4. Experimental Section

Dopamine–Hyaluronic Acid Conjugation: A dopamine/hyaluronic acid conjugate (d-HA) was prepared as described previously with slight modifications.[77] In brief, hyaluronic acid sodium salt from *Streptococcus equi* (HA; Alfa Aesar, Ward Hill, MA, USA) was dissolved to a concentration of 1 % (w/v) in 2-(*N*-morpholino)ethanesulfonic acid (MES) buffer (10×10^{-3} M, pH = 5). Afterward, 5×10^{-3} M 1-ethyl-3-(3-dimethylaminopropyl) carbo-diimide (EDC, Carl Roth, Karlsruhe, Germany) and 5×10^{-3} M *N*-hydroxysulfosuccinimide (sulfo-NHS, abcr, Karlsruhe, Germany) were added to this solution. After 3 h of incubation, this solution was mixed with 1% (w/v) dopamine hydrochloride (Sigma-Aldrich, St. Louis, MI, USA) solution (dissolved in 5× PBS, pH = 8), at a volumetric ratio of 1:1, and then incubated during shaking at 4 °C overnight. On the next day, the solution was transferred into dialysis tubes (MWCO = 300 kDa, Thermo Fisher Scientific, Waltham, MA, USA) and dialyzed against ultrapure water at 4 °C for two days. The dialyzed samples were freeze-dried for 2 days and stored at −80 °C until further use. The degree of catechol functionalization achieved with this procedure was determined spectrophotometrically by converting the absorbance value of d-HA solutions at 280 nm to a concentration value using a linear calibration curve obtained for pure dopamine solutions of different concentrations. Those absorption measurements were conducted on a specord 210 spectral photometer (Analytikjena, Jena, Germany).

Production of Bilayer Films: To generate the adhesive layer of the bilayer film, d-HA was solubilized in ddH_2O (10 mg mL^{-1}) and poured into a custom-made polycarbonate 6-well plate. Then, the solution in the wells was degassed under vacuum and left to dry at air at room temperature (RT) for 2 days. In the next step, the fibrous layer was generated by electrospinning a PVA/mucin solution onto a preformed d-HA film. To do so, first, PVA (500 mg, MW: ≈145 000 g mol^{-1}, Sigma-Aldrich) was solubilized in ddH_2O (5 mL) at 80 °C for 1 h; then, the solution was allowed to cool down to RT. Next, manually purified mucin (25 mg, MUC5AC, see the Supporting Information for MUC5AC purification) was solubilized in ddH_2O (5 mL) and gradually added to the PVA solution. Per sample, ≈0.25 mL of the final solution was deposited onto the preformed d-HA layer using a custom-made, laboratory-scale, vertical electrospinning device. The parameters of this process were selected as follows: voltage, 15 kV; distance between collector and syringe, 10 cm; flow rate, 0.03 mL min^{-1}. The final bilayer structure was stabilized by cross-linking the macromolecular components through exposure to glutaraldehyde (GA; 25 % aqueous solution, Sigma-Aldrich) vapor at RT for 12 h, followed by an incubation step in a vacuum chamber for 4 h. Completed samples were stored in a desiccator until further use.

Bilayer Film Characterization: Morphology: The morphology of the fibrous mat and the bilayer film was characterized using scanning electron microscopy (SEM; JEOL-JSM-6060LV, Jeol, Eching, Germany). Prior to tests, samples were coated with a thin gold layer using an MED 020 sputtering device (BAL-TEC, Balzers, Liechtenstein) under a saturated argon gas atmosphere. The diameter of PVA/MUC nanofibers was determined from those SEM images using the software ImageJ. Confocal laser scanning microscopy was used to quantitatively assess the isotropy of the fibrous layer (see the Supporting Information).

Wetting Properties: The wetting behavior of the samples was tested by contact angle measurements using a drop shape analyzer device (DSA25S, Krüss GmbH, Hamburg, Germany). For examination, samples were placed in front of the device-integrated high-resolution camera (acA1920, Basler, Ahrensburg, Germany). Imaging, processing, and image analysis were performed with the software ADVANCE (AD4021 v1.13, Krüss GmbH), which was used to initiate automatic imaging (15 fps for 5 s) once a droplet (4 µL ddH_2O) crossed a trigger line positioned just above the sample surface. 0.5 s after the first image of a

ADVANCED SCIENCE NEWS
www.advancedsciencenews.com

ADVANCED FUNCTIONAL MATERIALS
www.afm-journal.de

droplet (uninfluenced by the cannula) was captured, the images captured within the next 1.5 s were analyzed using the software-integrated ellipse (tangent-1) fit method. Contact angle values were determined as the water-enclosed angle between the surface and the edge of the droplet.

Mechanical Characterization: The tensile properties of the films (both, bilayer, and individual monolayers) were tested under uniaxial tension using a research-grade shear rheometer (MCR 302, Anton Paar, Graz Austria). In brief, rectangular samples were prepared by casting the adhesive layers in rectangular (10 mm × 30 mm) molds fabricated from polycarbonate. The measurements were performed by fixing the films at either end in custom-made clamp-like sample holders. The first of those clamps were fixed to the central shaft of the rheometer using a commercial adapter (D-CP/PP 7, Anton Paar); the second clamp was mounted onto a commercial bottom plate (P-PTD 200, Anton Paar). The measurement head of the rheometer was lifted at a constant speed of 10 µm s^{-1} until the film was ruptured, and the resulting normal force data were recorded at a sampling rate of 1/s (see Figure S6, Supporting Information, for the setup).

To evaluate the mechanical robustness of the films under tribological stress, they were probed in an oscillatory tribology setup as described in Winkeljann et al.[78] and subsequently examined optically. Here, both counterparts of the setup, i.e., polydimethylsiloxane (PDMS, SYLGARD 184, Dow Corning) pins with rounded edges in the measuring head and kidney-shaped PDMS samples in the sample holder, were cast in custom-made molds, activated by exposure to atmospheric plasma in a SmartPlasma2 oven (plasma technology GmbH, Herrenberg, Germany; settings: 0.4 mbar, 30 W, 1.5 min) to become hydrophilic,[79] and stored in ddH_2O until further use to avoid hydrophobic recovery.[79,80] d-HA and bilayer films were cast in circular molds (Ø = 20 mm) made from polycarbonate, and circular samples (Ø = 10 mm) were punched from the central areas of these films with a hand press (IstaBreeze Germany GmbH, Bad Rappenau, Germany). Before starting a measurement, the film samples were first hydrated in situ by applying each onto a moistened kidney-shaped PDMS sample. Then, 40 µL of PBS was added as a lubricant, and the friction response of the material pairing was recorded every 0.15 s in oscillatory mode over a deflection angle of 17° while applying a normal load *F* of 0.6 N, a sliding velocity of 0.7 mm s^{-1}, and a temperature of 37 °C. With those parameters, the resulting contact pressure is ≈0.028 MPa. To avoid evaporation of the lubricant as well as film drying, a moisture trap was installed. As control samples, plasma-activated PDMS specimens were probed without any film added (using PBS as a lubricant).

Once the oscillatory tribology measurements were concluded, any excess liquid was gently removed from the films, and they were allowed to dry at RT for two days. For both, macroscopic and microscopic examination of the film surfaces, a confocal laser scanning microscope (VK-X1000, Keyence, Oberhausen, Germany) was used. Combined laser confocal/light microscopy images were captured at 20× magnification (CF Plan, NA = 0.46; Nikon, Chiyoda, Tokyo, Japan). For obtaining a macroscopic overview of the films, several images acquired at 5× magnification (CF Plan, NA = 0.13; Nikon) were stitched together. The projected area of the films was determined using the open-source software ImageJ.

Degradation Behavior: For each layer of the bilayer film, the degradation behavior was assessed spectrophotometrically. To distinguish between the degradation products originating from either layer, chemical groups specific for each layer were selected, and their particular absorbance spectrum was tracked as they enter the liquid phase in which the bilayer samples were incubated. To represent the nonadhesive layer, a fluorescent dye covalently attached to mucins (Atto 488 – carboxy modified, ATTO-TEC GmbH, Siegen, Germany; Ex/Em = 488/535 nm) via carbodiimide coupling was selected (see the Supporting Information). To represent the adhesive layer, catechol groups (absorbance at 280 nm) were tracked. Samples immersed into aqueous solutions (see above) were placed onto an orbital shaker operating at 37 °C while avoiding light exposure. The supernatants were collected at predetermined time intervals and characterized using a multilabel plate reader (Victor3, Perkin Elmer, Rodgaum, Germany). To evaluate the degradation profile of the d-HA layer, PVA/mucin monolayers were incubated under similar conditions and their absorbance (at 280 nm) was subtracted from those obtained with d-HA films to avoid any interference.

Swelling Profile: For swelling tests, the measuring setup of the drop shape analyzer device used for the evaluation of the wetting behavior of the films was employed; also here, transversal images of the cross-section of the bilayer film were obtained and evaluated during the swelling process of the material. In detail, bilayer films were punched into circular samples (Ø 7 mm) using a manual eyelet press (Istabreeze Germany GmbH, Bad Rappenau, Germany); then, the initial height of each sample was measured using a digital caliper, and the initial cross-section of each sample was determined in a dry state. Afterward, a piece of lint-free laboratory wipe (≈6 cm × 6 cm) was fixated on a glass slide using adhesive tape to impede wrinkling of the laboratory wipe, and 750 µL of ddH_2O was added to fully wet the laboratory wipe. Then, the bilayer film samples (with the mucin/PVA side facing downward to prevent the films from rolling up during hydration) were placed onto the laboratory wipe, and images were automatically captured at different time steps for a total duration of 30 min. For evaluating the swelling behavior of each sample, $t = 0$ s was defined by the first image of the bilayer construct being in contact with the wet wipe. The captured images (including a scale bar) were exported using the ADVANCE software and were analyzed with the software ImageJ (version 1.53k) by setting the scale according to the displayed scale bar; here, the contrast was increased to 0.3% saturated pixels by enabling the option "equalize histogram." Then, the cross-sectional area was determined by identifying the outlines of the sample manually. Prior to averaging the results obtained from different film samples, the cross-sections measured at each time-step were normalized to the initial cross-section determined for each sample in a dry state.

Drug Loading and In Vitro Drug Release: TCL (Applichem, Darmstadt, Germany) was chosen as a model antibiotic and solubilized in a d-HA solution (0.86 mg mL^{-1}) before casting the bottom layer of the bilayer film. With this concentration of TCL in the d-HA solution, the expected TCL concentration in the bilayer film is ≈5.5 µg mm^{-2}. After the formation of the bilayer films, they were placed into wells of a 24-well plate equipped with permeable insert strips (BRANDplates insert system, pore size: 0.4 µm, Brand, Wertheim, Germany) to test their in vitro drug release behavior. The in vitro TCL release profile was determined by placing the TCL-loaded bilayer films into a range of solutions: simulated tear fluid, STF (NaCl: 6.78 g L^{-1}, $NaHCO_3$: 2.18 g L^{-1}, $CaCl_2{\cdot}2H_2O$: 0.084 g L^{-1}, KCl: 1.38 g L^{-1}, pH = 7.4); saliva mimetic, HSM (0.02% (w/v) manually purified human salivary MUC5B dissolved in 20×10^{-3} M TRIS, pH = 7.4; see the Supporting Information for MUC5B purification); SIF (KH_2PO_4: 6.8 g L^{-1}, NaOH: 0.896 g L^{-1}, pH = 6.8), and phosphate buffer saline, PBS (pH = 7.4). To mimic the salivary conditions with HSM, human salivary mucin (0.02% w/v in 20×10^{-3} M TRIS, pH = 7.4) was used manually purified to mimic the typical pH range and the average mucin concentration of human saliva.[81] Together, this set of solutions mimics the range of environmental conditions the bilayer film may encounter in an in vivo setting. The drug release quantification was then conducted as follows: the bilayer films were hydrated with 200 µL of the respective aqueous solution first; then, 2 mL of the same solution medium was placed into the bottom part of the chamber so that the bottom (drug-loaded) part of the bilayer film is fully wetted from below and can release drugs into this bottom part of the chamber over time. The absorbance of the liquid in this bottom chamber was then quantified at 360 nm at predetermined time intervals with a spectrophotometer (specord 210, Analytikjena, Jena, Germany) to detect drug molecules entering this liquid phase via diffusion. The released drug amount was quantified by converting the absorbance values of this liquid phase into absolute concentration values based on a TCL standard curve (Figure S8, Supporting Information).

Protein Adsorption: To assess the protein adsorption behavior to either side of the bilayer construct, a model protein, i.e., BSA (Albumin fraction V, Carl Roth) labeled with Atto488 (see the Supporting Information) was selected. The d-HA and PVA/mucin layers of the bilayer film were created separately, and each component was studied independently. Monolayer samples were placed into wells of a 24-well plate and incubated with

ADVANCED SCIENCE NEWS
www.advancedsciencenews.com

ADVANCED FUNCTIONAL MATERIALS
www.afm-journal.de

a fluorescently labeled BSA solution (0.1% (w/v) in PBS). Then, the samples were placed onto an orbital shaker while avoiding light and incubated at 37 °C for 1 h. After incubation, the supernatants were collected, and the fluorescence signal of this supernatant was quantified using a multilabel plate reader at Ex/Em = 488/535 nm. Then, the amount of BSA adsorbed onto the film was determined as the amount of fluorescent BSA depleted from the solution.

In Vitro Experiments with Procaryotic and Eucaryotic Cells: Prior to all in vitro tests involving cells, the bilayer film samples were placed into a sterilization chamber (BLX-254, Vilber Lourmat GmbH, Eberhardzell, Germany) and exposed to UV light (254 nm, 5 × 8 W) for 3 h. If not stated otherwise, all chemicals used for those in vitro tests were purchased from Sigma-Aldrich. Those experiments were conducted with human epithelial (HeLa) cells cultured in minimum essential medium supplemented with 10% (v/v) fetal bovine serum, 2×10^{-3} M L-glutamine solution, and 1% (v/v) nonessential amino acids. The cultivation of HeLa cells was conducted at 37 °C in a humidified atmosphere containing 5% CO_2.

Biocompatibility: A live/dead assay was applied to assess the biocompatibility of each side of the bilayer films. Here, bilayer film samples were placed into wells of an 8-well plate (µ-Slide ibidiTreat plate, ibidi GmbH, Gräfelfing, Germany), HeLa cells were seeded onto either the adhesive or the nonadhesive side of the bilayer film (30 000 cells per sample) and incubated for 24 h. Next, the samples were washed with DPBS and stained with 100 µL per well of a live/dead solution (1×10^{-6} M calcein-AM, 2×10^{-6} M ethidium homodimer 1, Invitrogen, Carlsbad, CA, USA). After 30 min of incubation, fluorescence images were acquired on a fluorescence microscope (DMi8, Leica, Wetzlar, Germany) using FITC (Ex = 460–500, DC = 505; Em = 512–542, Leica) and TXR filter cubes (Ex = 540–580, DC = 585; Em = 592 – 668, Leica), respectively. The exposure times were first optimized for each filter set and applied to all acquired images.

Bacterial Adhesion: Bacterial attachment tests were conducted with the strains *S. aureus* NCTC 8325-4 and *E. coli* ATCC 25922. Frozen vials containing bacteria at concentrations of 10^8 CFU mL^{-1} were reconstituted in PBS. The bilayer film samples were sterilized under UV light at a wavelength of 254 nm for 2 h. The bacterial suspensions were subsequently inoculated at a concentration of 10^7 CFU mL^{-1} onto the layer to be tested, i.e., the fibrous PVA/MUC layer and the d-HA layer, respectively. The samples were incubated at 37 °C for 2 h. Nonadherent bacteria were removed by washing the samples thrice in 5 mL sterile PBS. Then, the samples were vortexed in PBS for 1 min to remove the adherent bacteria, and the obtained suspensions were serially diluted. These serial dilutions were plated onto tryptic soy agar plates, which were incubated at 37 °C for 24 h. After this incubation period, the colonies were counted to determine the number of adherent bacteria for either sample layer.

In Vitro Cell Scratch Assay: An in vitro scratch test using cellular monolayers was applied to ensure that the sticky properties of the bilayer film do not prevent wound healing. First, HeLa cells were cultivated in a 48-well plate (80 000 cells per well) for 24 h. Then, a horizontal scratch was created in the middle part of the well using a pipette tip and a bilayer film was placed on top of this scratched cell layer (with the sticky side facing the cellular layer). The time-dependent closure of the damaged cell layer was observed on an inverted light microscope (DMi8, Leica) equipped with a 10× objective (Leica) and a digital camera (Orca Flash 4.0 C11440, Hamamatsu, Japan); images were acquired after 6, 12, and 24 h of incubation. As a control, scratched cellular layers without an additional bilayer film were used.

Pro/Anti-Inflammatory Cytokine Release of Macrophages In Vitro: The immune response to the bilayer system was evaluated by determining the cytokine expression of monocyte-derived macrophages. The human cell line U937 (ATCC) was cultured in RPMI 1640 medium (Gibco, Life Technologies, Paisely, UK) supplemented with 10% fetal calf serum (Gibco), 2×10^{-3} M L-glutamine (Gibco), 1×10^{-3} M sodium pyruvate (Gibco), 1 U mL^{-1} penicillin and 1 µg mL^{-1} streptomycin (Gibco). The cells were then differentiated into M0 macrophages using 100×10^{-9} M phorbol 12-myristate 13-acetate for 72 h and were allowed to rest in a complete culture medium for 24 h before the assay was conducted. These monocyte-derived M0 macrophages were seeded at a density of 800 000 cells mL^{-1} onto the samples, and the cytokine concentration in the macrophage culture supernatant was evaluated after 24 and 72 h of incubation at 37 °C with 5% CO_2. Quantification of the released proinflammatory (interleukin-6, tumor necrosis factor-α) and anti-inflammatory (interleukin-1 receptor antagonist, interleukin-10) cytokines was performed with the DuoSetELISA Development System (R&D Systems, Minneapolis, MN, USA) following the manufacturer's instructions using a multimode microplate reader (Spark, Tecan, Männedorf, Switzerland).

In Vivo Wound Healing Experiments: Prior to in vivo experiments, all film samples were sterilized by ethylene oxide exposure. The experimental protocol of the study was reviewed and approved by the Animal Experiments Local Ethics Committee of Bagcilar Training and Research Hospital (decision number: 2021/116). All procedures were applied according to the guide for the care and use of laboratory animals adopted by the National Institutes of Health (USA) and the Declaration of Helsinki. Tests were performed with Sprague-Dawley rats (body weight, 250–350 g, $N = 14$) at the University of Health Sciences, Bagcilar Training and Research Hospital Research Center, Istanbul, Turkey. The animals were housed in a controlled environment at a temperature of (24 ± 2) °C and at a humidity of 60% under a 12 h light/dark cycle. The animals were given free access to water and standard nutrition. The rats were anesthetized by intraperitoneal administration of ketamine/xylazine (90/10 mg kg^{-1}), and all efforts were made to minimize animal suffering. Prior to the experiments, the backs of the rats were shaved; then, two full-thickness skin defects (including epidermis and dermis) were created on the dorsal side of each rat using a 12 mm biopsy punch. One of the such created wounds was covered with a Janus-type bilayer film (either plain or antibiotic loaded, $N = 7$ each), and the defects were covered with a bandage to avoid uncontrolled animal reactions such as scratching or biting. On the 3rd, 7th, and 14th day of wound regeneration, a tissue sample was taken from both, the wound areas and a healthy skin tissue area using a 3 mm biopsy punch; those samples were fixed with paraformaldehyde (4% v/v) and then subjected to further histopathological examinations. To do so, 5 µm thick sections from paraffin-embedded tissue samples were stained with Harris hematoxylin/eosin and Masson trichrome (both obtained from Bio-Optika S.p.A, Milan, Italy) using routine procedures and afterward examined under a light microscope (Olympus BX53, Melville, NY, USA). The maximal epidermis thickness per image, the total number of hair follicles, and the average collagen density per image were calculated using the software ImageJ by analyzing $n = 10$ images per animal ($N = 6$) at each day of observation (day 0, 3, 7, and 14). Findings obtained with film treated samples were compared to untreated wounds and healthy skin tissue using a paired *t*-test; significant differences were marked with an asterisk if based on a *p*-value of $p \leq 0.05$.

Experiments Involving Ex Vivo Tissue Samples: Tissue Adhesion/Detachment Tests: Adhesion/detachment tests were performed on a commercial research-grade shear rheometer (MCR 302, Anton Paar, Graz Austria). Different ex vivo tissue samples (porcine eye, tongue, intestine, and cartilage samples) were tested, which were all obtained from a local butcher shop. The tissue samples were placed into a custom-made sample holder mounted to a commercial bottom plate (T-PTD 200, Anton Paar). In this step, the surface of each sample was smoothened by fixing the tissue with a stainless-steel ring; this step was necessary to remove macroscopic wrinkles on the tissue surface, which otherwise could negatively affect the adhesion/detachment test by rendering it less reproducible. Before mounting the samples into the sample holder, they were first hydrated with PBS. Then, the adhesion/detachment tests were conducted in a humidified atmosphere at a constant temperature of 37 °C. The bilayer film sample was fixed to the measuring shaft of the rheometer by attaching a custom-made clamp (see the Supporting Information) fabricated in a local workshop to a commercial adapter (D-CP/PP 7, Anton Paar). For each measurement, a fresh bilayer film and a fresh tissue sample were used. Each detachment test was then conducted as follows: the measuring head of the rheometer was lowered

ADVANCED SCIENCE NEWS
www.advancedsciencenews.com

ADVANCED FUNCTIONAL MATERIALS
www.afm-journal.de

until one side of the bilayer film (either its adhesive or nonadhesive side) was brought into contact with the tissue (the contact area was ≈64 mm^2). This contact was maintained for 10 s; afterward, the measuring head was lifted at a constant speed of 10 µm s^{-1}, and the resulting normal force was recorded at a measuring point density of 1/s until the measured force dropped to zero. The adhesion energy was calculated from the force–distance plot by calculating the area under the force–distance curve.

Topographical Evaluation of Bilayer Film-Treated Cornea Tissues: To assess whether the bilayer film would leave any residues or surface damage on a tissue after the film has been degraded, a topographical evaluation was performed. Here, porcine cornea samples were selected as they represent a particularly sensitive tissue variant. In detail, each sample was evaluated twice, i.e., before and after having been in contact with the adhesive side of a bilayer film for 3 days. To do so, fresh porcine eyes were first incubated in an antibiotic solution (0.2% TCL) for 1 h, gently rinsed with PBS, and kept on a tissue cloth for ≈10 min (to allow water droplets on the surface to evaporate). After eliminating the eye samples which exhibited visible, macroscopic defects, profilometric images of the corneal surfaces were obtained using a laser scanning microscope equipped with a 20× lens. For each sample, five images were acquired. Image quantification was then performed using the µsoft analysis extended software (version 7.2.7568, NanoFokus AG, Oberhausen, Germany). Prior to data analysis, a Gaussian filter (according to ISO 16610–61) with a cutoff wavelength of 80 µm was applied. For each topographical image, the following metrological parameters were calculated: the root-mean-square height (S_q), the developed interfacial area ratio (S_{dr}), the isotropy of the surface (S_{tr}), the maximum peak height (S_p), the root mean square gradient (S_{dq}), the arithmetic mean peak curvature (S_{pc}), the peak material volume (V_{mp}), and the dale void volume (V_{vv}); those parameters are all defined in ISO 25178-2 (see the Supporting Information). From those assessments, the set of eye samples was further narrowed down by eliminating those which showed noticeable microscopic defects; in detail, those samples that returned a surface roughness parameter (S_q) smaller than 0.3 µm were selected. With this procedure, it could be ensured that the population of cornea samples studied here had comparable, well-defined initial properties. Then, bilayer films were placed onto the hydrated surfaces of the cornea samples, and the eyes were immersed in STF (supplemented with 0.2% TCL) at 4 °C for 3 days until the bilayer films were fully degraded. As a control, similar incubation conditions were applied to a control group, i.e., eye samples that did not receive a film treatment. After 3 days of incubation, profilometric images were acquired again, and the same metrological parameters described above were calculated to quantify the effect of bilayer film treatment.

Statistical Analysis: The software GraphPad Prism (Prism 8, San Diego, CA, USA) was used to conduct all statistical analyses. All the data collected in this work were presented as mean ± standard deviation. Before each analysis, the normal distribution of the measured values was confirmed with a Shapiro-Wilk test. A two-tailed Student's *t*-test was performed for normally distributed populations with homogeneous variances, whereas a two-tailed Welch's *t*-test was used in case of unequal variances. Tukey's multiple comparison test were conducted for the comparison between multiple samples. If not stated otherwise, a *p*-value of $p \leq 0.05$ was chosen as a threshold for significance; accordingly, significant differences were marked with an asterisk where applicable.

Supporting Information

Supporting Information is available from the Wiley Online Library or from the author.

Acknowledgements

The authors thank Benjamin Winkeljann for designing custom-made sample molds, and Corinna Lieleg for helpful discussions regarding histology assessments. This project was funded by the Deutsche Forschungsgemeinschaft (DFG, German Research Foundation)—SFB-863—Project ID 111166240 and and Munich Multiscale Biofabrication Network.

Open access funding enabled and organized by Projekt DEAL.

Conflict of Interest

The authors declare no conflict of interest.

Author Contributions

The study was designed by C.K. and O.L. S.M. and P.M. designed the cytokine release experiments. M.G.B. conducted the tribology and swelling experiments. C.K. and M.B. performed the shearing tests and drug release studies. T.M.L. and S.M. performed experiments involving eukaryotic and prokaryotic cells. E.A., Z.D., and P.K. conducted the in vivo study. C.K. performed all other experiments and analyzed the data. The manuscript was written by C.K. and O.L. and was critically revised by all authors.

Data Availability Statement

The data that support the findings of this study are available from the corresponding author upon reasonable request.

Keywords

asymmetric designs, bioadhesives, hyaluronic acid, mucin, wound management

Received: June 14, 2021
Revised: March 22, 2022
Published online: April 30, 2022

[1] A. R. Parker, C. R. Lawrence, *Nature* **2001**, *414*, 33.
[2] H.-C. Yang, Y. Xie, J. Hou, A. K. Cheetham, V. Chen, S. B. Darling, *Adv. Mater.* **2018**, *30*, 1801495.
[3] A.-Y. Lu, H. Zhu, J. Xiao, C.-P. Chuu, Y. Han, M.-H. Chiu, C.-C. Cheng, C.-W. Yang, K.-H. Wei, Y. Yang, Y. Wang, D. Sokaras, D. Nordlund, P. Yang, D. A. Muller, M.-Y. Chou, X. Zhang, L.-J. Li, *Nat. Nanotechnol.* **2017**, *12*, 744.
[4] A. Kirillova, C. Marschelke, A. Synytska, *ACS Appl. Mater. Interfaces* **2019**, *11*, 9643.
[5] W. Wu, R. Cheng, J. Das Neves, J. Tang, J. Xiao, Q. Ni, X. Liu, G. Pan, D. Li, W. Cui, B. Sarmento, *J. Controlled Release* **2017**, *261*, 318.
[6] B. D. Ratner, *Annu. Rev. Biomed. Eng.* **2019**, *21*, 171.
[7] L. Wang, X. Zhang, K. Yang, Y.u V. Fu, T. Xu, S. Li, D. Zhang, L.u-N. Wang, C.-S. Lee, *Adv. Funct. Mater.* **2020**, *30*, 1904156.
[8] S. Li, N. Chen, X. Li, Y. Li, Z. Xie, Z. Ma, J. Zhao, X. Hou, X. Yuan, *Adv. Funct. Mater.* **2020**, *30*, 2000130.
[9] K. Xu, Y. Liu, S. Bu, T. Wu, Q. Chang, G. Singh, X. Cao, C. Deng, B. Li, G. Luo, M. Xing, *Adv. Healthcare Mater.* **2017**, *6*, 1700132.
[10] Y. Zhou, L. Gao, J. Peng, M. Xing, Y. Han, X. Wang, Y. Xu, J. Chang, *Adv. Healthcare Mater.* **2018**, *7*, 1800144.
[11] C. Gong, C. Lu, B. Li, M. Shan, G. Wu, *J. Biomed. Mater. Res., Part A* **2017**, *105*, 1000.
[12] T. M. Lutz, C. Kimna, A. Casini, O. Lieleg, *Mater. Today Bio* **2022**, *13*, 100203.

[13] X. Peng, X. Xia, X. Xu, X. Yang, B. Yang, P. Zhao, W. Yuan, P. W. Y. Chiu, L. Bian, *Sci. Adv.* **2021**, *7*, 8739.
[14] S. Hu, X. Pei, L. Duan, Z. Zhu, Y. Liu, J. Chen, T. Chen, P. Ji, Q. Wan, J. Wang, *Nat. Commun.* **2021**, *12*, 1689.
[15] W.-C. Huang, R. Ying, W. Wang, Y. Guo, Y. He, X. Mo, C. Xue, X. Mao, *Adv. Funct. Mater.* **2020**, *30*, 2000644.
[16] J. Shin, S. Choi, J. H. Kim, J. H. Cho, Y. Jin, S. Kim, S. Min, S. K. Kim, D. Choi, S.-W. Cho, *Adv. Funct. Mater.* **2019**, *29*, 1903863.
[17] M. M. Hasani-Sadrabadi, P. Sarrion, S. Pouraghaei, Y. Chau, S. Ansari, S. Li, T. Aghaloo, A. Moshaverinia, *Sci. Transl. Med.* **2020**, *12*.
[18] X. Zhao, Y. Liang, Y. Huang, J. He, Y. Han, B. Guo, *Adv. Funct. Mater.* **2020**, *30*, 1910748.
[19] T. Chen, Y. Chen, H. U. Rehman, Z. Chen, Z. Yang, M. Wang, H. Li, H. Liu, *ACS Appl. Mater. Interfaces* **2018**, *10*, 33523.
[20] C. Xuan, L. Hao, X. Liu, Y.e Zhu, H. Yang, Y. Ren, L. Wang, T. Fujie, H. Wu, Y. Chen, X. Shi, C. Mao, *Biomaterials* **2020**, *252*, 120018.
[21] M. Li, Z. Zhang, Y. Liang, J. He, B. Guo, *ACS Appl. Mater. Interfaces* **2020**, *12*, 35856.
[22] C. Cui, T. Wu, X. Chen, Y. Liu, Y. Li, Z. Xu, C. Fan, W. Liu, *Adv. Funct. Mater.* **2020**, *30*, 2005689.
[23] B. Xu, A. Li, R. Wang, J. Zhang, Y. Ding, D. Pan, Z. Shen, *Adv. Funct. Mater.* **2021**, *31*, 2105265.
[24] G. U. Ruiz-Esparza, X. Wang, X. Zhang, S. Jimenez-Vazquez, L. Diaz-Gomez, A.-M. Lavoie, S. Afewerki, A. A. Fuentes-Baldemar, R. Parra-Saldivar, N. Jiang, N. Annabi, B. Saleh, A. K. Yetisen, A. Sheikhi, T. H. Jozefiak, S. R. Shin, N. Dong, A. Khademhosseini, *Nano-Micro Lett.* **2021**, *13*, 1.
[25] B. R. Freedman, A. Kuttler, N. Beckmann, S. Nam, D. Kent, M. Schuleit, F. Ramazani, N. Accart, A. Rock, J. Li, M. Kurz, A. Fisch, T. Ullrich, M. W. Hast, Y. Tinguely, E. Weber, D. J. Mooney, *Nat. Biomed. Eng.* **2022**, 1.
[26] W. Liang, W. He, R. Huang, Y. Tang, S. Li, B. Zheng, Y. Lin, Y. Lu, H. Wang, D. Wu, *Adv. Mater.* **2022**, *34*, 2108992.
[27] G. Petrou, T. Crouzier, *Biomater. Sci.* **2018**, *6*, 2282.
[28] J. A. Burdick, G. D. Prestwich, *Adv. Mater.* **2011**, *23*, H41.
[29] Lu Han, X. Lu, K. Liu, K. Wang, L. Fang, L.u-T. Weng, H. Zhang, Y. Tang, F. Ren, C. Zhao, G. Sun, R. Liang, Z. Li, *ACS Nano* **2017**, *11*, 2561.
[30] H. Lee, S. M. Dellatore, W. M. Miller, P. B. Messersmith, *Science* **2007**, *318*, 426.
[31] B. Winkeljann, M. G. Bauer, M. Marczynski, T. Rauh, S. A. Sieber, O. Lieleg, *Adv. Mater. Interfaces* **2020**, *7*, 1902069.
[32] R. Nudelman, H. Alhmoud, B. Delalat, S. Fleicher, E. Fine, T. Guliakhmedova, R. Elnathan, A. Nyska, N. H. Voelcker, M. Gozin, S. Richter, *Adv. Funct. Mater.* **2019**, *29*, 1902783.
[33] A. W. Nugroho, H. Sosiati, P. Wijongko, *Int. J.* **2011**, *8*, 2431.
[34] M. Marczynski, K. Jiang, M. Blakeley, V. Srivastava, F. Vilaplana, T. Crouzier, O. Lieleg, *Biomacromolecules* **2021**, *22*, 1600.
[35] L. Shi, R. Ardehali, K. D. Caldwell, P. Valint, *Colloids Surf., B* **2000**, *17*, 229.
[36] J. Y. Co, T. Crouzier, K. Ribbeck, *Adv. Mater. Interfaces* **2015**, *2*, 1500179.
[37] H. Yan, C. Seignez, M. Hjorth, B. Winkeljann, M. Blakeley, O. Lieleg, M. Phillipson, T. Crouzier, *Adv. Funct. Mater.* **2019**, *29*, 1902581.
[38] T. Crouzier, K. Boettcher, A. R. Geonnotti, N. L. Kavanaugh, J. B. Hirsch, K. Ribbeck, O. Lieleg, *Adv. Mater. Interfaces* **2015**, *2*, 1500308.
[39] J. Klein, *Polym. Adv. Technol.* **2012**, *23*, 729.
[40] R. Jayasekara, I. Harding, I. Bowater, G. B. Y. Christie, G. T. Lonergan, *Polym. Test.* **2004**, *23*, 17.
[41] T. Yamaoka, Y. Tabata, Y. Ikada, *J. Pharm. Pharmacol.* **1995**, *47*, 479.
[42] A. Besheer, K. Maeder, S. Kaiser, J. Kressler, C. Weis, E. K. Odermatt, *J. Biomed. Mater. Res., Part B* **2007**, *82*, 383.
[43] W. D. Comper, L. M. Hilliard, D. J. Nikolic-Paterson, L. M. Russo, *Am. J. Physiol. Renal Physiol.* **2008**, *295*, F1589.
[44] Y. Jiang, et al., *J. Biomed. Mater. Res., Part B* **2010**, *93*, 275.
[45] A. Schädlich, T. Naolou, E. Amado, R. Schöps, J. Kressler, K. Mäder, *Biomacromolecules* **2011**, *12*, 3674.
[46] Y. Kaneo, S. Hashihama, A. Kakinoki, T. Tanaka, T. Nakano, Y. Ikeda, *Drug Metab. Pharmacokinet.* **2005**, *20*, 435.
[47] P. Dahiya, R. Kamal, *N. Am. J. Med. Sci* **2013**, *5*, 309.
[48] L. Shi, X. Liu, W. Wang, L. Jiang, S. Wang, *Adv. Mater.* **2019**, *31*, 1804187.
[49] R. A. Clark, *The Molecular and Cellular Biology of Wound Repair*, New York: Plenum Press **1996**, pp. 3–33.
[50] C. J. Wilson, R. E. Clegg, D. I. Leavesley, M. J. Pearcy, *Tissue Eng.* **2005**, *11*, 1.
[51] L. Anderson, N. G. Anderson, *Proc. Natl. Acad. Sci. USA* **1977**, *74*, 5421.
[52] R. R. R. Janairo, Y. Zhu, T. Chen, S. Li, *Tissue Eng., Part A* **2014**, *20*, 285.
[53] J. Song, T. M. Lutz, N. Lang, O. Lieleg, *Adv. Healthcare Mater.* **2020**, *10*, 2000831.
[54] T. Crouzier, H. Jang, J. Ahn, R. Stocker, K. Ribbeck, *Biomacromolecules* **2013**, *14*, 3010.
[55] W. Kafienah, J. D. Buttle, D. Burnett, P. A. Hollander, *Biochem. J.* **1998**, *330*, 897.
[56] G.-A. Junter, P. Thébault, L. Lebrun, *Acta Biomater.* **2016**, *30*, 13.
[57] G. A. Carlson, J. L. Dragoo, B. Samimi, D. A. Bruckner, G. W. Bernard, M. Hedrick, P. Benhaim, *Biochem. Biophys. Res. Commun.* **2004**, *321*, 472.
[58] J. E. Rayahin, J. S. Buhrman, Y. Zhang, T. J. Koh, R. A. Gemeinhart, *ACS Biomater. Sci. Eng.* **2015**, *1*, 481.
[59] B. Saleh, H. K. Dhaliwal, R. Portillo-Lara, E. Shirzaei Sani, R. Abdi, M. M. Amiji, N. Annabi, *Small* **2019**, *15*, 1902232.
[60] Z. Li, K. M. Bratlie, *Macromol. Biosci.* **2021**, *21*, 2100031.
[61] H. Yan, M. Hjorth, B. Winkeljann, I. Dobryden, O. Lieleg, T. Crouzier, *ACS Appl. Mater. Interfaces* **2020**, *12*, 19324.
[62] E. Nyman, J. Henricson, B. Ghafouri, C. D. Anderson, G. Kratz, *Plast. Reconstr. Surg. Global Open* **2019**, *7*, 2221.
[63] M. G. Neuman, R. M. Nanau, L. Oruña-Sanchez, G. Coto, *J. Pharm. Pharm. Sci.* **2015**, *18*, 53.
[64] A. Fallacara, S. Vertuani, G. Panozzo, A. Pecorelli, G. Valacchi, S. Manfredini, *Molecules* **2017**, *22*, 2104.
[65] Y. Ma, J. Yao, Q. Liu, T. Han, J. Zhao, X. Ma, Y. Tong, G. Jin, K. Qu, B. Li, F. Xu, *Adv. Funct. Mater.* **2020**, *30*, 2001820.
[66] B. Xu, A. Li, R. Wang, J. Zhang, Y. Ding, D. Pan, Z. Shen, *Adv. Funct. Mater.* **2021**, *31*, 2105265.
[67] Z. Ni, H. Yu, L. Wang, X. Liu, D. Shen, X. Chen, J. Liu, N. Wang, Y. Huang, Y. Sheng, *Adv. Healthcare Mater.* **2022**, *11*, 2101421.
[68] N. Pandey, A. Hakamivala, C. Xu, P. Hariharan, B. Radionov, Z. Huang, J. Liao, L. Tang, P. Zimmern, K. T. Nguyen, Y. Hong, *Adv. Healthcare Mater.* **2018**, *7*, 1701069.
[69] L. Han, M. Wang, P. Li, D. Gan, L. Yan, J. Xu, K. Wang, L. Fang, C. W. Chan, H. Zhang, H. Yuan, X. Lu, *ACS Appl. Mater. Interfaces* **2018**, *10*, 28015.
[70] H.-J. Park, Y. Jin, J. Shin, K. Yang, C. Lee, H. S. Yang, S.-W. Cho, *Biomacromolecules* **2016**, *17*, 1939.
[71] H. Jung, M. K. Kim, J. Y. Lee, S. W. Choi, J. Kim, *Adv. Funct. Mater.* **2020**, *30*, 2004407.
[72] D. Zhou, S. Li, M. Pei, H. Yang, S. Gu, Y. Tao, D. Ye, Y. Zhou, W. Xu, P. Xiao, *ACS Appl. Mater. Interfaces* **2020**, *12*, 18225.
[73] X. Fan, Y. Fang, W. Zhou, L. Yan, Y. Xu, H. Zhu, H. Liu, *Mater. Horiz.* **2021**, *8*, 997.
[74] K. Boettcher, B. Winkeljann, T. A. Schmidt, O. Lieleg, *Biotribology* **2017**, *12*, 43.
[75] C. A. Rickert, B. Wittmann, R. Fromme, O. Lieleg, *ACS Appl. Mater. Interfaces* **2020**, *12*, 28024.
[76] C. Kimna, B. Winkeljann, J. Song, O. Lieleg, *Adv. Mater. Interfaces* **2020**, *7*, 2000735.

[77] J. Shin, J. S. Lee, C. Lee, H.-J. Park, K. Yang, Y. Jin, J.i H. Ryu, K. S. Hong, S.-H. Moon, H.-M. Chung, H. S. Yang, S. H. Um, J.-W. Oh, D.-I. Kim, H. Lee, S.-W. Cho, *Adv. Funct. Mater.* **2015**, *25*, 3814.
[78] B. Winkeljann, A. B. Bussmann, M. G. Bauer, O. Lieleg, *Biotribology* **2018**, *14*, 11.
[79] S. H. Tan, N.-T. Nguyen, Y. C. Chua, T. G. Kang, *Biomicrofluidics* **2010**, *4*, 032204.
[80] D. T. Eddington, J. P. Puccinelli, D. J. Beebe, *Sens. Actuators, B* **2006**, *114*, 170.
[81] S. Raymentl, G. Liul, *J. Dent. Res.* **2000**, *79*, 1765.

A.2.1.2 Supplementary Information

ADVANCED FUNCTIONAL MATERIALS

Supporting Information

for *Adv. Funct. Mater.*, DOI: 10.1002/adfm.202105721

Multifunctional "Janus-Type" Bilayer Films Combine Broad-Range Tissue Adhesion with Guided Drug Release

*Ceren Kimna, Maria G. Bauer, Theresa M. Lutz, Salma Mansi, Enes Akyuz, Zuleyha Doganyigit, Percin Karakol, Petra Mela, and Oliver Lieleg**

Supplemental information

for

Multifunctional 'Janus-type' bilayer films combine broad-range tissue adhesion with guided drug release

Ceren Kimna [1,2], Maria G. Bauer [1,2], Theresa M. Lutz [1,2], Salma Mansi [3], Enes Akyuz [4], Zuleyha Doganyigit [5], Percin Karakol [6], Petra Mela [3], and Oliver Lieleg [1,2,*]

[1] School of Engineering and Design, Department of Materials Engineering, Technical University of Munich, Boltzmannstraße 15, 85748 Garching, Germany
[2] Center for Protein Assemblies (CPA), Technical University of Munich, Ernst-Otto-Fischer Straße 8, 85748, Garching, Germany
[3] Medical Materials and Implants, Department of Mechanical Engineering and Munich School of Bioengineering, Technical University of Munich, Boltzmannstraße 15, 85748 Garching, Germany
[4] University of Health Sciences, Faculty of Medicine, Department of Biophysics, Istanbul, Turkey
[5] Yozgat Bozok University, Faculty of Medicine, Department of Histology and Embryology, Yozgat, Turkey
[6] University of Health Sciences, Sisli Hamidiye Etfal Research and Training Hospital, Department of Plastic Reconstructive and Aesthetic Surgery, Istanbul, Turkey

*corresponding author

Prof. Dr. Oliver Lieleg
Center for Protein Assemblies (CPA),
Technical University of Munich,
Ernst-Otto-Fischer Straße 8, 85748 Garching, Germany

e-mail: oliver.lieleg@tum.de,
phone: +49 89 289 10952, fax: + 49 89 289 10801

1. Mucin purification

Porcine gastric mucin MUC5AC was purified manually as described previously[1]. In brief, the mucus content of the pig stomachs was collected by manually scraping the gastric tissue surfaces. The collected mucus was diluted 1:5 in 10 mM sodium phosphate buffer (pH = 7.0) containing 170 mM NaCl and 0.04 % sodium azide (Carl Roth), and then solubilized by stirring at 4 °C overnight. Next, cellular debris was removed *via* two centrifugation steps (30 min at 8,300 g and 45 min at 15,000 g, each step conducted at 4 °C), followed by a final ultracentrifugation step (150,000 g at 4 °C for 1 h). Subsequently, the mucins were purified by size exclusion chromatography using an ÄKTA purifier (GE Healthcare, Munich, Germany) and an XK50/100 column packed with Sepharose 6FF resin (GE Healthcare). The obtained mucin fractions were pooled, dialyzed against ultrapure water, and concentrated by crossflow filtration (MWCO: 100 kDa, Xampler Ultrafiltration Cartridge, GE Healthcare). The concentrate was then lyophilized and stored at -80 °C until further use.

Salivary mucin MUC5B was purified from unstimulated human whole saliva as described previously[2]. Saliva samples were freshly collected in ice-cooled tubes from healthy, non-smoking volunteers (age range: 25-30 years) who refrained from eating and drinking (except water) for one hour before donating saliva. Samples were diluted in ice-cold 10 mM sodium phosphate buffer (pH 7.0, 170 mM NaCl) to a ratio of 1:1 and purified according to the protocol used for MUC5AC as described above.

2. Fluorescence labeling of mucins and bovine serum albumin (BSA)

Purified mucins and a commercially obtained model protein (BSA) were labeled with a fluorescent dye (Atto 488 – carboxy modified, ATTO-TEC GmbH, Siegen, Germany) *via* carbodiimide coupling. The dye solution was first diluted in 1 mL MES buffer (10 mM, pH = 5) to a concentration of c_{ATTO} = 1.0 mg/mL. Afterwards, 5 mM EDC and 5 mM sulfo-NHS were added to this solution, and the mixture was allowed to incubate in the dark at RT for 3 h. This prolonged incubation time ensured that the remaining free EDC was hydrolyzed before mucin (or BSA) was added. In parallel, 40 mg of purified MUC5AC (or BSA) were dissolved in 19 mL PBS (10 mM, pH = 7). Then, the two solutions were thoroughly mixed and incubated at RT for 3 h. The mixture was dialyzed against ultrapure water (Spectrum™ Spectra/Por™ Float-A-Lyzer™ G2, MWCO: 300 kDa, Roth) to remove any unbound dye molecules. Finally, the labeled samples were lyophilized and stored at -80 °C until further use.

3. Topographical characterization of the fibrous layer

The surface topography of bilayer film was quantified by confocal laser scanning microscopy (using a Keyence VK-X1100 microscope equipped with a 20x lens; Keyence Corporation, Osaka, Japan). The acquired images were analyzed using the software µsoft (NanoFokus AG, Oberhausen, Germany). Images obtained from the fibrous mucin/PVA surface were first corrected for surface tilt by applying a first-grade polynomial filter. Then, three standardized surface roughness parameters were calculated according to ISO 25178-2: the root mean square height (S_q), the developed interfacial area ratio (S_{dr}), and the texture aspect ratio (S_{tr}):

- The root mean square value (S_q): This value is defined as the standard deviation of the measured height z in the xy-plane of the analyzed area A. This parameter can be calculated as:

$$S_q = \sqrt{\frac{1}{A}\iint_A \left(z(x, y)\right)^2 dxdy} \tag{3.1}$$

- The developed interfacial ratio value (S_{dr}): This parameter describes the complexity of a surface by comparing the actual surface and the projected surface. This value is calculated as:

$$S_{dr} = \frac{1}{A}\left[\iint_A \left(\sqrt{1 + \left(\frac{\partial z(x, y)}{\partial x}\right)^2 + \left(\frac{\partial z(x, y)}{\partial y}\right)^2} - 1\right) dxdy\right] \tag{3.2}$$

- The isotropy of a surface (S_{tr}): This parameter is defined as the ratio of the minimum autocorrelation length in any direction and the maximum autocorrelation length in any direction. Thus, this parameter can be calculated from the autocorrelation function (ACF) as:

$$S_{tr} = \frac{\min\limits_{(\tau x, \tau y)\in R} \sqrt{\tau x^2 + \tau y^2}}{\max\limits_{(\tau x, \tau y)\in Q} \sqrt{\tau x^2 + \tau y^2}} \text{ with } \begin{matrix} R = \{(\tau x, \tau y) : ACF(\tau x, \tau y) \le 0.2\} \\ Q = \{(\tau x, \tau y) : ACF(\tau x, \tau y) > 0.2\} \end{matrix} \tag{3.3}$$

$$ACF(\tau x, \tau y) = \frac{\iint_A z(x, y) z(x - \tau x, y - \tau y)\, dxdy}{\iint_A z^2(x, y)\, dxdy} \tag{3.4}$$

Results obtained with this metrological analysis of topographical images are compiled in **Figure S1**.

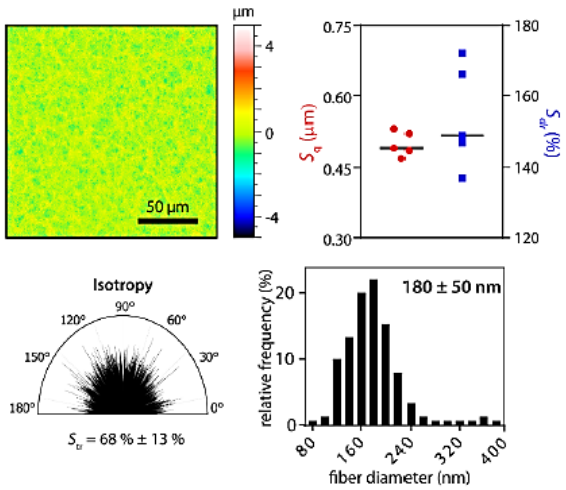

Figure S1. Topographical analysis of the fibrous, non-adhesive layer generated from a mucin/PVA mixture. The horizontal lines represent the mean values of S_q and S_{dr}, respectively, whereas the symbols denote results obtained from n = 5 independent samples. The good isotropy of the surface (bottom, left) and the homogeneous size distribution (bottom, right) of the PVA/mucin nanofibers as obtained by topographical analyses and SEM imaging, respectively, verify the excellent reproducibility of the film manufacturing procedure. n = 150 nanofibers were analyzed to determine the distribution of the fiber diameters.

4. Viscoelastic properties of the bilayer film

The viscoelastic properties of both, monolayer d-HA and bilayer films were determined using a commercial shear rheometer (MCR302, Anton Paar) equipped with a plate-plate measuring system (PP25, Anton Paar, Graz, Austria). For this set of experiments, circular films ($d = 25$ mm) were generated and placed onto the stationary bottom plate of the rheometer, where they were hydrated with 250 µL PBS *in situ*. Then, the measuring head was lowered to the measuring position, which was set to 500 µm for all measurements. A humidity chamber was installed to avoid evaporation of the hydration buffer, and the temperature was set to 37 °C. A torque-controlled ($M = 0.5$ µNm) frequency sweep (f_{start} = 0.1 Hz to f_{end} = 10 Hz) was performed to determine the frequency-dependent viscoelastic properties of the samples (**Figure S2**).

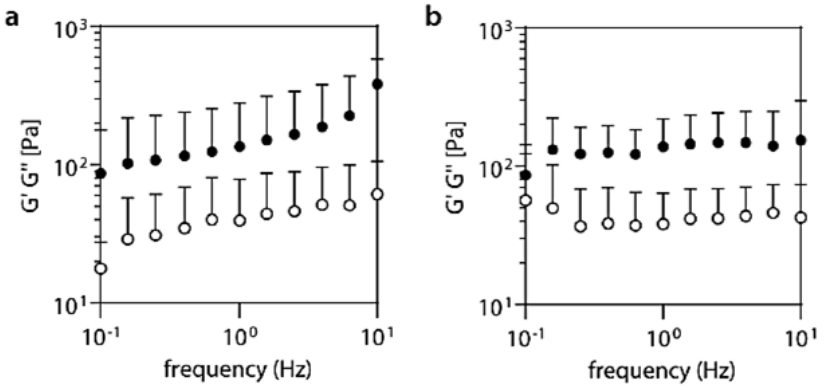

Figure S2. Viscoelastic properties of monolayer d-HA **(a)** and bilayer films **(b).** When hydrated, both variants behave as viscoelastic solids dominated by elastic properties (*i.e.*, the storage modulus *G'*). Data shown represent mean values; error bars denote the standard deviation as obtained from $n = 5$ independent samples.

5. Projected area of films after exposure to tribological stress

Table S1: Projected area (mm²) of four film sample sets (S1-S4) as determined after exposure to tribological stress; the data was determined with the software ImageJ for four independent d-HA and bilayer films each.

	d-HA	bilayer
S1	111.584	82.170
S2	120.515	93.449
S3	114.832	80.929
S4	102.398	89.839

6. Control experiments to confirm unidirectional drug release

To confirm the unidirectional release of drugs from bilayer films, control experiment were conducted, where the PVA/mucin layer was facing the semi-permeable membranes (see the main manuscript for experimental details). The obtained results are depicted in **Figure S3**.

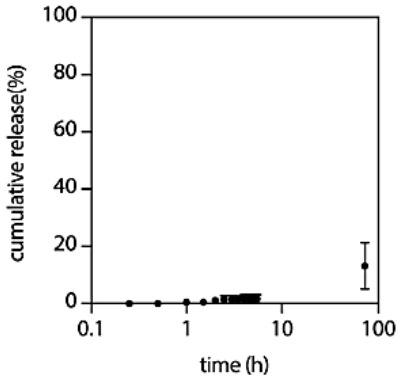

Figure S3. Control drug release experiment where the PVA/mucin non-adhesive layer is facing the semi-permeable membrane. Data shown represents mean values; error bars denote the standard deviation as obtained from $n = 7$ independent samples.

7. Cytotoxicity tests

To evaluate the putative cytotoxic effects of both, film surface and the degradation products occurring during the disintegration of the bilayer film, HeLa cells were seeded onto each surface of the bilayer film and subjected to Live/Dead assay (**Figure S4a**), and incubated with an extraction medium (*i.e.*, the culture medium, in which the films were incubated for 24 h) and then subjected to a colorimetric WST-1 cytotoxicity test (**Figure S4b**). This method follows the ISO 10993 standard.

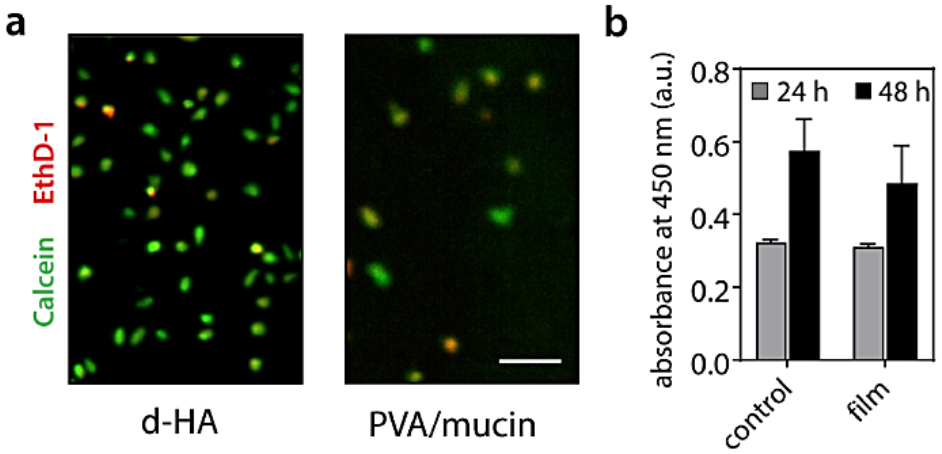

Figure S4. (a) Fluorescence microscopy images of HeLa cells (stained with dyes from a classical live/dead assay; scale bar: 100 µm. **(b)** *In vitro* cytotoxicity test of the degradation products generated by the decomposing bilayer film. Measurements were conducted after 24 and 48 h of incubation, respectively. Data shown represents mean values; error bars denote the standard deviation as obtained from $n = 5$ independent samples.

HeLa cells were cultivated as described in the main text, harvested, seeded into the wells of a 96-well plate (5,000 cells/well), and incubated for 24 h. Then, bilayer films were incubated in MEM medium for 24 h to allow for putative leeching effects to take place and afterwards sterilized by filtration. Then, the cell cultivation medium from the 96-well plate was replaced with this sterilized 'leeching' medium; cells incubated in fresh MEM were used as a control group. Cell viability was evaluated with a colorimetric WST-1 assay (2% v/v, Sigma Aldrich) after 24 and 48 h of incubation, respectively. The

absorbance of the medium was determined at a wavelength of 450 nm using a microplate reader (Viktor3, Perkin Elmer, Rodgaum, Germany). Results obtained with this assay show that the signal obtained for cells exposed to this 'leeching medium' was not significantly different compared to that of the control group (**Figure S4b**). This indicates that neither the bilayer film nor its degradation products entail measurable cytotoxic effects.

8. *Ex vivo* detachment tests with porcine cornea tissue samples

The effect of dopamine conjugation to hyaluronic acid on the mechanical properties of monolayer films was tested with porcine cornea samples as described in the section 'Tissue adhesion/detachment tests' of the main text. As depicted in **Figure 54,** the performance of different bilayer film variants was quite different: The data shows, that the good adhesive properties of the bilayer construct are indeed brought about by the dopamine groups that were conjugated to HA:

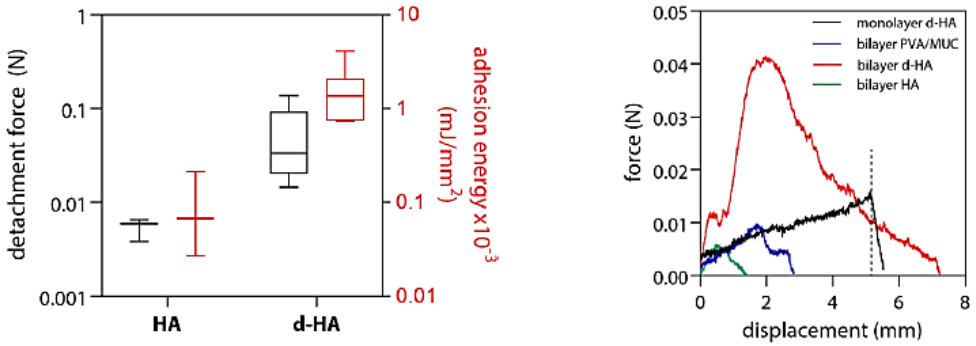

Figure 54. Detachment force (N) and adhesion energy (mJ/mm²) values as obtained for HA-PVA/MUC and d-HA/PVA/MUC bilayer films, respectively (left panel). The exemplary force-displacement curves obtained for different samples (right panel) demonstrate that film constructs making use of d-HA on their adhesive side clearly outperform the other groups.

9. Surface characterization of porcine cornea tissue by confocal laser scanning microscopy

To compare the surfaces of untreated and bilayer film-treated cornea tissues, the following additional metrological parameters (which are also defined in ISO 25178-2) were used:

- The maximum peak height (S_p): This parameter describes the height of the highest peak within the analyzed area.

$$S_p = \max z(x,y) \tag{3.5}$$

- The root mean square gradient (S_{dq}): This value represents the root mean square of slopes determined at all points in the analyzed area.

$$S_{dq} = \sqrt{\frac{1}{A}\iint_A \left[\left(\frac{\partial z(x,y)}{\partial x}\right)^2 + \left(\frac{\partial z(x,y)}{\partial y}\right)^2\right] dxdy} \tag{3.6}$$

6

- The arithmetic mean peak curvature (S_{pc}): This parameter quantifies the arithmetic mean of the principal curvature of the peaks on the surface.

$$S_{pc} = -\frac{1}{2}\frac{1}{n}\sum_{k=1}^{n}\left(\frac{\partial^2 z(x,y)}{\partial x^2}+\frac{\partial^2 z(x,y)}{\partial y^2}\right) \quad (3.7)$$

- The peak material volume ($V_{m(p)}$): This value represents the material volume of peaks at an areal material ratio of p = 10 %.

$$V_{m(p)} = \int_0^p \big(z(x) - z(p)\big)dx \quad (3.8)$$

- The dale void volume (V_w): This value represents the void volume of dales at an areal material ratio between p = 80 % and 100 %.

After applying the Gaussian filter (as described in the Methods section), the metrological parameters listed above were calculated for each group, *i.e.*, for untreated (= control group) and film-treated eyes, and both, before and after 3 days of incubation. The obtained results are compiled in **Table S2** and **Figure S6**.

Table S2. Metrological parameters used to quantify the effect of bilayer film treatment on the surface integrity of porcine cornea samples. Data shown represent mean values and error bars denote the standard deviation as obtained from $n = 5$ independent samples.

Parameters analyzed		Control group		Film treated group	
		before	after	before	after
S_q	[µm]	0.21 ± 0.06	0.24 ± 0.04	0.16 ± 0.06	0.20 ± 0.04
S_p	[µm]	3.4 ± 1.6	3.1 ± 0.8	2.3 ± 0.9	3.1 ± 0.8
S_{dr}	[%]	0.01 ± 0.01	0.01 ± 0.01	0.002 ± 0.01	0.01 ± 0.01
S_{dq}	[-]	0.11 ± 0.04	0.14 ± 0.04	0.06 ± 0.02	0.12 ± 0.02
S_{pc}	[1/µm]	228 ± 110	281 ± 102	103 ± 63	205 ± 58
V_m	[µm³ /µm²]	0.02 ± 0.01	0.02 ± 0.01	0.01 ± 0.01	0.01 ± 0.01
V_{vv}	[µm³ /µm²]	0.03 ± 0.01	0.03 ± 0.01	0.02 ± 0.01	0.02 ± 0.01

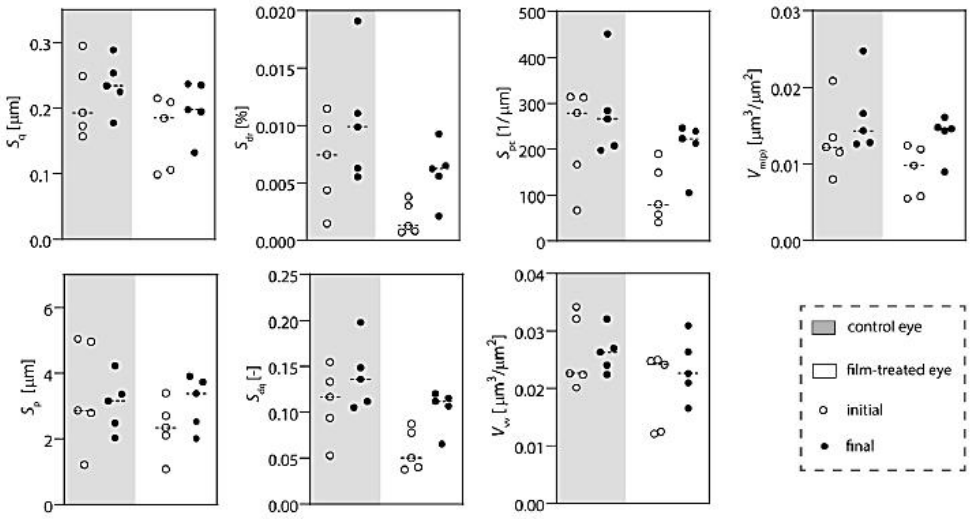

Figure S6. Topographical analyses of eye samples after bilayer film treatment for 3 days. The horizontal lines represent the mean values; open and closed circles represent the average value of five individual measurements conducted per sample. Data was acquired from five independent eye samples per group.

10. Additional information regarding the mechanical characterization tests

Setup used for the stretching tests:

Figure S7. Experimental setup used to determine the tensile strength of the films.

The bonding strength between the two interfaces was tested using samples that comprise a bilayer structure in the center (red) and monolayers of either d-HA (pink) or PVA/mucin (purple) at each end (**Figure S8**). To stabilize the monolayers for these stretching tests, a piece of laboratory wipe (~1 cm^2)

covered in nail polish was wrapped around each monolayer end, and the samples were allowed to dry overnight prior to mechanical testing. In each test, film rupture took place in the monolayer region, which shows that the bonding strength between the two layers of the bilayer construct is high.

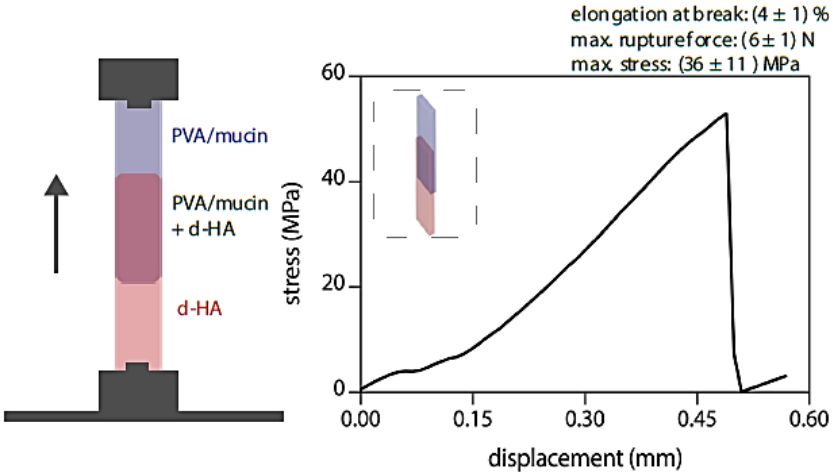

Figure S8. Schematic representation of partially overlapping bilayer film constructs fabricated to conduct bonding strength tests (left). An exemplary stress – distance curve obtained for such samples is shown on the right. Experiments were conducted as described in section 'mechanical characterization' of the main text using a total of $n = 8$ samples.

11. Quantification of drug release

A standard curve of the antibiotic TCL (**Figure S9**) was determined to convert the amount of drug release from the d-HA layer of the film into absolute concentration values. To do so, the absorbance of serially diluted TCL solutions was measured at 360 nm using a spectrometer (specord 210, Analytikjena, Jena, Germany). The concentration range, in which a linear relation was obtained, was then used to determine the drug concentration in the release medium (see the Methods section of the main text for details).

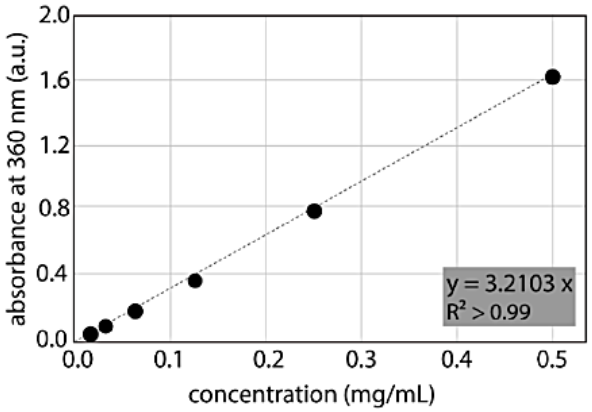

Figure S9. Tetracycline hydrochloride (TCL) standard curve as determined from serial dilutions of TCL.

12. *In vivo* wound healing experiments and histological assessments

The individual steps of *in vivo* wound healing experiments are shown in **Figure S10.** The applied procedures are described in detail in the main text.

1. Preparing the animals for the surgery and subsequent wound infliction

2. Placing a film onto one wound while keeping the other one untreated

3. Taking biopsies on days 0, 3, 7 and 14 for histological analysis

4. Observing the tissue closure (day 14)

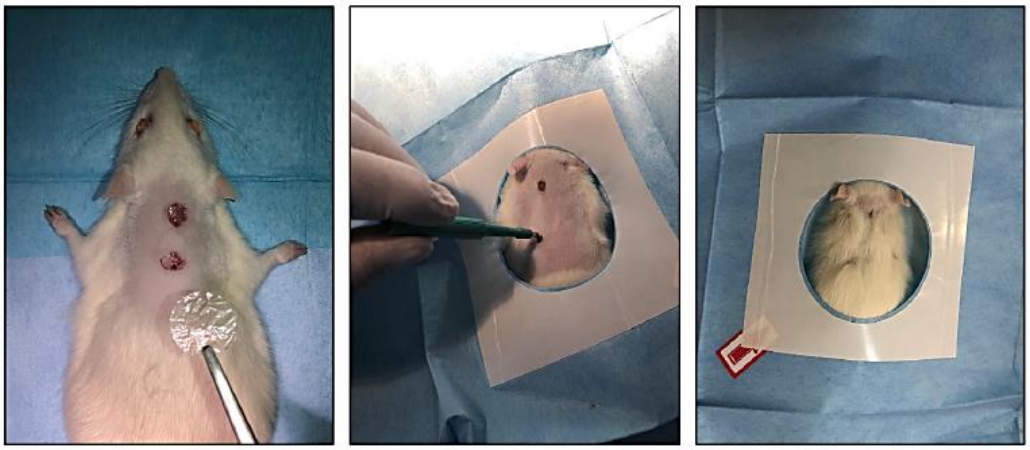

Figure S10. Macroscopic photographs documenting the procedure of the *in vivo* wound healing experiments.

In addition to the histological images shown in the main text, H&E and Masson's trichrome stained tissue samples (acquired on the 3rd and 7th postoperative day) are depicted in **Figure S11**. Since keratohyalin granules are present in the epidermis epithelium, it can be concluded that, for both groups (wounds treated with unloaded Janus-type bilayer film and wounds treated with drug-loaded films), reepithelization began before day 3. Histologically, a full recovery is observed for both film-treated wound types from the 7th day on.

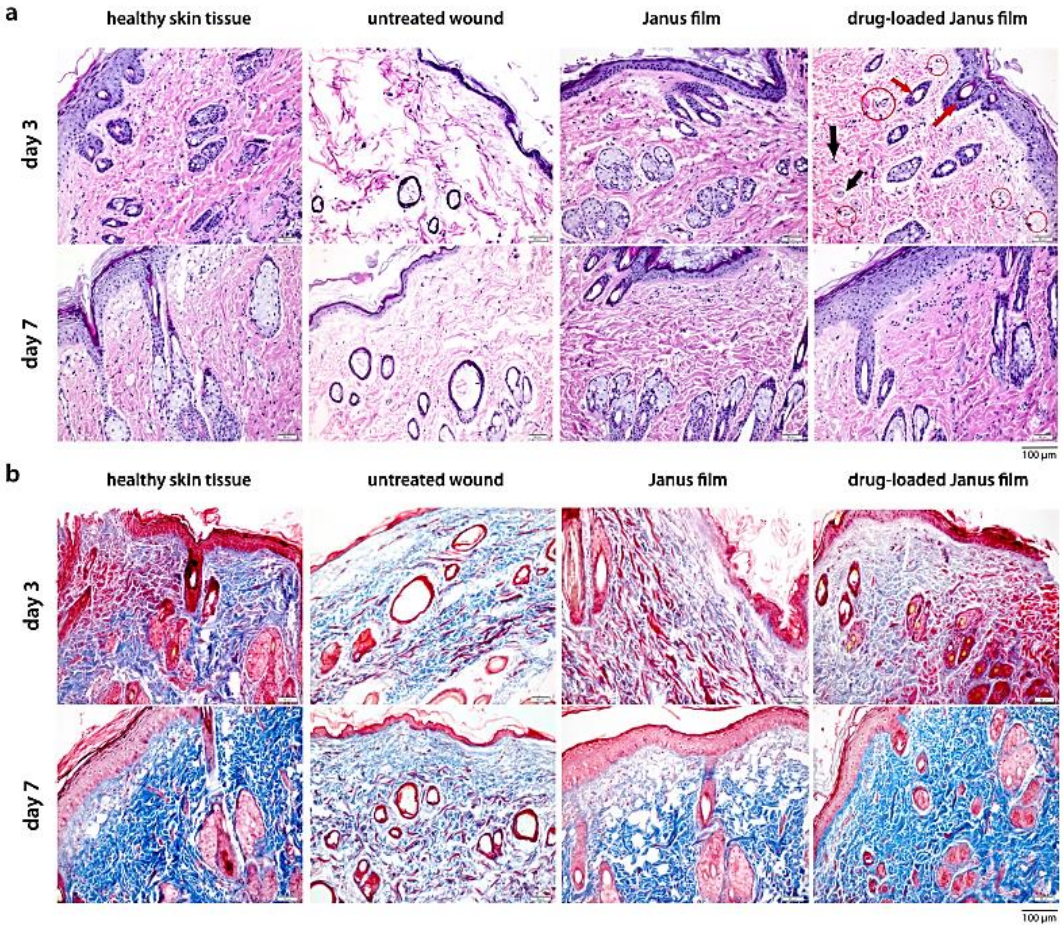

Figure S11. H&E **(a)** and Masson's trichrome **(b)** stained tissue sections taken on day 3 and day 7 post-surgery. The symbols in the upper right picture indicate specific tissue compartments as follows: black arrow: healthy corpuscles; red arrow: hair follicles; red circles: blood vessels. The scale bars denote 100 µm and apply to all images shown in this figure.

References

1 Schömig, V. J. *et al.* An optimized purification process for porcine gastric mucin with preservation of its native functional properties. *RSC Advances* **6**, 44932-44943 (2016).

2 Marczynski, M. *et al.* Charged glycan residues critically contribute to the adsorption and lubricity of mucins. *Colloids and Surfaces B: Biointerfaces* **187**, 110614 (2020).

3 van de Vyver, M. *et al.* Histology Scoring System for Murine Cutaneous Wounds. *Stem Cells Dev* **30**, 1141-1152, doi:10.1089/scd.2021.0124 (2021).

4 Gupta, A. & Kumar, P. Assessment of the histological state of the healing wound. *Plastic and Aesthetic Research* **2**, doi:10.4103/2347-9264.158862 (2015).

A.2.2 "Wetting Behavior and Stability of Surface-Modified Polyurethane Materials"

Received: 5 August 2021 | Revised: 7 September 2021 | Accepted: 10 September 2021

DOI: 10.1002/ppap.202100126

RESEARCH ARTICLE

PLASMA PROCESSES AND POLYMERS

Wetting behavior and stability of surface-modified polyurethane materials

Maria G. Bauer[1,2] | **Rosa Reithmeir**[1,2] | **Theresa M. Lutz**[1,2] | **Oliver Lieleg**[1,2]

[1]Department of Mechanical Engineering and Munich School of Bioengineering, Technical University of Munich, Garching, Germany

[2]Center for Protein Assemblies (CPA), Garching, Germany

Correspondence
Oliver Lieleg, Department of Mechanical Engineering and Munich School of Bioengineering, Technical University of Munich, Boltzmannstraße 11, 85748 Garching, Germany.
Email: oliver.lieleg@tum.de

Funding information
H2020 Future and Emerging Technologies, Grant/Award Number: 863183

Abstract

Even though polyurethanes (PU) constitute a class of highly versatile and customizable polymeric materials, being able to modify their surface properties, for example, their wettability, without altering the composition of the bulk material would often be desirable. However, PU-based materials can be both rather diverse and resilient to chemical modification. Thus, in this study, three PU variants are subjected to three different treatments that aim at altering the wetting properties of the materials: We assess the feasibility of plasma treatment, dopamine incubation, and chemical etching, and evaluate the stability of the obtained surface modifications with regard to wet and dry storage, UV exposure, and application-specific properties such as lubricity and colonization with eukaryotic cells. The results obtained here can be used to achieve an additional customization of PU surfaces to tailor their behavior for selected applications where dedicated surface properties are required.

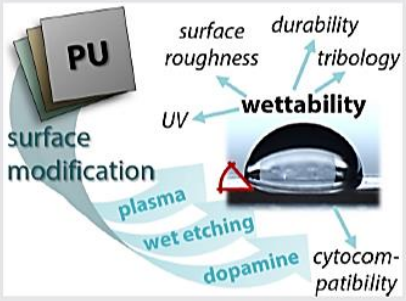

KEYWORDS
dopamine deposition, oxygen plasma treatment, polyurethanes, surface modification, water contact angle

1 | INTRODUCTION

The term polyurethane (PU) summarizes a large range of versatile and structurally diverse materials. Most PUs show interesting mechanical, physical, and chemical behaviors, and they can combine competing properties such as high robustness and strong flexibility. A chemical feature that all these materials share is a urethane group (–NH–CO–O–) as the major repeating motif in their backbone structure. To fit different requirements, PU-based materials can be tailored in terms of chemistry (by varying the type and degree of cross-linking) and appearance (they can be manufactured into solid materials, soft/hard foams, foils, adhesives, and coatings);

accordingly, the range of applications that PU materials can be used for is vast[1]: Examples range from technical applications in automotive and (aero)nautic industries (e.g., seating, instrument panels, chemically resistant/protective coatings),[2] over building and construction applications (e.g., thermal and acoustic insulators, floors, multi-material glues),[3] and everyday products (e.g., shoe soles, cushions)[4] to single-use (e.g., wound dressings, urinary catheters, hemodialysis tubes) and high-performance medical devices (such as cardiovascular implants).[5]

In some of these applications, a good interaction of the material with an aqueous environment, that is, hydrophilic properties, would be desirable. In biomedical applications, good wetting behavior is often related to, for example, enhanced interaction with cells and good biocompatibility of the material.[6] For technical and industrial applications, good interactions of polymeric materials with aqueous solutions are often required when preparing them for printing or coating and/or to improve their adhesive properties for optical, protective, or other functional layers/additives.[7]

However, as PU variants can be rather hydrophobic, this calls for a modification process that maintains the other highly interesting properties of PU materials. Accordingly, surface modification procedures appear to be most suitable to achieve this goal—altering the chemical properties of the PU polymers themselves before material generation would be likely to change the bulk behavior of the materials as well, and this is not desired.

A range of surface treatment procedures for polymeric materials have been reported in the literature; among those, some of the most prominent strategies are plasma treatment, chemical etching, and dopamine treatment. The phrase "plasma treatment" summarizes numerous methods/processes that generate (partially) ionized gas and/or radicals, which are frequently applied to various materials for surface modification, for example, for surface hydrophilization.[8,9] However, plasma processes often require specialized devices to provide either low ambient pressure (or even vacuum)[8] or high treatment temperatures (greater than or equal to several hundred degrees Celsius)[9], and these harsh conditions are not always suitable. For instance, when the inside of a hollow, flexible sample (like a balloon) or temperature-sensitive materials (i.e., most polymeric materials based on, e.g., polymethylmethacrylate, polystyrene, or polyvinylchloride) is to be treated, a different approach needs to be chosen. Similarly, for complexly shaped or porous samples, achieving a homogenous plasma treatment of the whole surface can be difficult,[10] especially when short exposure times (~10 s to 5 min), as typical for plasma activation of (polymeric) surfaces, are selected.[11] Conversely, longer exposure times can lead to undesired etching effects becoming dominant on the surfaces,[12,13] which can induce damage, especially to fragile objects or thin structures.

A second strategy to hydrophilize the surface of a material, which, in terms of its mechanistic working principle, is closely related to plasma activation, is chemical etching with fluids. Here, the samples are exposed to certain aggressive basic or acidic solutions, which modify the surface by creating new functional groups. Thus, similar to plasma treatment, also here, suitable conditions need to be identified that achieve the desired surface activation without damaging the material.[14]

Such issues should, however, not occur when dopamine treatment is used to alter the surface properties of a material. This solution-based, additive process was first introduced in 2007.[15] Here, under atmospheric conditions, dopamine molecules polymerize in basic solutions (pH ~8.5) and this leads to the deposition of a thin layer of (poly)dopamine onto the surface of a material exposed to such a dopamine solution. Even though the detailed mechanisms driving this layer formation are not fully understood yet (despite extensive studies),[16,17] it was shown that this strategy can be successfully applied to a broad range of materials including metals, glass, ceramics, and different polymeric materials.[15]

Here, we show that the efficiency of different surface modifications, which aim at improving the interaction of PU materials with aqueous solutions, varies with the type of PU. We compare the effect of plasma treatment, chemical etching, and dopamine treatment on the wettability of the different materials and evaluate the stability of these treatments after material storage under selected conditions. Additionally, the treated samples are evaluated after certain application-related challenges, that is, after disinfection with UV light, colonization with eukaryotic cells, and exposure to tribological load. Our results show that, depending on the desired application area, different surface treatment variants can fulfill the desired requirements for the PU materials tested here.

2 | EXPERIMENTAL SECTION

2.1 | PU materials

In this study, three different kinds of PU samples were investigated: first, the technical, elastomeric polyurethane THOMAPLAST®-PUR (PUR; Reichelt Chemietechnik GmbH + Co.) and second, two medical-grade polycarbonate-based thermoplastic PUs: the aliphatic Carbothane™ PC-3575A (PC; Lubrizol Advanced Materials [LAM]) and the aromatic Carbothane™ AC-4095A

(AC; LAM). PUR samples were commercially available in flat sheets with a thickness of 2 mm. In contrast, the material samples obtained from LAM had the form of thin, extruded films (thickness: 176 μm for PC and 250 μm for AC). These samples were provided to our project partners at the Fraunhofer Institute for Manufacturing Engineering and Automation who forwarded them to us to conduct surface modification tests with.

For cell culture tests and tribology measurements, round samples with diameters of 6 and 7 mm, respectively, were prepared. For all the other tests, rectangular samples with a size of ~1 cm^2 were used. Before any tests, all samples were thoroughly cleaned with 80% ethanol (EtOH; Carl Roth GmbH + Co. KG) and ultrapure water (ddH_2O), and then dried at room temperature overnight.

2.2 | Surface modifications

Three different surface treatment strategies were applied to improve the wettability of the materials and thus to enhance their performance for applications in aqueous environments.

2.2.1 | Oxygen plasma treatment

For plasma treatment, a commercial plasma system (Femto Model 1 base unit type B; Diener electronic GmbH & Co. KG) was used to facilitate the reproducibility of the process. This device uses a reactive-ion etching system to generate plasma at low pressure and ambient temperature; the usable power ranges from 0 to 100 W at a generator frequency of 40 kHz, and the cylindrical vacuum chamber has a volume of ~2 L. For treatment, the samples (prepared as described under Section 2.1) were placed onto a glass specimen carrier to (electrically) isolate them from the rest of the vacuum chamber. The chamber was then evacuated for ~5 min, and the desired low pressure of 0.4 mbar was obtained by manual adjustment via a needle valve. As the PU samples were—for practical reasons—simply dried under ambient conditions and the low pressure was established comparably quickly, the occurrence of residues of atmospheric air or water within the chamber or on the sample surface cannot be fully excluded. Then, the chamber was flushed with oxygen and the plasma was ignited. Based on a previously published process[18] used to activate different polymeric materials, plasma was generated for 90 s using the above-mentioned parameters. During this time span, fresh oxygen was constantly provided and ionized, and the used plasma/gas was removed by the vacuum system to maintain a steady and sufficient amount of unreacted oxygen plasma. The treated samples were used directly once the plasma treatment process had finished. Only the upper sample surfaces, where the nonpolar methyl groups could be reached by the plasma and thus converted into (mainly) hydroxy groups, were used for any further investigations.

2.2.2 | Dopamine treatment

For dopamine treatment, 0.4% (w/v) dopamine hydrochloride (Sigma-Aldrich Inc.) was dissolved in a buffer solution containing 20 mM HEPES (4-(2-hydroxyethyl)-1-piperazineethanesulfonic acid; Roth) and 154 mM sodium chloride (NaCl; Roth) adjusted to a pH value of 8.5. Under basic pH conditions, dopamine immediately starts to polymerize and deposit/adhere onto contact surfaces; this property can be used to generate a polydopamine layer on a broad range of materials by simply immersing the object into such a dopamine solution. Here, for practical reasons, always two samples (with their back sides aligned) were placed—standing upright—into a well of a 48-well plate. Then, the well was filled with ~1 ml of the dopamine solution until the samples were entirely covered. Subsequently, the samples were incubated on a slowly moving tilting shaker at room temperature for 3 h. Afterward, unbound dopamine molecules were removed by rinsing with ddH_2O, and the dopamine-treated samples were either directly used (if "wet" storage conditions were analyzed) or dried at room temperature overnight (if "dry" storage conditions were tested).

Since polydopamine tends to agglomerate into big particles (with sizes up to several micrometers), this could lead to inhomogeneous layers on the material surfaces and thus to unreproducible behavior of dopamine-treated samples. To avoid this, two different strategies were implemented here. First, as polydopamine agglomeration is a time-dependent process, the degree of dopamine polymerization was minimized by shortening the storage time of freshly prepared dopamine solutions as much as possible; this was achieved by dissolving the dopamine just before use (in this manuscript, this approach is referred to as "dopa-direct"). However, in such a short time, a fully homogeneous dopamine solution cannot be generated; because of this, variations in dopamine concentrations between different wells cannot be ruled out. The second approach is based on the scientific consensus that dopamine polymerization is initiated by oxidation processes.[19] Accordingly, here, we limited sample access to atmospheric oxygen. To achieve this, the incubation container was completely filled with the dopamine solution and the

container lid was closed and sealed with a laboratory film. Then, overnight incubation was conducted to allow the solution to equilibrate, while minimizing dopamine polymerization processes (in this manuscript, this approach is referred to as "dopa-overnight").

2.2.3 | Chemical etching

To chemically etch the material surfaces of the three PU variants tested here, each sample was completely immersed into the designated, concentrated acidic solution for 1 min at room temperature. The acidic solutions used here were 96% sulfuric acid (H_2SO_4; Roth) and 65% nitric acid (HNO_3; Roth). Consecutively, the etching reaction was interrupted by dipping the sample into 1 M sodium hydroxide (NaOH; Roth) and rinsing it with ddH_2O. For the subsequent surface analysis tests, the back sides of the samples were dried on a lint-free laboratory wipe; then, the samples were placed onto a glass slide with those back sides facing down.

In addition, as PC and AC are polycarbothane-based materials, for which the literature suggests that NaOH could be a suitable etching medium,[20] 32% NaOH was tested as well. Here, the same technique was used as that described for acidic solutions above, except that 1 M hydrogen chloride (HCl; Roth) was used to interrupt the etching reaction.

Furthermore, the literature suggests that etching of different materials can also be achieved by a mixture containing both an acidic solution and an oxidizing agent.[21] Here, such a mixed solution was prepared by combining 17.8 M H_2SO_4 and 11.6 M hydrogen peroxide (H_2O_2; Merck Chemicals GmbH) in a volume ratio of 3:1, which results in a very aggressive liquid known as "piranha solution." However, as the exposure of the examined materials to such a concentrated piranha solution entailed immediate and direct disintegration of the materials, the samples were instead treated with a diluted piranha solution, based on 5 M H_2SO_4, under constant stirring at 40°C for 5 h.

2.2.4 | Dry and wet reference samples

Here, as we compare a dry surface treatment (plasma treatment) with solution-based surface treatments (dopamine treatment/chemical etching), there are also different control groups to consider to ensure comparability. As "dry reference" samples, pristine, completely untreated materials are used. These serve as reference points for plasma-treated material samples characterized directly after this treatment, or for such samples treated with aqueous solutions, which were dried at room temperature overnight before characterization. In contrast, "wet reference" samples are untreated material samples that were immersed into distilled water for 3 h (this corresponds to the incubation time used for dopamine treatments). Such "wet reference" samples were used as reference points for all other conditions studied here.

2.3 | Storage conditions for stability tests

In addition to assessing the behavior of the PU samples immediately after surface treatment, the durability of the surface treatment was examined as well. Here, once more, two different storage conditions were compared: First, storage under wet (roughly physiological) conditions. Here, each sample was placed into a 24-well plate and the well was filled with 1 ml of Dulbecco's phosphate-buffered saline (DPBS; Sigma-Aldrich). Then, the well plate was stored in an oven at 37°C while avoiding evaporation. The second set of storage tests was conducted under dry conditions. Therefore, samples dried overnight were placed into a 24-well plate, which was stored at 7°C.

2.4 | Surface analysis

2.4.1 | Contact angle (CA) measurements

To determine the wetting behavior of the different PU variants before and after surface treatment, CA measurements were conducted. Therefore, samples were first gently cleaned and dried with particle-free pressurized air. Afterward, a droplet of 8 µl of ddH_2O water was placed onto each sample, and a transversal image of the liquid–solid interface was captured using a high-resolution camera (Point Gray Research). Then, the static CA value was determined using the software ImageJ and the "drop snake" plug-in (both open-source).

2.4.2 | Confocal laser scanning microscopy

Confocal laser scanning microscopy was conducted using a VK-X1000 microscope (Keyence) equipped with a ×50 lens (NA = 0.95; Nikon). Also, here, before performing measurements, all samples were gently cleaned and dried with particle-free pressurized air. Then, the samples were placed onto a glass slide using a droplet of 50 µl of distilled water as a thin spacer. This was necessary to allow the measuring device to automatically differentiate

between the very thin, transparent Carbothane foils and the glass slide. For each material/treatment combination, at least three samples were examined. On each sample, a stitched image was acquired such that a total area of 0.56 mm^2 could be analyzed. For this analysis, the software MultiFileAnalyzer (Keyence) was used. First, sample waviness (a wave form with correction strength 4 out of 20) and a linear tilt were removed from the topographical images. Additionally, to eliminate artifacts originating from the transparent nature of the samples (i.e., unrealistically deep valleys), the obtained profiles were inverted, a height cut (weak level) was applied, and the profiles were inverted back to the original configuration. From the adjusted topographical images, the metrological parameter S_q, the root-mean-square height (based on ISO 25178-2), was calculated as follows:

$$S_q = \sqrt{\frac{1}{A}\iint_A z^2(x,y)dxdy}. \quad (1)$$

Here, A denotes the definition area of the image.

2.5 | Water uptake

To examine the influence of the wet storage condition on the PU materials, water uptake tests were conducted for a time span of 50 days. Therefore, the samples (~1 mm^2) were first dried in a ventilated oven at 40°C for 4 days. Afterward, the initial mass of each sample was determined using a microscale (XSE205 DualRange; Mettler Toledo). Then, the samples were immersed into 1 ml of DPBS and incubated at 37°C while avoiding liquid evaporation. At various time steps, samples were removed from the incubation bath, their surface was dried with a laboratory wipe, and they were weighed again to determine the relative change in mass.

2.6 | UV treatment

For treatment with ultraviolet light, samples were placed in a commercial UV sterilization chamber (BLX-254; Vilber-Lourmat GmbH), working at a wavelength of 254 nm (4 × 8 W), and exposed to UV light for 10 and 30 min, respectively. In Rickert et al.,[22] it was shown that 10 min of direct exposure to UV generated by the very same device is sufficient to disinfect materials. However, here, immersed samples stored in buffer should also be disinfected; thus, the exposure time had to be increased to 30 min to ensure that a sufficient UV intensity reached the surface of the PU samples. To decide if any surface differences detected after UV irradiation were specific to the surface treatment applied before UV exposure or rather material-dependent alterations, both untreated (= control group) and treated (= plasma-treated or dopamine-treated) PU samples were exposed to UV light.

2.7 | In vitro tests with eukaryotic cells

2.7.1 | Cell cultivation

Human epithelial cells (HeLa) were cultured in Minimum Essential Medium Eagle (Sigma-Aldrich) containing 10% (v/v) fetal bovine serum (Sigma-Aldrich), 2 mM L-glutamine solution (Sigma-Aldrich), 1% non-essential amino acid solution (Sigma-Aldrich), and 1% penicillin/streptomycin (Sigma-Aldrich). Incubation was conducted in a humidified environment at 37°C with 5% CO_2.

2.7.2 | Biocompatibility test

Biocompatibility of the different PU sample surfaces was investigated using a water-soluble tetrazolium (WST-1) assay (Sigma-Aldrich). For this purpose, wells of a 96-well plate were filled with two medical-grade PU materials (AC and PC; at least three replicates for each material/surface modification combination). The sample-containing wells were then washed three times with sterile DPBS. Afterward, each sample was incubated with 30 000 cells for 24 h. After this incubation step, all samples were washed with sterile DPBS and, in each well, the buffer was replaced with 200 µl of media supplemented with a 2% (v/v) WST-1 solution. The cells were incubated for 1 h and, after transferring 100 µl from each well into a new plate, the absorption behavior of the solutions was quantified at an excitation wavelength of 450 nm (Varioskan LUX; Thermo Fisher Scientific). In addition, images of the treated cells were recorded on an inverted light microscope (DMi8 Leica; Leica) using phase-contrast settings, a ×10 lens (Leica, A-Plan, ×10/0.25 Ph1), and a digital camera (Orca Flash 4.0 C11440; Hamamatsu).

2.8 | Tribology

2.8.1 | Sample preparation

PUR samples were prepared as rectangular samples with a size of 5 × 12 mm; in this shape, they could be used directly in a ball-on-three-plates geometry making use of a commercial sample holder (Anton Paar). Before the

friction measurements, a subset of the prepared samples was plasma treated (as described above) and another subset was dopamine treated (as described above). To ensure a comparable hydration of the different PU variants, untreated and plasma-treated samples were additionally immersed into ddH_2O for 3 h (this is the same incubation time as that used during the dopamine treatment step).

2.8.2 | Friction measurements

For friction measurements, a commercial shear rheometer (MCR 302; Anton Paar) was equipped with a tribology unit (T-PTD 200; Anton Paar). As a counterpart, steel spheres with a diameter of 12.7 mm (1.4301, $S_q < 0.2\,\mu m$; Kugel Pompel) were used. Three PUR samples were mounted onto the sample holder and covered with 600 µl of 20 mM HEPES buffer (pH 7) as an aqueous lubricant. All tests were performed at a constant temperature of 21°C, and in each test, the sliding velocity was varied from 1000 to 0.1 mm s^{-1}. Measurements were conducted at a constant normal load of $F_N = 6$ N. This normal force was chosen such that, within the accessible speed range, friction in the boundary, mixed, and hydrodynamic regimes could be probed. Based on the Hertzian contact theory,[23] the average contact pressure p_0 was estimated as follows:

$$p_0 = \frac{2}{3}p_{max} = \frac{2}{3\pi}\sqrt[3]{\frac{6 \times F_{N,per\ pin} \times E'^2}{R^2_{sphere}}} \quad \text{with} \quad \frac{1}{E'} = \frac{1-\nu_1^2}{E_1} + \frac{1-\nu_2^2}{E_2}. \tag{2}$$

For steel, Young's modulus of $E_{steel} = 210$ GPa and a Poisson's ratio of $\nu_{steel} \approx 0.3$ were used. However, for PUR, the manufacturer lists neither of those material parameters in the material specification sheets; only the Shore A hardness ($Sh_A = 72$ A) is given. Thus, Young's modulus of PUR was estimated by combining the theory of Boussinesq[24] (which connects the indentation depth into a material with its Young's modulus) with linear correlations derived from the specifications given in the normed protocols to determine the Shore A hardness. Using this approach, the following estimation was obtained:

$$E_{est.} = \frac{1-\mu^2}{2R_{probe}C_1} \times \frac{C_1 + C_2 \times Sh_A}{100 - Sh_A}. \tag{3}$$

Here, $R_{probe} = 0.395$ mm is the radius of the indentation probe used in the hardness test and $C_1 = 0.549$ N, $C_2 = 0.07516$ N, and $C_3 = 0.025$ mm are constants derived from physical specifications of the Shore A hardness test.[25] With these values, an estimated Young's modulus of $\sim E_{PUR} = 8.6$ MPa was obtained. Furthermore, a Poisson's ratio of $\nu_{PU} = 0.45$ was assumed, as $0.4 \leq \nu \leq 0.5$ is typical for flexible (rubber-like) polymers such as elastomeric PUs.[26] Together, this results in an estimated average contact pressure of $p_0 = 0.77$ MPa and a contact area of $a = 0.88\,mm^2$.

2.8.3 | Statistical analysis

Tests for statistical significance were conducted for all quantitative results shown in Figures 1 and 3 as well as for biocompatibility tests shown in Figure 4. Each set of samples was first tested for a normal data distribution using a Lilliefors test; then, a two-sample F test was applied to check for equal variances. To test for significant differences between normally distributed samples, a two-sample t test was applied when homogeneity of variances was confirmed, whereas a Welch's t test was performed for heteroskedastic sets of samples. For samples that were not normally distributed, a Wilcoxon–Mann–Whitney test was performed. All statistical analyses were conducted using Microsoft® Excel® for Microsoft 365 (Version 2108; Microsoft Corporation) with add-in Real Statistics Resource Pack software (Release 7.6, Copyright 2013–2021; Charles Zaiontz); differences were considered statistically significant if a p value below 0.05 was obtained.

3 | RESULTS AND DISCUSSION

In a first step, the influences of different treatment strategies on the surface properties of three PU variants are examined. These PU variants comprise a technical polyurethane (PUR) and two medical-grade PUs (PC, AC—see Section 2). The aim of this first set of experiments is to test which of the three surface treatment strategies improves the wetting behavior of the polymeric material without inducing macroscopic or microscopic alterations to the surface properties of the PU materials. With initial CAs of 99.8 ± 0.65° and 93.9 ± 0.62°, the wetting properties of untreated PC and PUR, respectively, are located right in the transition zone between hydrophobic (CA > 90°) and hydrophilic (CA < 90°) behavior (Figure 1a,b); in contrast, untreated AC samples already show slightly hydrophilic behavior as indicated by CA values of 76.1 ± 0.78° (Figure 1c). Thus, a particular surface treatment is considered successful if those CAs are

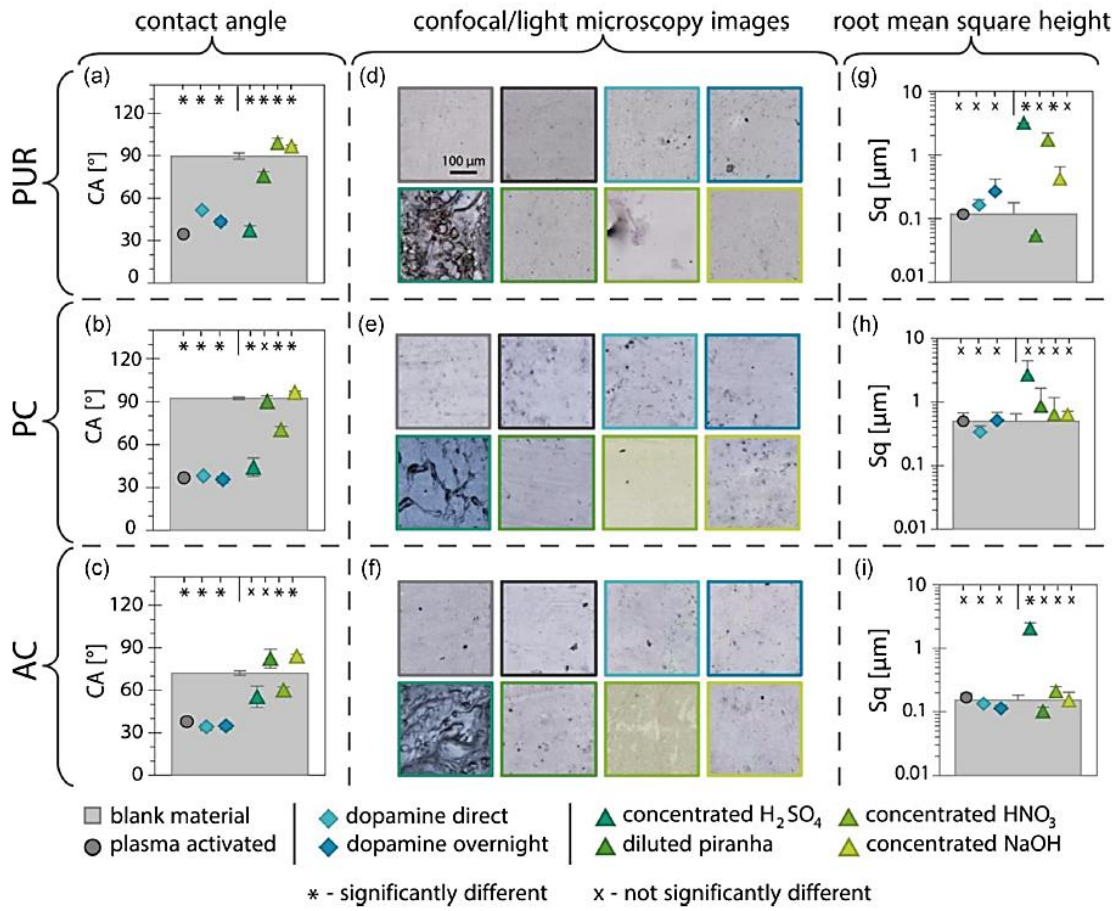

FIGURE 1 Influence of different treatment strategies on the surface properties of polyurethane materials: (a–c) the results of water contact angle measurements; (d–f) combined laser confocal and light microscopy images acquired at a ×50 magnification; and (g–i) quantification of the samples' surface roughness via the root-mean-square height S_q. Each aspect was assessed for three different polyurethane materials: (a, d, g), PUR; (b, e, h), PC; and (c, f, i), AC. Data were obtained before (light gray bars) and after the implementation of the designated surface activation strategies (other colors/symbols). The tested surface treatment strategies include plasma activation (dark gray/circles), two types of dopamine treatments (light blue and dark blue/diamonds), and four chemical etching approaches (different shades of green/triangles). The scale bar in (b) represents 100 µm and applies to all microscopy images in (d–f). Error bars denote the standard error of the mean as obtained from at least $n = 3$ measurements. If no error bars are visible, their size is on the order of the symbol size. Results determined to be significantly different from those obtained for the corresponding blank material sample are marked with an asterisk (based on a p value of 0.05); otherwise, the results are marked with a cross. AC, aromatic Carbothane™ AC-4095A; PC, aliphatic Carbothane™ PC-3575A; PUR, elastomeric polyurethane THOMAPLAST®-PUR

reduced to ~45° or below; such a result would represent a clearly hydrophilic wetting behavior. Indeed, both plasma treatment and dopamine treatment achieve this goal for all three PU variants. In contrast, the chemical etching strategies are less efficient as we only obtain satisfactory results with concentrated sulfuric acid (H_2SO_4).

However, as mentioned above, it is important that an improvement in the wetting properties does not arise at a too high price: Examples of undesired side effects that one of the surface treatment strategies could induce include noticeable color changes in the material or strong topographical alterations. To test for these alterations, the treated PU variants are next investigated under a confocal laser scanning microscope.

Combined confocal/light microscopy images (Figure 1d–f) clearly show that, for all three materials, a treatment with concentrated sulfuric acid leads to drastic

alterations of the sample surface: here, different from the even and homogeneous appearance of the untreated materials, major structural changes are visible. This qualitative impression is underscored when the surface roughness parameter S_q (i.e., the root-mean-square height) is calculated (Figure 1g–i) from the topographical information provided by the profilometric images: This metrological analysis shows that neither plasma treatment nor the two dopamine treatments lead to a significant alteration in the surface roughness. In contrast, exposure to sulfuric acid increases the roughness of all three PU variants. In other words, all etching solutions tested here either fail to sufficiently decrease the CA of the PU materials (piranha solution, NaOH) or induce obvious surface alterations (i.e., topographical changes in the case of H_2SO_4 and color alterations in the case of HNO_3). Thus, in the rest of this article, chemical etching of the different PU materials is not considered further.

For many applications, in addition to being efficient, it is equally important that a surface treatment entails changes in the material properties that are stable over an extended time period. Thus, in a next step, we investigate the durability of the hydrophilizing effect achieved by the different surface treatments. In detail, two storage conditions are examined: first, wet incubation at body temperature (i.e., samples immersed in DPBS and stored at 37°C) and second, dry incubation in the cold (i.e., storage at 4°C without any added buffer). Here, the first scenario mimics conditions that the PU variants will encounter in or on the human body, for example, when used as materials for implants or medical devices; in contrast, the second set of storage parameters can be relevant for medical products before their application in vivo or for PU-based materials that are used outside a living organism.

As control groups, untreated samples are immersed into a buffered solution and stored at 37°C. For those untreated samples, such wet storage gives rise to a slight decrease in the CA. This effect takes place within the first 5 days of storage and is the mildest for AC and the strongest for PUR; after this time point, the CA values stabilize and remain constant for the rest of the observation period (see Figure 2a–c). A similar trend is observed when the water uptake behavior of these samples is quantified: we find the strongest effect for PUR (where we measure an increase of ~2% [w/w]) and weaker changes (i.e., a weight increase ~1% [w/w]) for AC and PC (Figure 2d). This suggests that these two phenomena, water uptake and a decrease in the CA upon storage in aqueous solutions, are related.

Overall, when comparing wet and dry storage of treated samples, the former seems to be preferable for all three PU variants and for all treatment strategies tested; here, the CA values stabilize at much smaller numbers than under dry storage conditions (Figure 2e–g). This suggests that using the treated samples in an application where they are continuously exposed to an aqueous environment would be ideal. For dopamine-treated PU samples stored under wet conditions, we measure CA values as low as 20–30°, and these are stable for at least 2 weeks. Plasma-treated samples slightly recover over time and stabilize at somewhat larger CAs between 40° and 50°; however, also, these values correspond to clearly hydrophilic behavior. When stored under wet conditions, we find the best durability of all surface treatments for AC samples (Figure 2c): here, after the 4th day, we detect virtually no change in the measured CA values anymore.

In contrast, when stored under dry conditions, all surface-treated PU variants lose, to a certain extent, their initially strong hydrophilic properties over time. Such a behavior is known as "hydrophobic recovery" and resembles previous results obtained with other polymeric materials such as polydimethylsiloxane (PDMS),[27–30] polypropylene,[31–33] polyethylene,[34] and polytetrafluorethylene.[35,36] For most of these materials (when stored in air), this hydrophobic recovery occurs within the first 2–7 days.[28,30,31,36] In these publications, this effect was mainly attributed to a migration of the polar groups created by the plasma treatment from the surface of the material into the sub-surficial polymeric volume, for example, via diffusive motion of polymer chains or by reorientation/rotation of polymer segments carrying the hydrophilic residues.[37] Also, for those other polymeric materials, this process of hydrophobic recovery slowed down when the samples were stored in a polar medium (e.g., phosphate-buffered saline); there, this was attributed to stabilizing effects arising from interactions between the surface-bound polar (hydroxyl) groups created by plasma treatment and the polar solvent covering the surface.[27,28,35,36]

Of course, in addition to the storage conditions (including storage time, temperature, and the surrounding medium),[28,31,35] hydrophobic recovery can also be influenced by certain treatment parameters such as the plasma type[13,38] and the technical settings used during the plasma treatment[32,36] as well as the specific properties (e.g., the degree of crystallinity[32,33] and the glass transition temperature[39]) of the treated material. Thus, it is not surprising that the kinetics of hydrophobic recovery is slightly different for all three PU variants examined here. For plasma-treated AC samples, hydrophobic recovery is the strongest; in contrast, for PUR samples, we still observed a considerably reduced CA at the end of the stability test.

Even though dry storage of all treated samples leads to a clear increase in the CA within the first few days (all

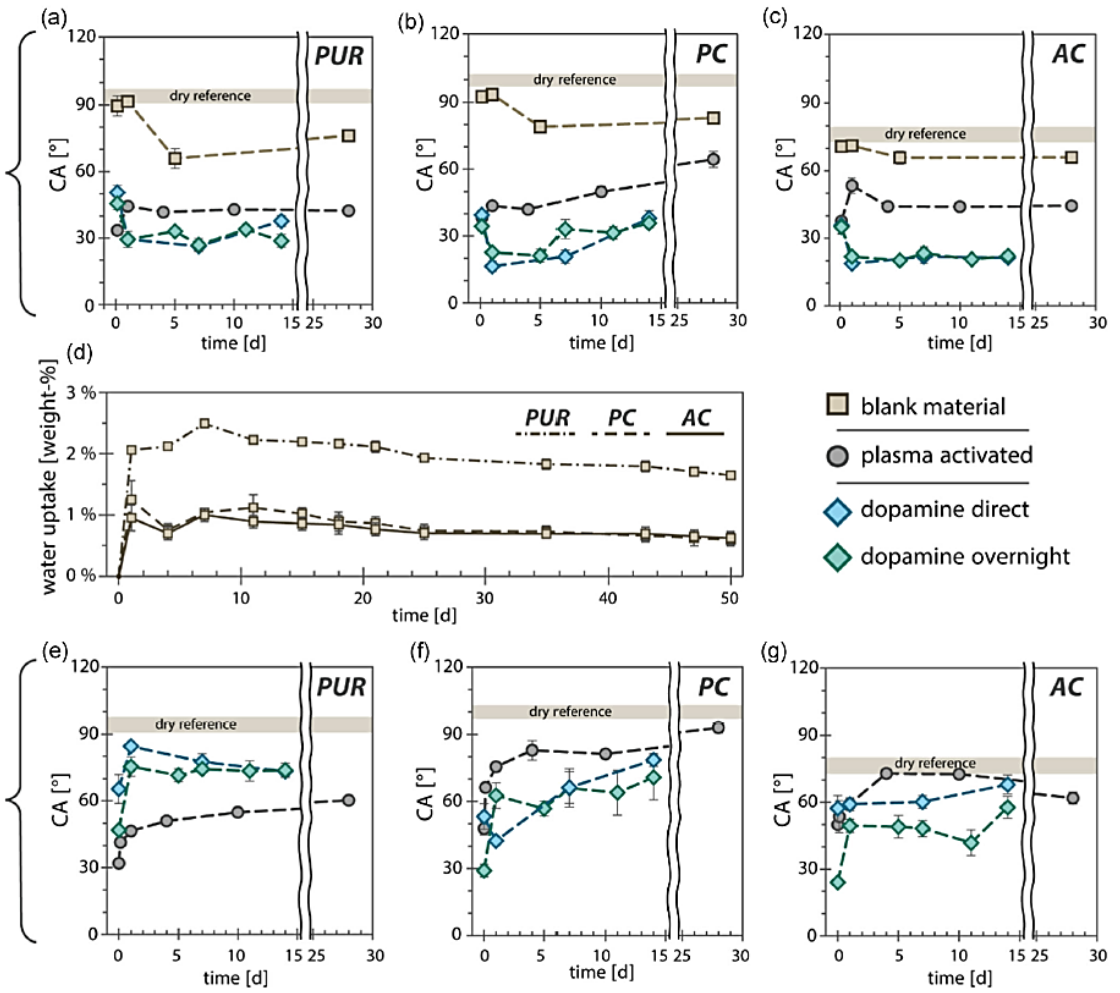

FIGURE 2 Durability of different surface modifications of PU materials during sample storage: Contact angle measurements conducted over a period of 2–4 weeks are shown for untreated/blank (beige squares), plasma-activated (gray circles), "dopamine-direct"- and "dopamine-overnight"-treated (blue/turquoise diamonds) samples. Samples were either stored in the wet state (i.e., in physiological buffer at 37°C; a–d) or in the dry state (at 4°C; e–g). For wet storage, the data shown in (d) describe the water uptake behavior of the PU samples as determined by the relative change in weight. Error bars denote the standard error of the mean as obtained from at least $n = 3$ measurements. If no error bars are visible, their size is on the order of the symbol size. AC, aromatic Carbothane™ AC-4095A; PC, aliphatic Carbothane™ PC-3575A; PU, polyurethane; PUR, elastomeric polyurethane THOMAPLAST®-PUR

CA values are above 45° after 5 days of dry storage), it is worth noting that the "dopamine overnight"-treated AC samples, all treated PC samples, and all treated PUR samples maintain improved wetting properties (i.e., at least 15–20° difference) and did not fully recover their initial CA values for at least 2 weeks. Plasma-treated PUR samples performed the best: here, even after a month of storage, the measured CA values were still lower by ~50° than those determined for untreated samples.

As no clear difference between the outcomes of dopamine-overnight- and dopamine-direct-treated samples in any of the previous tests could be observed, for practical reasons, the following tests are only performed with one type of dopamine treatment. Thus, for the rest of this article, the dopamine-direct treatment of the different PU materials is not considered further.

For many applications, a germ-free material surface is required. However, as the conditions of an autoclave

treatment (high temperature + high humidity + high pressure) are expected to adversely affect the shape and structure of the samples (due to, e.g., softening, hydrolysis, and pyrolysis), milder disinfection methods are needed to reduce potential microbial contamination of the materials. Here, we use UV irradiation as a possible disinfection method and investigate the influence of such UV exposure on the material properties of the three PU variants and the different hydrophilizing surface treatments applied to them. As described above, the wettability of the differently treated surfaces (as quantified by the CA) is a good indicator of successful surface modification. Thus, we again use CA measurements to evaluate the influence of UV exposure on the surface properties of the different activated PU variants.

First, blank (= not surface modified) samples are tested to assess the putative effects that a UV exposure might have on the base materials themselves. Yet, we detect only minor differences between the wetting properties of untreated and UV-treated samples (Figure 3), independent of whether the UV exposure occurred in a "wet state" or a "dry state." Consequently, all obvious changes in the CA of surface-treated samples that we might detect later are likely to originate from alterations in the surface activations as induced by the UV exposure. Interestingly, we find that UV irradiation only affects selected conditions: For plasma-treated samples, hydrophobic recovery seems to be accelerated by a UV treatment conducted in the dry state. This effect is the weakest on PUR, which is in line with our findings described above (see Figure 2e), where plasma-treated PUR samples were most stable when stored in the dry state. The plasma-treated PUR samples in the wet state are the only plasma-treated samples that do not show any changes for either of the exposure times.

In contrast, for dopamine-treated AC and PC samples in a wet state, UV exposure of samples even significantly decreases the CA values. As dopamine is reported to be UV sensitive,[40] we speculate that this effect might be due to further stabilization of the wet dopamine layer by the UV light. However, in the dry state, the UV irradiation once more seems to have negative effects on the dopamine-treated surfaces.

Having shown that most hydrophilized PU samples can be subjected to a UV treatment without compromising the surface activation effect, we next investigate the interaction of the PU materials with eukaryotic cells. For this subset of tests, we focus on AC and PC, as these two materials (in contrast to PUR) have been developed for medical use. As a model cell line to conduct colonization and cytotoxicity tests with, we select the well-established epithelial cell line HeLa.[16,41] Such HeLa

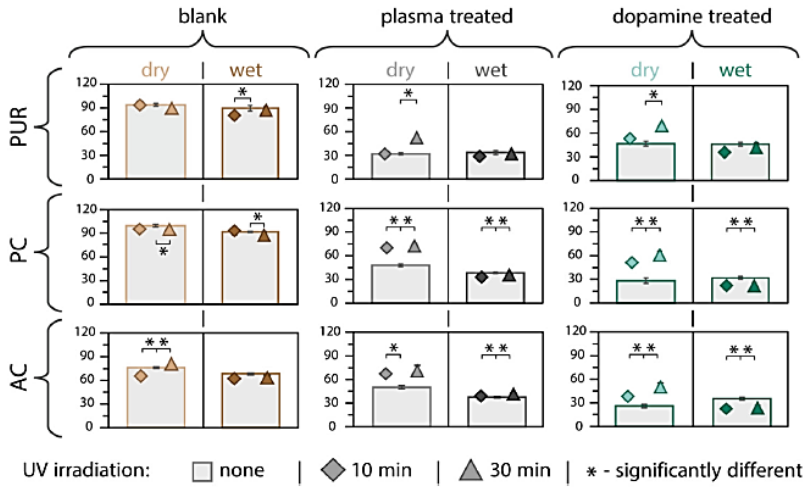

FIGURE 3 Influence of UV irradiation on the surface wettability of different PU samples: Contact angles were determined on all three materials before UV irradiation (gray bars), and after 10 min (diamonds) and 30 min (triangles) of UV exposure. Results are shown for untreated (blank, left column), plasma-treated (middle column), and "dopamine overnight"-treated (right column) samples. The samples were either exposed to UV light in a "dry state" (light colors) or a "wet state," that is, when covered by a water layer of ~1 cm thickness (dark colors). Error bars denote the standard error of the mean as obtained from at least $n = 3$ measurements. If no error bars are visible, their size is on the order of the symbol size obtained from at least $n = 3$ measurements. Results determined to be significantly different from those obtained for the corresponding blank material sample are marked with an asterisk (based on a p value of 0.05). AC, aromatic Carbothane™ AC-4095A; PC, aliphatic Carbothane™ PC-3575A; PU, polyurethane; PUR, elastomeric polyurethane THOMAPLAST®-PUR

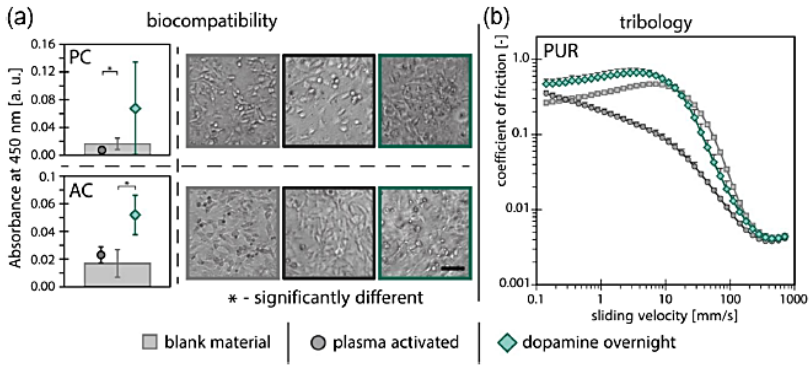

FIGURE 4 Functional examination of surface-treated PU variants. (a) To assess the biomedical functionality of PC and AC, the viability of HeLa cells seeded onto the PU materials is determined using a WST-1 test (left), and phase-contrast images show the morphology of adherent cells (right). The scale bar corresponds to 50 μm and applies to all microscopy images in this subfigure. The error bars denote the standard deviation as obtained from six independent samples obtained from at least $n = 3$ measurements. If no error bars are visible, their size is on the order of the symbol size. Results determined to be significantly different from those obtained from the corresponding blank material sample are marked with an asterisk (based on a p value of 0.05). (b) A technical application of PUR samples is tested via a tribological examination of (un)treated PUR samples in a rotational ball-on-three-plates setup. Error bars denote the standard error of the mean as determined from at least $n = 3$ sample sets. If no error bars are visible, their size is on the order of the symbol size. AC, aromatic Carbothane™ AC-4095A; PC, aliphatic Carbothane™ PC-3575A; PU, polyurethane; PUR, elastomeric polyurethane THOMAPLAST®-PUR

cells are seeded onto the two PU variants to investigate the morphology and metabolic activity of those cells when colonizing AC and PC surfaces, respectively (Figure 4a, left).

On both untreated AC and PC material surfaces, we find good surface coverage with HeLa cells, and the well-spread asymmetric morphology of these cells is consistent with what one would expect for viable epithelial cells seeded onto a stiff substrate (Figure 4a, right). This result is in line with statements of the manufacturer that Carbothanes are biocompatible, medical-grade PUs.[42]

Whereas plasma activation of the two PU materials hardly entails any alterations with regard to cell colonization, dopamine treatment improves this material property. This is demonstrated by a higher cell density that we find on the dopamine-treated samples that is accompanied by a stronger signal obtained from a WST-1 test: On the dopamine-treated surfaces, the metabolic activity reported by the absorbance signals is ~2 (AC) or ~3 times (PC) as high as that for unmodified AC and PC samples, respectively. This result is in agreement with similar tests conducted with other synthetic materials coated with dopamine[43,44] and demonstrates that this surface treatment strategy can promote cell colonization while avoiding cytotoxic effects.

Finally, for the PUR samples, which are not used in a medical context, we also assess a material property that is relevant for an important application area; as PUR samples are used in many technical settings, here, we chose a rotational tribology test to examine the influence of the different surface treatments on the friction behavior of PUR. Compared to untreated PUR, we observe that dopamine treatment mostly maintains the friction response of the sample; only in the boundary lubrication regime do we detect a slightly increased friction factor (Figure 4b). Even though one might have assumed that an improved interaction with the lubricant as brought about by the dopamine treatment could lead to reduced friction, this finding agrees with previous results from the literature: dopamine forms an adhesive layer to which other objects readily stick. Whereas this property is beneficial for attaching other molecules to the dopamine layer,[45] here, it counteracts the improved interaction of the surface with aqueous solutions by restricting the sliding motion of the steel sphere, thus resulting in increased coefficients of friction, yet only at slow sliding speeds. This result can be explained by the Stribeck theory[46]: as stated there, with increasing relative sliding velocities, the contact of the two surfaces in a tribological material pairing is reduced as a thin lubricating liquid layer is formed in between the surfaces. Accordingly, the stickiness of a surface becomes less relevant when moving from the boundary lubrication regime into the mixed (or even hydrodynamic) lubrication regime, as the contact of the steel sphere with the adhesive layer is reduced. In full agreement with this picture, we find that plasma-treated samples (which show enhanced wettability, but have non-sticky surfaces) show

a reduced friction response in both the mixed and most of the boundary lubrication regime, and this can be attributed to improved interactions of the hydrophilized surface with the aqueous lubricant. As a consequence of the improved surface wetting behavior, one or more of the following two effects can occur: first, as the plasma treatment leads to a more polar surface, the (polar) water molecules have more possibilities (with higher degrees of freedom) to interact with the material surface. Second, a thin hydration layer can be generated on the surface of the PUR, which might promote separation of the two tribological partners even at slower sliding velocities. Thus, at intermediate sliding speeds of ~10 mm s^{-1}, the resulting friction reduction is approximately on the order of a factor of 5, which is high for a high-friction material such as PUR.

4 | CONCLUSIONS

In summary, here, we have shown that oxygen plasma treatment and dopamine deposition are two highly suitable surface treatment strategies to enhance the wettability of different PU materials. With either method, we observed good stability of the achieved surface modification for at least 2 weeks, and these modifications are robust toward UV irradiation (when applied to samples stored in the wet state) as required for sample disinfection. In terms of certain aspects, the dopamine treatment appeared somewhat superior to the plasma treatment; nevertheless, the best treatment option depends on the specific material as well as the intended application. Also, for each application/material combination, optimization of the process parameters used for the surface modification process could further improve the properties of the differently treated PU variants. An interesting advantage provided by the dopamine-based strategy could be that it allows for an easy attachment of a macromolecular top layer to enable hydration lubrication (thus reducing friction) or to initiate multistep coatings as useful for drug storage/release approaches.[47] Similarly, also, the plasma treatment can serve as an initial step for further surface functionalization, for example, when followed by silanization and subsequent carbodiimide-mediated coupling of a macromolecular layer.[48] Indeed, both approaches have previously been used to reduce friction and wear generation[44,48,49] and to reduce the adsorption of proteins, cells, and bacteria[18,44]; however, to date, such multifunctional coatings have been mainly applied to other polymeric materials such as PDMS or polytetrafluorethylene. Existing coatings of PU materials, in contrast, often aim at merely individual characteristics, *e.g.*,hemocompatibility or antibacterial properties of the material.[50] Certainly, PU materials would benefit from more complex, multifunctional coatings, and the corresponding additional properties (in particular, an improved friction behavior) brought about by their use would further increase the range of applications that they can be used for.

ACKNOWLEDGMENTS

The authors thank their APRICOT project partners at the Fraunhofer Institute for Manufacturing Engineering and Automation (IPA, Stuttgart, Germany) for procurement and supply of the extruded Carbothane™ films. This project has received funding from the European Union's Horizon 2020 research and innovation program under grant agreement No. 863183. This publication represents the views of the author(s) only. The European Commission is not responsible for any use that may be made of the information it contains. Open Access funding enabled and organized by Projekt DEAL.

CONFLICT OF INTERESTS

The authors declare that there are no conflict of interests.

AUTHOR CONTRIBUTIONS

This study was conceptualized by Maria Bauer and Oliver Lieleg; Rosa Reithmeir contributed to contact angle measurements; Theresa Lutz performed experiments involving eukaryotic cells; and Maria Bauer performed all other experiments and analyzed the data. The manuscript was written by Maria Bauer and Oliver Lieleg and was critically revised by all authors.

DATA AVAILABILITY STATEMENT

The data that support the findings of this study are available from the corresponding author upon reasonable request.

ORCID

Maria G. Bauer https://orcid.org/0000-0001-7592-9904
Theresa M. Lutz http://orcid.org/0000-0002-5072-3931
Oliver Lieleg http://orcid.org/0000-0002-6874-7456

REFERENCES

[1] (a) A. Das, P. Mahanwar, *Adv. Ind. Eng. Polym. Res.* **2020**, *3*, 93.; (b) H.-W. Engels, H.-G. Pirkl, R. Albers, R. W. Albach, J. Krause, A. Hoffmann, H. Casselmann, J. Dormish, *Angew. Chem., Int. Ed. Engl.* **2013**, *52*, 9422.; (c) F. Zafar, *Polyurethane*, InTech, **2012**.; (d) M. M. Rahman, M. M. Rabbani, J. K. Saha, *Polymers and Polymeric Composites: A Reference Series* (Ed: M. I. H. Mondal), Springer International Publishing, Cham **2018**, p. 1.; (e) J. O. Akindoyo, M. D. H. Beg, S. Ghazali, M. R. Islam, N. Jeyaratnam, A. R. Yuvaraj, *RSC Adv.* **2016**, *6*, 114453.

[2] (a) R. Deng, P. Davies, A. K. Bajaj, *J. Sound Vib.* **2003**, *262*, 391.; (b) M. Modesti, F. Simioni, *Polym. Eng. Sci.* **1996**, *36*,

2173.; (c) D. K. Chattopadhyay, K. Raju, *Prog. Polym. Sci.* **2007**, *32*, 352.

[3] (a) G. Tibério Cardoso, S. Claro Neto, F. Vecchia, *Front. Archit. Res.* **2012**, *1*, 348.; (b) S. Chen, Y. Jiang, *Polym. Compos.* **2018**, *39*, 1370.; (c) R. Höfer, P. Daute, R. Grützmacher, A. Westfechtel, *J. Coat. Technol.* **1997**, *69*, 65.; (d) A. Zahn, J. Grimm, *Adhes. Sealants* **2013**, *10*, 32.

[4] (a) R. J. Galan, T. Narayan, R. A. Markovs, *J. Elastomers Plast.* **1990**, *22*, 22.; (b) M. M. Hirschler, *Polym. Adv. Technol.* **2008**, *19*, 521.

[5] (a) J. Joseph, R. M. Patel, A. Wenham, J. R. Smith, *Trans. IMF* **2018**, *96*, 121.; (b) W. Wang, C. Wang *Woodhead Publishing Reviews: Mechanical Engineering Series* (Ed: J. Paulo Davim), Woodhead Publishing Limited, Cambridge, UK **2012**, p. 115.; (c) F. J. Davis, G. R. Mitchell, *Bio-Materials and Prototyping Applications in Medicine* (Eds: P. Bártolo, B. Bidanda), Springer, Boston, MA **2008**, p. 27.

[6] (a) A. Riveiro, A. L. B. Maçon, J. del Val, R. Comesaña, J. Pou, *Front. Phys.* **2018**, *6*, 16.; (b) L. Sun, J. Guo, H. Chen, D. Zhang, L. Shang, B. Zhang, Y. Zhao, *Adv. Sci.* **2021**, 2100126.

[7] (a) M. Iqbal, D. K. Dinh, Q. Abbas, M. Imran, H. Sattar, A. Ul Ahmad, *Surfaces* **2019**, *2*, 349.; (b) N. Encinas, M. Pantoja, J. Abenojar, M. A. Martínez, *J. Adhes. Sci. Technol.* **2010**, *24*, 1869.; (c) M. Berczeli, Z. Weltsch, *Polymers* **2021**, *13*, 901.; (d) J. Song, B. Winkeljann, O. Lieleg, *Adv. Mater. Interfaces* **2020**, *7*, 2000850.

[8] F. L. Tabares, I. Junkar, *Molecules (Basel, Switzerland)* **2021**, *26*, 1903.

[9] K. Bazaka, M. V. Jacob, R. J. Crawford, E. P. Ivanova, *Acta Biomater.* **2011**, *7*, 2015.

[10] (a) R. Radjef, K. Jarvis, B. L. Fox, S. L. McArthur, *Plasma Processes Polym.* **2020**, *17*, 2000017.; (b) T. Wang, L. Shi, L. Lv, J. Liu, *Plasma Processes Polym.* **2020**, *17*, 2000056.

[11] (a) J. Šimončicová, S. Kryštofová, V. Medvecká, K. Ďurišová, B. Kaliňáková, *Appl. Microbiol. Biotechnol.* **2019**, *103*, 5117.; (b) D. Braný, D. Dvorská, E. Halašová, H. Škovierová, *Int. J. Mol. Sci.* **2020**, *21*, 2932.

[12] M. Aliofkhazraei, *Surface Energy*, IntechOpen **2015**.

[13] D. Hegemann, H. Brunner, C. Oehr, *Nucl. Instrum. Methods Phys. Res., Sect. B* **2003**, *208*, 281.

[14] (a) D. Zhuang, J. H. Edgar, *Mater. Sci. Eng., R* **2005**, *48*, 1.; (b) J. S. Mijovic, J. A. Koutsky, *Polym.-Plast. Technol. Eng.* **1977**, *9*, 139.

[15] H. Lee, S. M. Dellatore, W. M. Miller, P. B. Messersmith, *Science (New York, N.Y.)* **2007**, *318*, 426.

[16] J. Yang, M. A. Cohen Stuart, M. Kamperman, *Chem. Soc. Rev.* **2014**, *43*, 8271.

[17] (a) P. Kord Forooshani, B. P. Lee, *J. Polym. Sci., Part A: Polym. Chem.* **2017**, *55*, 9.; (b) H. A. Lee, E. Park, H. Lee, *Adv. Mater. (Deerfield)* **2020**, *32*, e1907505.

[18] B. Winkeljann, M. G. Bauer, M. Marczynski, T. Rauh, S. A. Sieber, O. Lieleg, *Adv. Mater. Interfaces* **2020**, *7*, 1902069.

[19] (a) H. W. Kim, B. D. McCloskey, T. H. Choi, C. Lee, M.-J. Kim, B. D. Freeman, H. B. Park, *ACS Appl. Mater. Interfaces* **2013**, *5*, 233.; (b) J. H. Ryu, P. B. Messersmith, H. Lee, *ACS Appl. Mater. Interfaces* **2018**, *10*, 7523.; (c) S. Hong, Y. S. Na, S. Choi, I. T. Song, W. Y. Kim, H. Lee, *Adv. Funct. Mater.* **2012**, *22*, 4711.; (d) V. Ball, J. Gracio, M. Vila, M. K. Singh, M.-H. Metz-Boutigue, M. Michel, J. Bour, V. Toniazzo, D. Ruch, M. J. Buehler, *Langmuir* **2013**, *29*, 12754.

[20] P. H. Geil, *Product R&D* **1975**, *14*, 59.

[21] (a) B. Schwartz, H. Robbins, *J. Electrochem. Soc.* **1976**, *123*, 1903.; (b) V. Paredes, E. Salvagni, E. Rodríguez-Castellón, J. M. Manero, *Metall. Mater. Trans. A* **2017**, *48*, 3770.; (c) P. Sun, G. Liu, D. Lv, X. Dong, J. Wu, D. Wang, *RSC Adv.* **2015**, *5*, 52916.; (d) I. Borisov, A. Ovcharova, D. Bakhtin, S. Bazhenov, A. Volkov, R. Ibragimov, R. Gallyamov, G. Bondarenko, R. Mozhchil, A. Bildyukevich, V. Volkov, *Fibers* **2017**, *5*, 6.; (e) L. Hallmann, A. Mehl, N. Sereno, C. H. Hämmerle, *Appl. Surf. Sci.* **2012**, *258*, 7213.

[22] C. A. Rickert, T. M. Lutz, M. Marczynski, O. Lieleg, *Macromol. Biosci.* **2020**, *20*, e2000090.

[23] H. Hertz, *J. Reine Angew. Math.* **1882**, 156.

[24] (a) M. J. Boussinesq, *Application des potentiels à l'étude de l'équilibre et du mouvement des solides élastiques*, Gauthier-Villars, Paris **1885**.; (b) V. L. Popov, *Handbuch der Kontaktmechanik*, Springer Berlin, Heidelberg **2018**.

[25] J. Kunz, M. Studer, *Kunststoffe International* **2006**, *6*, 92.

[26] (a) R. D. Widdle, A. K. Bajaj, P. Davies, *Int. J. Eng. Sci.* **2008**, *46*, 31.; (b) Y. M. Poplavko, *Electronic Materials: Principles and Applied Science*, Elsevier, Amsterdam, NL **2019**, p. 71.; (c) D. Rosato, D. Rosato, *Plastics Engineered Product Design*, Elsevier, Amsterdam, NL **2003**, p. 161.; (d) J. Karpiesiuk, *Mod. Approaches Mater. Sci.* **2020**, *2(3)*, 251.

[27] S. H. Tan, N.-T. Nguyen, Y. C. Chua, T. G. Kang, *Biomicrofluidics* **2010**, *4*, 32204.

[28] R. A. Lawton, C. R. Price, A. F. Runge, W. J. Doherty, S. S. Saavedra, *Colloids Surf., A* **2005**, *253*, 213.

[29] S. Hemmilä, J. V. Cauich-Rodríguez, J. Kreutzer, P. Kallio, *Appl. Surf. Sci.* **2012**, *258*, 9864.

[30] D. T. Eddington, J. P. Puccinelli, D. J. Beebe, *Sens. Actuators, B* **2006**, *114*, 170.

[31] R. Morent, N. de Geyter, C. Leys, L. Gengembre, E. Payen, *Surf. Coat. Technol.* **2007**, *201*, 7847.

[32] Y. I. Yun, K. S. Kim, S.-J. Uhm, B. B. Khatua, K. Cho, J. K. Kim, C. E. Park, *J. Adhes. Sci. Technol.* **2004**, *18*, 1279.

[33] I. Novák, Š. Florián, *J. Mater. Sci.* **2004**, *39*, 2033.

[34] (a) M. Pascual, R. Sanchis, L. Sánchez, D. García, R. Balart, *J. Adhes. Sci. Technol.* **2008**, *22*, 1425.; (b) M. R. Sanchis, V. Blanes, M. Blanes, D. Garcia, R. Balart, *Eur. Polym. J.* **2006**, *42*, 1558.; (c) M. Pascual, R. Balart, L. Sánchez, O. Fenollar, O. Calvo, *J. Mater. Sci.* **2008**, *43*, 4901.

[35] D. J. Wilson, R. L. Williams, R. C. Pond, *Surf. Interface Anal.* **2001**, *31*, 397.

[36] J. Nakamatsu, L. F. Delgado-Aparicio, R. Da Silva, F. Soberon, *J. Adhes. Sci. Technol.* **1999**, *13*, 753.

[37] M. Mortazavi, M. Nosonovsky, *Appl. Surf. Sci.* **2012**, *258*, 6876.

[38] D. J. Wilson, R. L. Williams, R. C. Pond, *Surf. Interface Anal.* **2001**, *31*, 385.

[39] J. Zhou, A. V. Ellis, N. H. Voelcker, *Electrophoresis* **2010**, *31*, 2.

[40] X. Du, L. Li, J. Li, C. Yang, N. Frenkel, A. Welle, S. Heissler, A. Nefedov, M. Grunze, P. A. Levkin, *Adv. Mater. (Deerfield)* **2014**, *26*, 8029.

[41] S.-I. Sawada, Y. Iwasaki, N. Nakabayashi, K. Ishihara, *J. Biomed. Mater. Res. A.* **2006**, *79*, 476.

[42] (a) The Lubrizol Cooperation, Carbothane™ TPU, **2021**. https://www.lubrizol.com/Health/Medical/Polymers/Carbothane-TPU (accessed: July 2021).; (b) Lubrizol Life Science, Benefits of Medical-Grade TPU Over Non-Medical Grade Alternatives, 2020. https://www.lubrizol.com/Health/Medical/Resource-Hub (accessed: September 2021).; (c) Lubrizol Life Science, Medical Device TPU Product Guide, 2020. https://www.lubrizol.com/Health/Medical/Resource-Hub (accessed: September 2021).

[43] S. H. Ku, J. Ryu, S. K. Hong, H. Lee, C. B. Park, *Biomaterials* **2010**, *31*, 2535.

[44] J. Song, T. M. Lutz, N. Lang, O. Lieleg, *Adv. Healthcare Mater.* **2021**, *10*, e2000831.

[45] H. Lee, J. Rho, P. B. Messersmith, *Adv. Mater. (Deerfield)* **2009**, *21*, 431.

[46] (a) R. Stribeck, *Zeitschrift des Vereins Deutscher Ingenieure (VDI)* **1901**, *45*, 73.; (b) R. Stribeck, *Zeitschrift des Vereins Deutscher Ingenieure (VDI)* **1902**, *46*, 1341.; (c) B. Jacobson, *Tribol. Int.* **2003**, *36*, 781.

[47] (a) C. Kimna, B. Winkeljann, J. Song, O. Lieleg, *Adv. Mater. Interfaces* **2020**, *7*, 2000735.; (b) M. J. Garcia-Fernandez, L. Martinez-Calvo, J.-C. Ruiz, M. R. Wertheimer, A. Concheiro, C. Alvarez-Lorenzo, *Plasma Processes Polym.* **2012**, *9*, 540.

[48] B. Winkeljann, P.-M. A. Leipold, O. Lieleg, *Adv. Mater. Interfaces* **2019**, *6*, 1900366.

[49] C. A. Rickert, B. Wittmann, R. Fromme, O. Lieleg, *ACS Appl. Mater. Interfaces* **2020**, *12*, 28024.

[50] (a) S. Zanini, A. Polissi, E. A. Maccagni, E. C. Dell'Orto, C. Liberatore, C. Riccardi, *J. Colloid Interface Sci.* **2015**, *451*, 78.; (b) H.-S. Lee, N. Tomczyk, J. Kandel, R. J. Composto, D. M. Eckmann, *J. Mater. Chem. B* **2013**, *1*, 6382.; (c) C. Luo, W. Liu, B. Luo, J. Tian, W. Wen, M. Liu, C. Zhou, *Carbohydr. Polym.* **2017**, *156*, 235.; (d) P. Alves, S. Pinto, H. C. de Sousa, M. H. Gil, *J. Appl. Polym. Sci.* **2011**, *122*, 2302.; (e) P. Alves, R. Cardoso, T. R. Correia, B. P. Antunes, I. J. Correia, P. Ferreira, *Colloids Surf., B* **2014**, *113*, 25.; (f) K. Fujimoto, H. Tadokoro, Y. Ueda, Y. Ikada, *Biomaterials* **1993**, *14*, 442.; (g) F. Noorisafa, A. Razmjou, N. Emami, Z.-X. Low, A. H. Korayem, A. A. Kajani, *J. Exp. Nanosci.* **2016**, *11*, 1087.

SUPPORTING INFORMATION

Additional Supporting Information may be found online in the supporting information tab for this article.

How to cite this article: M.G. Bauer, R. Reithmeir, T.M. Lutz, O. Lieleg, *Plasma Processes Polym.* **2021**, e2100126.
https://doi.org/10.1002/ppap.202100126

A.2.3 "Bio-Macromolecular Surface Coatings for Autohesive, Transparent, Elastomeric Foils"

RESEARCH ARTICLE

Macromolecular Materials and Engineering
Open Access
www.mame-journal.de

Bio-Macromolecular Surface Coatings for Autohesive, Transparent, Elastomeric Foils

*Maria G. Bauer and Oliver Lieleg**

Thin materials made from elastomeric polymers such as polydimethylsiloxane (PDMS) and polyurethane (PU) can be both, compliant and resilient. Their mechanical robustness and flexibility will make them great candidates for applications in the human body where space is limited and repeated deformations occur. Nonetheless, current medical applications of elastomeric foil-like products are mainly restricted to inflatable balloon parts of stents or intubation tubes. Here, a key limiting factor is the autohesive behavior of those foils, that is, their propensity to stick to themselves. This property impedes handling and processing and can also interfere with the designated tasks of such foils. To mitigate this undesired behavior, different bio-macromolecular coatings are applied here and assess their influence on the autohesive behavior, flexibility, and transparency of the materials. A non-covalent, dopamine-assisted coating approach is compared to a covalent coating strategy employing carbodiimide chemistry and investigated both, anionic and cationic macromolecules as top layers. The results show that especially the carbodiimide-mediated mucin coating can efficiently suppress the autohesive behavior of the foils while maintaining the flexibility and transparency of the material. Thus, such coatings can not only broaden the medical application range of foil-based elastomeric devices but may also prove beneficial for applications in soft robotics.

1. Introduction

Applying coatings to surfaces is a ubiquitous tool to adjust the surface properties of a material. In addition to changing the optical appearance of the product,[1] coatings are mainly applied to protect the bulk material from undesired environmental impacts, for example, from corrosion,[2] wear,[3,4] heat damage,[5] cellular or bacterial colonization,[6a,6b,7] or to activate the surface so it gains additional functions. Examples of such surface-associated functionalities are catalysis[8] and filtering tasks,[9] local drug release,[10] control over cellular adhesion,[7,11] as well as photo- and thermochromic[12] or self-healing properties.[13] Thus, coatings are employed in almost any kind of industry, ranging from aeronautic and automotive applications,[14] over materials used in construction and infrastructure,[15] to a broad range of problems in biochemical, medical, and pharmaceutical areas.[16a–d,17] In addition, coatings can play an important role in achieving more environmentally friendly and sustainable products. Examples include energy-efficient paintings/coatings for buildings,[18] coatings improving the efficiency of photovoltaic systems and batteries,[19] coatings to enhance the function of filters and membranes for water and air cleaning purposes,[20] coatings prolonging the lifetime of a product.[21]

For medical purposes, but also when targeting pharmaceutical applications or developing biocompatible surfaces on synthetic materials, biomacromolecules are frequently chosen as top-layer molecules in coatings. In addition to being well biocompatible, those large and often very complex molecules can come with a variety of beneficial properties, such as antimicrobial activity, lubricious behavior, the ability to hold and release bioactive molecules, and to enhance/weaken cell adhesion.[17] Especially when dealing with medical devices, a biomacromolecule coating created on the product surface can establish such beneficial multifunctionality on the device.

The range of materials used in the medical field is broad as it includes ceramics, metals, and polymeric materials. For many reasons, however, polymeric materials are often preferred. For instance, thin polymeric products such as foils can be both, transparent and flexible, and this enables a range of applications for which metals and ceramics are inappropriate. Two examples of such elastomeric polymer materials frequently used in the biomedical field are polydimethylsiloxane (PDMS) and polyurethane (PU). Since these materials combine different ben-

M. G. Bauer, O. Lieleg
School of Engineering and Design
Department of Materials Engineering
Technical University of Munich
Boltzmannstraße 15, 85748 Garching, Germany
E-mail: oliver.lieleg@tum.de
M. G. Bauer, O. Lieleg
Center for Protein Assemblies and Munich Institute of Biomedical Engineering
Technical University of Munich
Ernst-Otto-Fischer Str. 8, 85748 Garching, Germany
The ORCID identification number(s) for the author(s) of this article can be found under https://doi.org/10.1002/mame.202200681

DOI: 10.1002/mame.202200681

ADVANCED SCIENCE NEWS
www.advancedsciencenews.com

Macromolecular Materials and Engineering
Open Access
www.mame-journal.de

eficial properties, they are used in a broad range of applications. Whereas PDMS is used, for example, for catheters, micropumps, bandages, and implants.[22] PU has previously been applied as a coating to create antibacterial surfaces, to fabricate drug delivery vehicle, stents, surgical dressings, tissue engineering scaffolds, and cardiac patches.[23] However, thin polymeric foils typically also come with an issue: they tend to be quite adhesive to other materials and to themselves, the latter of which is a mechanism typically referred to as autohesion.[24] Handling or processing such autohesive foils is challenging, and this particular material property sometimes also interferes with the intended function of the foils: intravenous bags and the inflatable balloon parts of stents or intubation tubes would open up more easily if the polymer material would be less sticky. Similarly, fluidic elastomeric actuators (FEA), a very adaptive type of actuator used for soft robotics, could benefit from such coatings as well. Those FEAs comprise thin structural compartments made of elastomeric polymers which are actuated by changing the internal pressure—either by pneumatic or hydraulic means. Here, every time the chambers are deflated, the elastomeric walls of the chambers repeatedly come into contact with each other, and autohesive properties are undesired here. Of course, the application range of such FEAs is not limited to medical devices such as endoscopes; they are anticipated to be particularly suitable for applications promoting active safety in automotive, in industrial applications, and for haptic-interface tasks.[25] Overall, the current application range of polymer foils would certainly be extended if the autohesion of the foils could be mitigated—without losing the flexibility and transparency of the thin polymer material. Here, applying macromolecular coatings might be a good solution to achieve this goal.

Compared to the bulk material of a product, coatings are typically very thin. They rarely exceed a thickness of a few hundred micrometers, and they can even be constituted by a single monolayer of (macro)molecules.[26] Nonetheless, whenever coatings are applied, the idea is that the surface properties of the material are afterwards dominated by the coating—and that the coating does not influence the bulk properties of the material. If the coating procedure requires multiple treatment steps, it is expected that the last, final treatment creating the top layer of the coating is most important—and any influence the potential intermediate layers might have, is typically not investigated in detail.

In the past, two coating strategies were mainly put forward to immobilize biomacromolecules onto products. The first coating strategy, a carbodiimide-mediated coating process, is well established, frequently used, and creates covalent bonds between the substrate, the intermediate layer, and the top-layer of the coating. This strategy, however, can only be applied to certain materials, which limits its use. In contrast, the second coating strategy, a dopamine-assisted process, is comparably new and establishes an adhesive, intermediate layer on a very broad range of materials; with this approach, attaching a macromolecular top layer based on a combination of covalent and non-covalent bonds is very easily possible.[27]

Here, we ask how macromolecular coatings generated with either of the two coating strategies mentioned above affect the material properties of transparent, flexible polymer foils made from carbonate-based polyurethane (PCU) and PDMS, respectively. As biomacromolecules forming the top layer of the coatings, we select examples that come with different charge states: first, manually purified mucins, which are poly-anionic glycoproteins with a molecular weight (MW) of a few megadaltons; second, two dextrans variants, that is, synthetic polysaccharides, with a molecular weight of MW = 150 kDa that are functionalized with cationic residues (either with quaternary amine groups or with the cationic amino acid lysine). Then, we compare a range of material properties for coated and uncoated foils, including their flexibility, transparency, and autohesive behavior, and relate them to alterations in wettability, surface potential, and (putatively) surface roughness as brought about by the coating application.

2. Results and Discussion

For all following results two different materials, that is, polydimethylsiloxane (PDMS) and carbonate-based polyurethane (PCU), are tested either uncoated or coated with mucins, Lysine-Dextrans (LDex), or Q-Dextrans (QDex) via either a carbodiimide-mediated strategy (carbo) or a dopamine-based strategy (dopa). To clearly identify the different material/coating combinations studied in this manuscript, they will be referred to as follows: "material"—"coating strategy"—"top-layer molecule" with PCU/PDMS, uncoated/carbo/dopa, and mucin/LDex/QDex as alternatives for the respective sections.

As depicted in **Figure 1**, both foil materials tested here exhibit (in their untreated form) hydrophobic properties as indicated by contact angle (CA) values above 90°: we measure 113° ± 2° for PDMS and 107° ± 2° for PCU. However, the surface wettability of both materials should be considerably altered by applying a macromolecular coating. In fact, three different aspects of the two coating strategies tested here can contribute to rendering the base materials more hydrophilic: the plasma activation (which is the first step of the carbodiimide-based coating process), the dopamine pre-coating, as well as the mostly hydrophilic structures of the selected macromolecules.[28] And indeed, all tested surface coatings can reduce the CA of the foils—at least to some extent (Figure 1). On PDMS (Figure 1a), the hydrophilizing effect achieved with the two mucin coatings is clearly stronger than the effect obtained with the two dextran coatings. Probably, owing to their much larger molecular weight, the mucins (MW ≈ 4–6 MDa) can alter the surface properties of the material more efficiently than the smaller dextrans (MW = 150 kDa). Such a clear difference between the different coatings is, however, not visible for PCU (Figure 1b). Maybe here, on a material that is less hydrophobic than PDMS, the smaller dextrans are sufficient to achieve a similarly strong hydrophilization as the larger mucins.

Of course, whereas a change in the wetting behavior of the foils is a clear indication that the surface treatment has worked, this result may not correlate with a putative alteration in the autohesive properties of a foil (which typically occur in the dry state of a foil). Thus, we next compare the strength of these autohesive properties of differently coated foils to that of their uncoated counterparts. To do so, two different pulling tests are conducted, in which the orientation of the pulling direction with respect to the contact interface of two foil samples differs: As depicted in the schematics of **Figure 2**a,b, lap shear tests probe a configuration where the pulling force is applied in parallel to the sample interface (Figure 2a); in contrast, in detachment tests, the pulling force is orientated orthogonally to the interface (Figure 2b).

ADVANCED SCIENCE NEWS
www.advancedsciencenews.com

Macromolecular Materials and Engineering
www.mame-journal.de

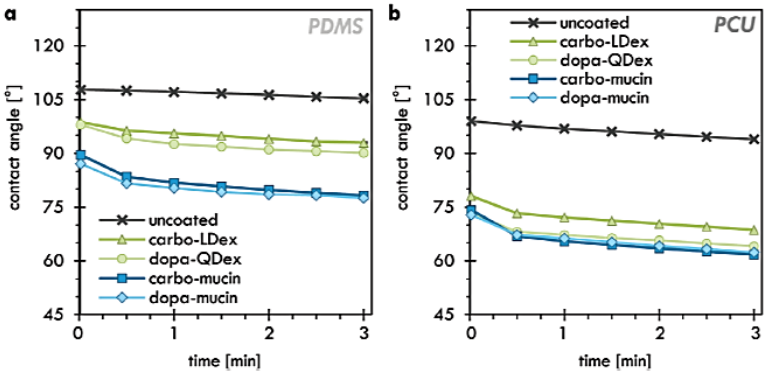

Figure 1. Influence of surface modifications on the wettability of PDMS and of PCU foils. The development of the water CA determined on uncoated (cross symbols), carbo-LDex coated (triangles), dopa-QDex coated (circles), carbo-mucin coated (squares), and dopa-mucin coated (diamonds) surfaces of a) PDMS samples and b) PCU samples is shown over a time period of 3 min. The error bars depict the error of the mean determined from at least 10 samples. If no error bars are visible, they are in the range of the size of the symbols.

The results in Figure 2c show that all coating variants—partial and full coatings—slightly increase the resistance of the PDMS foils against lap shear movement (compared to uncoated PDMS foils); however, no difference was found between the base coated samples (i.e., carbo coated and dopa coated) and their corresponding fully coated counterparts. For the "dopa"-based coatings, one explanation for this outcome could be that, at some spots of the interface, the sticky dopamine layer is not entirely covered by the top layer of macromolecules. However, for the "carbo"-based coatings, such an explanation does not apply. Interestingly, the results we obtain for the detachment tests (Figure 2d) indicate the opposite behavior, that is, a significant reduction in the detachment resistance—at least for the full "carbo"-coatings. Additionally, here, a significant difference between the results of each intermediate step and the corresponding completed coatings was observed, indicating that PDMS-carbo and PDMS-dopa foils exhibit a stronger autohesive behavior than fully coated PDMS foils.

For PCU samples (Figure 2e, f), the observed behavior follows the same trend as for the detachment tests conducted with PDMS samples. Here, both in the lap shear tests (Figure 2e) as well as in the detachment tests (Figure 2f), the "carbo"-coatings significantly decrease the resistance of the material towards the respective movement. For the carbo-mucin coating, this effect is even so strong that the two foil samples sometimes spontaneously separate before the lap shear measurement can be started. Because of this behavior, the number of measuring points we report for the PCU-carbo-mucin samples is lower than for the other samples, and the determined value should be interpreted as an upper limit rather than a real average. A similar effect is observed for the PCU-carbo-LDex samples as well as PCU-carbo samples; however, here, it occurred less frequently. Owing to this complication, which affects the comparability of the sample sets, the horizontal lines indicating significant differences in Figure 2e are dashed. In contrast, we did not find a significant difference between the results obtained for samples fully treated with the dopamine-based coating strategy compared to those obtained for the uncoated materials, but such a difference was observed between the dopa-coated and the dopa-QDex coated as well as the dopa-LDex coated samples. In the detachment tests (Figure 2f), such a premature separation of the samples is technically not possible, but the overall trend is similar to the behavior observed in the lap shear tests: the "carbo"-coatings significantly reduce the resistance to lap shear and detachment, respectively, whereas the "dopa"-coatings do not. Moreover, we note that the values obtained for the PCU-carbo-mucin samples are extremely low, that is, two to three orders of magnitude smaller than those determined for uncoated samples. We speculate that a combination of two effects might be responsible for the observed behavior. First, the more efficient hydrophilization obtained for the mucin coatings (see Figure 1) indicates a more efficient surface coverage achieved with this particular macromolecule; second, the larger mucins might generate a stronger steric hindrance effect compared to the smaller dextrans. The latter might reduce the probability that a local, uncovered spot of the sticky dopamine layer can get in direct contact with the opposing sample surface thus decreasing its detachment resistance.

To further investigate those somewhat unexpected results, we determine the zeta potentials of the surfaces of the differently coated and uncoated foils. All uncoated materials are clearly negatively charged; we measure − 45 mV ± 0.6 mV for PDMS (Figure 3a, left) and − 41 mV ± 2 mV for PCU (Figure 3a, right). Based on the structural formulas of the polymers comprising those foils, finding such strongly anionic properties is not obvious (especially for the PDMS samples, which contain mostly uncharged and non-polar methyl groups). However, a similar behavior has been observed previously on PDMS[29] as well as on other solid surfaces which were anticipated to be inert due to the lack of ionizable surface groups.[30,31] There, this behavior was rationalized by an asymmetric adsorption of water ions; however, the origin of this effect and whether hydroxide ions or hydronium ions show a higher affinity towards the polymeric surface is still under discussion.[31,32] In the presence of the full coating, those surface zeta potentials should be changed—and both, the respec-

ADVANCED SCIENCE NEWS
www.advancedsciencenews.com

Macromolecular Materials and Engineering
www.mame-journal.de

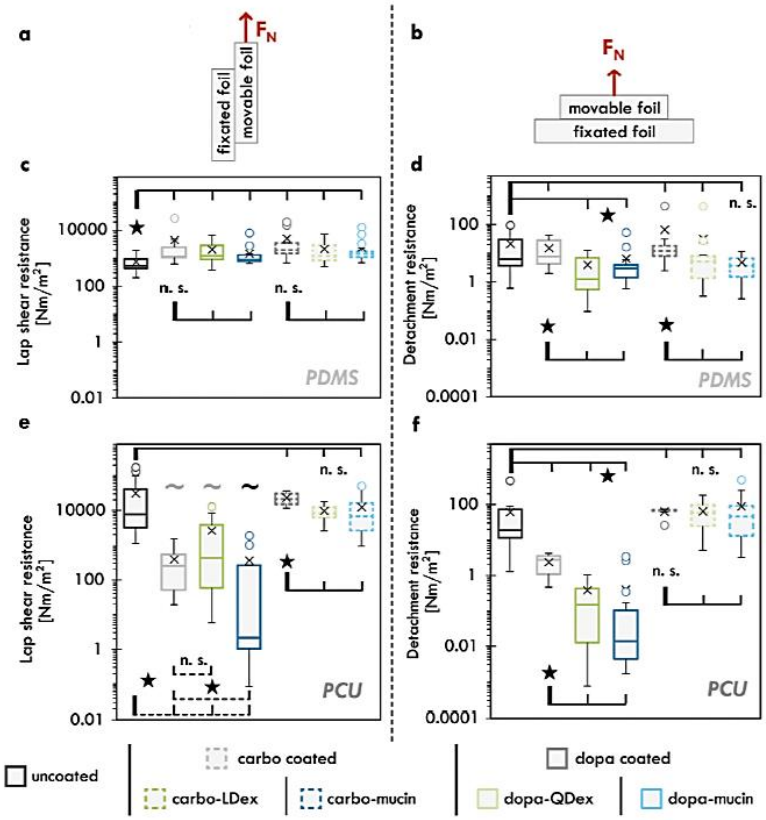

Figure 2. Resistance of (surface modified) foils against lap shear and detachment. a,b) Schematics depicting the two pulling modes tested here. For the lap shear tests (a, c, e), a force was applied parallel to the interface of the two foils; for the detachment tests (b, d, f), a force was applied orthogonally to the interface. c,e) Results of the lap shear tests. The tilde symbols in d) mark conditions where some sets of foils detached before the measurements could be started (grey tilde: 20% of the test sets; black tilde: 50% of the test sets). d,f) Results of the detachment tests. All diagrams display data obtained for uncoated samples (black lines), carbo coated samples (full grey lines), carbo-LDex coated samples (full green lines), carbo-mucin coated samples (full blue lines), dopa coated samples (dashed grey lines), dopa-QDex coated samples (dashed green lines), and dopa-mucin coated samples (dashed blue lines). The boxes denote the median (central line), the median plus the first quartile (top line), and the median minus the third quartile (bottom line) as determined for at least 8 sample sets. Cross symbols indicate the mean, and circles depict outliers based on an outlier multiplier of 2.2. Asterisks indicate significant differences ($p = 0.05$) and n.s. indicates that no significant difference was found. The legend at the bottom of the figure applies to all diagrams.

tive pre-treatment (dopamine incubation vs plasma activation/vs silane coupling) as well as the macromolecule used for creating the top layer in the coating should have an influence here. Ideally, the surface properties of the foil would become clearly dominated by the properties of the macromolecule used; and zeta potential measurements conducted on macromolecular solutions containing ether mucin, QDex, or LDex (which are all conducted at identical conditions to ensure comparability, that is, at a pH value of ≈ 5.6 and in the presence of 1 mM KCl) clearly show that those macromolecules have very different charge states (Figure 3b): mucin (−28 mV ± 0.3 mV) is clearly anionic, QDex (13 mV ± 4 mV) is clearly cationic, and LDex (−1 mV ± 0.3 mV) is almost uncharged at this pH value.

Dopamine carries an amine group and thus is cationic; therefore, applying a dopamine pre-coating should render the foils less anionic. On PDMS, this alteration in the surface charge state induced by dopamine is only small (Figure 3c); in contrast, we find a strong shift by 25 mV for the PCU foils (Figure 3d). For the full, dopamine-assisted coatings generated on PDMS, we find very similar values as for the dopamine pre-coating alone.

Apparently, the surface properties of PDMS are—in terms of charge—so strong that it is not easily possible to override them with a macromolecular coating as we attempt it here. On the PCU samples, however, either macromolecule entails a strong change in the surface charge state, and the obtained result agrees with those of the macromolecules used: Attaching the QDex

ADVANCED SCIENCE NEWS
www.advancedsciencenews.com

Macromolecular Materials and Engineering
Open Access
www.mame-journal.de

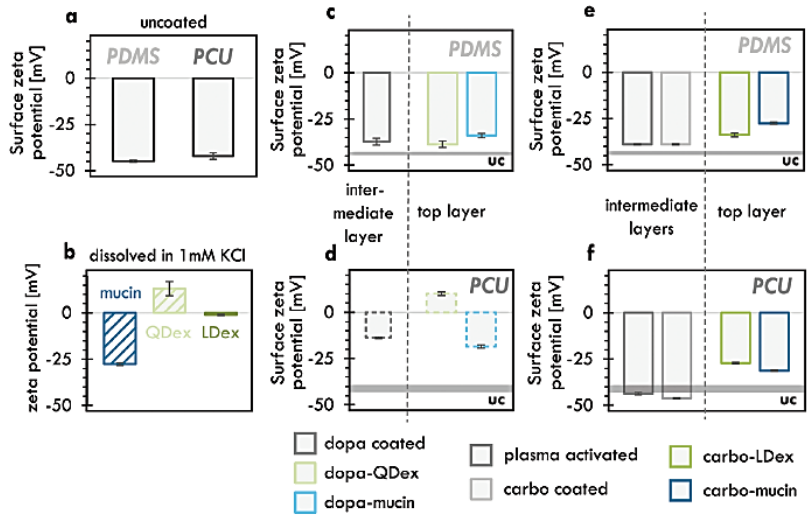

Figure 3. Zeta potentials of bare and coated substrate materials as well as of the molecules used as top layers in the coatings. All values shown were determined at a pH value of 5.6. a) Surface potentials of the uncoated (uc) materials. b) Zeta potentials of the macromolecules used as top-layers. c,d) Results obtained for the dopamine-based coating strategy. e,f) Results obtained for the carbodiimide-mediated coating strategy. The grey bar labeled with "uc" in diagrams (c–f) indicates results obtained for the uncoated substrate as displayed in (a). The legend at the bottom of the figure applies to diagrams (c–f). Error bars depict the error of the mean as determined from at least 3 (sets of) samples. If no error bars are visible, they are in the range of the size of the symbols.

molecules leads to an overall cationic surface whereas attaching the mucins leads to an anionic surface, which is (in absolute numbers) less strongly charged than pure PCU itself. However, neither of the two coatings fully reach the zeta potential values we determined for the corresponding macromolecule in solution. This indicates that, even if a rather efficient coating is created, the intermediate dopamine layer still affects the surface properties of the coating.

For the carbodiimide-mediated coating process, the two pre-conditioning steps seem to have only minor influences on the measured zeta potential, and this holds true for both foil materials tested here (Figure 3e,f). However, when the full coatings are applied, we do find relevant alterations in the measured surface zeta potentials. When using mucins as a top layer molecule, the measured surface potentials are very similar to that of mucins in solution, indicating a very efficient alteration of either foil surface by the carbodiimide-mediated coating strategy. When using LDex molecules for those covalent coatings, the obtained surface potentials are still strongly anionic and comparable to those achieved with mucins. However, the measured values are "less negative" than those obtained for "incomplete" coatings carrying the pre-conditioning, intermediate layers only. In other words, also here, attaching the final macromolecule layer has a clear influence on the final surface potential of the material.

So far, mainly desired alterations of surface properties as induced by the different coatings were examined; however, surface coatings might also lead to undesired changes of certain surface properties (e.g., the surface roughness) or they could even negatively impact the bulk behavior of the sample—and neither is typically desired. Accordingly, when modifying the surfaces of a foil, it is crucial that the other characteristic properties of the material, that is, its transparency and flexibility, are maintained. Ideally, of course, the applied coatings were to only alter the surface properties of the foils, but this needs to be verified. Therefore, in another set of tests, we ask if the desirable material properties of PDMS and PCU foils are affected by the different coatings investigated here.

First, the transparency of foils with and without coatings is compared by quantifying their absorbance behavior in the UV–vis range, that is, between wavelengths of 190 to 900 nm (**Figure 4**a,b). Importantly, we find that none of the coatings alters the transparency of PDMS or PCU foils in a considerable manner.

This good transparency of both, PDMS and PCU foils, agrees with the very low surface roughness values (the root-mean-square-height S_q and the developed interfacial ratio S_{dr}) we determine for them using laser scanning profilometry: we obtain $S_{q,PDMS} = (0.4 \pm 0.2)$ µm and $S_{q,PCU} = (0.2 \pm 0.1)$ µm, as well as $S_{dr,PDMS} = (1 \pm 1)$ % and $S_{dr,PCU} = (0.6 \pm 0.2)$ % (Figure 4c,d,f,g). After applying the different coatings, these roughness values remain in a very similar range. Additionally, we find very similar S_{pc} values for coated and uncoated samples (and this holds true for both foil materials investigated here). As this particular metrological parameter quantifies the curvature of peak structures on the surface, this finding suggests that the different coating procedures do not entail a local accumulation of chemicals/molecules (especially dopamine is known for forming agglomerates) but rather lead to spatially homogenous coatings.

ADVANCED SCIENCE NEWS
www.advancedsciencenews.com

Macromolecular Materials and Engineering
www.mame-journal.de

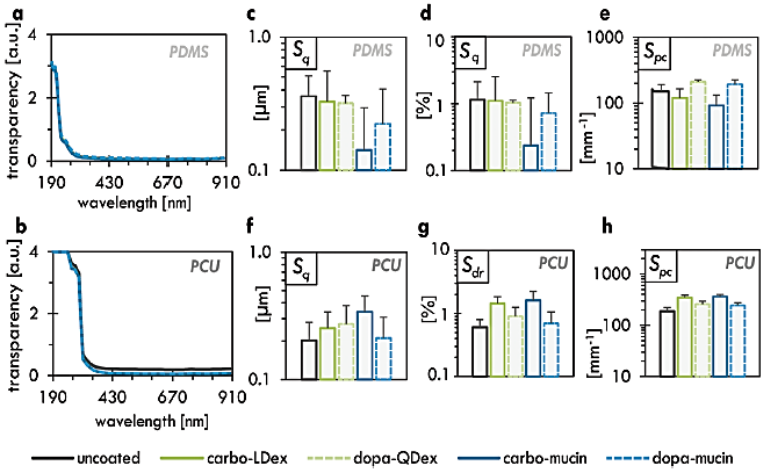

Figure 4. Transparency and surface roughness of uncoated and coated PDMS and PCU foils. a,b) Absorbance behavior of the samples in the UV–vis range. c–h) Metrological parameters quantifying different features of the foil surfaces: the root-mean-square-height S_q (c, f), the developed interfacial ratio S_{dr} (d, g), and the arithmetic mean peak curvature S_{pc} (e, h) are compared. All diagrams display results for uncoated samples (black lines), carbo-LDex coated samples (full green lines), dopa-QDex coated samples (dashed green lines), carbo-mucin coated samples (full blue lines), and dopa-mucin coated samples (dashed lines). The legend at the bottom of the figure applies to all diagrams. Error bars depict the error of the mean as determined from at least 6 samples. If no error bars are visible, they are in the range of the size of the symbols.

To compare the flexibility of the foils before and after coating, we determine the torque required to twist a foil sample and compare the surface topography of each sample before and after such a twisting experiment. Again, our aim is to test whether the coating application changes the material behavior rather than interpreting the absolute values obtained from those measurements. Thus, to ensure optimal comparability of the results obtained with different samples, all measured torque values are normalized to the cross-section of the corresponding sample. Similarly, we only evaluate the difference between the determined surface roughness parameters before and after torque application.

Our first observation is that all tested foil samples (i.e., uncoated and coated ones) show a similar overall behavior: at first, the measured torque values are comparably high; then, they decrease within ≈ 1 min to a plateau value, which is maintained for the rest of the measurement (which had a total duration of 10 min). To facilitate a quantitative comparison of those time-dependent results, we focus on the initial torque value (**Figure** 5a, c) as well as the plateau value (Figure 5b, d), which we determine as the mean of all torque values recorded after 60 s. For the initial torque values, we find no significant differences between the coated samples and the uncoated samples, respectively (and this holds true for both, PDMS and PCU samples).

Moreover, for all samples, the drop in the torque values (from the initial value to the plateau value) is about one magnitude of order. Thus, all measured plateau values are very similar—only the results obtained for the PCU-carbo-mucin samples are slightly lower than the values determined for uncoated PCU samples. Accordingly, we find no significant differences when we compare the change in the surface texture of the foil samples: neither when analyzing the height parameter S_q (Figure 5e, g) nor when investigating the hybrid parameter S_{dr} (Figure 5f, h), we find significant differences between any of the coated samples and the respective uncoated control samples. This result is confirmed when we compare the width of the foil samples before and after the flexibility testing (Figure 5 i, k): here, we detect no sign of plastic deformation/narrowing as the results obtained for coated and uncoated samples are virtually identical. Thus, the flexibility of the thin films tested here is not altered by the applied coatings.

Taking into account all the results presented above, we conclude: Eliminating the autohesive behavior of transparent, elastomeric foils is not a trivial task. Here, among the different options tested, the carbo-mucin coating generated on PCU (the material that initially showed the stronger autohesion behavior) achieved this goal best. On PDMS foils, the obtained effects were comparably weak—which is somewhat surprising considering that both substrate materials examined here are transparent, autohesive elastomers with initially similar wettabilites and very similar surface zeta potentials. Our analysis of the surface zeta potentials obtained after different steps of the coating procedures suggests that, for the PDMS samples, the initial surface properties cannot be fully altered even if the coatings are successfully applied. Moreover, we found that, even if eventually the same top-layer macromolecule is applied, the carbodiimide-mediated coatings perform better in reducing the very strong autohesive properties of the PCU samples than dopamine-assisted coatings. For the latter, it seems that the intermediate layer is not fully covered by the macromolecular top layer (even after overnight incubation), which is why (locally) some uncovered, sticky dopamine molecules might still give rise to undesired adhesive properties. Nevertheless, none of the coating variants tested here had any detectable negative impact on the flexibility, transparency, or

ADVANCED SCIENCE NEWS
www.advancedsciencenews.com

Macromolecular Materials and Engineering
Open Access
www.mame-journal.de

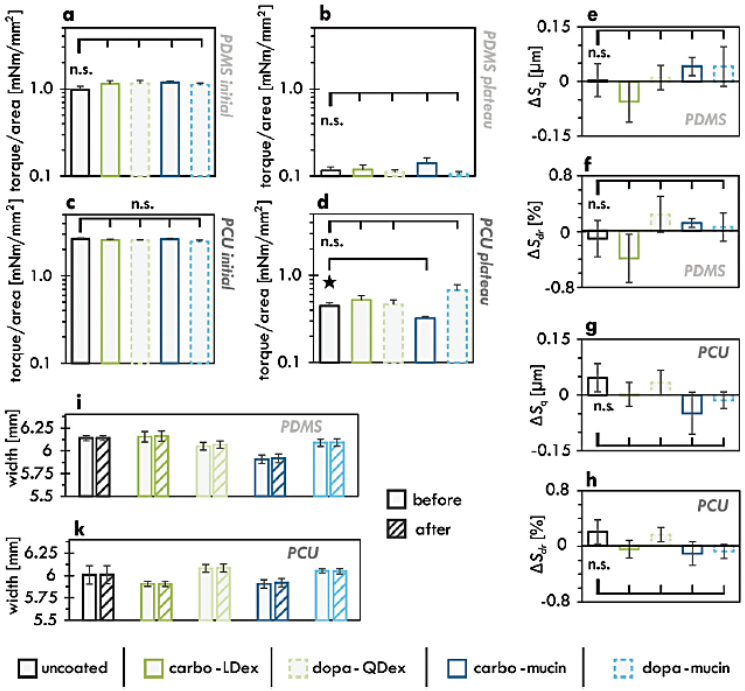

Figure 5. Torsional flexibility of bare and coated polymer foils and topographical analysis of the foils after twisting tests. a–d) Torque values determined at the beginning (a, c) and in the plateau phase (b, d) of the flexibility tests. e–h) Differences in the surface roughness parameters S_q (e, g) and S_{dr} (f, h) as determined before and after the flexibility tests. i,k) Widths of the foil samples before (empty bars) and after (striped bars) conducting the flexibility tests. All diagrams display results for uncoated samples (black lines), carbo-LDex coated samples (full green lines), dopa-QDex coated samples (dashed green lines), carbo-mucin coated samples (full blue lines), and dopa-mucin coated samples (dashed blue lines). Error bars depict the error of the mean determined from at least 5 samples. Asterisks indicate significant differences ($p = 0.05$); n.s. indicates no significant differences. The legend at the bottom of the figure applies to all diagrams.

roughness of the foils they were generated on—and this is a very promising result.

3. Conclusions

Here, we could show that the final surface properties of coated polymeric foils are not only dominated by the properties of the applied top layer-molecules but can still be significantly influenced by the substrate and the selected coating strategy. Two aspects should be kept in mind: first, even though dopamine-based coatings are applicable to a wide range of substrates and can immobilize various top-layer molecules, the intermediate dopamine layer seems to affect the final surface properties of the coated material more strongly than the intermediate layers required for the more complex and more time-consuming carbodiimide-based coatings. Second, the results presented here underscore the importance of choosing a substrate-specific coating strategy on the one hand and a suitable top-layer molecule combination on the other hand—and quantifying the properties of the created coatings in detail is key when tailoring them for a specific application.

4. Experimental Section

If not stated differently all chemicals were obtained from Carl Roth, Karlsruhe, Germany.

Polymeric Materials: In this study, the following two different polymeric materials were examined:

Polydimethylsiloxane (Sylard 184, Dow Corning, Midland, MI, USA): PDMS samples were prepared manually by first mixing PDMS oil in a 10:1 (w/w) ratio with the curing agent and exposing the mixture to vacuum for 1 h to remove air bubbles. The mixture was then filled into a well plate (Ø 15 cm, Greiner Bio-One GmbH, Frickenhausen, Germany) such that the PDMS could spread evenly; this process led to samples with a thickness of ≈ 300–400 µm. Silicone curing was allowed to take place at 70 °C for 4 h, subsequently, the samples were further tempered at 110 °C for 2 h. Only the surface properties of the side facing the bottom of the well plate during curing were evaluated.

Polycarbonate-Based Polyurethane (Carbothane AC-4085A, Lubrizol Advanced Materials, USA): This was a medical grade, polycarbonate-based, thermoplastic, aromatic polyurethane and was extruded by Gerlinger Industries GmbH (Netzschkau, Germany) into foils with a thickness of ≈ 150–200 µm; those foils had a better surface quality on one side, and only the surface properties of this high-quality side were evaluated.

All further preparation steps to shape the samples into the desired dimensions were conducted manually: either they were cut with scissors

ADVANCED SCIENCE NEWS
www.advancedsciencenews.com

Macromolecular Materials and Engineering
Open Access
www.mame-journal.de

and scalpels or punched into a circular shape with a manual eyelet press (Istabreeze Germany GmbH, Bad Rappenau, Germany). Prior to any modifications or tests, all samples were cleaned in 80 % (v/v) ethanol and deionized water (ddH_2O) for 15 min each and then dried.

Surface Coatings: All samples were examined in an uncoated and a coated version. Coatings were applied either via a multi-step carbodiimide-mediated coating process or via a two-step dopamine-based coating process.

CARBOdiimide-Mediated Coating (carbo): For this coating process to be feasible on both materials, several coating conditions had to be adjusted to meet the specific properties of each material. Whereas the coating process for PDMS was conducted as published by Winkeljann et al.,[33] the process parameters had to be adjusted for the thermoplastic PCU. This was, on the one hand, necessary to achieve a similarly efficient plasma activation on the more resilient PCU; on the other, to compensate for the reduction of the incubation temperature (as PCU has a relatively low Vicat temperature), the concentrations of reactants and/or prolonged treatment times were increased to maintain the efficiency of the multi-step coating procedure. In the following process descriptions, different conditions applied to PDMS and PCU, respectively, will be listed in curved brackets as follows: {applied to PDMS/applied to PCU}.

The surfaces of the samples were activated by applying an atmospheric plasma treatment at a low pressure of 0.4 mbar using a power supply of {30 W/56 W} for {1.5 min/25 min}. As soon as the plasma activation step was completed, each sample was immersed into ≈ 1 mL of a silane solution containing 1 % (w/v) TMS-EDTA (N-[(3-trimethoxysilyl)propyl] ethylenediamine triacetic acid trisodium salt, abcr GmbH, Karlsruhe, Germany) dissolved in 10 mM acetate buffer at pH 4.5 and incubated at {60 °C/37 °C} for {5 h/8.5 h} to create a silane pre-coating. Subsequently, the samples were removed from the silane solution and dipped into isopropanol to wash off any excess solution. To stabilize the silane pre-coating, the samples were exposed to {110 °C & atmospheric pressure/room temperature (RT) & at $p_{rel} = -800$ to -600 mbar} for {1 h/16 h}. Afterwards, the samples were washed in 96 % (v/v) ethanol on a rolling shaker (≈60 rpm) for 1 h to remove any unbound silane molecules; then, they were dipped into ddH_2O to wash off any ethanol residues. To initiate the macromolecular coupling step, the samples were immersed into a solution containing 5 mM EDC (1-ethyl-3-(3-dimethylaminopropyl)carbodiimide-hydrochloride) and 5 mM sulfo-NHS (N-hydroxysulfosuccimid sodium salt, abcr) dissolved in 100 mM MES (2-(N-morpholino ethanesulfonic acid, AppliChem GmbH, Darmstadt, Germany) buffer at pH 5 (≈ 1 mL per sample). This solution was prepared just before use to avoid preliminary hydrolysis of the coupling agents. Incubation at RT was allowed to take place on a slowly moving tilting shaker for 30 min. Subsequently, the samples were immediately transferred into ≈ 1 mL/sample Dulbecco's phosphate buffered saline (pH = 7.4, DPBS, Sigma-Aldrich Inc., Darmstadt, Germany) containing either 0.05 % (w/v) lysine-dextran (MW = 150 kDa, TdBlabs, Uppsala, Sweden) or 0.05 % (w/v) lab-purified mucins (mainly MUC5AC, which was manually purified from pig stomachs as described by Marczynski et al.).[34] During an incubation step of at least 16 h, the samples were slowly moved by a tilting shaker at 7 °C. Once the macromolecular coupling was finalized, to remove unbound macromolecules, the samples were cleaned in 80 % (w/v) ethanol by placing them onto a slowly moving tilting shaker for 30 min.

DOPAmine-Based Coating (dopa): For the dopamine coating variant, both materials were treated in the same way. To achieve a smooth and homogenous surface coating, and to prohibit the undesired sedimentation and attachment of larger (poly-)dopamine agglomerates onto the surfaces, the samples were positioned vertically in a suitable coating container, a freshly prepared solution (≈ 1 mL/sample) containing 0.4 % (w/v) dopamine hydrochloride (Sigma-Aldrich) dissolved in 20 mM HEPES buffer (4-(2-hydroxyethyl)-1-piperazineethanesulfonic acid; pH 8.5) was added, and the container was placed onto a slowly moving tilting shaker for 3 h. To wash off excess, not fully attached dopamine, the samples were dipped into ddH_2O and subsequently immersed into 20 mM HEPES buffer (pH 7) containing either 0.1 (w/v) % Q-dextran (MW = 150 kDa, TdBlabs) or 0.1 % (w/v) of lab-purified mucins. Then, the samples were once more placed onto a slowly moving tilting shaker at RT overnight. To remove any unbound macromolecules, the samples were dipped into ddH_2O, into 80 % ethanol, and again into ddH_2O.

Finally, all samples (independent of how they were coated) were either placed into 20 mM HEPES buffer (pH 7) and stored at 7 °C until further use, or they were dried at RT for at least 24 h (for tests conducted with dry samples).

The specific top-layer molecules studied here were chosen for the following reasons: mucins have recently been introduced as powerful components of coatings for medical devices,[4,7,35] and both coating strategies can be used to immobilize those anionic glycoproteins on PDMS and PCU films. As a counterpart for those large biomacromolecules, dextrans were selected, which were also regularly used in biomedical studies—especially as base material for drug delivery applications, and tissue engineering purposes.[36,37] Such dextrans were commercially available at different molecular weights and can carry different functionalizations (i.e., charged residues).[36,38a,38b] To serve as a positively charged counterpart to the anionic mucin, QDex was chosen due to its strong cationic character (according to the manufacturer) and its strong interaction with dopamine layers which was observed in pretests. However, since such QDex molecules do not possess primary amine groups, applying the carbodiimide-mediated-coating strategy to them was chemically not feasible. Thus, as a suitable alternative, the zwitterionic LDex was used for carbo-coatings since this molecule comprises the same dextran backbone, was available at the same molecular weight, and, at least locally, carries cationic groups.

Contact Angle Measurements: CA measurements were conducted using a drop shape analyzer device (DSA25S, Krüss GmbH, Hamburg, Germany). For examining the influence of the coatings on the time-dependent wetting behavior of the materials, dried samples were placed in front of the device-integrated high-resolution camera (ac1920, Basler, Ahrensburg). For imaging, image processing, and image analysis, the device-specific software ADVANCE (AD4021 v 1.13, Krüss GmbH) was used. An automatic imaging protocol was employed that was initiated by a water droplet (6 µL ddH_2O) crossing a trigger line positioned just above the sample surface. For the first two seconds after triggering, the camera captured images with a frequency of 10 fps. For evaluation, only the first image of the droplet uninfluenced by the cannula as well as the last image of this first series were used. Subsequently, images were captured (each for 1 s at 3 fps) at various additional time steps up to 20 min after the trigger line was crossed. Here, only the second image of each series was evaluated, provided that its quality (sharpness, lighting, no vibration) was sufficient; otherwise, the remaining images served as fallback alternatives. On each image, the CA values were determined as the water-enclosed angle between the surface and the edge of the droplet (using a manually adjusted baseline and the software-integrated Young–Laplace fit method).

Lap Shear Tests: For all mechanical examinations, that is, lap shear tests, detachment tests, and flexibility tests, a commercial shear rheometer (MCR 302, Anton Paar, Graz, Austria) equipped with a sample holder unit for disposable bottom plates (P-PTD200/80/I, Anton Paar) was used.

For lap shear tests, two foil samples (≈ 12 mm x 25 mm each) were placed on top of each other such that the overlap region was ≈ 10 mm; then, they manually were pressed together for 10 s, and the contact area was precisely measured using a digital caliper. Both foil samples were inserted into one clamp each and the normal force was reset. Finally, the measuring head was lifted at a velocity of 30 µm s^{-1} until both samples fully detached from each other. For comparing the obtained results, the determined force values were divided by the measured contact area to receive a shear stress.

Detachment Tests: For adhesion tests, a round foil with a diameter of 10 mm was attached to a commercial PP08 measuring shaft (Anton Paar) using double-sided adhesive tape. First, the zero gap was detected on a disposable aluminum bottom plate (Cat. No. 302 234, Anton Paar), and then a second foil was attached to the bottom plate using double-sided adhesive tape. Afterwards, the normal force was reset, and the shaft was further lowered until a normal force of 5 N was reached, which was maintained for 30 s. Subsequently, reached z-position was held for 60 s to give the foil materials some time to relax. Then, the measuring head was lifted up at a constant speed of 15 µm s^{-1}, and a measuring point was recorded every 0.2 s.

ADVANCED SCIENCE NEWS
www.advancedsciencenews.com

Macromolecular Materials and Engineering
www.mame-journal.de

Zeta Potential Measurements: Zeta potentials were determined for the bare and the coated foil surfaces as well as for the macromolecules (in solution) used as top-layers in the coatings. To ensure comparability of the results, both types of experiments were performed with the same electrolyte solution, that is, ultrapure water containing 1 mM KCl (pH ≈ 5.6).

Zeta Potential Analysis of Solid Surfaces: The zeta potentials of solid foil surfaces were determined using a SurPASS 3 Eco device (Anton Paar) equipped with an adjustable gap measuring cell for planar samples (Cat. No. 159 880, Anton Paar). To avoid (re-) hydration effects of the coatings or substrates affecting the measurements in different ways, all samples (i.e., bare, partially coated, or fully coated) were stored in ultrapure water for at least 4 h prior to any measurement. Then the samples were cut into shape (rectangles of 10 mm x 20 mm), and a set of two identical samples was inserted into the measuring cell following the instructions of the device's manufacturer. The gap height was adjusted to a value between 95 and 110 µm and the cell containing the samples was flushed at least twice with the electrolyte solution before a measurement was started at room temperature.

Zeta Potential Analysis of Macromolecular Solutions: To assess the zeta potentials of the different macromolecules in solution, the electrophoretic light scattering mode of a LiteSizer500 (Anton Paar) was used. Therefore, an omega cuvette (Mat. No. 155 765, Anton Paar) was filled with the electrolyte solution containing 0.05 % (w/v) of the desired top-layer macromolecule and inserted into the machine. The zeta potentials were then analyzed at 21 °C after an equilibration time of 2 min.

UV/Vis Measurements: To examine the influence of the coatings on the transparency of the materials, light absorption measurements in a wavelength range from 190 to 900 nm (in 10 nm steps) were conducted using a microplate reader with cuvette port (SpectraMax ABS Plus, Molecular Devices, LLC, San Jose, US). For each material/coating combination, a UV-cuvette was filled with 1.4 mL of ultrapure water and used as a reference. In those measurements, special care was taken to ensure that all samples were placed at the same position in the laser beam path.

Confocal Laser Scanning Microscopy: Confocal laser scanning microscopy was conducted using a VK-X1000 microscope (Keyence, Oberhausen, Germany) equipped with a 20x magnification lens (CF Plan, NA = 0.46; Nikon, Chiyoda, Tokyo, Japan). Prior to performing the measurements, all samples were dried and cleaned with particle-free pressurized air. Then, the samples were placed onto a glass slide using a droplet of distilled water or 80 % (w/v) ethanol as a thin spacer for PCU and PDMS, respectively. This was necessary to allow the measuring device to automatically differentiate between the very thin, transparent foils and the glass slide.

All material/coating combinations were examined before and after subjecting them to torsion tests. At least four samples were analyzed per condition. To determine the full sample width (which later enables a comparison of this sample width before and after the torsion tests), 2×11 images were acquired across the smaller dimension of each sample. To evaluate the surface roughness of the samples (using the software MultiFileAnalyzer (Keyence)), single images were analyzed (by excluding those displaying the edges of the samples). Here, the images were preprocessed as follows: First, a linear tilt based on the full image area was removed; second, the sample waviness (a wave form with correction strength 5 out of 20) was subtracted; third, missing points were filled by estimating the mean height value of the surrounding points. From the adjusted topographical images, the following metrological parameters (based on ISO 25178-2) were calculated: the root-mean-square-height S_q:

$$S_q = \sqrt{\frac{1}{A}\int\int_A z^2(x,y)\,dxdy} \tag{1}$$

the developed interfacial ratio S_{dr}:

$$S_{dr} = \frac{1}{A}\left[\int\int_A \left\{\sqrt{\left[1+\left(\frac{\partial z(x,y)}{\partial x}\right)^2+\left(\frac{\partial z(x,y)}{\partial y}\right)^2\right]}-1\right\}dxdy\right] \tag{2}$$

the arithmetic mean peak curvature S_{pc}:

$$S_{pc} = -\frac{1}{2}\frac{1}{n}\sum_{k=1}^{n}\left(\frac{\partial^2 z(x,y)}{\partial x^2}+\frac{\partial^2 z(x,y)}{\partial y^2}\right) \tag{3}$$

This set of parameters was chosen as S_q (which evaluates the height distribution) and S_{dr} (which describes the relative increase of the determined surface area due to roughness features compared to an entirely planar sample) were frequently used surface roughness parameters that give a good overview over the surface structure of a sample. Additionally, S_{pc} was selected as a specific parameter evaluating the curvature of the detected peaks; this feature was used to investigate whether any dopamine agglomerates had settled onto the surface as a consequence of the surface modification procedure.

Torsion Tests: For torsion measurements, the rheometer was equipped with a measuring shaft for disposable measuring heads (CP/DP70, Anton Paar). To both, the sample holder unit and the measuring shaft, an in-house manufactured aluminum clamp was attached as described in Kimna et al.[39] Both clamps were positioned in a parallel orientation, and a foil sample (5 mm x 10 mm) was fixated such that the free length of the samples was always comparable (≈12 mm). The normal force was reset, and the top clamp was moved upwards to pre-stretch the sample until a normal force of −0.3 N was achieved. For the actual torsion measurements, the measuring head performed an oscillating movement over 116.5° to each side at a frequency of 0.2 Hz; measuring points were collected every 0.6 s for a total duration of 10 min. To account for differences in sample thickness, the thickness of each sample was determined using an electronic micrometer screw (Filetta, Schut Geometrische Meettechniek bv, Groningen, Netherlands). The exact width of each sample was determined from the stitched images obtained from confocal laser scanning microscopy (see above). To ensure comparability, all determined torque values were divided by the cross-section (determined by multiplying the sample thickness and width) of the corresponding sample. To examine the influence of the torsional deformation on the material structure, confocal laser scanning microscopy images across the middle section of each sample were captured as described above; images acquired before and after the torsion tests at the same position on each sample were compared.

Statistical Analysis: Tests for statistical significance were conducted for all quantitative results shown in Figure 2 and Figure 5. Each set of results was first tested for a normal data distribution using a Shapiro–Wilk test, then, a two-sample F-test was applied to check for equal variances. To test for significant differences between normally distributed samples, a two-sample t-test was applied when the homogeneity of variances was confirmed, whereas a Welch's t-test was performed for heteroskedastic sets of samples. For samples that were not normally distributed, a Wilcoxon–Mann–Whitney test was performed. All statistical analyses were conducted using Microsoft Excel for Microsoft 365 (Version 2206; Microsoft Corporation) employing the add-in Real Statistics Resource Pack software (Release 7.6, Copyright 2013–2021; Charles Zaiontz); differences were considered statistically significant if a p-value below 0.05 was obtained.

Acknowledgements

The authors thank Tobias Fuhrmann for his assistance with the mucin purification and their APRICOT project partners at the Fraunhofer Institute for Manufacturing Engineering and Automation (IPA, Stuttgart, Germany) for procuring and supplying the extruded Carbothane films. This project has received funding from the European Union's Horizon 2020 research and innovation program under grant agreement No 863183. This publication represents the views of the author(s) only. The European Commission is not responsible for any use that may be made of the information it contains.

Open access funding enabled and organized by Projekt DEAL.

ADVANCED SCIENCE NEWS
www.advancedsciencenews.com

Macromolecular Materials and Engineering
Open Access
www.mame-journal.de

Conflict of Interest

The authors declare no conflict of interest.

Author Contributions

The study was conceptualized by M.G.B. and O.L.; M.G.B. performed experiments and analyzed the data. The manuscript was written and critically revised by M.G.B. and O.L.

Data Availability Statement

The data that support the findings of this study are available from the corresponding author upon reasonable request.

Keywords

carbodiimide coupling, detachment tests, dextrans, dopamine, mucins, surface zeta-potentials

Received: December 6, 2022
Revised: January 25, 2023
Published online:

[1] D. C. Rich, *J. Coat Technol. Res.* **2016**, *13*, 1.
[2] a) M. F. Montemor, *Surf. Coat. Technol.* **2014**, *258*, 17; b) P. A. Sørensen, S. Kiil, K. Dam-Johansen, C. E. Weinell, *J. Coat Technol. Res.* **2009**, *6*, 135.
[3] A. A. Voevodin, M. S. Donley, J. S. Zabinski, *Surf. Coat. Technol.* **1997**, *92*, 42.
[4] J. Song, T. M. Lutz, N. Lang, O. Lieleg, *Adv. Healthcare Mater.* **2021**, *10*, 2000831.
[5] T. Mariappan, *J. Fire Sci.* **2016**, *34*, 120.
[6] a) M. Cloutier, D. Mantovani, F. Rosei, *Trends Biotechnol.* **2015**, *33*, 637; b) R. O. Darouiche, *Int. Artif. Organs* **2007**, *30*, 820.
[7] B. Winkeljann, M. G. Bauer, M. Marczynski, T. Rauh, S. A. Sieber, O. Lieleg, *Adv. Mater. Interfaces* **2020**, *7*, 1902069.
[8] S. Mehla, J. Das, D. Jampaiah, S. Periasamy, A. Nafady, S. K. Bhargava, *Catal. Sci. Technol.* **2019**, *9*, 3582.
[9] B. Winkeljann, B. T. Käsdorf, J. Boekhoven, O. Lieleg, *Macromol. Biosci.* **2018**, https://doi.org/10.1002/mabi.201700311
[10] a) C. Kimna, B. Winkeljann, J. Song, O. Lieleg, *Adv. Mater. Interfaces* **2020**, *7*, 2000735; b) F. Siepmann, J. Siepmann, M. Walther, R. J. Macrae, R. Bodmeier, *J. Controlled Release* **2008**, *125*, 1.
[11] Y. Liu, G. Wu, K. de Groot, *J. R Soc. Interface* **2010**, *7*, 631.
[12] a) M. Avella-Oliver, S. Morais, R. Puchades, Á. Maquieira, *Trends Analyt. Chem.* **2016**, *79*, 37; b) M. A. Chowdhury, M. Joshi, B. S. Butola, *J. Eng. Fiber Fabr.* **2014**, *9*, 155892501400900.
[13] a) M. Samadzadeh, S. H. Boura, M. Peikari, S. M. Kasiriha, A. Ashrafi, *Prog. Org. Coat.* **2010**, *68*, 159; b) F. Zhang, P. Ju, M. Pan, D. Zhang, Y. Huang, G. Li, X. Li, *Corros. Sci.* **2018**, *144*, 74.
[14] a) L. D. Chambers, K. R. Stokes, F. C. Walsh, R. J. K. Wood, *Surf. Coat. Technol.* **2006**, *201*, 3642; b) F. Guy *Super-Hydrophobic Coatings as a Part of the Aircraft Ice Protection System*, SAE Technical Paper, Warrendale, PA, United States **2017**; c) C. Seubert, K. Nietering, M. Nichols, R. Wykoff, S. Bollin, *Coatings* **2012**, *2*, 221.
[15] a) E. K. Arya, B. S. Dharaya, *IOP Conf. Ser.: Mater. Sci. Eng.* **2021**, *1114*, 012006; b) B. Shojaei, M. Najafi, A. Yazdanbakhsh, M. Abtahi, C. Zhang, *Polym. Adv. Technol.* **2021**, *32*, 2797; c) C. M. Collins, M. Safiuddin, *Infrastructures* **2022**, *7*, 46.
[16] a) V. B. Møller, K. Dam-Johansen, S. M. Frankær, S. Kiil, *J. Coat Technol. Res.* **2017**, *14*, 279; b) G. A. Ellis, S. A. Díaz, I. L. Medintz, *Curr. Opin Biotechnol.* **2021**, *71*, 77; c) S. M. Thomas, R. Dicosimo, V. Nagarajan, *Trends Biotechnol.* **2002**, *20*, 238; d) H. J. Griesser, *Woodhead Publishing Series in Biomaterials*, Woodhead Publishing, Duxford, UK **2016**.
[17] J. Song, B. Winkeljann, O. Lieleg, *Adv. Mater. Interfaces* **2020**, *7*, 2000850.
[18] a) P. S. Aklujkar, B. Kandasubramanian, *J. Coat. Technol. Res.* **2021**, *18*, 19; b) M. Kamalisarvestani, R. Saidur, S. Mekhilef, F. S. Javadi, *Renewable Sustainable Energy Rev.* **2013**, *26*, 353.
[19] a) P. Guan, L. Zhou, Z. Yu, Y. Sun, Y. Liu, F. Wu, Y. Jiang, D. Chu, *J. Energy Chem.* **2020**, *43*, 220; b) A. S. Sarkin, N. Ekren, S. Saglam, *Sol. Energy* **2020**, *199*, 63.
[20] a) D. J. Miller, D. R. Dreyer, C. W. Bielawski, D. R. Paul, B. D. Freeman, *Angew. Chem., Int. Ed.* **2017**, *56*, 4662; b) A. Rabajczyk, M. Zielecka, W. Klapsa, A. Dziechciarz, *Materials* **2021**, *14*, 2161.
[21] K. Czerwinski, T. Rydzkowski, J. Wróblewska-Krepsztul, V. K. Thakur, *Coatings* **2021**, *11*, 1504.
[22] I. Miranda, A. Souza, P. Sousa, J. Ribeiro, E. M. S. Castanheira, R. Lima, G. Minas, *J. Funct. Biomater.* **2021**, *13*, 2.
[23] J. Joseph, R. M. Patel, A. Wenham, J. R. Smith, *Trans. IMF* **2018**, *96*, 121.
[24] F. Awaja, *Polymer* **2016**, *97*, 387.
[25] P. Boyraz, G. Runge, A. Raatz, *Actuators* **2018**, *7*, 48.
[26] Y. Choi, H.-V. Tran, T. R. Lee, *Coatings* **2022**, *12*, 1462.
[27] J. H. Ryu, P. B. Messersmith, H. Lee, *ACS Appl. Mater. Interfaces* **2018**, *10*, 7523.
[28] a) V. Jokinen, P. Suvanto, S. Franssila, *Biomicrofluidics* **2012**, *6*, 016501; b) M. G. Bauer, R. Reithmeir, T. M. Lutz, O. Lieleg, *Plasma Proceseses Polym.* **2021**, *18*, 2100126; c) H.-C. Yang, R. Z. Waldman, M.-B. Wu, J. Hou, L. Chen, S. B. Darling, Z.-K. Xu, *Adv. Funct. Mater.* **2018**, *28*, 1705327; d) M. Marczynski, B. Winkeljann, O. Lieleg, in *Biopolymers for Biomedical and Biotechnological Applications*, Wiley, Hoboken **2021**, p. 181; e) R. Bansil, B. S. Turner, *Curr. Opin. Colloid Interface Sci.* **2006**, *11*, 164.
[29] a) G. Ocvirk, M. Munroe, T. Tang, R. Oleschuk, K. Westra, D. J. Harrison, *Electrophoresis* **2000**, *21*, 107; b) J. K. Beattie, *Lab. Chip* **2006**, *6*, 1409.
[30] B. J. Kirby, E. F. Hasselbrink, *Electrophoresis* **2004**, *25*, 203.
[31] R. Zimmermann, U. Freudenberg, R. Schweiß, D. Küttner, C. Werner, *Curr. Opin. Colloid Interface Sci.* **2010**, *15*, 196.
[32] a) Y. Uematsu, *J. Phys. Condens Matter.* **2021**, https://doi.org/10.1088/1361-648X/ac15d5; b) A. Barisic, J. Lützenkirchen, N. Bebic, Q. Li, K. Hanna, A. Shchukarev, T. Begovic, *Colloids Interfaces* **2021**, *5*, 6; c) Y. Uematsu, D. J. Bonthuis, R. R. Netz, *Curr. Opin. Electrochem.* **2019**, *13*, 166; d) B. J. Kirby, E. F. Hasselbrink, *Electrophoresis* **2004**, *25*, 187.
[33] B. Winkeljann, P.-M. A. Leipold, O. Lieleg, *Adv. Mater. Interfaces* **2019**, https://doi.org/10.1002/admi.201900366
[34] M. Marczynski, C. A. Rickert, T. Fuhrmann, O. Lieleg, *Sep. Purif. Technol.* **2022**, *294*, 121209.
[35] a) M. Caldara, R. S. Friedlander, N. L. Kavanaugh, J. Aizenberg, K. R. Foster, K. Ribbeck, *Curr. Biol.* **2012**, *22*, 2325; b) G. Petrou, T. Crouzier, *Biomater. Sci.* **2018**, *6*, 2282; c) C. A. Rickert, B. Wittmann, R. Fromme, O. Lieleg, *ACS Appl. Mater. Interfaces* **2020**, *12*, 28024.
[36] Q. Hu, Y. Lu, Y. Luo, *Carbohydr. Polym.* **2021**, *264*, 117999.
[37] S. Tiwari, R. Patil, P. Bahadur, *Polymers* **2018**, *11*, 1.
[38] a) J. Maia, M. B. Evangelista, H. Gil, L. Ferreira, *Carbohydrates Applications in Medicine*, (Ed: M. H. Gil), Research Signpost, Trivandrum, Kerala, India **2014**; b) W. B. Neely, *Adv. Carbohydr. Chem.* **1960**, *15*, 341.
[39] C. Kimna, M. G. Bauer, T. M. Lutz, S. Mansi, E. Akyuz, Z. Doganyigit, P. Karakol, P. Mela, O. Lieleg, *Adv. Funct. Mater.* **2022**, *32*, 2105721.

A.2.4 "Comparing the Resilience of Macromolecular Coatings on Medical-Grade Polyurethane Foils"

A.2.4.1 Full Research Article

Surfaces and Interfaces 41 (2023) 103231

Contents lists available at ScienceDirect

Surfaces and Interfaces

journal homepage: www.sciencedirect.com/journal/surfaces-and-interfaces

Comparing the resilience of macromolecular coatings on medical-grade polyurethane foils

Maria G. Bauer [a,b], Kjetil Baglo [a,c], Luca Reichert [a,c], Jan Torgersen [a,c], Oliver Lieleg [a,b,*]

[a] School of Engineering and Design, Department of Materials Engineering, Technical University of Munich, Boltzmannstraße 15, 85748 Garching, Germany
[b] Center for Protein Assemblies and Munich Institute of Biomedical Engineering, Technical University of Munich, Ernst-Otto-Fischer Str. 8, 85748 Garching, Germany
[c] Institute of Materials Science, Technical University of Munich, Boltzmannstraße 15, 85748 Garching, Germany

ARTICLE INFO

Keywords:
Dopamine coatings
Carbodiimide coatings
Linear tribology
Long-term testing
Sterilization

ABSTRACT

Foils made from elastomeric polymers, such as polycarbonate-based polyurethane (PCU), can combine desirable properties including flexibility, durability, and compliance. Still, their usage is often limited by their strongly autohesive behavior. To overcome this issue, surface coatings can be applied. Here, dopamine-based (dopa) and carbodiimide-mediated (carbo) coatings are compared by assessing their tribological performance and surface properties after long-term sliding tests, and after storage or sterilization. Even though both coating strategies achieve very good lubricity, the dopa-coatings are less resilient than the carbo-coatings. Thus, for such applications where extended sample storage or sterilization is required, covalent coatings should be preferred.

1. Introduction

For medical applications thin, flexible polymeric materials are regularly used [1,2]; they often require anti-adhesive properties, *e.g.*, on the inner sides of intravenous bags or on medical tubings such as catheters. Here, uncontrolled biofouling can (partially) block the device, entail undesired cell ingrowth, lead to infections, and eventually entail device failure [3–5]. For certain applications, the accessible space such an artificial object needs to fit into can be quite limited; thus, the material must be as thin as possible but still sufficiently stable and flexible to fulfill its purpose. For example, when polymeric foils are envisioned as components for cushion-like implants aiming at separating damaged articular surfaces in small joints or replacing intervertebral disks, the polymeric material must endure continuous mechanical loads and deformations and enable a smooth relative movement of the opposing surfaces. Yet, thin spacer materials with appropriate bulk and surface properties are scarce. Thus, coating (thin) polymeric materials to improve their surface properties is the currently preferred method to render them suitable for such medical applications [6–10].

Here, two methods to alter the surface properties of medical-grade carbonate-based polyurethane (PCU) films with initially strongly autohesive properties are compared [11]: first, rather novel dopamine-based (dopa) coatings [12–16], which have gained particular attention as they can readily generate bio-based, intermediate adhesion layers between an extensive range of substrate materials and various top-layer molecules, thus establishing multifaceted properties for bio-medical applications (*e.g.*, anti-biofouling, optimized cell/blood contact surfaces, drug delivery, or bioimaging/-sensing) [17–21]; second, well-established but substrate-/top-layer-wise more restricted, work-intensive carbodiimide-mediated (carbo) coatings [22–25]. Both hydrophilic surface treatments can – when employing a suitable top-layer macromolecule (establishing a hydration layer) combined with a corresponding macromolecular lubricant – enable an efficient gliding motion of two PCU foils by utilizing hydration lubrication and (potentially) sacrificial layer formation [11,26–29]. However, the coatings generated with either method may differ in terms of their stability. Thus, here, the resilience of these coatings towards storage/application conditions, sterilization processes, and prolonged sliding movements is assessed. Additionally, the coatings' ability to prevent wear and abrasion is compared.

2. Experimental section

Unless stated otherwise, all chemicals were obtained from Carl Roth, Karlsruhe, Germany.

* Corresponding author at: Department of Mechanical Engineering and Munich School of Bioengineering, Technical University of Munich, Boltzmannstraße 11, 85748 Garching, Germany.
E-mail address: oliver.lieleg@tum.de (O. Lieleg).

https://doi.org/10.1016/j.surfin.2023.103231
Received 26 May 2023; Received in revised form 24 July 2023; Accepted 30 July 2023
Available online 2 August 2023

2.1. Sample preparation

2.1.1. Polycarbonate-based polyurethane samples

Thermoplastic, aromatic, and medical grade polycarbonate-based polyurethane (PCU, Carbothane™ AC-4085A, Lubrizol Advanced Materials, USA)) was obtained as extruded foils (thickness of ≈ 150–200 μm) from Gerlinger Industries GmbH (Netzschkau, Germany). Those foils had a better surface quality on one side, and all following modifications and examinations were performed on this side only. All further preparation steps required to shape the samples into the desired dimensions were conducted manually: either they were cut with scissors and scalpels or punched into a circular shape with a manual eyelet press (Istabreeze Germany GmbH, Bad Rappenau, Germany).

2.1.2. Cylindrical polydimethylsiloxane (PDMS) samples

Cylindrical polydimethylsiloxane (PDMS) samples (pins) served as a model material to conduct preliminary rotational tribology examinations for assessing coating-lubricant interactions. As previously described by Winkeljann et al. [30], those pins were prepared from the commercially available PDMS system Sylgard 184 (Dow Corning, Midland, MI, USA). A curable solution was prepared by mixing PDMS in a 10:1 ratio with the curing agent and exposing the mixture to vacuum for 1 h (to remove air bubbles). To create pins ($\varnothing = 6.2$ mm), the mixture was filled into a custom-made aluminum mold using a transfer pipette before curing the silicone at 70 °C for 4 h. Since previous studies indicated that there might be unreacted low molecular weight residues left after curing the PDMS [31,32], the samples were further tempered at 110 °C for 2 h.

Prior to any modifications, treatments or tests, all samples (whether made from PDMS or PCU) were cleaned in 80% (v/v) ethanol and deionized water (ddH2O) for 15 min each and then dried.

2.2. Macromolecular lubricants

Here anionic biomacromolecules were examined only (polyanionic macromolecules are typical for biolubricants in the human body) [33]. Further selection criteria: commercial availability in adequate quality/purity; intermediate molecular weight/viscosity. Alginic acid (AlgA, $c = 6\%$, viscosity $\eta_{c=1\%,temp=25\cdot C} = 5 - 40$ mPa ∗ s, Sigma Aldrich, Darmstadt, Germany), γ-poly-glutamic acid (gPGA, $c = 10\%$, MW > 700kDa, Biosynth Ltd., Berkshire, UK), and carboxymethyl-dextran (CM-Dex, $c = 12\%$, $MW = 500$kDa, TdB Labs AB, Uppsala, Sweden) were compared to hyaluronic acid (HA, $c = 8\%$, $MW = 70 - 80$kDa, Biosynth). The respective macromolecule concentrations were adjusted such that a comparable, good tribological performance was achieved. Unless stated differently, the lubricants were prepared in phosphate buffered saline (PBS, $pH = 7.4$, Sigma).

2.3. Surface coatings

To promote interactions with the anionic lubricants, the top-layers in each coating were created from dextran variants which locally provide cationic groups (amines), *i.e.*, Lysine-Dextran and Q-Dextran (TdB Labs). Coatings were applied by employing either a multi-step carbodiimide-mediated coating process [11,21,23,24], or a two-step dopamine-based coating process [12,18,19]. Previously it was shown that those coatings have no undesired effects on the surface roughness, transparency, or flexibility of the employed substrate [11], and this could be confirmed by Fourier-transformed infrared (FTIR, see supplementary information SI 1) and DSC scans (see SI 2).

2.3.1. Carbodiimide-mediated coating process

The coating process for PDMS was conducted as published by Winkeljann et al. [30]. For coating the thermoplastic PCU, the process parameters as described by Bauer, Lieleg [11] were applied. Different process parameters were required to account for differences in the materials' susceptibility to plasma treatment and to compensate for the reduced incubation temperature applicable to PCU (which is due to its relatively low Vicat temperature). In the following process descriptions, different conditions applied to PDMS and PCU, respectively, will be listed in curved brackets as follows: {applied to PDMS/applied to PCU}.

In brief, the surfaces of the samples were activated by employing a low-pressure atmospheric plasma ($p_{abs} = 0.4$ mbar, power supply: {30 W/56 W}, treatment time: {1.5 min/25 min}). Immediately afterwards, each sample was immersed into a silane solution containing 1% (w/v) TMS-EDTA (N-[(3-trimethoxysilyl)propyl] ethylenediamine triacetic acid trisodium salt, abcr GmbH, Karlsruhe, Germany) dissolved in 10 mM acetate buffer at pH 4.5 and incubated at {60 °C/37 °C} for {5 h/8.5 h} to create a silane pre-coating. Subsequently, the samples were dipped into isopropanol to wash off any excess solution. Silane stabilization was conducted at {110 °C & atmospheric pressure/room temperature (RT) & $p_{rel} = -800$ mbar to -600 mbar} for {1 h/16 h}. Afterwards, the samples were washed in 96% (v/v) ethanol to remove any unbound silane molecules. To initiate the macromolecular coupling step, the samples were incubated in a freshly prepared solution containing 5 mM EDC (1-ethyl-3-(3-dimethylaminopropyl)carbodiimide-hydrochloride) and 5 mM sulfo-NHS (N-hydroxysulfosuccimid sodium salt, abcr) dissolved in 100 mM MES (2-(N-morpholino ethanesulfonic acid, AppliChem GmbH, Darmstadt, Germany) buffer at pH 5 for 30 min. Subsequently, the samples were immediately transferred into Dulbecco's phosphate buffered saline (pH = 7.4, DPBS, Sigma-Aldrich Inc., Darmstadt, Germany) containing 0.05% (w/v) lysine-dextran (MW = 150 kDa, TdBlabs, Uppsala, Sweden). After an incubation period of at least 16 h at 7 °C, the macromolecular coupling was finalized, and the samples were cleaned in 80% (w/v) ethanol.

2.3.2. Dopamine-based coating process

As described in [11], both PDMS pins and PCU foils were treated in the same way. To prevent undesired sedimentation and attachment of larger (poly-)dopamine agglomerates onto the surfaces, the samples were positioned vertically in a freshly prepared solution containing 0.4% (w/v) dopamine hydrochloride (Sigma-Aldrich) dissolved in 20 mM HEPES buffer (4-(2-hydroxyethyl)−1-piperazineethanesulfonic acid; pH 8.5) and incubated for 3 h. To wash off excess (poly-)dopamine, the samples were dipped into ddH_2O and subsequently incubated in 20 mM HEPES buffer (pH 7) containing 0.1 (w/v)% Q-dextran (MW = 150 kDa, TdBlabs) at RT overnight. To remove any unbound macromolecules, the samples were dipped into ddH_2O, then into 80% ethanol, and again into ddH_2O. Finally, all samples (independent of how they were coated) were either placed into 20 mM HEPES buffer (pH 7) and stored at 7 °C until further use, or they were dried at RT for at least 24 h (for tests conducted with dry samples).

The successful application of the coatings was assessed by contact angle measurements [11] and FTIR scans (SI 1).

As top-layer molecules, dextrans (MW: 150 kDa) were selected. Such dextrans were previously used in various biomedical studies – especially as a base material for drug delivery applications and tissue engineering purposes [34,35]. Dextrans are commercially available at different molecular weights, and they can carry different functionalizations (*e.g.*, charged residues) [34,36,37]. Based on the findings presented by Imamura et al. [38], a glass transition temperature of > 100 °C was estimated for dextrans with a molecular weight of 150 kDa; this indicates that, at the applied testing temperatures used in this study (max. 30 °C), the dextran layer should not exhibit autohesive behavior. To enable good electrostatic interactions with the anionic macromolecules present in the studied lubricants, Q-dextran was chosen due to its strong cationic character (according to the manufacturer). Moreover, in pretests, we observed a strong interaction of this Q-dextran with dopamine layers, which renders those dextrans suitable components for a dopamine-based coating. However, since such Q-dextran molecules do not possess primary amine groups, applying the carbodiimide-mediated coating

strategy to them was chemically not feasible. Thus, as a suitable alternative, the zwitterionic lysine-dextran was used for carbo-coatings since this molecule comprises the same dextran backbone, was available at the same molecular weight, and, at least locally, carries cationic groups as well.

2.4. Rotational tribology

Friction examinations conducted in static contact between the tribological partners were performed as described in detail in [30]. In brief: a commercial shear rheometer (MCR 302, Anton Paar, Graz, Austria) was equipped with a tribology unit (T-PTD 200, Anton Paar), and a ball-on-cylinder geometry was employed. As a counterpart to the (coated) PDMS cylinders (see above), a steel sphere ($Ø$ = 12.7 mm, Kugel Pompel, Vienna, Austria) was selected. Measurements were performed at a constant normal force of F_N = 6 N such that friction responses in the boundary, mixed, and hydrodynamic regimes could be probed within the accessible speed range, which additionally corresponds to a reasonable velocity range for biomedical applications [39–42]. Based on the Hertzian contact theory [43], an average contact pressure $p_0 \approx 0.31$ MPa was estimated (Young's moduli: E_{steel} = 210 GPa, $E_{PDMS} \approx 2$ MPa; Poisson's ratios: $\nu_{steel} \approx 0.30$, $\nu_{PDMS} \approx 0.49$) [44]. The speed-dependent friction behavior (reported by the coefficient of friction, CoF) was evaluated by running a logarithmic speed ramp decreasing from ≈ 700 to 0.001 mm/s^{-1}. For each measurement, 600 µL of lubricant were required; as all measurements were conducted at 28 °C, a moisture trap was installed around the setup to avoid evaporation of the lubricant.

2.5. Linear tribology: basic measurements

To conduct tribological measurements in migrating contact between the tribological partners, an oscillatory tribology setup employing the same commercial shear rheometer as for rotational tribology measurements was used. However, now it was equipped with a measuring unit (P-PTD200/80/I, Anton Paar) that allows for connecting dedicated sample holders *via* a thread. For all oscillatory tribology experiments conducted here, a sample holder made from stainless steel (which provides a planar surface) was connected to this measuring unit. On the opposing side, a custom-made, maneuverable measuring head (which was based on the measuring head described in detail by Winkeljann et al. [45]) was connected to a measuring shaft for disposable measuring heads (D-CP/PP 7, Anton Paar). The measuring head used here has the same main geometric specifications as the one described in [45]; however, instead of steel spheres, each of the three sample holders was equipped with a custom-made, dedicated PDMS pin (cylinder (Ø 7 mm) having a rounded edge (radius = 3 mm) on the side facing the opposing sample holder); owing to their rounded edges, those dedicated PDMS pins provide a planar surface ($Ø$ = 3 mm), which allows for conducting friction measurements without generating edge artefacts.

For each measurement run, three sets of samples comprising a rectangular sample (~ 12 mm x 8 mm, attached to the stainless-steel bottom plate *via* double-sided adhesive tape) and a circular one ($Ø$ = 6 mm, attached *via* spontaneous adhesion to the PDMS pins mounted in the measuring head) were required. The circular shape of the second sample further reduces the occurrence of undesired edge effects when this circular sample is moved over the rectangular sample during the tribological measurement.

For all linear tribology measurements conducted here, 225 µL of the desired lubricant were applied per set of samples. Since all measurements were conducted at 28 °C, a moisture trap was installed around the setup to avoid evaporation of the lubricant. During the measurements, the circular samples were moved over the rectangular samples at a sliding frequency of 1 Hz and over a sliding angle of 0.15 rad; for such a small ratio of the sliding angle/distance to the radius of the measuring head (18 mm), the movement can be approximated to be almost a straight line. This specific frequency and sliding angle were chosen as they result in maximum sliding velocities of ~ 10 mm/s, which lie in the intermediate range of sliding velocities examined *via* rotational tribology and do not induce inertia-based artefacts at the turning points. Basic measurements were conducted with coated samples in combination with a macromolecular lubricant only. For these measurements, the average contact pressure was (compared to the rotational tribology setup) raised to 0.5 MPa; this was necessary as, in pretests (when employing contact pressures close to the previously employed 0.3 MPa for longer periods) it was observed that the circular foils would tend to lose contact with the PDMS pin mounted in the measuring head. Measurements were run continuously for 45 min and data points were acquired five times per minute.

2.6. Scanning electron microscopy

Uncoated or coated PCU samples were sputtered with gold and examined on a scanning electron microscope (SEM, Jeol JSM-7600F, Jeol (Germany) GmbH, Freising, Germany), employing an acceleration voltage of 10 kV, a working distance of 10 mm, a spot size of 45 and a detector for secondary electrons. Images were acquired such that the interface between the PCU foil and the background was clearly visible. For image evaluation, the software IMS (Imagic, Bildverarbeitung AG, Glattbrugg, Switzerland) was used. The thickness of each coating was estimated by subtracting the mean value obtained for the uncoated samples from the mean value of the coated samples and conducting error propagations.

2.7. Linear tribology: long-term measurements

These long-term tests were run with coated as well as with uncoated samples; in all cases, a 12% CM-Dex solution was used as a lubricant, and the total testing period was 9 h. To enable measurements running effectively also on the uncoated samples, several adaptions and compromises had to be made: in addition to reducing the applied load during the long-term tests to 0.4 MPa, this load was not applied directly in full, but stepwise, *i.e.*, starting at 0.15 MPa and increasing the load every 3 min by 0.5 MPa until the full load was reached. If the foils stuck to each other or if the circular foil detached from the PDMS pin, the measurement was interrupted, the circular samples were cleaned and reattached to the PDMS pins, and the test was restarted (on the same area of the rectangular samples as before) but the time for each load step until the full load was reached was reduced to 90 s each. The resulting CoF was recorded twice per minute; additionally, to evaluate the measurement reliability, the following three parameters were traced:

- 'sets': average number of sets required to identify a set of samples effectively enabling a tribological measurement (if the measurement initiation was unsuccessful for ~7 times, a new sample set was used)
- 'runs': average number of effective measuring runs required per set of samples to achieve the full run time
- '(re-)starts': average number of measurement initiations required per set of samples to achieve the full run time

Once the full runtime of 9 h (running at full load) was reached on a set of samples, the measurement was terminated.

2.8. Confocal laser scanning microscopy

Confocal laser scanning microscopy was conducted using a VK-X1000 microscope (Keyence, Oberhausen, Germany) equipped with a 20x magnification lens (CF Plan, NA = 0.46; Nikon, Chiyoda, Tokyo, Japan). Prior to performing the measurements, all samples were dried and cleaned with particle-free pressurized air. Then, the samples were placed onto a glass slide using a droplet of distilled water as a thin spacer to allow the measuring device to automatically differentiate between the

very thin, transparent foils and the glass slide.

For samples that had been exposed to the long term tribological testing, the entire visible contact area was captured as one stitched image. Therefore, the lubricant employed for the long-term tests was removed by thoroughly cleaning the samples in ddH_2O.

To derive quantitative surface roughness parameters from the captured images, the software MultiFileAnalyzer (Keyence) was used. To preprocess the images, first, a linear tilt was removed; second, the sample waviness (a wave form with correction strength of 10 out of 20) was subtracted; third, artefact valleys (created when the measurement process penetrated into the transparent material) were removed by inverting the height, cropping the peaks (employing medium intensity as defined by the program), and inverting the height once more such that the sample was in its original orientation again. On each adjusted topographical image, a rectangular area ($\sim 7\ mm^2$) was defined that was located centrally within each contact area. Then, the following metrological parameters (based on ISO 25178-2) were calculated: the root-mean-square-height S_q:

$$S_q = \sqrt{\frac{1}{A}\int\int_A z^2(x,y)\,dx\,dy} \quad (1)$$

and the peak extreme height S_{xp} which is defined as the difference in height z between an areal material ratio of 2.5% and of 50%. This set of parameters was chosen as S_q is a frequently used surface roughness parameter giving a general overview over the height distribution of a sample surface. Additionally, S_{xp} was selected as a peak-related parameter to detect any signs of wear or abrasion generated in response to the long-term treatment.

2.9. Resilience assessments

Coated samples were exposed to different application-oriented treatments to compare the resilience of the coatings towards such relevant processes. Subsequently, those coated and treated samples were examined by employing linear tribology tests, surface zeta potential measurements, a surface morphology analysis, and FTIR scans (see SI 4 & 5).

2.9.1. UV disinfection

For treatment with ultraviolet light, samples were immersed into PBS, placed into a commercial UV sterilization chamber (BLX-254; Vilber-Lourmat GmbH, Eberhardzell, Germany) and exposed to UV light (wavelength of 254 nm; 4 × 8 W) for 1 h.

2.9.2. Storage

To assess the storability of the samples, coated samples were UV disinfected and dipped into 80% ethanol (to avoid bacterial contamination) and then stored either immersed in PBS at $T = 7$ °C (cold) or at $T = 30$ °C (warm) or dehydrated and stored at T~ 21 °C (dry).

2.9.3. Sterilization

Two different sterilization methods were applied. Treatments with γ-irradiation ('gamma'; dose: 25–50 kGy; system type: JS9000; complied standards: EN ISO 9001, EN ISO 13 485, EN ISO 11137-1) or ethylene oxide ('ETO'; duration: 5 h, temperature: 45 °C, pressure: 610 mbar, average ETO concentration: 700 mg L^{-1}) were conducted by employing commercial standard processes available at the company steripac GmbH (Calw, Germany). For both treatments, the samples were stored in sterilization bags.

2.9.4. Evaluation measurements after resilience treatments

2.9.4.1. Linear tribology measurements. Coated samples subjected to either of the treatments described above were examined employing linear tribology to investigate the influence of the different treatments on the coating functionality, *i.e.*, the tribological performance of the coated foils. If the samples were previously stored or treated in a dried state, they were rehydrated in PBS at 7 °C for at least 24 h. The average contact pressure was set to 0.5 MPa, data points were acquired every 20 s, and the maximal run time was 20 min. In case the foils stuck to each other during testing, the measurement was terminated preliminarily. Then, this shortened run time, *i.e.*, the time for which the movable foil slid over the fixated foil without the autohesive foils sticking together, was defined as effective run time and traced for all samples in addition to the CoFs.

2.9.4.2. Surface zeta potentials. Zeta potentials for bare, coated, as well as coated and treated foil surfaces were determined using a SurPASS 3 Eco device (Anton Paar) equipped with an adjustable gap measuring cell for planar samples (Cat. No. 159880, Anton Paar). To avoid (re-)hydration effects of the coatings or substrates affecting the measurements in different ways, all samples were stored in PBS for at least 4 h prior to any measurement. A set of two identical samples was inserted into the measuring cell and the gap height was adjusted to a value between 95 μm and 110 μm. Prior to each measurement, the cell was flushed at least twice with an electrolyte solution (2% PBS at pH 7.4).

2.9.4.3. Fourier-transformed infrared spectroscopy. The FTIR spectra were acquired using a Nicolet iS50 Smart ITX ATR Diamond - FTIR spectrometer. Spectra were recorded at a 2 μm resolution, with 20 scans per sample, and in acquisition mode attenuated total reflectance (ATR). Spectra were detected for wavenumbers ranging from 4000 cm^{-1} to 525 cm^{-1} and evaluated in absorbance format. The background was characterized by scanning the empty sample stage only.

3. Results and discussion

To identify the most suitable lubricant to be combined with the two examined coatings, the friction responses obtained with different lubricants are compared. On uncoated samples, all four macromolecular lubricants show a similar and clearly improved lubricity compared to ddH_2O (Fig. 1a). Only at very high sliding velocities above ~ 200 mm/s this trend is reversed. However, those high sliding speeds are not relevant for biomedical applications, where velocities over a few hundred mm/s are rarely exceeded [40–42].

If lubricated with ddH_2O only, samples carrying either a carbo-coating (Fig. 1b) or a dopa-coating (Fig. 1c) return similar coefficients of friction (CoF) as uncoated samples. However, once combined with one of the macromolecular lubricants, a strong decrease of the CoF is observed, especially in the boundary and mixed lubrication regime, resulting in CoFs constantly below 0.04 (which is not achieved when using either coatings or lubricants only).

Next, a linear tribology setup is employed, which enables measuring the friction response between two identical samples, *i.e.*, two polymeric foils carrying the same coating. Here, a reciprocating motion is applied at a constant frequency and stroke length. The CoFs determined for either coating/lubricant combination (Fig. 1d-e) are around ~ 0.1 or below and stable over time. Owing to the strongly autohesive behavior of the PCU films (glass transition temperature $T_g = -10°C$ [46], transition range confirmed by DSC scans, see SI 2) used here and in all following tests [11], it is not possible to reliably measure samples carrying either only a coating (and not a biopolymer lubricant) or samples carrying no coating. Consistent with the results of the rotational tribology measurements, CM-Dex solutions somewhat outperform the other lubricant options for both coating variants; consequently, all further measurements are conducted with this lubricant.

Prior to assessing the durability of the coatings, their thickness is analyzed. Therefore, images depicting the sideview of the samples are captured *via* scanning electron microscopy; here, the bulk material and the interface (containing the surface coatings) are clearly differentiable (Fig. 2). Consequently, the thickness of the coatings can be estimated by

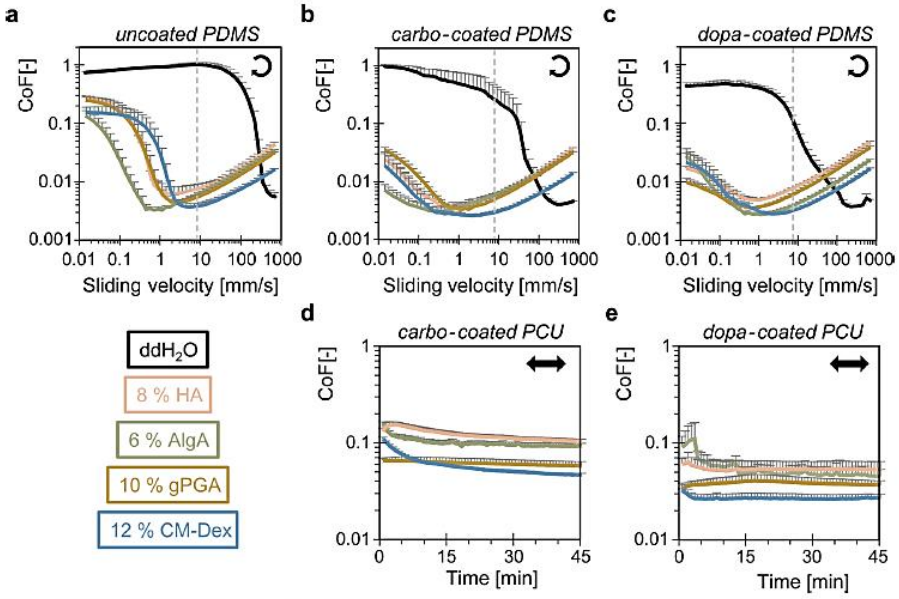

Fig. 1. *Lubrication performance of bio-macromolecular solutions on differently coated polymer substrates:* **a) – c)** static contact (rotational tribology setup; steel on PDMS) and **d)** & **e)** migrating contact (using two identically coated PCU films) results for a) uncoated, b) & d) carbo-coated, or c) & e) dopa-coated samples. The legend (referring to the used lubricant) applies to all subfigures. Error bars depict the standard error of the mean as determined from at least three sets of samples.

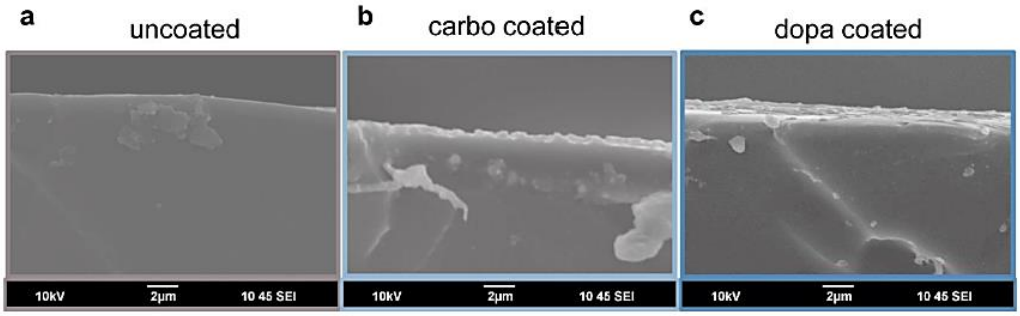

Fig. 2. *SEM images of (un-)coated PCU films:* representative SEM images acquired from side-views of a) uncoated, b) carbo-coated, and c) dopa-coated PCU-foils are displayed.

subtracting the mean interface thickness determined for uncoated samples from the mean interface thickness determined for both coated samples and applying error propagations. With this approach, a thickness d for the carbo-coating and the dopa-coating of $d_{carbo} \approx (0.25 \pm 0.07)\mu m$ and $d_{dopa} \approx (0.95 \pm 0.29)\mu m$), respectively, is estimated. The individual values determined for the interface thicknesses can be found in SI 3.

To assess the durability of the very thin coatings, first extended linear tribology measurements (total run-time: 9 h) are performed and the influence of the coatings on wear generation is assessed. For comparison, measurements on uncoated samples are conducted as well. Such long-term tests are possible for all samples (Fig. 3a-c). However, they require varying effort as indicated by the number of sample sets needed to effectively start a measurement (if the measurement initiation was unsuccessful for ~7 times, a new sample set was used). For carbo-coated samples, each set allows for starting a measurement; for uncoated samples, typically two sets are required. During the measurement, the carbo-coated samples show a highly reproducible behavior without any stick-slip-effects and without any interruption of the sliding movement. Uncoated and dopa-coated samples return less steady CoF traces; moreover, for both sample types, several interruptions of the sliding movement occur, and several measurement initiations/restarts are required. This undesirable behavior is also associated with wear generation: for uncoated samples, scratches and surface distortions are clearly visible after tribological treatment; in contrast, carbo-coated samples show now clear signs of wear (Fig. 3d-e).

On tribologically treated dopamine-coated samples, some surface distortions are observed (Fig. 3f). For surface morphologies of single images of the different coating/treatment combinations, see SI 4. Surface roughness parameters derived from such profilometric images confirm this impression: the root mean square height S_q and the peak extreme height S_{xp} remain constant for carbo-coated samples; in contrast, for the other two samples, those two parameters are increased by the tribological treatment (Fig. 3g–h). Thus, it can be concluded that the carbo-coating provides better wear protection.

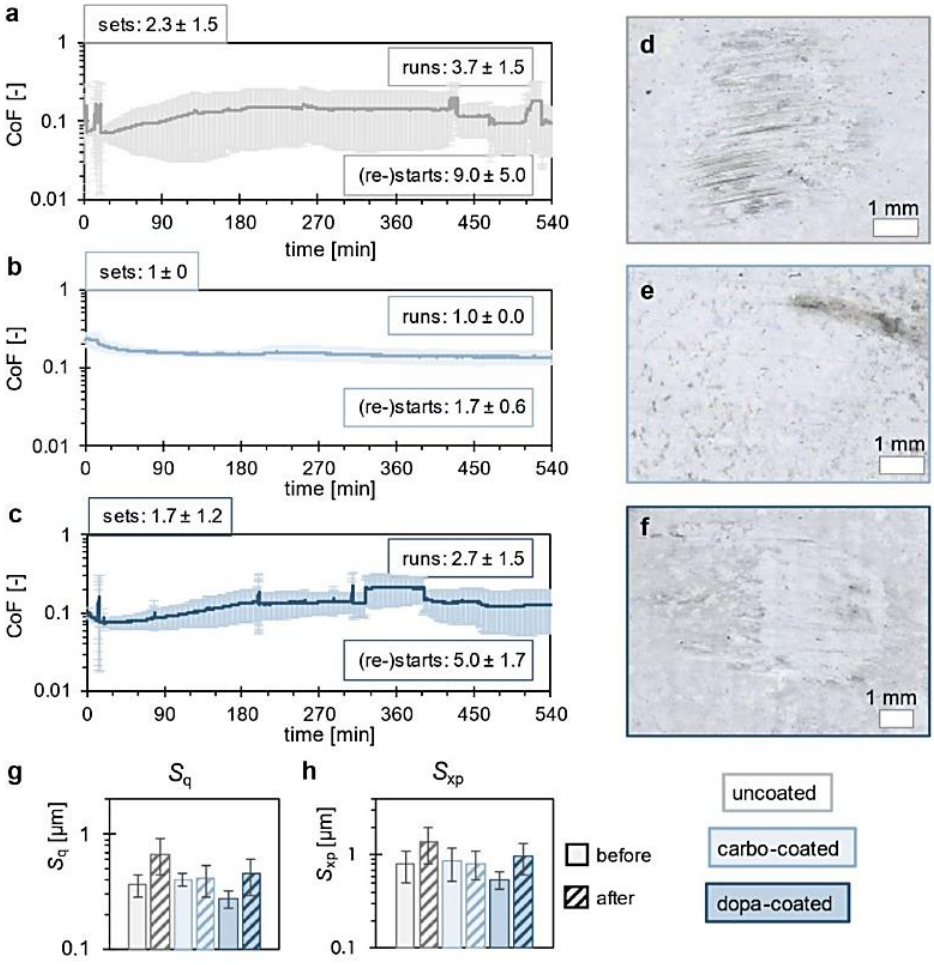

Fig. 3. *Long-term tribological treatment of the coatings*: **a) - c)** average CoF determined during linear tribology measurements running for 9 h. For definitions of 'sets', 'runs', and '(re-)starts', see method section (2.7). **d) – f)** exemplary profilometric images of (coated) samples after treatment. **g) – h)** comparison of two surface roughness parameters before and after treatment. The legend below f) applies to all subfigures, the legend next to h) applies to g) and h). Error bars depict the standard deviation as determined for at least 3 (sets of) samples.

Next, the resilience of the coatings towards different storing conditions (Fig. 4) and sterilization methods (Fig. 5) is compared. In addition to the CoF, the effective runtime (eRT; maximum runtime per measurement: 20 min) is monitored, which is defined as the time for which the movable foil slides over the fixated foil without the autohesive foils sticking together. A coating/lubricant combination is rated to be functional if it continuously separates the two foils. In those tests, always the same lubricant is used; thus, differences in the tribological performance of the systems are dictated by the coating.

To avoid bacterial contaminations, all samples used for storage tests were disinfected by treating them with UV-irradiation; accordingly, UV-treated coated samples serve as an additional reference group (Fig. 4a). Such UV treatment has only an effect on the surface charge of the carbo-coated samples (*bottom diagram*), which is probably caused by interactions of the UV irradiation with the silane layer [47] used during the carbo-coating process. The tribological behavior of the carbo-coatings seems not to be affected by the UV treatment; however, the CoFs recorded for dopa-coatings are slightly increased (*top diagram, bars*). Nonetheless, both UV-treated coatings enable successful lubrication as they achieve decent CoFs of ~ 0.1 and eRTs of 20 min (*top diagram, circles*).

For samples stored at different conditions, the obtained CoFs are plotted over the eRTs (Fig. 4b-d). In such a diagram, a well-performing coating would lie in the bottom right area of the diagram; and indeed, this is where most of the carbo-coatings are located independent of their storage conditions. In contrast, dopa-coatings tend to show increased

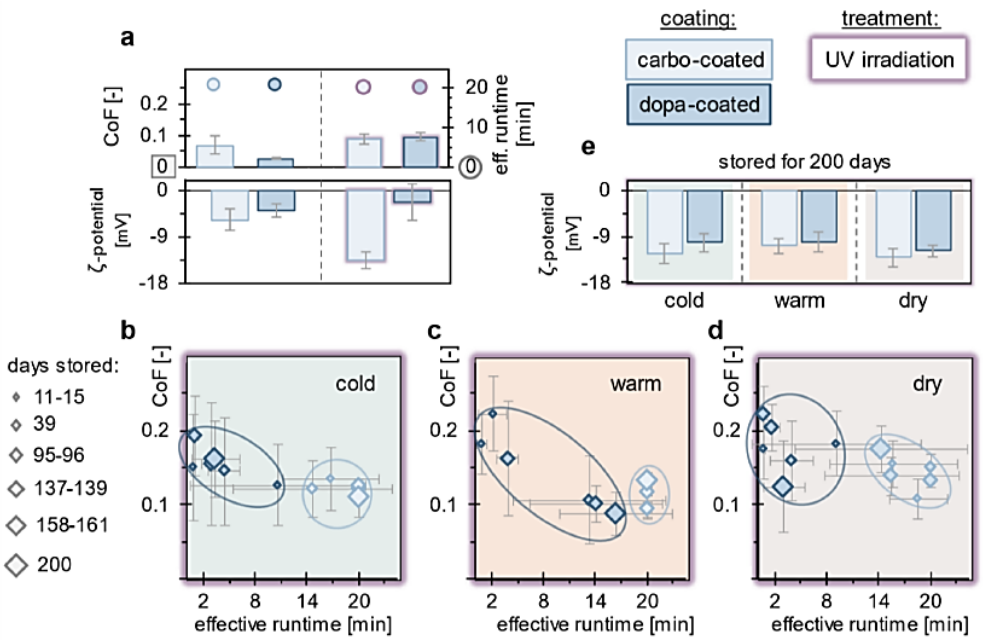

Fig. 4. *Influence of storage conditions on the coatings:* In **a),** in addition to untreated samples (left), coated and UV-treated samples (right) are shown as references. For **b)-d)** the samples were either stored b) cold, c) warm, or d) dry. e) Surface zeta potentials (at pH = 7.4) of coated samples stored for 200 days. The legend above e) applies to all subfigures, the legend next to b) applies to b) - d). For all tribology measurements, 12% CM-Dex was used as a lubricant. Error bars depict the standard error of the mean as determined from at least three sets of samples.

CoFs and/or reduced eRTs. Possibly, the dextrans bound to the dopamine layer detach over time, thus exposing the sticky dopamine layer; this, in turn, would trigger a rapid inhibition of the relative movement between the foils. However, an unexpected behavior is observed for both coatings when stored 'warm': here, the carbo-coating enables successful lubrication for each tested sample even after a storage period of 200 days with only weakly increased CoFs. Furthermore, the lubrication performance of the dopa-coated samples, which suffers after short periods of storage, appears to improve again with longer storage times. Such a behavior might be explainable by consecutive failure of the two layers comprising the coating, *i.e.,* if first the dextran layer detaches and later also the sticky dopamine-layer detaches from the PCU foils. Independent of the storage condition, the surface zeta potentials of carbo-coated samples remain unchanged when compared to the UV-treated references samples (Fig. 4b-d). In contrast, dopa-coated samples exhibit decreased surface potentials, which underscores the previous notion that those coatings are not fully stable over time.

However, for many medical devices, disinfection is not sufficient, but sterilization is required. Thus, next, the influence of common sterilization methods, *i.e.,* treatments with ethylene oxide or with γ-irradiation, on the coatings are examined. Since such sterilization processes can also affect the bulk material [48], alterations in the behavior of uncoated samples are monitored as well (Fig. 5, *white symbols*). Moreover, since the full sterilization processes (which include sample drying, shipment forth and back, sterilization, degassing, and rehydration) are very time-consuming, the sterilized samples are compared to stored samples (which were prepared and tested on the same days).

In line with our expectation, the storing process itself has hardly any influence on the friction response of the uncoated and carbo-coated samples; however, the response of the dopa-coated samples is somewhat affected. Interestingly, the uncoated material appears to be affected by the sterilization processes as the eRT is reduced to less than 2 min for ethylene oxide treated samples and to less than 1 min for γ-irradiated samples. In contrast, both coatings seem to mitigate this undesired effect. A similar picture emerges when analyzing the surface zeta potentials (Fig. 5, *bottom*): Storage of the uncoated material leads to a strong decrease of the overall surface charge, but this effect is reduced by the coatings. The same trend is obtained for the sterilized samples and confirmed by FTIR scans (as well as images of the surface morphologies, see SI 4), for which the most strongly influenced wavenumber ranges, which are associated with aliphatic hydrogen vibrations, are depicted in Fig. 5c. Here, both coatings appear to offer improved resistance to the sterilization treatments, with carbo-coated samples experiencing basically no change and the dopa-coated samples only minor changes compared to the uncoated samples (for the full FTIR scans as well as a detailed analysis and discussion of the observed bands, see SI 5). Overall, for all presented evaluations, the carbo-coated samples appear to be affected the least.

4. Conclusions

With both coating types, two PCU surfaces can be sufficiently lubricated to allow for a smooth relative sliding movement. During long-term load or storage, the more labor-intensive carbodiimide-mediated

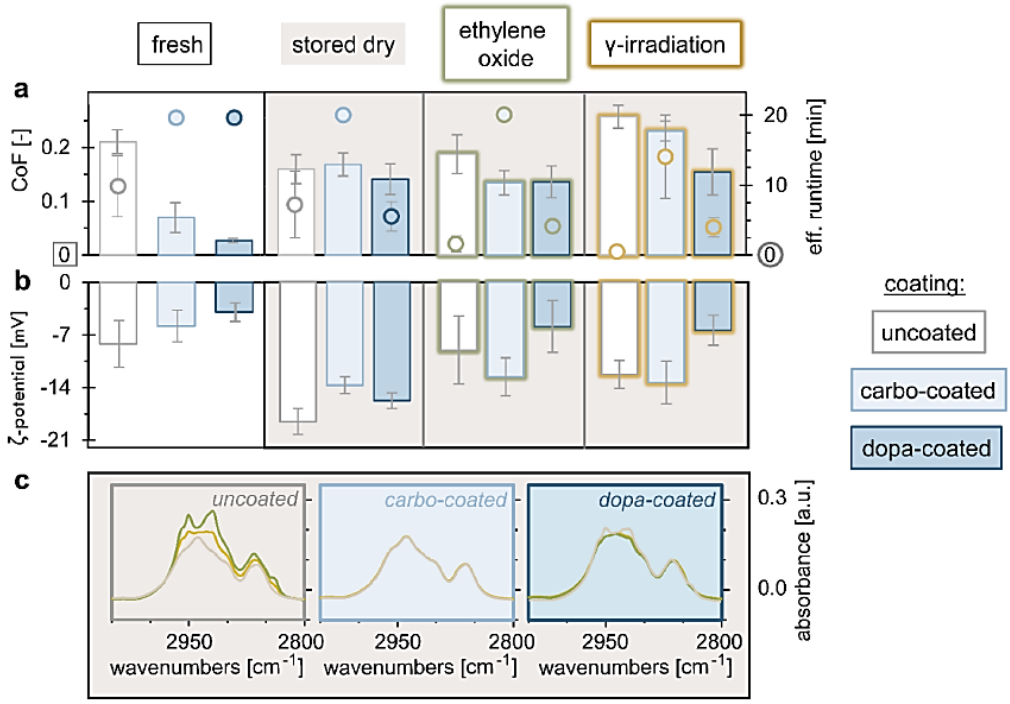

Fig. 5. *Influence of sterilization processes on the coatings*: a) linear tribology results (lubricated with 12% CM-Dex), b) surface zeta potential measurements (at pH = 7.4), and c) FTIR scans for uncoated (white/gray), carbo-coated (light blue), or dopa-coated (dark blue) samples after treatment with ethylene oxide (green outline/curve) or with γ-irradiation (yellow outline/curve). References: freshly prepared samples (white background) and stored (but unsterilized) samples (beige background). Error bars depict the standard error of the mean as determined from at least three sets of samples.

coatings outperform the easy-to-generate dopamine-coatings; this holds true with regard to reliability, the ability to avoid stick-slip events, and durability.

Statement of ethics approval

Approval of ethics is not required for the experiments conducted in this manuscript.

CRediT authorship contribution statement

Conceptualization and writing of the original draft: M.G.B. and O.L.; Data curation, formal analysis, investigation, methodology, and visualization: M.G.B., except for all content regarding DSC measurements: K. B., investigation of FTIR scans: K.B., and data acquisition and formal analysis of SEM images: L.R.; Funding acquisition, resources, supervision: O.L., J.T.; Writing (reviewing and editing): all authors;

Declaration of Competing Interest

The authors declare that they have no known competing financial interests or personal relationships that could have appeared to influence the work reported in this paper.

Data availability

The data that support the findings of this study are available from the corresponding author upon reasonable request.

Acknowledgments

The authors thank their APRICOT project partners at the Fraunhofer Institute for Manufacturing Engineering and Automation (IPA, Stuttgart, Germany) for procuring and supplying the extruded Carbothane™ films. This project has received funding from the European Union's Horizon 2020 research and innovation program under grant agreement No 863183. This publication represents the views of the author(s) only. The European Commission is not responsible for any use that may be made of the information it contains.

Supplementary materials

Supplementary material associated with this article can be found, in the online version, at doi:10.1016/j.surfin.2023.103231.

References

[1] J. Joseph, R.M. Patel, A. Wenham, J.R. Smith, Biomedical applications of polyurethane materials and coatings, Trans. IMF 96 (2018) 121–129, https://doi.org/10.1080/00202967.2018.1450209.
[2] R. Yoda, Elastomers for biomedical applications, J. Biomater. Sci. Polym. Ed. 9 (1998) 561–626, https://doi.org/10.1163/156856298X00046.
[3] S. Kumar, D.N. Roy, V. Dey, A comprehensive review on techniques to create the anti-microbial surface of biomaterials to intervene in biofouling, Colloid Interface Sci. Commun. 43 (2021), 100464, https://doi.org/10.1016/j.colcom.2021.100464.
[4] H.Y. Ahmadabadi, K. Yu, J.N. Kizhakkedathu, Surface modification approaches for prevention of implant associated infections, Colloids Surf. B 193 (2020), 111116, https://doi.org/10.1016/j.colsurfb.2020.111116.

[5] A.B. Asha, Y. Chen, R. Narain, Bioinspired dopamine and zwitterionic polymers for non-fouling surface engineering, Chem. Soc. Rev. 50 (2021) 11668–11683, https://doi.org/10.1039/d1cs00658d.
[6] N.J. Irwin, M.G. Bryant, C.P. McCoy, J.L. Trotter, J. Turner, Multifunctional, low friction, antimicrobial approach for biomaterial surface enhancement, ACS Appl. Bio Mater. 3 (2020) 1385–1393, https://doi.org/10.1021/acsabm.9b01042.
[7] J. Song, B. Winkeljann, O. Lieleg, Biopolymer-based coatings: promising strategies to improve the biocompatibility and functionality of materials used in biomedical engineering, Adv. Mater. Interfaces 7 (2020), 2000850, https://doi.org/10.1002/admi.202000850.
[8] J.L. Lanigan, S. Fatima, T.V. Charpentier, A. Neville, D. Dowson, M. Bryant, Lubricious ionic polymer brush functionalised silicone elastomer surfaces, Biotribology 16 (2018) 1–9, https://doi.org/10.1016/j.biotri.2018.08.001.
[9] F. Poncin-Epaillard, G. Legeay, Surface engineering of biomaterials with plasma techniques, J. Biomater. Sci. Polym. Ed. 14 (2003) 1005–1028, https://doi.org/10.1163/15685620376923153 8.
[10] H. Rashidi, J. Yang, K.M. Shakesheff, Surface engineering of synthetic polymer materials for tissue engineering and regenerative medicine applications, Biomater. Sci. 2 (2014) 1318–1331, https://doi.org/10.1039/c3bm60330j.
[11] M.G. Bauer, O. Lieleg, Bio-macromolecular surface coatings for autohesive, transparent, elastomeric foils, Macro Materials & Eng (2023) 2200681. doi:10.1002/mame.202200681.
[12] H. Lee, S.M. Dellatore, W.M. Miller, P.B. Messersmith, Mussel-inspired surface chemistry for multifunctional coatings, Science 318 (2007) 426–430, https://doi.org/10.1126/science.1147241.
[13] S. Hong, Y.S. Na, S. Choi, I.T. Song, W.Y. Kim, H. Lee, Non-covalent self-assembly and covalent polymerization co-contribute to polydopamine formation, Adv. Funct. Mater. 22 (2012) 4711–4717, https://doi.org/10.1002/adfm.201201156.
[14] J. Jiang, L. Zhu, L. Zhu, B. Zhu, Y. Xu, Surface characteristics of a self-polymerized dopamine coating deposited on hydrophobic polymer films, Langmuir 27 (2011) 14180–14187, https://doi.org/10.1021/la202877k.
[15] J.H. Ryu, P.B. Messersmith, H. Lee, Polydopamine surface chemistry: a decade of discovery, ACS Appl. Mater. Inter. 10 (2018) 7523–7540, https://doi.org/10.1021/acsami.7b19865.
[16] J. Song, T.M. Lutz, N. Lang, O. Lieleg, Bioinspired dopamine/mucin coatings provide lubricity, wear protection, and cell-repellent properties for medical applications, Adv. Healthc. Mater. 10 (2021), e2000831, https://doi.org/10.1002/adhm.202000831.
[17] Y.H. Ding, M. Floren, W. Tan, Mussel-inspired polydopamine for bio-surface functionalization, Biosurf. Biotribol. 2 (2016) 121–136, https://doi.org/10.1016/j.bsbt.2016.11.001.
[18] F. Liu, X. Liu, F. Chen, Q. Fu, Mussel-inspired chemistry: a promising strategy for natural polysaccharides in biomedical applications, Prog. Polym. Sci. 123 (2021), 101472, https://doi.org/10.1016/j.progpolymsci.2021.101472.
[19] M.E. Lynge, P. Schattling, B. Städler, Recent developments in poly(dopamine)-based coatings for biomedical applications, Nanomedicine 10 (2015) 2725–2742, https://doi.org/10.2217/nnm.15.89.
[20] C. van Mai, Di Li, H. Duan, Phenolic-compound-based functional coatings: versatile surface chemistry and biomedical applications, Langmuir 39 (2023) 1709–1718, https://doi.org/10.1021/acs.langmuir.2c03227.
[21] B. Winkeljann, M.G. Bauer, M. Marczynski, T. Rauh, S.A. Sieber, O. Lieleg, Covalent mucin coatings form stable anti-biofouling layers on a broad range of medical polymer materials, Adv. Mater. Interfaces 7 (2020), 1902069, https://doi.org/10.1002/admi.201902069.
[22] H.G. Khorana, The chemistry of carbodiimides, Chem. Rev. 53 (1953) 145–166, https://doi.org/10.1021/cr60165a001.
[23] J.V. Staros, R.W. Wright, D.M. Swingle, Enhancement by N-hydroxysulfosuccinimide of water-soluble carbodiimide-mediated coupling reactions, Anal. Biochem. 156 (1986) 220–222, https://doi.org/10.1016/0003-2697(86)90176-4.
[24] G.T. Hermanson, Bioconjugate Techniques, 3rd ed., Elsevier/AP, London, Waltham MA, 2013.
[25] B.R. Coad, M. Jasieniak, S.S. Griesser, H.J. Griesser, Controlled covalent surface immobilisation of proteins and peptides using plasma methods, Surf. Coat. Technol. 233 (2013) 169–177, https://doi.org/10.1016/j.surfcoat.2013.05.019.
[26] J. Klein, Hydration lubrication, Friction 1 (2013) 1–23, https://doi.org/10.1007/s40544-013-0001-7.
[27] D. Laage, T. Elsaesser, J.T. Hynes, Water dynamics in the hydration shells of biomolecules, Chem. Rev. 117 (2017) 10694–10725, https://doi.org/10.1021/acs.chemrev.6b00765.
[28] M. Marczynski, K. Jiang, M. Blakeley, V. Srivastava, F. Vilaplana, T. Crouzier, O. Lieleg, Structural alterations of mucins are associated with losses in functionality, Biomacromolecules 22 (2021) 1600–1613, https://doi.org/10.1021/acs.biomac.1c00073.
[29] B.T. Käsdorf, F. Weber, G. Petrou, V. Srivastava, T. Crouzier, O. Lieleg, Mucin-inspired lubrication on hydrophobic surfaces, Biomacromolecules 18 (2017) 2454–2462, https://doi.org/10.1021/acs.biomac.7b00605.
[30] B. Winkeljann, P.-M.A. Leipold, O. Lieleg, Macromolecular coatings enhance the tribological performance of polymer-based lubricants, Adv. Mater. Interfaces (2019), 1900366, https://doi.org/10.1002/admi.201900366.
[31] J. Kim, M.K. Chaudhury, M.J. Owen, Hydrophobic recovery of polydimethylsiloxane elastomer exposed to partial electrical discharge, J. Colloid Interface Sci. 226 (2000) 231–236, https://doi.org/10.1006/jcis.2000.6817.
[32] D.T. Eddington, J.P. Puccinelli, D.J. Beebe, Thermal aging and reduced hydrophobic recovery of polydimethylsiloxane, Sens. Actuators B 114 (2006) 170–172, https://doi.org/10.1016/j.snb.2005.04.037.
[33] J. Klein, Polymers in living systems: from biological lubrication to tissue engineering and biomedical devices, Polym. Adv. Technol. 23 (2012) 729–735, https://doi.org/10.1002/pat.3038.
[34] Q. Hu, Y. Lu, Y. Luo, Recent advances in dextran-based drug delivery systems: from fabrication strategies to applications, Carbohydr. Polym. 264 (2021), 117999, https://doi.org/10.1016/j.carbpol.2021.117999.
[35] S. Tiwari, R. Patil, P. Bahadur, Polysaccharide based scaffolds for soft tissue engineering applications, Polymers (2018) 11, https://doi.org/10.3390/polym11010001.
[36] M.H. Gil (Ed.), Carbohydrates Applications in Medicine, Research Signpost, Trivandrum, Kerala, India, 2014.
[37] W.B. NEELY, Dextran: structure and synthesis, Adb. Carbohyd. Chem. 15 (1960) 341–369, https://doi.org/10.1016/S0096-5332(08)60191-5.
[38] K. Imamura, A. Fukushima, K. Sakaura, T. Sugita, T. Sakiyama, K. Nakanishi, Water sorption and glass transition behaviors of freeze-dried sucrose-dextran mixtures, J. Pharm. Sci. 91 (2002) 2175–2181, https://doi.org/10.1002/jps.10218.
[39] K. Boettcher, S. Grumbein, U. Winkler, J. Nachtsheim, O. Lieleg, Adapting a commercial shear rheometer for applications in cartilage research, Rev. Sci. Instrum. 85 (2014) 93903, https://doi.org/10.1063/1.4894820.
[40] K.-A. Kwon, R.J. Shipley, M. Edirisinghe, D.G. Ezra, G. Rose, S.M. Best, R. E. Cameron, High-speed camera characterization of voluntary eye blinking kinematics, J. R. Soc. Interface 10 (2013), 20130227, https://doi.org/10.1098/rsif.2013.0227.
[41] M. Klarhöfer, B. Csapo, C. Balassy, J.C. Szeles, E. Moser, High-resolution blood flow velocity measurements in the human finger, Magn. Reson. Med. 45 (2001) 716–719, https://doi.org/10.1002/mrm.1096.
[42] M. Grimmer, A.A. Elshamanhory, P. Beckerle, Human lower limb joint biomechanics in daily life activities: a literature based requirement analysis for anthropomorphic robot design, Front. Robot. AI 7 (2020) 13, https://doi.org/10.3389/frobt.2020.00013.
[43] H. Hertz, Ueber die Berührung fester elastischer Körper, CRLL 1882 (1882) 156–171, https://doi.org/10.1515/crll.1882.92.156.
[44] I.D. Johnston, D.K. McCluskey, C.K.L. Tan, M.C. Tracey, Mechanical characterization of bulk Sylgard 184 for microfluidics and microengineering, J. Micromech. Microeng. 24 (2014) 35017, https://doi.org/10.1088/0960-1317/24/3/035017.
[45] B. Winkeljann, A.B. Bussmann, M.G. Bauer, O. Lieleg, Oscillatory tribology performed with a commercial shear rheometer, Biotribology 14 (2018) 11–18, https://doi.org/10.1016/j.biotri.2018.04.002.
[46] The Lubrizol Corporation, Aromatic Carbothane™ AC Series TPU: Transparent Thermoplastic Polyurethane, 2020. https://www.lubrizol.com/Health/Medical/Polymers/Carbothane-TPU (Accessed 12 July 2023).
[47] T. Iline-Vul, N. Kanovsky, D. Yom-Tov, M. Nadav-Tsubery, S. Margel, Design of silane-based UV-absorbing thin coatings on polyethylene films, Colloids Surf. A 648 (2022), 129164, https://doi.org/10.1016/j.colsurfa.2022.129164.
[48] E.-S.A. Hegazy, T. Sasuga, M. Nishii, T. Seguchi, Irradiation effects on aromatic polymers: 1. Gas evolution by gamma irradiation, Polymer 33 (1992) 2897–2903, https://doi.org/10.1016/0032-3861(92)90074-7.

A.2.4.2 Supplementary Information

Supplementary information

for

Comparing the Resilience of Macromolecular Coatings on Medical-Grade Polyurethane Foils

Maria G. Bauer[1,2], Kjetil Baglo[1,3], Luca Reichert[1,3], Jan Torgerson[1,3], Oliver Lieleg[1,2,*]

[1] School of Engineering and Design, Department of Materials Engineering, Technical University of Munich, Boltzmannstraße 15, 85748 Garching, Germany

[2] Center for Protein Assemblies and Munich Institute of Biomedical Engineering, Technical University of Munich, Ernst-Otto-Fischer Str. 8, 85748 Garching, Germany

[3] Institute of Materials Science, Technical University of Munich, Boltzmannstraße 15, 85748 Garching, Germany

*corresponding author:

Prof. Dr. Oliver Lieleg

Department of Mechanical Engineering and Munich School of Bioengineering,

Technical University of Munich, Boltzmannstraße 11, 85748 Garching, Germany

e-mail: oliver.lieleg@tum.de,

phone: +49 89 289 10952, fax: + 49 89 289 10801

SI 1 Fourier-transformed infrared spectroscopy (FTIR)

Spectra determined for uncoated and coated PCU samples are displayed in **Figure SI 1**.

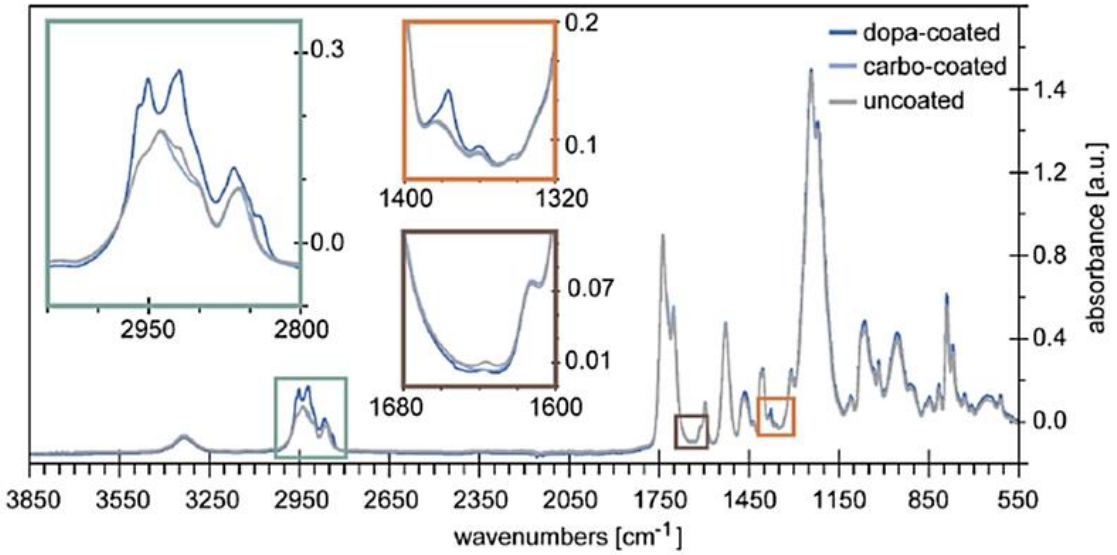

Figure SI 1: FTIR spectra of uncoated and coated PCU samples: Results obtained for uncoated PCU (grey), carbo-coated PCU (light blue), and dopa-coated PCU (dark blue) foils are displayed. Important ranges in the spectra are marked by the colored frames (turquoise, grey, and orange) and depicted as enlarged details in frames of the corresponding color.

Even though these FTIR spectra are – overall – rather similar, it is possible to detect some differences, especially within the following wavenumber ranges:

1) 2800 – 3050 cm^{-1} (turquoise frame),
2) 1600 – 1680 cm^{-1} (brown frame),
3) 1320 – 1440 cm^{-1} (orange frame).

The most noticeable changes in the spectra occur in the 2800 cm^{-1} to 3000 cm^{-1} range, where aliphatic hydrogen vibrations are observed. The coated samples each consist of at least three different compounds (*i.e.,* the PCU substrate, the intermediate layer, and the top-layer molecule), all of which have spectra reported in literature we can use to make comparisons with. [1–6]

For the ***uncoated PCU sample***, the highest abundance of peaks is expected for CH2 asymmetric and symmetric stretching occurring at 2938 cm^{-1} and 2862 cm^{-1}, respectively. The shoulder at 2955 cm^{-1} of medium to low intensity is likely CH_3 asymmetric stretch, with the lower intensity symmetric stretch overlapping with the CH_2 symmetric stretch. Other than these vibrations, there are peaks of medium to low abundance at 2920 cm^{-1} and 2905 cm^{-1}, which may be aliphatic vibrations from polymer additives such as plasticizers, solvents, or from certain parts of the polymer that are not accounted for by considering the functional groups. Without detailed knowledge about the synthesis and preparation of the commercial polymer material, a more detailed discussion is not possible.

For the ***dopa-coated PCU***, the spectrum shows two distinct peaks at 2920 cm^{-1} and 2950 cm^{-1} identified as CH_3 and CH_2 asymmetric stretch, with complementary symmetric vibrations at 2855 cm^{-1} and 2835 cm^{-1}. The shift to lower wavenumbers of these groups is consistent with a positively charged group such as a quaternary amine, and the peak positions correspond well with the spectra reported for quaternary amine. [6] A peak at 1377 cm^{-1} can be seen for the dopa-coated PCU sample; this peak is also strong in the spectrum of a quaternary amine and is likely to represent a CH_3 vibration mode. The lack of a similar increase in the ~1450 cm^{-1} CH_2 peak may indicate a dominant CH_3 content over CH_2 in the dopa coating – but this notion is not supported by the C-H stretching modes. It should also be noted that a C-H stretching is by no means unique to a quaternary amine and could be the result of other constituents. For instance, if the main functionalization of the surface is achieved through hydrogen bonding, then this would also show up in this range as a shift in C-H vibrations. To specifically assign the observed changes to the compositional chemistry, a more in-depth study would be needed. The primary amine band is present at 1635 cm^{-1}, but with a low abundance; the complimentary N-H stretching in the range 3450-3160 cm^{-1} is not observed, likely due to the low abundance. The secondary amine N-H stretch at 3335 cm^{-1} has a high abundance but is present for both, coated PCU films and the uncoated PCU film alike, making an evaluation difficult.

For the ***carbo-coated PCU*** sample, there is almost no change in the recorded absorbance (compared to uncoated PCU foils) except for a decrease in intensity for the peak at 2920 cm^{-1}. The lower abundance of this peak is likely due to a change in the PCU film rather than the coating, as the abundance of all other peaks remains unchanged. This change may be due to

the removal of lighter aliphatic species dissolved in the polymer network, and such a removal may occur during the atmospheric plasma treatment (@ 60 W for 25 min) and/or as a consequence of the foil exposure to highly concentrated solvents (*e.g.,* 96 % ethanol for 1 h).

Mainly, those results indicate that applying the coatings has induced minor changes to the material. For the dopa coating, the influence of the coating components is detectable in the spectra, whereas for the carbo-coating, the processing itself appears to have the greatest influence. It should be noted that FTIR tends to favor chemical groups with a strong dipole, and a more in-depth study would be required if the chemical composition of the coating and the polymer were to be described in full.

SI 2 Differential scanning calorimetry

To analyze how the applied coatings influence the heat thermal behavior, differential scanning calorimetry (DSC) scans were conducted. Therefore, a differential scanning calorimeter (DSC 300 Caliris, Netzsch Gerätebau GmbH, Selb, Germany) was employed and DSC scans were performed from -40°C to 300°C at 10°C/min. A protective flow of nitrogen at 20 ml/min was used for all measurements with sample weights of 10.2 mg, 11.3 mg, and 11.5 mg for the uncoated, dopa-, and carbo-coated samples, respectively. To fit the DSC pans, the samples were cut into squares using lab scissors and sealed in lidded aluminum pans. The heat flow recorded by DSC for the uncoated, carbo-coated, and dopa-coated PCU films are presented **Figure SI 2.**

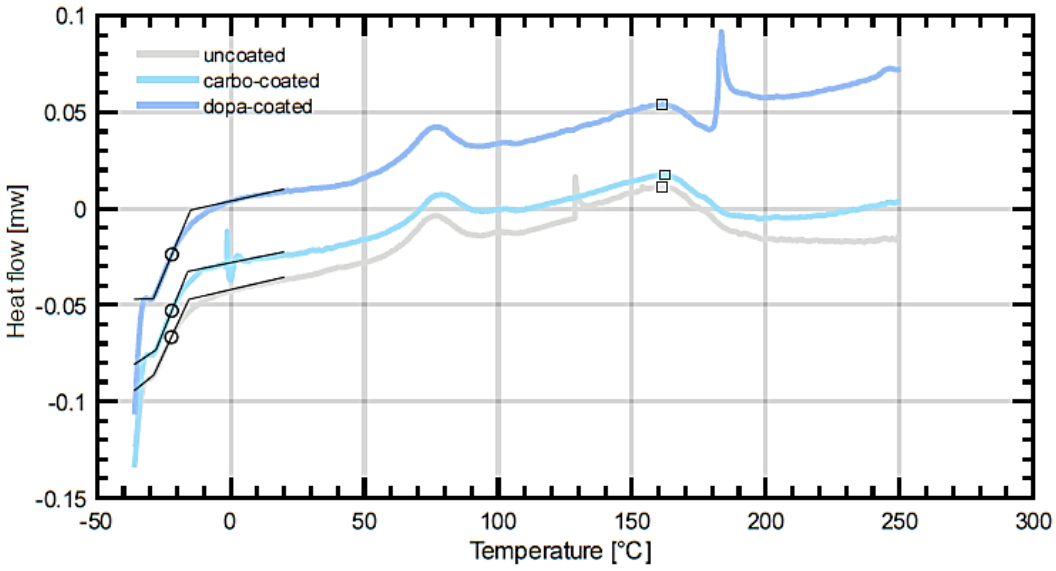

***Figure SI 2**: Influence of the coatings on the thermal behavior of the PCU foils*: The heat flow detected for temperatures ranging from -40 °C to 250 °C is displayed for uncoated (grey), carbo-coated (light blue), and dopa-coated (dark blue) PCU samples.

For all three sample types, the onset of the glass transition was estimated to be at -29 °C, while the inflection point was estimated to be at -22 °C. The melting temperature was recorded from the maximum of each broad melting peak and was determined to be 161°C for the uncoated and dopa-coated sample, and at 162°C for the carbo-coated sample. This melting temperature

is within the expected range for poly(urethane carbonates). [7] The difference between the T_g and T_m values we obtained for the uncoated PCU and the values stated by the manufacturer might be caused by different measurement conditions and/or sample dimensions/preparations. Nonetheless, especially the T_g values are still in a similar range and – more importantly – clearly below the temperature ranges used in this study.

For the carbo-coated sample, a sharp exothermic peak followed by an endothermic peak is observed around 0°C. The second feature may represent the melting of N-[3-(Trimethoxysilyl)propyl]-ethylenediamine which is reported to have a melting temperature of 0°C; and the exothermic behavior is expected for a crystalline material and is often observed for amines owing to strong hydrogen bonding. [8] Additionally, for all samples, there is an endothermic peak around 76°C followed by a slight endothermic peak at 100°C; the origin of those two peaks are most likely ethanol and water evaporation.

Overall, the DSC data suggests that the coatings do not significantly change T_g nor T_m.

SI 3 Scanning electron microscopy (SEM)

The individual interface thicknesses d_{int} derived from the acquired SEM images are listed in **Table SI 1.**

Table SI 1: Individual interface thicknesses derived from SEM images

$d_{int,uncoated}$ [µm]	$d_{int,carbo}$ [µm]	$d_{int,dopa}$ [µm]
0.458	0.353	1.573
0.390	0.606	1.504
0.407	0.641	0.576
0.274	0.672	1.000
0.462	0.925	0.865
0.356	0.673	0.424
0.119	0.504	0.712
0.390	1.052	1.001
0.256	0.475	1.068
0.222	0.407	4.525
0.084	0.527	5.288
	0.628	0.797
	0.477	0.763
	0.441	0.848
	0.202	1.017
	0.370	0.966
	0.289	0.949
	0.322	0.133
	1.441	0.687
	0.814	0.599
	0.678	
	0.538	
	0.404	
	0.356	
	0.441	
	0.407	

These values result in mean interface thicknesses of $\bar{d}_{int,uncoated} = (0.31 \pm 0.04)\,\mu m$ $\bar{d}_{int,carbo} = (0.56 \pm 0.05)\,\mu m$, and $\bar{d}_{int,dopa} = (1.26 \pm 0.29)\,\mu m$, respectively. The lowe number of values determined for uncoated samples is caused by the fact, that the visibl interface was for several images so thin, that it was not possible to reliably determine ar interface thickness.

SI 4 Surface Morphologies

To compare the influence of the coatings and/or treatments on the surface morphologies of the PCU foils, profilometric images were captured as stitched collections of 3 horizontal and 4 vertical single images. To display the surface morphologies, the single images were preprocessed as described in methods section (2.6) in the manuscript; then, representative images for each coating/treatment combination were chosen and compared qualitatively to each other together with the corresponding laser microscopy images. Such morphologies are displayed for coated and long-term treated samples in **Figure SI 3,** and for coated and sterilized samples in **Figure SI 4**.

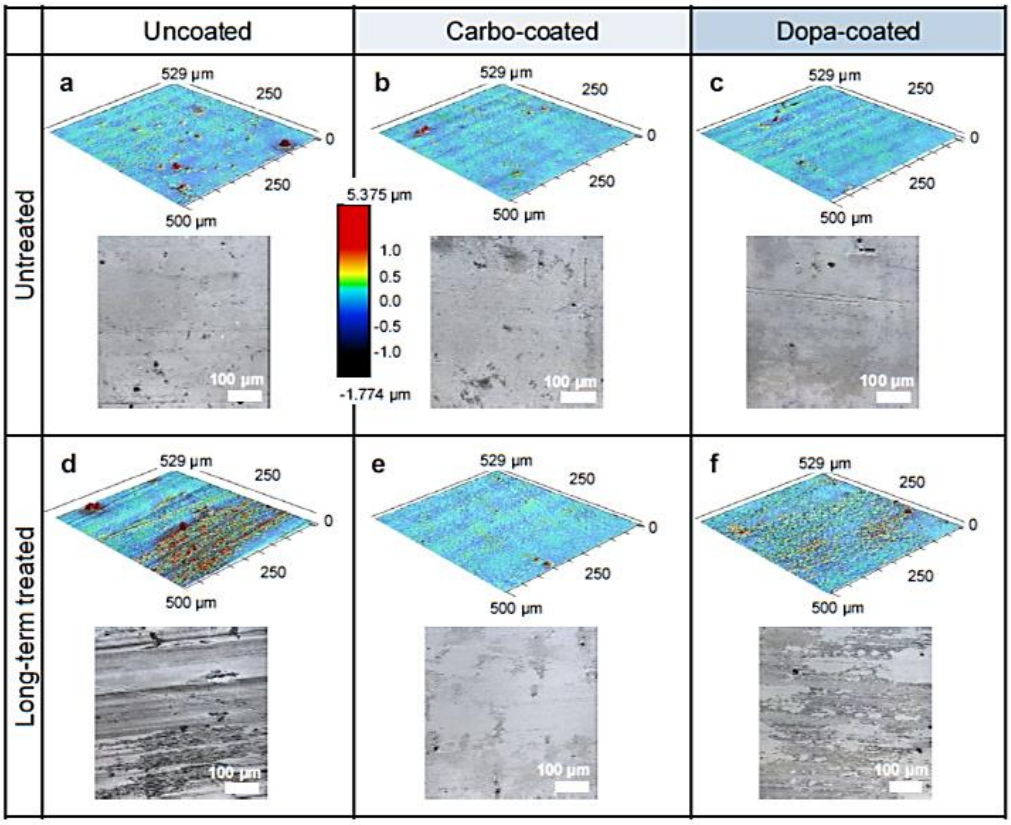

Figure SI3: *Surface morphologies and laser microscopy images of coated and long-term treated samples:* For each coating/treatment combination, a representative set of images (taken with 20x magnification) of the resulting surface structure is displayed; colored images represent height-scaled 3D surface morphologies (top pictures); grey-scale images represent laser microscopy image (bottom pictures). The color scale located between subfigures a) and b) applies to all images depicting surface morphologies.

In **Figure SI 3**, when comparing the images of the untreated samples displayed in the top row, the impression is confirmed, that neither coating appears to have a major influence on the surface morphologies of the samples. However, when each untreated sample is compared to the corresponding long-term treated sample (*i.e.,* samples exposed to 9 h of tribological load) clear differences can be observed. Whereas, on the images of the uncoated, long-term treated sample obvious grooves and valleys from the continuous linear movement are evident, almost no change is perceptible if the images associated with the carbo-coating are compared. On the images of the long-term treated, dopa-coated samples some signs of increased roughness and abrasion are visible.

If the images in **Figure SI 4** are compared with respect to the coating type, *i.e.,* column-wise, neither of the two sterilization treatments appears to have a strong influence on the surface structures or appearance of the foils when compared to each corresponding "stored" sample. Overall, the microscopy images are quite similar, and all surface morphology images can be colored using the same color scheme as their surface roughness is close to zero. However, there seems to be a small difference between the treated, uncoated samples and the control group (uncoated, untreated – only stored), which is not observable for either of the coated samples. This indicates that the applied surface coatings might help reduce putative influences the sterilization procedures have on the substrate material itself.

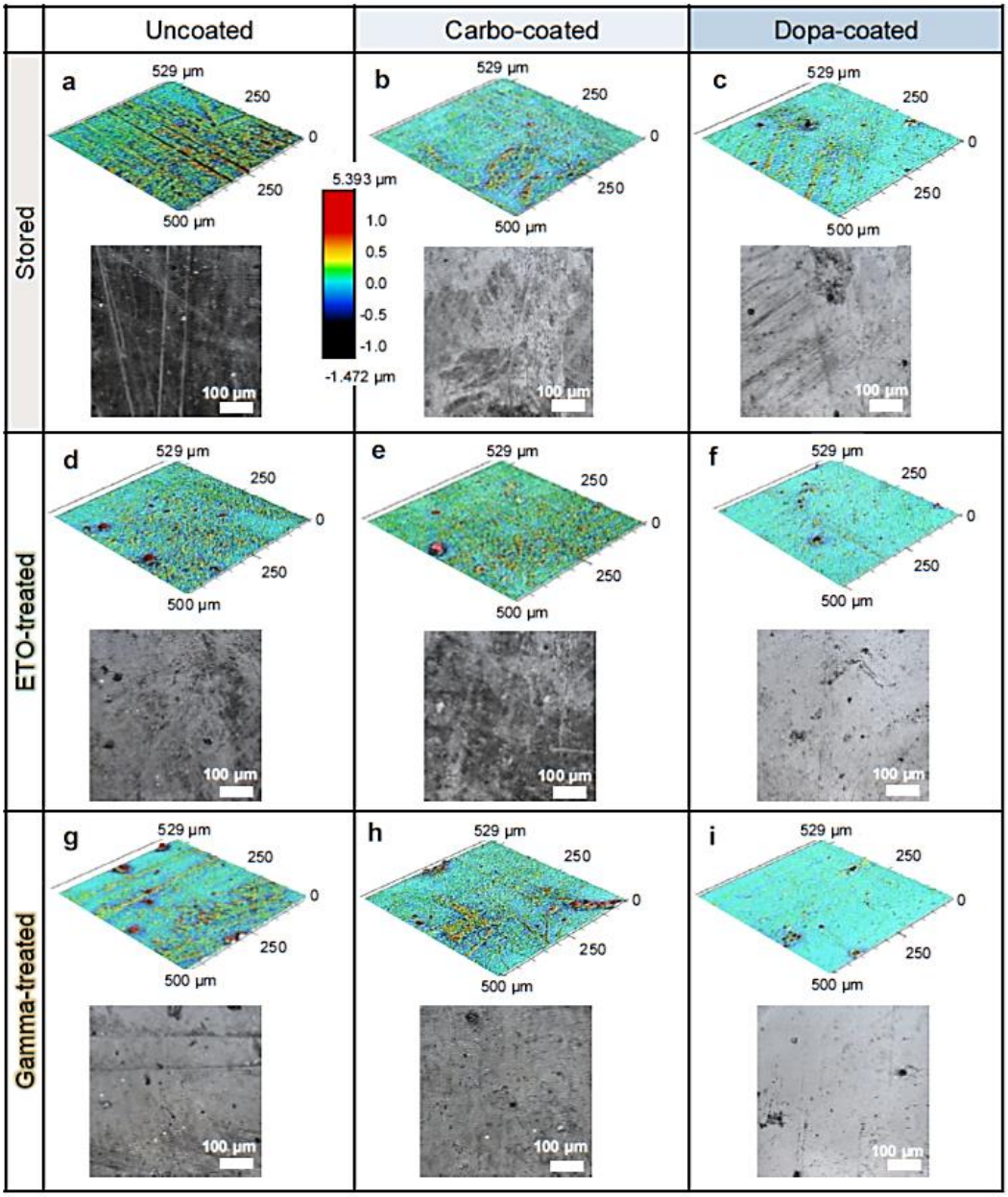

Figure SI 4: *Surface morphologies and laser microscopy images of coated and sterilized samples:* For each coating/treatment combination, a representative set of images (taken with 20x magnification) of the resulting surface structure is displayed; colored images represent height-scaled 3D surface morphologies (top pictures); grey-scale images represent laser microscopy image (bottom pictures). The color scale located between subfigures a) and b) applies to all images depicting surface morphologies.

SI 5 FTIR scans of sterilized samples

To examine putative influences of the sterilization processes on the substrate material or coating composition, FTIR scans were conducted as described in **SI 1**. In **Figure SI 5**, the spectra obtained for stored (uncoated or coated) samples are compared to spectra determined for samples subjected to a sterilization treatment.

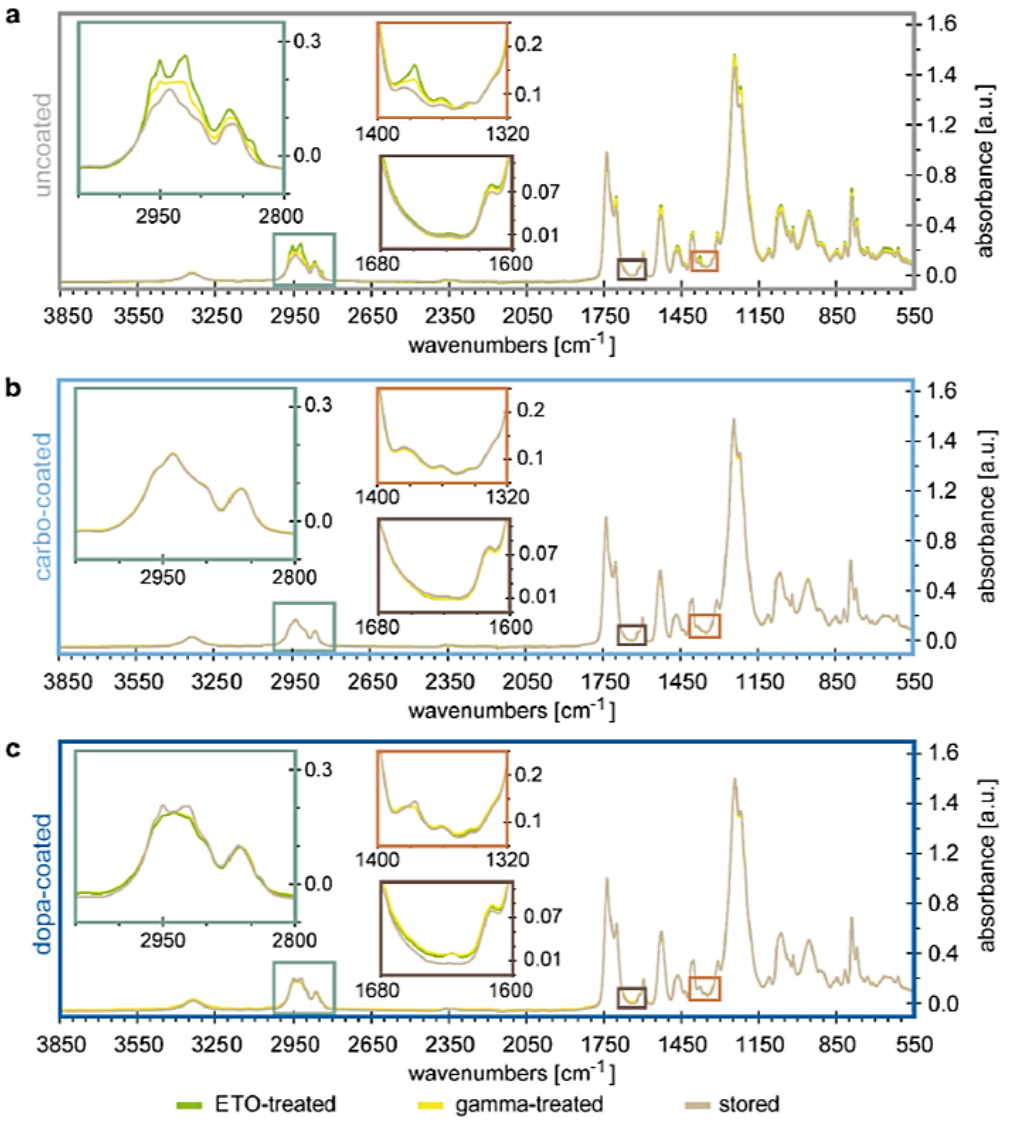

***Figure SI 5:** FTIR spectra of different foil samples:* spectra are shown for a) uncoated, b) carbo-coated, and c) dopa-coated samples which were treated with either ethylene oxide fumigation (ETO, green) or γ-irradiation (gamma, yellow), or simply stored in a dry state (stored, beige). The legend at the bottom of the figure applies to all subfigures.

When using the stored samples as a reference, for each sterilization treatment, the changes caused by the sterilization process can be studied. For the uncoated samples, there is a strong change in the abundance of aliphatic C-H stretching vibrations in the 3000-2800 cm^{-1} range and in the vibrations around 1377 cm^{-1}. The ETO-treatment seems to trigger the appearance of two strong peaks indicating CH_3 and CH_2 asymmetric stretching. These peaks are similar to the bands we notice for the unsterilized dopa-coated sample in **Figure SI 1**; for uncoated samples, those must originate from the ethylene oxide fumigation. The simplest explanation would be that the observed bands are caused by hydrogen bonding of residual ethylene oxide molecules.

For carbo-coated samples, we detect no noticeable change in the FTIR spectra upon either sterilization treatment. It is, however, not fully clear why this is the case. Potentially, a change in the surface properties caused by the plasma treatment (@ 60 W for 25 min), removal of lighter aliphatic species upon exposure to highly concentrated solvents (*e.g.,* 96 % ethanol for 1 h), or the presence of the dextran layer on the surface could have rendered the foils more resistant to alterations by sterilization. In any case, the result indicates that the carbo-coated samples exhibit an increased inertness toward the two sterilization methods than uncoated foils.

For the dopa-coated sample, both sterilization treatments reduction the abundance of the CH_2 and CH_3 asymmetric stretch at 2920 cm^{-1} and 2950 cm^{-1}, as well as the 1377 cm^{-1} CH_3 peak. This result could indicate a change in the coating or of selected exposed groups from the coating; however, without spectral changes outside the aliphatic C-H vibrations, it is difficult to make a more detailed assessment.

Overall, both coatings appear to provide the foils with improved resistance towards the two sterilization treatments tested here – with the carbo-coated samples experiencing basically no change and the dopa-coated samples only minor changes compared to the uncoated samples. However, to fully assess and understand the origin of this enhanced resilience introduced by the coatings, further studies would be needed.

SI 6 References

[1] SpectraBase, Dopamine hydrochloride: Attenuated Total Reflectance Infrared (ATR-IR) Spectrum. https://spectrabase.com/spectrum/9HdJ7pFzgn1 (accessed July 18th, 2023).

[2] SpectraBase, N1-[3-(Trimethoxysilyl)propyl]-1,2-ethanediamine: Attenuated Total Reflectance Infrared (ATR-IR) Spectrum. https://spectrabase.com/spectrum/KB8BLkV1YdM (accessed July, 18th 2023).

[3] SpectraBase, Dextran: Attenuated Total Reflectance Infrared (ATR-IR) Spectrum. https://spectrabase.com/spectrum/BDKq1MblXC4 (accessed July 18th 2023).

[4] IRUG, Dextran from Leuconostoc mesenteroides: Interactive IRUG Spectrum. http://www.irug.org/jcamp-details?id=7047 (accessed July 18zh 2023).

[5] SpectraBase, DL-lysine: Attenuated Total Reflectance Infrared (ATR-IR) Spectrum. https://spectrabase.com/spectrum/89KyMH3B2yR (accessed July 18th 2023).

[6] SpectraBase, Quarternary ammonium compound: Transmission Infrared (IR) Spectrum. https://spectrabase.com/spectrum/GIeuiZ5tVi6 (accessed July 18th 2023).

[7] Z. Chen, N. Hadjichristidis, X. Feng, Y. Gnanou, Poly(urethane–carbonate)s from Carbon Dioxide, Macromolecules 50 (2017) 2320–2328. https://doi.org/10.1021/acs.macromol.7b00142.

[8] ChemicalBook, N-[3-(Trimethoxysilyl)propyl]ethylenediamine. https://www.chemicalbook.com/ChemicalProductProperty_EN_CB3129690.htm (accessed July 24th 2023).

A.2.5 "Effects of Sterilization Methods on the Integrity and Functionality of Covalent Mucin Coatings on Medical Devices"

RESEARCH ARTICLE

ADVANCED MATERIALS INTERFACES
www.advmatinterfaces.de

Effects of Sterilization Methods on the Integrity and Functionality of Covalent Mucin Coatings on Medical Devices

*Carolin A. Rickert, Maria G. Bauer, Julia C. Hoffmeister, and Oliver Lieleg**

Recent advances in the field of biomedical materials have demonstrated that covalent mucin coatings generated on polymeric materials have the potential to greatly improve the surface properties of medical devices such as their wettability, lubricity, and resistance toward biofouling. For such biopolymer-based coatings to be used in a medical application, sterilization of the coated devices is mandatory. However, common sterilization methods such as autoclavation, ethylene oxide fumigation, as well as γ- or ultraviolet-irradiation, create harsh conditions during the device treatment, and this might compromise the structural integrity and thus functionality of macromolecular coatings. Here, it is demonstrated that covalent mucin coatings generated on medical devices made from polyvinyl chloride, polyurethane, or polydimethylsiloxane are able to withstand such treatments—albeit to different extents. Among all treatments tested, ethylene oxide fumigation is identified as the most promising method as it maintains the coatings the best. The findings imply that the beneficial properties demonstrated for mucin coatings in vitro should indeed be transferable to applications in vivo.

1. Introduction

Whether as implants or as tools for invasive procedures or patient care, products made from polymer-based materials are indispensable helpers in many fields of modern medicine. Endotracheal tubes comprising polyvinyl chloride (PVC), for instance, are commonly used in medical emergencies to secure a patient's supply with air.[1] Catheters made from polyurethane (PU) have become an integral tool for drainage purposes and to support surgical procedures in cardiovascular, urological, or neurovascular medicine.[2,3] Polydimethylsiloxane (PDMS) is the material of choice for implantable tubes or devices.[4,5] However, when those synthetic materials come into direct contact with human tissue or if they remain in the body for a longer time period, complications can arise. The significantly higher stiffness of polymeric materials compared to human epithelia can, for example, entail damage to the tissue during friction processes. The resulting injuries render the tissue more susceptible to infections, which can promote severe inflammations. Moreover, medical devices themselves may constitute a major infection risk, as germs or other contaminants from the environment can attach to the device and are then transported into the human body.[5,6]

One strategy to combat these issues is based on the application of coatings to the surfaces of the medical devices.[7,8] In this context, coatings generated from the endogenic macromolecule mucin have been put forward as highly interesting candidates that can provide multiple functionalities at the same time: Covalent mucin coatings were recently shown to efficiently reduce bacterial adhesion to a broad variety of artificial materials,[9] to improve the surface wettability,[10] to reduce friction,[11] and to prevent wear formation on (corneal) tissue under tribological stress.[12] Furthermore, by repeatedly reassessing the surface wettability of coated samples, the good stability of such coatings has been proven previously: there, the mucin coatings maintained their functionality very well even when stored for 90 days.[12] Mucins are large glycoproteins that constitute an essential part of the inherent immune barrier of mammalians.[13–15] Here, as the main functional component of mucus, the viscoelastic hydrogel covering all mucosal tissues, mucins not only establish a stable barrier against bacteria and viruses, they also provide excellent lubricity.[16–18] From a molecular point of view, the multifaceted properties of mucins are brought about by its complex microarchitecture: the long protein backbone (>5600 amino acids) contains both, a densely glycosylated, hydrophilic core region and two sparsely glycosylated, but partially folded hydrophobic termini.[19] A mucin variant commonly used in research is MUC5AC, and decent amounts of this highly functional mucin type can be obtained from porcine stomachs by performing a multi-stage purification process.[20] Moreover, these lab-purified mucins have previously been shown to be highly biocompatible[21]—both as hydrogels and coatings.[11,22] As a purified product of animal

C. A. Rickert, M. G. Bauer, J. C. Hoffmeister, O. Lieleg
TUM School of Engineering & Design
Department of Materials Engineering
Technical University of Munich
Boltzmannstr. 15, 85748 Garching b. München, Germany
E-mail: oliver.lieleg@tum.de
C. A. Rickert, M. G. Bauer, J. C. Hoffmeister, O. Lieleg
Center for Functional Protein Assemblies (CPA)
Technical University of Munich
Ernst-Otto-Fischer Straße 8, 85748 Garching b. München, Germany
The ORCID identification number(s) for the author(s) of this article can be found under https://doi.org/10.1002/admi.202101716.

DOI: 10.1002/admi.202101716

ADVANCED SCIENCE NEWS
www.advancedsciencenews.com

ADVANCED MATERIALS INTERFACES
www.advmatinterfaces.de

origin, however, sterility cannot be guaranteed. Thus, when envisioned to be used as a component of medical devices, mucin-based coatings generated on medical devices need to be sterilized before usage.

Typical examples of standardized procedures suitable for sterilizing medical devices include irradiation with either γ or ultraviolet (UV)-rays, AC, or fumigation with ethylene oxide.[23,24] However, all those methods might negatively influence the biochemical integrity of mucin coatings: Thermal stress, for example, often disrupts intramolecular forces that stabilize the conformation of protein domains, and this can entail protein denaturation.[25] UV- and γ-irradiation might induce oxidation or cleavage of covalent bonds located in the protein backbone or in aromatic amino acid side chains.[26,27] Treatments with ethylene oxide are suspected to modify methionine and cysteine residues in proteins, and this, in turn, can decrease their stability and agglomeration propensity.[28,29] To what extent such issues may limit the functionality of covalent mucin coatings is, however, to date unclear.

In this study, we test the integrity and functionality of covalent MUC5AC coatings. Such mucin coatings are generated on medical devices made from PU, PVC, and PDMS and then subjected to different sterilization treatments. By employing two specific detection methods, we show that the glycosylated part of the mucin molecule is more robust toward those physico-chemical challenges than its hydrophobic termini. Contact angle measurements demonstrate that, for nearly all treatments, the hydrophilic character of surfaces coated with mucins can be maintained to a certain extent. Rotational tribology experiments show that the lubricity provided by mucin coatings is not impaired by any of the sterilization treatments tested here. Lastly, lipid adsorption tests illustrate the superior functionality of coatings subjected to ethylene oxide compared to the other techniques, which underscores the overall finding that this sterilization method has the least impact on the integrity and functionality of the mucin coatings.

2. Experimental Section

Unless stated otherwise, all chemicals were purchased from Carl Roth GmbH & Co. KG (Karlsruhe, Germany).

2.1. Medical Devices

In this study, mucin coatings were tested on three different medical devices: contact lenses, endotracheal tubes, and urinary catheters (**Figure 1**a). As described previously,[12] the contact lenses studied here (curvature: 0.07 mm^{-1}, surface roughness: 0.66 ± 0.08 µm) consist of a highly biocompatible, aliphatic Pt-catalyzed liquid silicone based on Si-H and Si-vinyl poly-dimethyl-siloxane (PDMS; Polymer Systems Technology, High Wycombe, UK) without any further additives. They were kindly provided by Woehlk Contactlinsen GmbH (Schönkirchen, Germany). The endotracheal tubes (Super

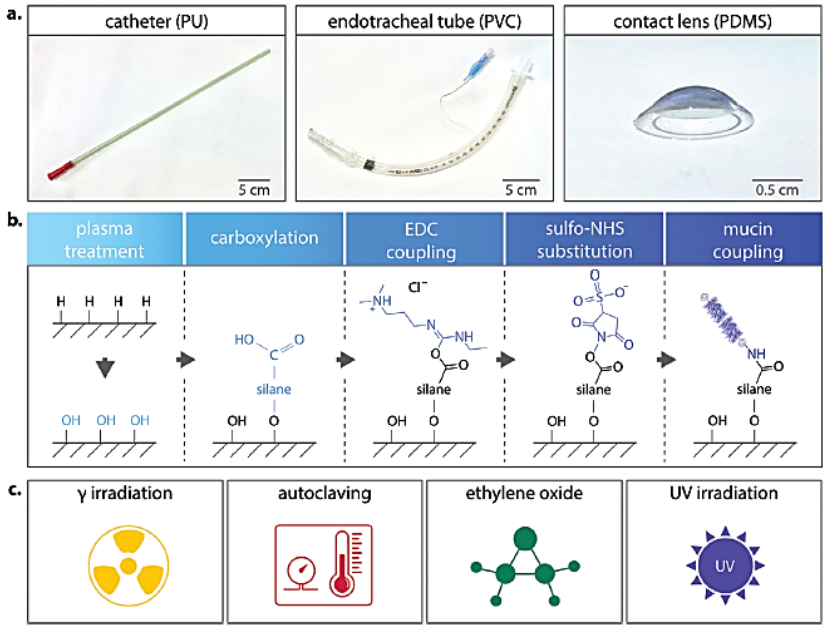

Figure 1. Overview of the medical devices, the mucin coating process, and the sterilization techniques used in this study. a) Exemplary images of a urinary catheter (made from PU), an endotracheal tube (made from PVC), and a PDMS-based contact lens as used in this study. b) The coating process employed here starts with plasma activation of the material, followed by carboxylation using a silane precursor, and a final carbodiimide coupling step to covalently attach the mucins onto the surfaces of the medical devices. c) Sterilization of the coated devices was conducted via γ-irradiation, autoclaving, ethylene oxide fumigation, or UV irradiation.

ADVANCED SCIENCE NEWS
www.advancedsciencenews.com

ADVANCED MATERIALS INTERFACES
www.advmatinterfaces.de

Safetyclear, 10.0 mm, CH40) were purchased from Radecker Notfallmedizin (Ammerbuch/Entringen, Germany) and are made from latex-free polyvinyl chloride (PVC). The urinary catheters (SpeediCath Standard, CH/FR 18/6.0 mm) are fabricated from polyurethane (PU) and were purchased from Coloplast (Hamburg, Germany). To obtain uniform specimens from the latter two medical devices, round samples with a diameter of 7 mm were cut from the endotracheal tubes (curvature of the samples: 0.1 mm^{-1}, surface roughness: 0.4 ± 0.5 µm) and the catheters (curvature of the samples: 0.17 mm^{-1}, surface roughness: 2.3 ± 0.5 µm) using an eyelet press (IstaBreeze Germany GmbH, Bad Rappenburg, Germany). The surface roughness (expressed by the arithmetical mean height S_q according to ISO 25178-2) of each sample was measured on a laser-scanning microscope (VK-X1000, Keyence, Neu-Isenburg, Germany) equipped with a 20× lens (CF Plan, NA = 0.46; Nikon, Chiyoda, Tokyo, Japan). A Gaussian filter with a cut-off wavelength of 0.2 mm was applied before calculating the roughness parameter with the MultiFileAnalyzer software (v2.1.3.89, Keyence). The endotracheal tubes and the urinary catheters are commercial medical products approved for clinical usage in the European market (Conformité Européenne, CE) labeled). Before further usage, all samples were first washed in 70% (v/v) ethanol and then in ddH_2O by incubating them in the respective solution while being placed onto a rolling shaker (RS-TR 05, Phoenix Instrument GmbH; Garbsen, Germany) for 30 min.

2.2. Mucin Purification

Porcine gastric mucins (MUC5AC) were manually purified.[30] In brief, raw mucus was manually collected from the mucosal tissue of fresh pig stomachs obtained from a local slaughterhouse (Schlacht- und Viehhof, München, Germany). The harvested material was diluted 1:5 in phosphate buffered saline (pH 7.0) containing 170 × 10^{-3} M sodium chloride and 0.04% sodium azide, and then homogenized at 4 °C overnight by stirring. To remove mesoscopic impurities and cellular debris, two centrifugation steps (17 590 × g for 30 min and 158 306 × g for 1 h) were conducted. Afterward, the mucins were separated from other molecules via size exclusion chromatography using an ÄKTA purifier system (GE Healthcare, Chicago, IL, USA) equipped with an XK50/100 column packed with Sepharose 6FF (GE Healthcare). The collected mucin-containing fractions were pooled, and 1 M NaCl was added. The mixture was then dialyzed against ultrapure water and concentrated by crossflow filtration using an ultrafiltration hollow fiber cartridge with a molecular weight cut-off of 100 kDa (UFP-100-E-3MA, GE Healthcare). After lyophilization, the mucin was stored at −80 °C. For further processing, the lyophilized mucin was solubilized in the desired buffer, vortexed for 1 min and kept at 4 °C on a shaking incubator (set to 750 rpm) for 2 h to generate a homogeneous solution.

2.3. Covalent Mucin Coating Process

The mucin macromolecules were covalently attached to the surfaces of the medical devices by performing a carbodiimide coupling process (Figure 1b).[31] For this purpose, the sample surfaces were first activated by exposing them to plasma generated with ambient air (60 W, 0.4 mbar, 90 s; plasma oven "SmartPlasma 2," plasma technology GmbH, Herrenberg, Germany). Subsequently, surface carboxylation was achieved by incubating the specimens in 10 × 10^{-3} M acetate buffer (pH 4.5) supplemented with 1.0% (v/v) of the coupling agent *N*-[(3-trimethoxysilyl)propyl]ethylenediamine triacetic acid trisodium salt (TMS-EDTA, abcr GmbH, Karlsruhe, Germany) at 60 °C for 5 h. To remove loosely bound silanes, the samples were first dipped into iso-propanol (>99. 5%) and then washed in 96% (v/v) ethanol on a rolling shaker (70 rpm; RS-TR 05, Phoenix Instrument GmbH, Garbsen, Germany) for 1 h. The generated siloxane bonds were stabilized by baking the samples at 80 °C for 2 h (for PDMS samples) or at room temperature for 24 h (for PVC and PU samples). To finally attach the MUC5AC macromolecules via EDC-NHS coupling, the carboxyl groups previously generated on the sample surfaces were activated by incubating the samples in 100 × 10^{-3} M 2-(N-morpholino)-ethanesulfonic acid buffer (MES buffer, pH 5.0) comprising 5 × 10^{-3} M 1-ethyl-3-(3-(dimethylamino)propyl)carbodiimide (EDC) and 5 × 10^{-3} M *N*-hydroxysulfosuccinimide (sulfo-NHS, acbr GmbH) for 30 min while moderately shaking (35 rpm). The samples were then immersed into Dulbecco's phosphate buffered saline (DPBS; Lonza, Verviers, Belgium) containing 0.1% (w/v) MUC5AC and kept there at 4 °C for 18 h. Last, if not stated otherwise, the coated samples were gently washed in 80% (v/v) ethanol, air-dried, stored in sterilization bags (Medi Pack GmbH, Mönchengladbach, Germany), and rehydrated in DPBS for 24 h before each experiment. Importantly, all specimens used in a given set of experiments were coated at the same time and stored for the same duration—independently of whether or not a sterilization process was conducted.

As described earlier, small specimens of the different medical devices were subjected to the covalent coating process—but not whole devices. For other small samples of similar sizes, a uniform density of such mucin coatings was demonstrated in a previous study.[9] However, once full-length endotracheal tubes or catheters are supposed to be coated, a suitable technical process needs to be developed and its success (i.e., the uniformity of the coating) needs to be verified.

2.4. Sterilization Methods

Four different sterilization methods were conducted (Figure 1c). For autoclaving (AC), sterilization bags (Medi Pack GmbH, Mönchengladbach, Germany) containing the dried samples were placed into an autoclave (Systec VX-150, Systec GmbH, Linden, Germany), and a standard sterilizing process (121 °C, 20 min) was applied. Treatments with γ-irradiation (dose: 25–50 kGy; system type: JS9000; complied standards: EN ISO 9001, EN ISO 13 485, EN ISO 11137-1) or ethylene oxide (EO; duration: 5 h, temperature: 45 °C, pressure 610 mbar, average EO concentration: 700 mg L^{-1}) were conducted by employing commercial standard processes available at the company steripac GmbH (Calw, Germany). Here, the samples were stored in sterilization bags as well. For sterilization via UV irradiation, the samples were directly placed into a petri dish, placed into a sterilization

ADVANCED SCIENCE NEWS
www.advancedsciencenews.com

ADVANCED MATERIALS INTERFACES
www.advmatinterfaces.de

chamber (BLX-254, Vilber Lourmat GmbH, Eberhardzell, Germany), and exposed to UV irradiation (254 nm, 5 × 8 W) for 30 min. After irradiation, the samples were moved into sterilization bags for further storage.

2.5. ELISA

An indirect enzyme-linked immunosorbent assay (ELISA) was conducted that targets the unglycosylated, hydrophobic termini of the surface-bound MUC5AC molecules. Therefore, the PU and PVC samples were used as prepared earlier (round shaped), and the contact lenses were cut into four identical parts to fit into the wells of a 48-well plate. The specimens were incubated in blocking buffer (5% [w/v] milk powder dissolved in DPBS containing 1 mg/mL Tween 20) at 4 °C overnight. Additionally, empty wells of a 48-well plate (one per sample) were blocked using the same blocking buffer. After overnight incubation, all wells were washed with DPBS-Tween, and the samples were transferred into empty, blocked wells. Then, 300 µL of blocking buffer supplemented with a specific antibody for MUC5AC detection (1:400; ABIN966608, antibodies-online GmbH, Aachen, Germany) were added into each well, and the well plate was placed on a shaker (35 rpm) at 4 °C for 1 h. Before adding the secondary antibody, the wells were washed thrice with DPBS-Tween. A horse radish peroxidase (HRP) conjugated goat anti-mouse (murine) IgG antibody (ABIN237501, antibodies-online GmbH) was diluted 1:5000 in blocking buffer, and 200 µL of this solution were added to each sample. Antibody incubation was allowed to take place on a shaker (35 rpm) at 4 °C for 2 h.

After washing the wells with DPBS (without any Tween), 150 µL of QuantaRed Working Solution were added to each well. This solution comprises of 50 parts QuantaRed Enhancer Solution, 50 parts QuantaRed Stable Peroxide, and 1 part QuantaRed ADHP Concentrate (QuantaRed Enhanced Chemifluorescent HRP Substrate Kit 15 159; Thermo Fisher Scientific, Waltham, MA, USA). After 30 min of incubation at RT, 100 µL of the solution were removed from each well and transferred into an empty well plate, and the fluorescence signal created by the converted substrate was quantified using a plate reader (ex.: 540 nm, em.: 590 nm; Fluoroskan Ascent FL, Thermo Labsystems, Waltham, MA, USA). The measured values were normalized to the intensities measured for coated but untreated reference samples (of the respective group).

2.6. Lectin Depletion Assay

To complement the ELISA measurements, the presence of surface-bound MUC5AC molecules was probed with a lectin depletion assay that targets the glycosylated, central region of the MUC5AC glycoprotein. For this purpose, coated samples (similar geometries as described for the ELISA assay) were washed thrice with DPBS and placed into wells of a 48-well plate. Then, 300 µL of DPBS containing 12.5 µg mL^{-1} fluorescently labeled lectins (FITC conjugated lectin from *triticum vulgaris*, wheat, Sigma Aldrich) were added to each well. Those lectins specifically target sialic acids (in detail, *N*-acetylneuraminic acid and *N*-glycolylneuraminic acid) and *N*-acetylglucosamin.[32] The well-plate was placed on a shaker (35 rpm) under light exclusion for 12 h. Afterward, 200 µL of the lectin solution were removed from each well and transferred into an empty well plate. The fluorescence signal obtained from those lection solutions was then quantified using a plate reader (ex.: 485 nm, em.: 538 nm; Fluoroskan Ascent FL, Thermo Labsystems). The measured values were normalized to the intensities measured for the blank reference samples of each group.

2.7. Tribological Measurements

Tribological experiments were conducted on a commercial shear rheometer (MCR 302, Anton Paar, Graz, Austria) equipped with a rotational tribology setup (T-PTD 200, Anton Paar) as described previously.[33] In brief, a ball-on-3-pins geometry was established by combining a rotating steel sphere (Ø 12.7 mm, Kugel Pompel, Wien, Austria) with PDMS-pins (Ø 5.5 mm). The cylindrical PDMS-pins were produced by adding one part crosslinker to ten parts of the PDMS prepolymer (PDMS, Sylgard 184, Dow-Corning, Wiesbaden, Germany), placing the mixture into a vacuum chamber for 1 h, pouring the degassed mixture into custom-made molds, and finally curing the pins at 80 °C for 4 h. Before each measurement, the pins were gently washed with 70% (v/v) ethanol and inserted into a pin holder; here, special care was taken to achieve symmetric pin positions (to ensure centric rotation of the ball on the three pins). 600 µL of HEPES buffer (4-[2-hydroxyethyl]-1-piperazineethanesulfonic acid buffer) were then pipetted onto the pin-holder such that the pins were fully covered. The HEPES buffer had a pH of 7.3, which corresponds to the average pH value of the human tear film.[34] The temperature control was set to $T = 20$ °C, which represents the standard storage conditions (room temperature) of such devices. A normal force of $F_N = 6$ N was applied, which corresponds to a contact pressure of ≈ 0.35 MPa (according to Hertzian contact theory).[35] Then, friction coefficients were measured for sliding velocities ranging from 10^3 to 10^{-2} mm s^{-1} (by applying logarithmic speed ramps with ten measuring points per decade; sliding velocities were varied from "fast" to "slow" to minimize stick-slip effects) using an acquisition time of 10 s per data point.

2.8. Contact Angle Measurements

To assess the wetting behavior of the different medical devices, contact angle measurements were performed using a drop shape analyzer device (DSA25S, Krüss GmbH, Hamburg, Germany). Therefore, the coated samples were removed from the buffer solution and dried with oil-free pressurized air (Aero Duster 105/2) for ≈3 s. Uncoated samples were used as described above (see Section 2.1). Afterward, a droplet of 2 µL of ultrapure water was placed onto each sample, and lateral images of the droplets were captured with a high-resolution camera (acA1920, Basler, Ahrensburg, Germany) integrated into the device. These images were processed with the software ADVANCE (AD4021 v1.13, Krüss GmbH) using the integrated ellipse (tangente-1) fit method; static contact angles were defined as the water enclosed angle between the surface and the edge of the droplet.

ADVANCED SCIENCE NEWS
www.advancedsciencenews.com

ADVANCED MATERIALS INTERFACES
www.advmatinterfaces.de

2.9. Assessment of the Break-up Time (BUT)

The BUT quantifies the duration that a liquid film completely covers a surface exposed to air without rupturing. To measure this BUT, contact lenses were hydrated in DPBS overnight. Afterward, the lenses were removed from the liquid, and the excess water was removed by gently blotting the lenses with a low-lint laboratory paper towel, and the lenses were placed onto a dry glass slide. Then, a stopwatch was started immediately, and the time point at which a first rupture of the fluid film appeared was recorded.

2.10. Lipid Deposition Tests

To assess lipid deposition on the sample surfaces, a depletion assay was conducted. Therefore, the samples (similar geometries as described for the ELISA assay) were gently washed in 70% (v/v) ethanol and ddH_2O, and then placed into a 48-well plate. Then, 300 µL of DPBS supplemented with 25×10^{-6} M of fluorescently labeled 1,2-dioleoyl-sn-glycero-3-phosphoethanolamine (DOPE-Atto590, ATTO-TEC GmbH, Siegen, Germany) were added to each sample. After an incubation step at 4 °C for 4 h (while gently shaking at 25 rpm), 200 µL of the lipid solution were removed from each well and transferred into an empty well plate. The fluorescent signals of those transferred solutions were then quantified using a plate reader (ex.: 584 nm, em.: 620 nm; Fluorskan FL, Thermo Labsystems), and the measured values were normalized to the intensity values measured for an empty well.

2.11. Tests for Statistical Significance

To test for normal data distribution, a Lilliefors test was applied; a two-sample F-test was employed to check for equal variances. To test for significant differences between normally distributed samples, a two-sample *t*-test was applied when homogeneity of variances was met, whereas a Welch's t test was performed for unequal variances. For samples that were not normally distributed, a Wilcoxon–Mann–Whitney test was performed. All statistical analyses were performed using Matlab (version R2019a, MathWorks, Natick, MA, USA), and differences were considered statistically significant if a *p*-value below 0.05 was obtained.

3. Results and Discussion

Covalent coatings with MUC5AC macromolecules were established on samples of three medical devices: urinary catheters (PU), endotracheal tubes (PVC), and contact lenses (PDMS). In a first set of experiments, we aim at assessing the durability of those covalent mucin coatings by probing the structural integrity of mucins after exposing the coated specimens to different sterilization procedures. More precisely, we first employ an antibody-based detection method (ELISA) that specifically targets the non-glycosylated, hydrophobic termini of the MUC5AC glycoproteins (**Figure** 2a–c).

For all three tested materials, the fluorescence signals obtained after sterilization with either γ-irradiation or autoclavation are significantly lower than those obtained for untreated

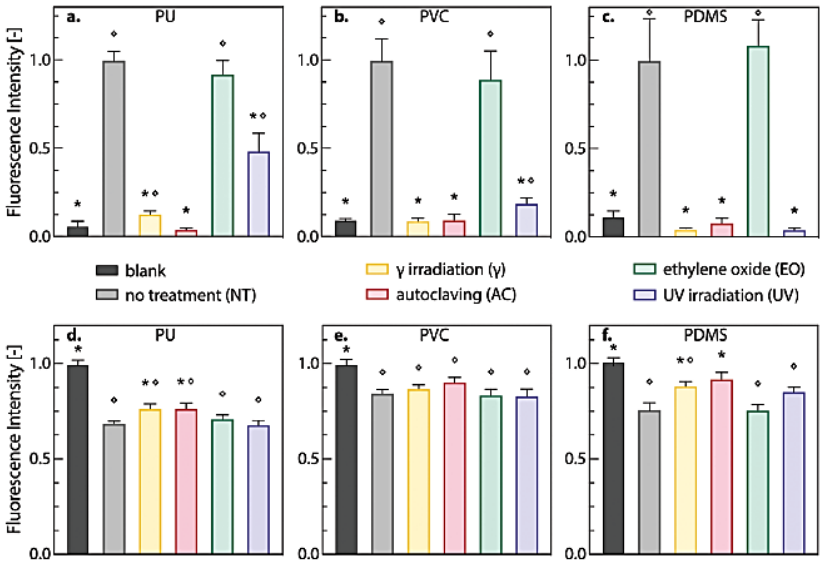

Figure 2. Detection of surface-bound mucins MUC5AC via ELISA and lectin-binding. The normalized fluorescence intensities obtained with an ELISA (a–c) and a lectin-based depletion assay (d–f) are shown for different medical devices coated with mucins. The coated samples were either stored without any further treatment, or sterilized via γ-irradiation, autoclavation, ethylene oxide fumigation, or UV irradiation. The error bars denote the standard error of the mean as obtained from $n \geq 4$ samples. Asterisks and rhombi denote statistically significant differences between a treated sample group and the untreated references or the blank sample, respectively (based on a *p*-value of 0.05).

ADVANCED SCIENCE NEWS
www.advancedsciencenews.com

ADVANCED MATERIALS INTERFACES
www.advmatinterfaces.de

mucin coatings. In fact, the measured values are comparable to those obtained for a blank sample. This indicates that these two sterilization approaches induce severe damage to or even full cleavage of the hydrophobic MUC5AC termini. The same picture arises for UV irradiated mucin coatings generated on PDMS or PVC. On PU, in contrast, somewhat higher values are obtained for UV irradiated samples; yet, also here, those values are still considerably lower than those obtained for untreated coatings. In marked contrast to those observations, samples that were subjected to ethylene oxide fumigation return fluorescent signals that are similarly high as those determined for untreated coatings—and this assessment applies to coatings generated on any of the three materials. From these tests, we conclude that the integrity of the hydrophobic termini of the mucin molecules is impaired by autoclavation and irradiation with either gamma or UV rays, respectively. In contrast, sterilization with ethylene oxide maintains the integrity of the terminal polypeptide chains.

So far, we focused on the unglycosylated, hydrophobic terminal regions of mucins; however, the glycosylated core region of the MUC5AC constitutes the largest part of the macromolecule and plays a key role for many of the molecule's important properties. Thus, in a next step, the presence and accessibility of this glycosylated part of surface-attached mucins is probed by employing a lectin binding assay that specifically detects a structural motif from the glycosylation pattern of the mucin glycoprotein (Figure 2d–f). Here, the coatings are incubated with a solution of fluorescent lectins, and the lectin solution is analyzed after this incubation step. Thus, low fluorescence intensity values represent a strong depletion of the lectin molecules and this, in turn, indicates the presence of a high number of glycosylated groups on the mucin coatings. Consistently, for almost all coatings, the obtained values are significantly lower than those obtained for blank, uncoated samples; only for autoclaved mucin coatings generated on PDMS, the measured difference is not significant. Importantly, for all coatings that were sterilized by either ethylene oxide exposure or UV irradiation, the lectin depletion induced by the coatings is equally high as for untreated reference coatings. This is a good indication that, for those particular samples, the density of glycan groups (and thus the glycosylated area in general) in the treated coatings is not affected by the sterilization treatment.

Together, the two assays show that the glycosylated regions of the mucin coatings seem to be more resistant toward the applied sterilization methods than the non-glycosylated terminal regions. This agrees with our expectations since the glycosylation pattern was already observed to protect the protein backbone from proteolytic degradation.[35] The terminal, non-glycosylated parts of the polypeptide backbone, in turn, are more vulnerable. Moreover, the results discussed so far suggest that both parts of the MUC5AC glycoprotein seem to survive a treatment with ethylene oxide gas very well. Here, with either assay, no significant differences were observed compared to untreated coatings.

Having probed the structural integrity of the covalent mucin coatings after subjecting them to the different sterilization

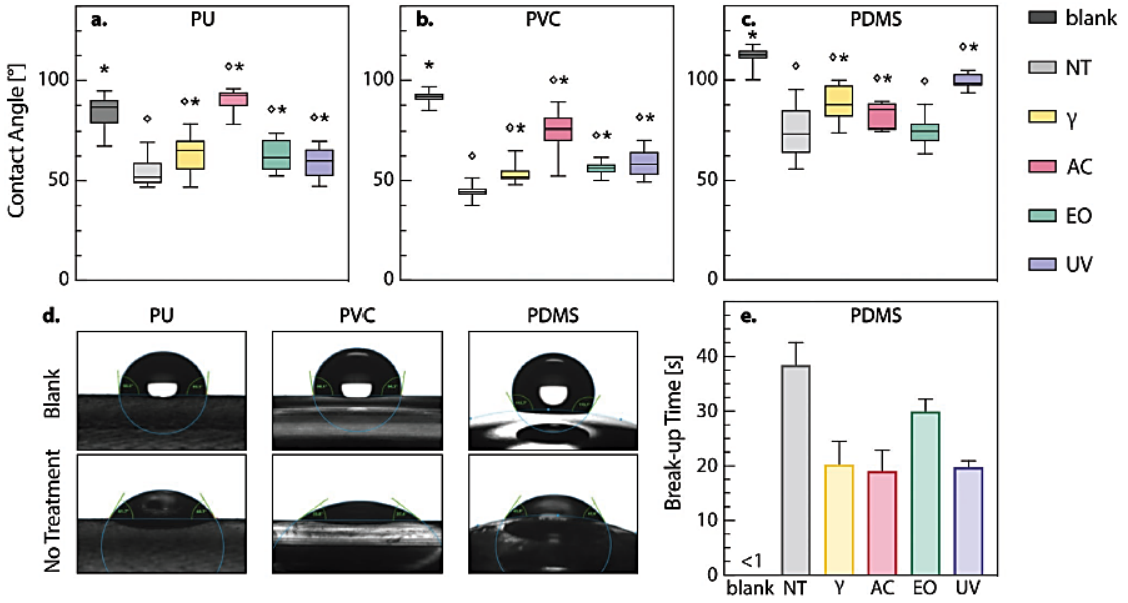

Figure 3. Wettability of sterilized mucin coatings generated on different medical devices. Contact angles ($n \geq 10$) quantify the wettability of the surfaces and are displayed for a) PU, b) PVC, and c) PDMS based medical devices. Contact angles larger than 90° denote hydrophobic behavior, whereas values smaller than 90° represent hydrophilic surfaces. Asterisks and rhombi denote statistically significant differences between a treated sample and the untreated reference or the blank sample, respectively (based on a p-value of 0.05). d) Exemplary images of the three blank device surfaces and the same set of surfaces carrying a mucin coating (that has not been subjected to any sterilization process). e) Break-up times as determined for PDMS-based contact lenses (blank, coated, or coated and sterilized). Error bars indicate the standard error of the mean as obtained from $n = 3$ samples.

ADVANCED SCIENCE NEWS
www.advancedsciencenews.com

ADVANCED MATERIALS INTERFACES
www.advmatinterfaces.de

techniques, our next goal is to test if selected functions of the coatings are compromised by the different treatments. More specifically, we first compare the wettability of the different samples (**Figure** 3a–c), which plays a key role for the antibiofouling and friction-reducing effects of mucin coatings.[9,11] A reliable quantification of the wetting behavior of a sample is provided by the static contact angle (CA) of a water droplet that is placed onto a sample surface: here, contact angles above 90° denote hydrophobic behavior, whereas contact angles smaller than 90° indicate hydrophilic surface properties. Exemplary images of droplets placed onto the different materials with and without covalent mucin coatings, respectively, are depicted in Figure 3d.

Our first observation is that, as expected, the wettability of the uncoated base materials differs. The CA values obtained for PU and PVC are located around the threshold between hydrophobic and hydrophilic behavior, whereas PDMS exhibit clear hydrophobic behavior with high contact angles around 110°. On all three materials, however, the mucin coatings decrease the contact angles by ≈40°–50°, which corresponds to an alteration of the surface properties into hydrophilic behavior. Remarkably, this strong alteration in the wetting properties is maintained for all materials after exposure to ethylene oxide; in addition, after irradiation with gamma or UV rays, coatings generated on PU or PVC still provide clearly hydrophilic properties as well. Autoclaving, in contrast, leads to a strong increase of the contact angles, and this result agrees with the findings discussed above, which illustrated that this particular sterilization method induces severe damage to the mucin macromolecules.

Even though determining CA values is a standard approach in material science, in the context of contact lenses, a more application-oriented characterization of their wetting behavior is used. Here, the liquid film BUT is determined as this measure is of high relevance for the performance of a contact lens on the cornea: maintaining a full tear film coverage on the lens without rupture between blinking is essential to ensure comfort and to protect the underlying tissue from harm. For uncoated, blank PDMS lenses (Figure 3e), we measure very small values below 1 s; in other words, the liquid film ruptures immediately after removing the sample from the liquid. Contact lenses that are covalently coated with mucins, in turn, perform way better (Figure 3e): here, the measured BUT values are in the range of ≈38 s. After sterilization with ethylene oxide, the BUT still reaches 30 s, and the corresponding values are ≈20 s for AC, γ, or UV irradiation. Thus, all those values are much larger than the average duration of a human blinking period, which is ≈5 s.[36] Also, these results support our findings obtained from the CA measurements and demonstrate that all treatments maintain the wetting improvement brought about by the mucin coating—at least to a certain extent.

In addition to improving the wettability of surfaces, another important property brought about by mucins is providing lubricity. Mucins typically achieve this via a combination of two effects: sacrificial layer formation and hydration lubrication. On hydrophobic surfaces such as PDMS, sacrificial layer formation is primarily driven by the molecule's unglycosylated termini: since they are hydrophobic, they enable transient mucin adsorption onto hydrophobic surfaces but allow the adsorbed glycoprotein to become sheared off again under tribological stress. Owing to the covalent coupling of mucins to surfaces as performed in this study focusing on coatings of medical devices, however, this particular mechanism will be suppressed. In contrast, the second mechanism, hydration lubrication, should still be fully operable: as the densely glycosylated central region of the mucin glycoprotein can bind lots of water molecules, it maintains a surface-bound lubricating liquid film even under tribological loads and thus reduces friction.

To assess the lubricating abilities of sterilized mucin coatings, we perform tribological measurements with flat PDMS samples (see methods). For blank, uncoated PDMS samples (**Figure** 4a), we obtain a typical Stribeck's curve showing low friction coefficients in the regime of hydrodynamic lubrication only (i.e., at high sliding velocities, which correspond to blinking movements of the upper eye lid[37]). After a steep transition zone (mixed lubrication regime), the boundary lubrication regime is entered, which is most relevant for sliding speeds as they are expected to occur between a contact lens and the cornea;[38] here, very high friction coefficients around 1 are

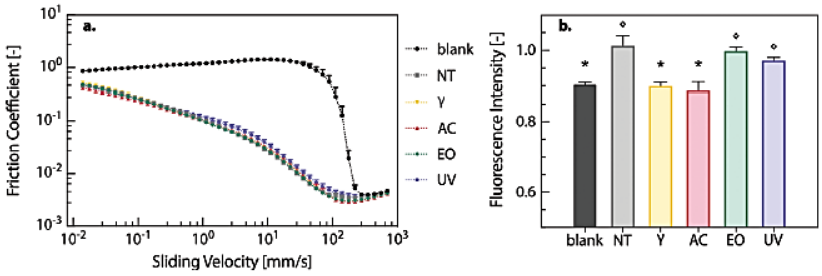

Figure 4. Tribological behavior and lipid adsorption as observed for mucin-coated PDMS samples. The Stribeck curves shown in (a) were obtained for PDMS samples that were either left uncoated (blank) or were covalently coated with mucin. The coated samples were either stored without any further treatment, or they were sterilized via γ-irradiation, autoclavation, ethylene oxide fumigation, and UV irradiation, respectively. For all tribological data, a steel-on-PDMS material pairing was used in a rotational tribology setup (see the Experimental Section). Error bars denote the standard error of the mean as obtained from $n = 4$ independent measurements per condition. The fluorescence intensities displayed in (b) were obtained in a lipid depletion assay. Higher values denote lower depletion of the lipids from the solution, hence lower adsorption of the lipids onto the sample surfaces. The error bars denote the standard error of the mean as obtained from $n \geq 4$ samples. Asterisks and rhombi denote statistically significant differences between a treated sample and the untreated reference or the blank sample, respectively (based on a p-value of 0.05).

ADVANCED SCIENCE NEWS
www.advancedsciencenews.com

ADVANCED MATERIALS INTERFACES
www.advmatinterfaces.de

obtained. For mucin-coated samples, however, we find reduced friction coefficients across almost the whole range of sliding speeds probed. Now, instead of a steep transition from low to high friction coefficients, we observe a slow, gentle increase of friction with decreasing sliding speed. Even at the slowest sliding speed probed, the coated samples still outperform the uncoated ones. Remarkably, none of the sterilization methods tested here shows a measurable influence on the lubricity of the coating. With the previous results from the ELISA test and lectin assay in mind, this can be rationalized very well: As discussed above, the predominant lubrication mechanisms provided by covalent coatings is hydration lubrication, and this mechanism relies on the glycosylated parts of the mucin glycoprotein. As the results compiled in Figure 2 showed, the glycan pattern of mucins is more resilient toward the sterilization methods tested here than the unglycosylated, hydrophobic termini of mucin. Apparently, even with minor damages to this glycosylation pattern, the sterilized mucin layer can still bind sufficient amounts of water to provide hydration lubrication.

In addition to providing lubricity, a second key function established by mucin coatings is to counteract biofouling events, i.e., to reduce the undesired adsorption of molecules or cells onto surfaces.[9,11] For the medical devices studied here, this aspect is most relevant for contact lenses, which are optical devices that need to maintain a high transparency to allow for maximal light transmission. This property, however, can be drastically compromised by the deposition of molecules—typically lipids—that are present in the physiological tear film. Indeed, covalent mucin coatings have previously been shown to strongly reduce such lipid adsorption onto contact lenses,[12] thus preserving the transparency of the optical device. Hence, in a last set of experiments, we test if this lipid-repellent effect is still present after sterilization of the mucin coatings, and we conduct a depletion assay to assess this question (see the Experimental Section).

When exposing PDMS contact lenses to a lipid-rich liquid environment, we observe a substantially higher depletion of lipids for blank, uncoated samples than for unsterilized mucin-coated contact lenses (Figure 4b). Importantly, for the latter samples, the measured fluorescence values suggest that, here, lipid adsorption onto the coated contact lens surface is negligibly low. This finding is in full agreement with previous results and demonstrates the suitability of the employed depletion assay to study lipid deposition onto surfaces. Similarly, good results as those obtained for untreated coatings are also reached with coated samples that were either subjected to ethylene oxide or UV sterilization. After γ-irradiation or autoclavation, however, the outcome of this lipid deposition test is similar to that obtained for blank, uncoated PDMS lenses. Overall, these findings are consistent with the results obtained from the structural integrity tests shown in Figure 2d–f: Owing to the hydrophobic nature of PDMS, lipid adsorption can easily occur via hydrophobic interactions acting between the fatty acid chains of the lipids and the lens surface. For an intact mucin coating, the hydrophilic central region (which represents the largest part of the macromolecule) covers the surface and prevents the adsorption of hydrophobic objects. Accordingly, those sterilization methods that maintain the glycosylation pattern of the MUC5AC glycoprotein the best (i.e., ethylene oxide exposure, and UV treatment), also preserve the lipid-resistance properties of the coating.

4. Conclusion

The results discussed in this study show that, among the sterilization methods investigated here, mucin coatings are most robust toward ethylene oxide exposure; here, the biochemical integrity of the mucins and the properties brought about by the coating were maintained the best. One major concern associated with an ethylene oxide-based sterilization process, however, is the putative retention of toxic residues in the material. To enable clinical usage of medical products that have been subjected to ethylene oxide fumigation, the amount of such toxic residues needs to be minimized, which is typically achieved by extensive aeration of the treated devices after sterilization. Yet, the efficiency of different aeration methods (such as air circulation under heat, pulsed vacuum postprocessing, or microwave desorption) and the necessary duration or intensity of such post-sterilization treatments needs to be individually studied for each medical device. Moreover, even though lab-purified mucin macromolecules were shown to be highly biocompatible,[21] assessing the biocompatibility of mucin coatings before and after sterilization should be tested following detailed ISO protocols (including endotoxin tests) so mucin-coated medical devices can enter the next stage toward medical application.

Overall, the results obtained here for sterilized medical devices carrying a mucin coating are very positive as they indicate that making use of the various beneficial properties established by such mucin coatings should be very well possible in a clinical context: The three medical devices tested here find broad usage in many medical disciplines. Moreover, they represent an even broader range of objects made from the same set of polymeric materials, which can equally profit from the hydrophilizing, anti-biofouling, or friction-reducing effects brought about by such mucin coatings.

Acknowledgements

The authors thank Matthias Marczynski for his kind assistance with the mucin purification. Furthermore, the authors thank Woehlk Contactlinsen GmbH for providing PDMS contact lenses. This research received funding from the German Federal Ministry for Economic Affairs and Energy through the Central Innovation Programme for small- and medium-sized enterprises (ZIM). Moreover, financial support from the Deutsche Forschungsgemeinschaft (DFG) through grant LI 1902/15-1 (project number 460209889) is gratefully acknowledged.

Open access funding enabled and organized by Projekt DEAL.

Conflict of Interest

The authors declare no conflict of interest.

Author Contributions

C.A.R., M.G.B., and O.L. designed the experiments. C.A.R. and J.C.H. performed the experiments and analyzed data. The manuscript was written by O.L. and C.A.R. All authors gave approval to the final version of the manuscript.

ADVANCED SCIENCE NEWS
www.advancedsciencenews.com

ADVANCED MATERIALS INTERFACES
www.advmatinterfaces.de

Data Availability Statement

The data that support the findings of this study are available from the corresponding author upon reasonable request.

Keywords

autoclavation, contact lens, endotracheal tube, ethylene oxide, gamma irradiation, urinary catheter, UV irradiation

Received: September 8, 2021
Revised: October 26, 2021
Published online:

[1] P. J. Featherstone, C. M. Ball, R. N. Westhorpe, *Anaesth. Intensive Care* **2015**, *43*, 435.
[2] Z. K. Zander, P. Chen, Y.-H. Hsu, N. Z. Dreger, L. Savariau, W. C. Mcroy, A. E. Cerchiari, S. D. Chambers, H. A. Barton, M. L. Becker, *Biomaterials* **2018**, *178*, 339.
[3] P. Poli, A. Scocca, F. Di Puccio, G. Gallone, L. Angelini, E. M. Calabrò, *J. Vasc. Access* **2016**, *17*, 175.
[4] A. Victor, J. E. Ribeiro, F. Araújo, *J. Mech. Eng. Biomech.* **2019**, *4*, 1.
[5] B. Y. Yoo, B. H. Kim, J. S. Lee, B. H.o Shin, H. Kwon, W.-G. Koh, C. Y. Heo, *Acta Biomater.* **2018**, *76*, 56.
[6] H. R. Thorarinsdottir, T. Kander, A. Holmberg, S. Petronis, B. Klarin, *Crit. Care* **2020**, *24*, 1.
[7] P. Singha, J. Locklin, H. Handa, *Acta Biomater.* **2017**, *50*, 20.
[8] H. Liu, S. Shukla, N. Vera-González, N. Tharmalingam, E. Mylonakis, B. B. Fuchs, A. Shukla, *Fron. Cell. Infect. Microbiol.* **2019**, *9*, 37.
[9] B. Winkeljann, M. G. Bauer, M. Marczynski, T. Rauh, S. A. Sieber, O. Lieleg, *Adv. Mater. Interfaces* **2020**, *7*, 1902069.
[10] J. Song, B. Winkeljann, O. Lieleg, *Adv. Mater. Interfaces* **2020**, *7*, 2000850.
[11] J. Song, T. M. Lutz, N. Lang, O. Lieleg, *Adv. Healthcare Mater.* **2021**, *10*, 2000831.
[12] C. A. Rickert, et al, *ACS Appl. Mater. Interfaces* **2020**, *12*, 28024.
[13] D. A. Dartt, *Prog. Retinal Eye Res.* **2002**, *21*, 555.
[14] S. K. Linden, P. Sutton, N. G. Karlsson, V. Korolik, M. A. Mcguckin, *Mucosal Immunol.* **2008**, *1*, 183.
[15] A. P. Corfield, *Biochim. Biophys. Acta, Gen. Subj.* **2015**, *1850*, 236.
[16] J. A. Voynow, B. K. Rubin, *Chest* **2009**, *135*, 505.
[17] D. J. Thornton, K. Rousseau, M. A. Mcguckin, *Annu. Rev. Physiol.* **2008**, *70*, 459.
[18] M. E. V. Johansson, G. C. Hansson, *Nat. Rev. Immunol.* **2016**, *16*, 639.
[19] R. Bansil, B. S. Turner, *Curr. Opin. Colloid Interface Sci.* **2006**, *11*, 164.
[20] V. J. Schömig, B. T. Käsdorf, C. Scholz, K. Bidmon, O. Lieleg, S. Berensmeier, *RSC Adv.* **2016**, *6*, 44932.
[21] O. Lieleg, C. Lieleg, J. Bloom, C. B. Buck, K. Ribbeck, *Biomacromolecules* **2012**, *13*, 1724.
[22] H. Yan, C. Seignez, M. Hjorth, B. Winkeljann, M. Blakeley, O. Lieleg, M. Phillipson, T. Crouzier, *Adv. Funct. Mater.* **2019**, *29*, 1902581.
[23] W. A. Rutala, D. J. Weber, *Am. J. Infect. Control* **2013**, *41*, S2.
[24] N. P. Tipnis, D. J. Burgess, *Int. J. Pharm.* **2018**, *544*, 455.
[25] S. Ray, R. P. Cooney, *Handbook of Environmental Degradation of Materials*, **2018**, Elsevier, Amsterdam pp. 185–206.
[26] E. V. Khoroshilova, Y. A. Repeyev, D. N. Nikogosyan, *J. Photochem. Photobiol., B* **1990**, *7*, 159.
[27] J. A. Reisz, et al, *Antioxid. Redox Signaling* **2014**, *21*, 260.
[28] K. Funatsu, H. Kiminami, Y. Abe, J. F. Carpenter, *J. Pharm. Sci.* **2019**, *108*, 770.
[29] L. Chen, C. Sloey, Z. Zhang, P. V. Bondarenko, H. Kim, D.a R. Sekhar Kanapuram, *J. Pharm. Sci.* **2015**, *104*, 731.
[30] M. Marczynski, K. Jiang, M. Blakeley, V. Srivastava, F. Vilaplana, T. Crouzier, O. Lieleg, *Biomacromolecules* **2021**, *22*, 1600.
[31] B. Winkeljann, P.-M. A. Leipold, O. Lieleg, *Adv. Mater. Interfaces* **2019**, *6*, 1900366.
[32] J. T. Gallagher, M. Harding, R. E. Dale, *Proc. of the Fifth Lectin Meet. Bern*, De Gruyter, Berlin **1982**,
[33] K. Boettcher, S. Grumbein, U. Winkler, J. Nachtsheim, O. Lieleg, *Rev. Sci. Instrum.* **2014**, *85*, 093903.
[34] M. B. Abelson, I. J. Udell, J. H. Weston, *Arch. Ophthalmol.* **1981**, *99*, 301.
[35] B. T. Käsdorf, F. Weber, G. Petrou, V. Srivastava, T. Crouzier, O. Lieleg, *Biomacromolecules* **2017**, *18*, 2454.
[36] L. G. Carney, R. M. Hill, *Acta Ophthalmol.* **1982**, *60*, 427.
[37] M. G. Doane, *Am. J. Ophthalmol.* **1980**, *89*, 507.
[38] A. C. Dunn, J. A. Tichy, J. M. Urueña, W. G. Sawyer, *Tribol. Int.* **2013**, *63*, 45.

A.3 Licenses for the Presented Publications

A.3.1 **"Multifunctional "Janus-Type" Bilayer Films Combine Broad-Range Tissue Adhesion with Guided Drug Release"**

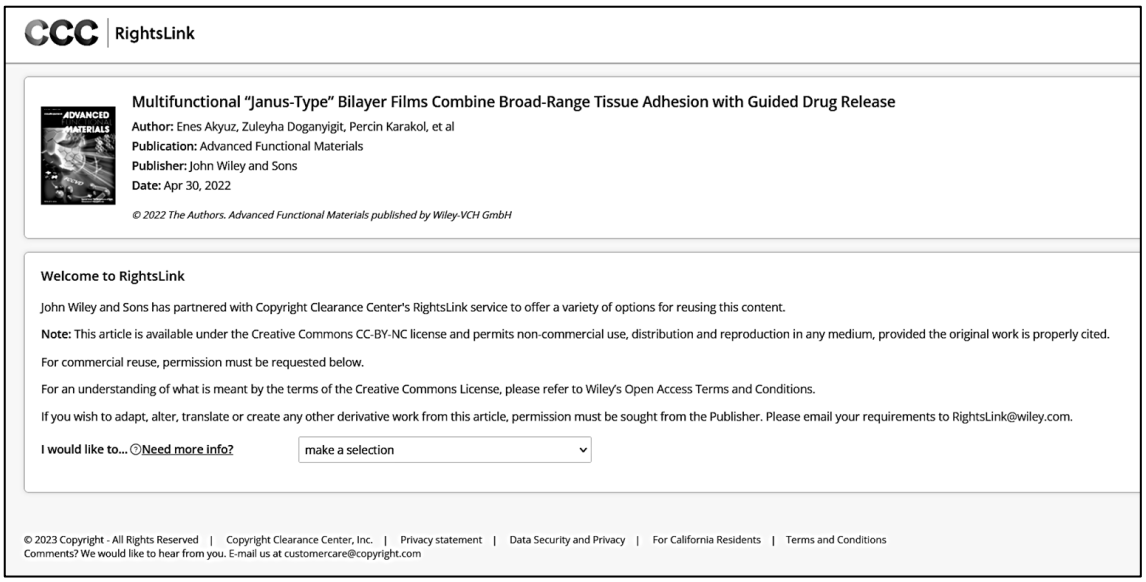

CCC | RightsLink

Multifunctional "Janus-Type" Bilayer Films Combine Broad-Range Tissue Adhesion with Guided Drug Release

Author: Enes Akyuz, Zuleyha Doganyigit, Percin Karakol, et al
Publication: Advanced Functional Materials
Publisher: John Wiley and Sons
Date: Apr 30, 2022

© 2022 The Authors. Advanced Functional Materials published by Wiley-VCH GmbH

Welcome to RightsLink

John Wiley and Sons has partnered with Copyright Clearance Center's RightsLink service to offer a variety of options for reusing this content.

Note: This article is available under the Creative Commons CC-BY-NC license and permits non-commercial use, distribution and reproduction in any medium, provided the original work is properly cited.

For commercial reuse, permission must be requested below.

For an understanding of what is meant by the terms of the Creative Commons License, please refer to Wiley's Open Access Terms and Conditions.

If you wish to adapt, alter, translate or create any other derivative work from this article, permission must be sought from the Publisher. Please email your requirements to RightsLink@wiley.com.

I would like to... Need more info? make a selection

© 2023 Copyright - All Rights Reserved | Copyright Clearance Center, Inc. | Privacy statement | Data Security and Privacy | For California Residents | Terms and Conditions
Comments? We would like to hear from you. E-mail us at customercare@copyright.com

Accessed on October 22nd, 2023

A.3.2 **"Wetting Behavior and Stability of Surface-Modified Polyurethane Materials"**

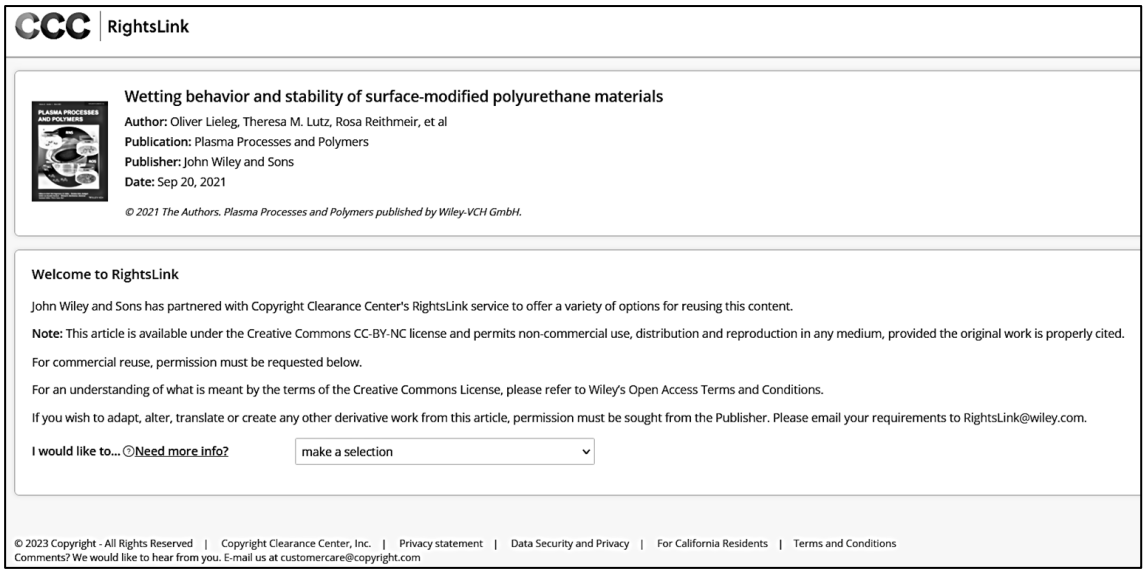

CCC | RightsLink

Wetting behavior and stability of surface-modified polyurethane materials

Author: Oliver Lieleg, Theresa M. Lutz, Rosa Reithmeir, et al
Publication: Plasma Processes and Polymers
Publisher: John Wiley and Sons
Date: Sep 20, 2021

© 2021 The Authors. Plasma Processes and Polymers published by Wiley-VCH GmbH.

Welcome to RightsLink

John Wiley and Sons has partnered with Copyright Clearance Center's RightsLink service to offer a variety of options for reusing this content.

Note: This article is available under the Creative Commons CC-BY-NC license and permits non-commercial use, distribution and reproduction in any medium, provided the original work is properly cited.

For commercial reuse, permission must be requested below.

For an understanding of what is meant by the terms of the Creative Commons License, please refer to Wiley's Open Access Terms and Conditions.

If you wish to adapt, alter, translate or create any other derivative work from this article, permission must be sought from the Publisher. Please email your requirements to RightsLink@wiley.com.

I would like to... Need more info? make a selection

© 2023 Copyright - All Rights Reserved | Copyright Clearance Center, Inc. | Privacy statement | Data Security and Privacy | For California Residents | Terms and Conditions
Comments? We would like to hear from you. E-mail us at customercare@copyright.com

Accessed on October 22nd, 2023

A.3.3 **"Bio-Macromolecular Surface Coatings for Autohesive, Transparent, Elastomeric Foils"**

CCC | RightsLink

Bio-Macromolecular Surface Coatings for Autohesive, Transparent, Elastomeric Foils

Author: Oliver Lieleg, Maria G. Bauer
Publication: Macromolecular Materials & Engineering
Publisher: John Wiley and Sons
Date: Feb 20, 2023

© 2023 The Authors. Macromolecular Materials and Engineering published by Wiley-VCH GmbH

Open Access Article

This is an open access article distributed under the terms of the Creative Commons CC BY license, which permits unrestricted use, distribution, and reproduction in any medium, provided the original work is properly cited.

You are not required to obtain permission to reuse this article.

For an understanding of what is meant by the terms of the Creative Commons License, please refer to Wiley's Open Access Terms and Conditions.

Permission is not required for this type of reuse.

Wiley offers a professional reprint service for high quality reproduction of articles from over 1400 scientific and medical journals. Wiley's reprint service offers:

- Peer reviewed research or reviews
- Tailored collections of articles
- A professional high quality finish
- Glossy journal style color covers
- Company or brand customisation
- Language translations
- Prompt turnaround times and delivery directly to your office, warehouse or congress.

Please contact our Reprints department for a quotation. Email corporatesaleseurope@wiley.com or corporatesalesusa@wiley.com or corporatesalesDE@wiley.com.

© 2023 Copyright - All Rights Reserved | Copyright Clearance Center, Inc. | Privacy statement | Data Security and Privacy | For California Residents | Terms and Conditions
Comments? We would like to hear from you. E-mail us at customercare@copyright.com

Accessed on October 22nd, 2023

A.3.4 **"Comparing the Resilience of Macromolecular Coatings on Medical-Grade Polyurethane Foils"**

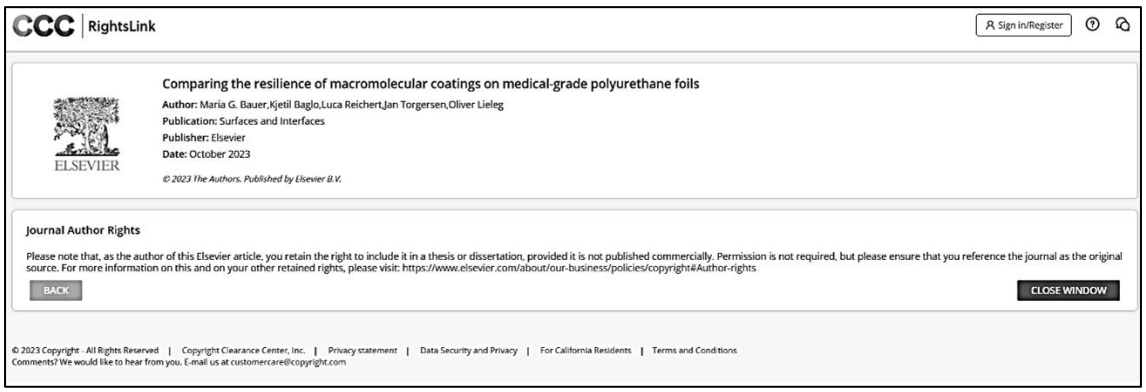

CCC | RightsLink

Sign in/Register

Comparing the resilience of macromolecular coatings on medical-grade polyurethane foils

Author: Maria G. Bauer,Kjetil Baglo,Luca Reichert,Jan Torgersen,Oliver Lieleg
Publication: Surfaces and Interfaces
Publisher: Elsevier
Date: October 2023

© 2023 The Authors. Published by Elsevier B.V.

Journal Author Rights

Please note that, as the author of this Elsevier article, you retain the right to include it in a thesis or dissertation, provided it is not published commercially. Permission is not required, but please ensure that you reference the journal as the original source. For more information on this and on your other retained rights, please visit: https://www.elsevier.com/about/our-business/policies/copyright#Author-rights

BACK CLOSE WINDOW

© 2023 Copyright - All Rights Reserved | Copyright Clearance Center, Inc. | Privacy statement | Data Security and Privacy | For California Residents | Terms and Conditions
Comments? We would like to hear from you. E-mail us at customercare@copyright.com

Accessed on October 22nd, 2023

A.3.5 "Effects of Sterilization Methods on the Integrity and Functionality of Covalent Mucin Coatings on Medical Devices"

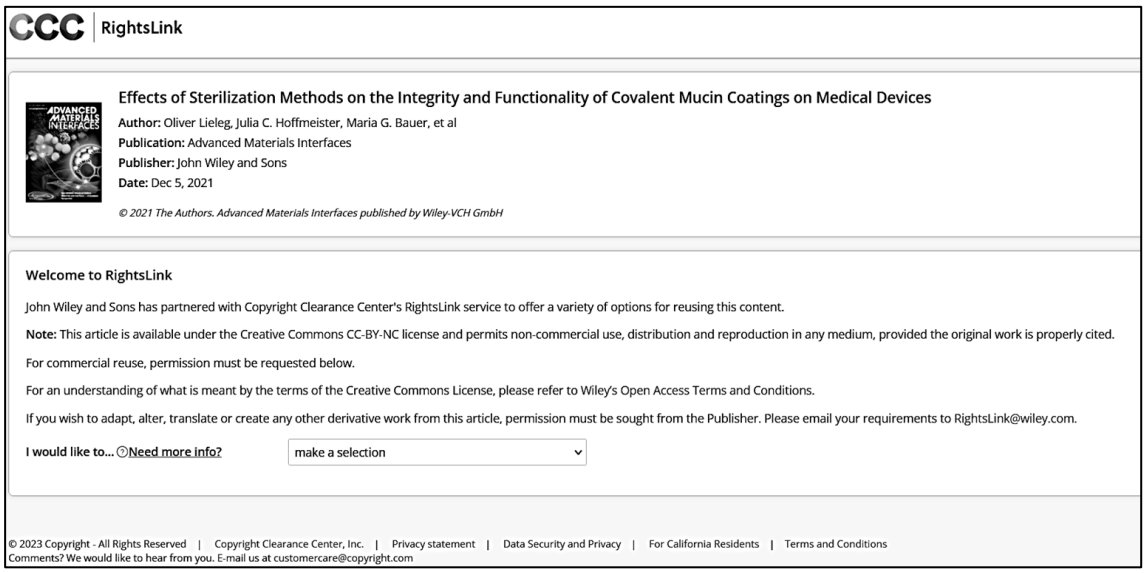

CCC | RightsLink

Effects of Sterilization Methods on the Integrity and Functionality of Covalent Mucin Coatings on Medical Devices

Author: Oliver Lieleg, Julia C. Hoffmeister, Maria G. Bauer, et al
Publication: Advanced Materials Interfaces
Publisher: John Wiley and Sons
Date: Dec 5, 2021

© 2021 The Authors. Advanced Materials Interfaces published by Wiley-VCH GmbH

Welcome to RightsLink

John Wiley and Sons has partnered with Copyright Clearance Center's RightsLink service to offer a variety of options for reusing this content.

Note: This article is available under the Creative Commons CC-BY-NC license and permits non-commercial use, distribution and reproduction in any medium, provided the original work is properly cited.

For commercial reuse, permission must be requested below.

For an understanding of what is meant by the terms of the Creative Commons License, please refer to Wiley's Open Access Terms and Conditions.

If you wish to adapt, alter, translate or create any other derivative work from this article, permission must be sought from the Publisher. Please email your requirements to RightsLink@wiley.com.

I would like to... Need more info? make a selection

© 2023 Copyright - All Rights Reserved | Copyright Clearance Center, Inc. | Privacy statement | Data Security and Privacy | For California Residents | Terms and Conditions
Comments? We would like to hear from you. E-mail us at customercare@copyright.com

Accessed on October 22nd, 2023

A.4 Full List of Publications (all peer-reviewed)

Bauer, M. G., Reithmeir, R., Lutz, T. M., Lieleg, O. (2021), 'Wetting behavior and stability of surface-modified polyurethane materials', *Plasma Processes and Polymers,* 18 (11).
Available at: https://doi.org/10.1002/ppap.202100126

Rickert, C. A., **Bauer, M. G.,** Hoffmeister, J. C., Lieleg, O., (2021), 'Effects of Sterilization Methods on the Integrity and Functionality of Covalent Mucin Coatings on Medical Devices', *Advanced Materials Interfaces*, 9 (3).
available at: https://doi.org/10.1002/admi.202101716

Kimna, C., **Bauer, M. G.,** Lutz, T. M., Mansi, S., Akyuz, E., Doganyigit, Z., Karakol, P., Mela, P., Lieleg, O., (2022), 'Multifunctional "Janus-Type" Bilayer Films Combine Broad-Range Tissue Adhesion with Guided Drug Release', *Advanced Functional Materials,* 32 (30).
Available at: https://doi.org/10.1002/adfm.202105721

Bauer, M. G., Lieleg, O. (2023), 'Bio-Macromolecular Surface Coatings for Autohesive, Transparent, Elastomeric Foils', *Macromolecular Materials and Engineering,* 308 (7).
Available at: https://doi.org/10.1002/mame.202200681

Bauer, M. G., Baglo, K., Reichert, L., Torgersen, J., Lieleg, O., (2023), 'Comparing the resilience of macromolecular coatings on medical-grade polyurethane foils', *Surfaces and Interfaces*, 41.
Available at: https://doi.org/10.1016/j.surfin.2023.103231

B References

1. A. Ram. *Fundamentals of Polymer Engineering*. Boston, MA: Springer US; 1997.
2. D. I. Bower. *An introduction to polymer physics*. Cambridge, New York: Cambridge University Press; 2002.
3. Domb A, Mizrahi B, Farah S. *Biomaterials and Biopolymers*. Cham: Springer International Publishing; 2023.
4. Rehm B, Moradali MF (eds.). *Biopolymers for Biomedical and Biotechnological Applications*: Wiley; 2021.
5. Bártolo PJ. *Bio-Materials and Prototyping Applications in Medicine*. 2nd ed. Cham: Springer International Publishing AG; 2021.
6. Yoda R. *Elastomers for biomedical applications*. *J Biomat Sci-Polym E* 1998;**9**(6):561–626, DOI: 10.1163/156856298X00046.
7. Joseph J, Patel RM, Wenham A, Smith JR. *Biomedical applications of polyurethane materials and coatings*. *Int J Surf Eng Coat* 2018;**96**(3):121–9, DOI: 10.1080/00202967.2018.1450209.
8. Miranda I, Souza A, Sousa P, Ribeiro J, Castanheira EMS, Lima R et al. *Properties and Applications of PDMS for Biomedical Engineering: A Review*. *J Funct Biomater* 2021;**13**(1):2, DOI: 10.3390/jfb13010002.
9. Zare M, Ghomi ER, Venkatraman PD, Ramakrishna S. *Silicone-based biomaterials for biomedical applications: Antimicrobial strategies and 3D printing technologies*. *J. Appl. Polym. Sci.* 2021;**138**(38), DOI: 10.1002/app.50969.
10. Joshi P, Riley PR, Denning W, Shukla S, Khosla N, Narayan J et al. *Laser-patterned carbon coatings on flexible and optically transparent plastic substrates for advanced biomedical sensing and implant applications*. *J. Mater. Chem. C* 2022;**10**(8):2965–75, DOI: 10.1039/D1TC05176H.
11. Butterworth ML, Ugrinich M. *First Metatarsophalangeal Joint Implant Options*. *Clin Podiatr Med Surg* 2019;**36**(4):577–96, DOI: 10.1016/j.cpm.2019.07.003.
12. Wintermantel E, Ha S-W. *Medizintechnik*. Berlin: Springer; 2009.
13. Martin Browne. *APRICOT: The APRICOT Factsheet*. Anatomically Precise Revolutionary Implant for bone Conserving Osteoarthritis Treatment. [October 25, 2023]; Available from: https://apricot-project.eu/.
14. Kumar S, Roy DN, Dey V. *A comprehensive review on techniques to create the anti-microbial surface of biomaterials to intervene in biofouling*. *Colloid Interf Sci Comm* 2021;**43**:100464, DOI: 10.1016/j.colcom.2021.100464.
15. Chambers LD, Stokes KR, Walsh FC, Wood R. *Modern approaches to marine antifouling coatings*. *J Surf Coat* 2006;**201**(6):3642–52, DOI: 10.1016/j.surfcoat.2006.08.129.
16. Fujimoto K, Tadokoro H, Ueda Y, Ikada Y. *Polyurethane surface modification by graft polymerization of acrylamide for reduced protein adsorption and platelet adhesion*. *Biomaterials* 1993;**14**(6):442–8, DOI: 10.1016/0142-9612(93)90147-T.
17. Awaja F. *Autohesion of polymers*. *J Polymer* 2016;**97**:387–407, DOI: 10.1016/j.polymer.2016.05.043.
18. Stacer RG, Schreuder-Stacer HL. *Time-dependent autohesion*. *Int J Fract* 1989;**39**(1-3):201–16, DOI: 10.1007/BF00047450.
19. Packham DE. Theories of Fundamental Adhesion. In: L. F. M. da Silva, A. Oechsner, R. Adams. *Handbook of Adhesion Technology*. Cham: Springer; 2019, p 1–31.
20. Pizzi A, Mittal, Kashmiri, L. (eds.). *Handbook of adhesive technology*. 2nd ed. New York, Basel: Marcel Dekker Inc; 2003.
21. Irwin NJ, Bryant MG, McCoy CP, Trotter JL, Turner J. *Multifunctional, Low Friction, Antimicrobial Approach for Biomaterial Surface Enhancement*. *ACS Appl Bio Mater* 2020;**3**(3):1385–93, DOI: 10.1021/acsabm.9b01042.
22. Song J, Winkeljann B, Lieleg O. *Biopolymer-Based Coatings: Promising Strategies to Improve the Biocompatibility and Functionality of Materials Used in Biomedical Engineering*. *Adv Mater Inter* 2020;**7**(17), DOI: 10.1002/admi.202000850.
23. Lanigan JL, Fatima S, Charpentier TV, Neville A, Dowson D, Bryant M. *Lubricious ionic polymer brush functionalised silicone elastomer surfaces*. *J Biotri* 2018;**16**:1–9, DOI: 10.1016/j.biotri.2018.08.001.
24. Poncin-Epaillard F, Legeay G. *Surface engineering of biomaterials with plasma techniques*. *J Biomater Sci Polym Ed* 2003;**14**(10):1005–28, DOI: 10.1163/156856203769231538.
25. Rashidi H, Yang J, Shakesheff KM. *Surface engineering of synthetic polymer materials for tissue engineering and regenerative medicine applications*. *Biomater. Sci.* 2014;**2**(10):1318–31, DOI: 10.1039/C3BM60330J.
26. Peacock AJ. *Polymer chemistry: Properties and applications*. Munich: Carl Hanser Verlag; 2006.
27. Boinovich LB, Emelyanenko AM. *Hydrophobic materials and coatings: principles of design, properties and applications*. *Russ. Chem. Rev.* 2008;**77**(7):583–600, DOI: 10.1070/RC2008v077n07ABEH003775.
28. Jokinen V, Suvanto P, Franssila S. *Oxygen and nitrogen plasma hydrophilization and hydrophobic recovery of polymers*. *Biomicrofluidics* 2012;**6**(1):16501–1650110, DOI: 10.1063/1.3673251.
29. Pearce AK, O'Reilly RK. *Polymers for Biomedical Applications: The Importance of Hydrophobicity in Directing Biological Interactions and Application Efficacy*. *Biomacromolecules* 2021;**22**(11):4459–69, DOI: 10.1021/acs.biomac.1c00434.
30. Marczynski M, Winkeljann B, Lieleg O. Advances in Mucin Biopolymer Research: Purification, Characterization, and Applications. In: Rehm B, Moradali MF. *Biopolymers for Biomedical and Biotechnological Applications*: Wiley; 2021, p 181–208.
31. Bansil R, Turner BS. *Mucin structure, aggregation, physiological functions and biomedical applications*. *Curr Opin Colloid In* 2006;**11**(2-3):164–70, DOI: 10.1016/j.cocis.2005.11.001.
32. Voynow JA, Rubin BK. *Mucins, mucus, and sputum*. *Chest* 2009;**135**(2):505–12, DOI: 10.1378/chest.08-0412.
33. Kronberg B. *The hydrophobic effect*. *Curr Opin Colloid In* 2016;**22**:14–22, DOI: 10.1016/j.cocis.2016.02.001.
34. Kyte J. *The basis of the hydrophobic effect*. *Biophys Chem* 2003;**100**(1-3):193–203, DOI: 10.1016/S0301-4622(02)00281-8.
35. Pratt LR. *Theory of Hydrophobic Effects*. *Annu. Rev. Phys. Chem.* 1985;**36**(1):433–49, DOI: 10.1146/annurev.pc.36.100185.002245.

36. Marczynski M, Balzer BN, Jiang K, Lutz TM, Crouzier T, Lieleg O. *Charged glycan residues critically contribute to the adsorption and lubricity of mucins*. *Colloids Surf B Biointerfaces* 2020;**187**:110614, DOI: 10.1016/j.colsurfb.2019.110614.
37. Winkeljann B, Boettcher K, Balzer BN, Lieleg O. *Mucin Coatings Prevent Tissue Damage at the Cornea–Contact Lens Interface*. *Adv Mater Inter* 2017;**4**(19), DOI: 10.1002/admi.201700186.
38. Co JY, Crouzier T, Ribbeck K. *Probing the Role of Mucin-Bound Glycans in Bacterial Repulsion by Mucin Coatings*. *Adv Mater Inter* 2015;**2**(17), DOI: 10.1002/admi.201500179.
39. Shi L, Ardehali R, Caldwell KD, Valint P. *Mucin coating on polymeric material surfaces to suppress bacterial adhesion*. *Colloids Surf B Biointerfaces* 2000;**17**(4):229–39, DOI: 10.1016/S0927-7765(99)00121-6.
40. Coles JM, Chang DP, Zauscher S. *Molecular mechanisms of aqueous boundary lubrication by mucinous glycoproteins*. *Curr Opin Colloid In* 2010;**15**(6):406–16, DOI: 10.1016/j.cocis.2010.07.002.
41. Käsdorf BT, Weber F, Petrou G, Srivastava V, Crouzier T, Lieleg O. *Mucin-Inspired Lubrication on Hydrophobic Surfaces*. *Biomacromolecules* 2017;**18**(8):2454–62, DOI: 10.1021/acs.biomac.7b00605.
42. Jung B, Theato P. Chemical Strategies for the Synthesis of Protein–Polymer Conjugates. In: Schlaad H. *Bio-synthetic Polymer Conjugates*. Berlin, Heidelberg: Springer Berlin Heidelberg; 2013, p 37–70.
43. Vandermeulen GWM, Klok H-A. *Peptide/protein hybrid materials: enhanced control of structure and improved performance through conjugation of biological and synthetic polymers*. *Macromol Biosci* 2004;**4**(4):383–98, DOI: 10.1002/mabi.200300079.
44. Hermanson GT. *Bioconjugate techniques*. Amsterdam: Academic Press; 2013.
45. Park H-J, Jin Y, Shin J, Yang K, Lee C, Yang HS et al. *Catechol-Functionalized Hyaluronic Acid Hydrogels Enhance Angiogenesis and Osteogenesis of Human Adipose-Derived Stem Cells in Critical Tissue Defects*. *Biomacromolecules* 2016;**17**(6):1939–48, DOI: 10.1021/acs.biomac.5b01670.
46. Han L, Lu X, Liu K, Wang K, Fang L, Weng L-T et al. *Mussel-Inspired Adhesive and Tough Hydrogel Based on Nanoclay Confined Dopamine Polymerization*. *ACS Nano* 2017;**11**(3):2561–74, DOI: 10.1021/acsnano.6b05318.
47. Lee H, Dellatore SM, Miller WM, Messersmith PB. *Mussel-inspired surface chemistry for multifunctional coatings*. *Science* 2007;**318**(5849):426–30, DOI: 10.1126/science.1147241.
48. Lee H, Rho J, Messersmith PB. *Facile Conjugation of Biomolecules onto Surfaces via Mussel Adhesive Protein Inspired Coatings*. *Adv Mater* 2009;**21**(4):431–4, DOI: 10.1002/adma.200801222.
49. Ding YH, Floren M, Tan W. *Mussel-inspired polydopamine for bio-surface functionalization*. *Biosurf Biotribol* 2016;**2**(4):121–36, DOI: 10.1016/j.bsbt.2016.11.001.
50. Lee HA, Park E, Lee H. *Polydopamine and Its Derivative Surface Chemistry in Material Science: A Focused Review for Studies at KAIST*. *Adv Mater* 2020;**32**(35):e1907505, DOI: 10.1002/adma.201907505.
51. Du X, Li L, Li J, Yang C, Frenkel N, Welle A et al. *UV-triggered dopamine polymerization: control of polymerization, surface coating, and photopatterning*. *Adv Mater* 2014;**26**(47):8029–33, DOI: 10.1002/adma.201403709.
52. Hong S, Na YS, Choi S, Song IT, Kim WY, Lee H. *Non-Covalent Self-Assembly and Covalent Polymerization Co-Contribute to Polydopamine Formation*. *Adv Funct Mater* 2012;**22**(22):4711–7, DOI: 10.1002/adfm.201201156.
53. Jiang J, Zhu L, Zhu L, Zhu B, Xu Y. *Surface characteristics of a self-polymerized dopamine coating deposited on hydrophobic polymer films*. *Langmuir* 2011;**27**(23):14180–7, DOI: 10.1021/la202877k.
54. Zhou D, Li S, Pei M, Yang H, Gu S, Tao Y et al. *Dopamine-Modified Hyaluronic Acid Hydrogel Adhesives with Fast-Forming and High Tissue Adhesion*. *ACS Appl Mater Interfaces* 2020;**12**(16):18225–34, DOI: 10.1021/acsami.9b22120.
55. Winkeljann B, Bauer MG, Marczynski M, Rauh T, Sieber SA, Lieleg O. *Covalent Mucin Coatings Form Stable Anti-Biofouling Layers on a Broad Range of Medical Polymer Materials*. *Adv Mater Interfaces* 2020;**7**(4), DOI: 10.1002/admi.201902069.
56. Li H, Jiang B, Li J. *Recent advances in dopamine-based materials constructed via one-pot co-assembly strategy*. *Adv Colloid Interface Sci* 2021;**295**:102489, DOI: 10.1016/j.cis.2021.102489.
57. M. R. Dewar, G. J. Parfitt. *An investigation of the physical properties of saliva and their relationship to the mucin content*. *J Dent Res* 1954;**33**(5):596–605, DOI: 10.1177/00220345540330050301.
58. K. Nisizawa WP. *The composition and properties of the mucin clot from cattle submaxillary glands*. *Arch Oral Biol* 1959;**1**:161–70, DOI: 10.1016/0003-9969(59)90008-1.
59. Y. Hashimoto, S. Hashimoto, W. Pigman. *Purification and properties of porcine submaxillary mucin*. *Arch Biochm Biophys* 1964;**104**:282–91, DOI: 10.1016/S0003-9861(64)80015-1.
60. Sweeney MP, Bagg J, Baxter WP, Aitchison TC. *Clinical trial of a mucin-containing oral spray for treatment of xerostomia in hospice patients*. *Palliat Med* 1997;**11**(3):225–32, DOI: 10.1177/026921639701100307.
61. Kuduk SD, Schwarz JB, Chen X-T, Glunz PW, Sames D, Ragupathi G et al. *Synthetic and Immunological Studies on Clustered Modes of Mucin-Related Tn and TF O-Linked Antigens: The Preparation of a Glycopeptide-Based Vaccine for Clinical Trials against Prostate Cancer*. *J. Am. Chem. Soc.* 1998;**120**(48):12474–85, DOI: 10.1021/ja9825128.
62. Pecher G, Häring A, Kaiser L, Thiel E. *Mucin gene (MUC1) transfected dendritic cells as vaccine: results of a phase I/II clinical trial*. *Cancer Immunol Immunother* 2002;**51**(11-12):669–73, DOI: 10.1007/s00262-002-0317-z.
63. Rivalland G, Loveland B, Mitchell P. *Update on Mucin-1 immunotherapy in cancer: a clinical perspective*. *Expert Opin Biol Ther* 2015;**15**(12):1773–87, DOI: 10.1517/14712598.2015.1088519.
64. Schömig VJ, Käsdorf BT, Scholz C, Bidmon K, Lieleg O, Berensmeier S. *An optimized purification process for porcine gastric mucin with preservation of its native functional properties*. *RSC Adv* 2016;**6**(50):44932–43, DOI: 10.1039/C6RA07424C.
65. Marczynski M, Rickert CA, Fuhrmann T, Lieleg O. *An improved, filtration-based process to purify functional mucins from mucosal tissues with high yields*. *Sep Purif Technol* 2022;**294**:121209, DOI: 10.1016/j.seppur.2022.121209.
66. Marczynski M, Jiang K, Blakeley M, Srivastava V, Vilaplana F, Crouzier T et al. *Structural Alterations of Mucins Are Associated with Losses in Functionality*. *Biomacromolecules* 2021;**22**(4):1600–13, DOI: 10.1021/acs.biomac.1c00073.
67. Kwan C-S, Cerullo AR, Braunschweig AB. *Design and Synthesis of Mucin-Inspired Glycopolymers*. *ChemPlusChem* 2020;**85**(12):2704–21, DOI: 10.1002/cplu.202000637.

68. Marcaurelle LA. *Recent advances in the chemicalsynthesis of mucin-like glycoproteins*. *Glycobiology* 2002;**12**(6):69R-77, DOI: 10.1093/glycob/12.6.69R.
69. W. B. Neely. *Dextran: structure and synthesis*. *Adv Carbohyd Chem* 1960;**15**:341–69, DOI: 10.1016/S0096-5332(08)60191-5.
70. Heinze T, Liebert T, Heublein B, Hornig S. Functional Polymers Based on Dextran. In: Klemm D, Heinze T. *Polysaccharides*. Berlin: Springer; 2006, p 199–291.
71. Sidebotham RL. *Dextrans*. *Adv Carbohydr Chem Biochem* 1974;**30**:371–444, DOI: 10.1016/S0065-2318(08)60268-1.
72. M. Atik. *The uses of dextran in surgery: A current evaluation*. *Surgery* 1969(65):548–62, DOI: 10.5555/uri:pii:0039606069901251.
73. Luanda A, Badalamoole V. *Past, present and future of biomedical applications of dextran-based hydrogels: A review*. *Int J Biol Macromol* 2023;**228**:794–807, DOI: 10.1016/j.ijbiomac.2022.12.129.
74. Hu Q, Lu Y, Luo Y. *Recent advances in dextran-based drug delivery systems: From fabrication strategies to applications*. *Carbohydr Polym* 2021;**264**:117999, DOI: 10.1016/j.carbpol.2021.117999.
75. Winkeljann B, Leipold P-MA, Lieleg O. *Macromolecular Coatings Enhance the Tribological Performance of Polymer-Based Lubricants*. *Adv Mater Inter* 2019;**6**(16), DOI: 10.1002/admi.201900366.
76. Kimna C, Bauer MG, Lutz TM, Mansi S, Akyuz E, Doganyigit Z et al. *Multifunctional "Janus-Type" Bilayer Films Combine Broad-Range Tissue Adhesion with Guided Drug Release*. *Adv Funct Mater* 2022;**32**(30), DOI: 10.1002/adfm.202105721.
77. Bauer MG, Reithmeir R, Lutz TM, Lieleg O. *Wetting behavior and stability of surface-modified polyurethane materials*. *Plasma Process Polym* 2021;**18**(11), DOI: 10.1002/ppap.202100126.
78. Bauer MG, Lieleg O. *Bio-Macromolecular Surface Coatings for Autohesive, Transparent, Elastomeric Foils*. *Macro Mater Eng* 2023;**308**(7), DOI: 10.1002/mame.202200681.
79. Bauer MG, Baglo K, Reichert L, Torgersen J, Lieleg O. *Comparing the resilience of macromolecular coatings on medical-grade polyurethane foils*. *J Surf Interf* 2023;**41**:103231, DOI: 10.1016/j.surfin.2023.103231.
80. Rickert CA, Bauer MG, Hoffmeister JC, Lieleg O. *Effects of Sterilization Methods on the Integrity and Functionality of Covalent Mucin Coatings on Medical Devices*. *Adv Mater Inter* 2021;**9**(3), DOI: 10.1002/admi.202101716.
81. Das A, Mahanwar P. *A brief discussion on advances in polyurethane applications*. *Adv Ind Eng Polym Res* 2020;**3**(3):93–101, DOI: 10.1016/j.aiepr.2020.07.002.
82. Akindoyo JO, Beg MDH, Ghazali S, Islam MR, Jeyaratnam N, Yuvaraj AR. *Polyurethane types, synthesis and applications – a review*. *RSC Adv* 2016;**6**(115):114453–82, DOI: 10.1039/C6RA14525F.
83. Davis FJ, Mitchell GR. Polyurethane Based Materials with Applications in Medical Devices. In: Bártolo P, Bidanda B, Bártolo P. *Bio-materials and prototyping applications in medicine*. New York, NY: Springer; 2008, p 27–48.
84. Lubrizol Life Science. *Aromatic Carbothane AC Series TPU: technical data sheet*. document no.: 20-244218. [October 29, 2023]; Available from: https://www.lubrizol.com/Health/Medical/Polymers/Carbothane-TPU.
85. Victor A, Ribeiro J, F. Araújo F. *Study of PDMS characterization and its applications in biomedicine: A review*. *JMEB* 2019;**4**(1):1–9, DOI: 10.24243/JMEB/4.1.163.
86. Volkov A. Polydimethylsiloxane (PDMS). In: Drioli E, Giorno L. *Encyclopedia of Membranes*. Berlin, Heidelberg: Springer; 2019, p 1–2.
87. Crouzier T, Boettcher K, Geonnotti AR, Kavanaugh NL, Hirsch JB, Ribbeck K et al. *Modulating Mucin Hydration and Lubrication by Deglycosylation and Polyethylene Glycol Binding*. *Adv Mater Inter* 2015;**2**(18), DOI: 10.1002/admi.201500308.
88. Song J, Lutz TM, Lang N, Lieleg O. *Bioinspired Dopamine/Mucin Coatings Provide Lubricity, Wear Protection, and Cell-Repellent Properties for Medical Applications*. *Adv Healthc Mater* 2021;**10**(4):e2000831, DOI: 10.1002/adhm.202000831.
89. Naessens M, an Cerdobbel, Soetaert W, Vandamme EJ. *Leuconostoc dextransucrase and dextran: production, properties and applications*. *J Chem Tech Biotech* 2005;**80**(8):845–60, DOI: 10.1002/jctb.1322.
90. Yalpani M, Hedman PO. *Preparation and Applications of Dextran-Derived Products in Biotechnology and Related Areas*. *Crit Rev Biotechnol* 1985;**3**(4):375–421, DOI: 10.3109/07388558509150789.
91. TdB Labs AB. *lysine-dextran: datafile*. document no: LD010. [29.10.23]; Available from: https://tdblabs.se/products/other-derivatives-and-polysaccharides/lysine-dextran/.
92. TdB Labs AB. *Q-dextran: datafile*. document no.: QD010. [29.10.23]; Available from: https://tdblabs.se/products/other-derivatives-and-polysaccharides/q-dextran/.
93. TdB Labs AB. *CM-dextran: datafile*. document no.: CMD010. [29.10.23]; Available from: https://tdblabs.se/products/other-derivatives-and-polysaccharides/cm-dextran/.
94. Burdick JA, Prestwich GD. *Hyaluronic acid hydrogels for biomedical applications*. *Adv Mater* 2011;**23**(12):H41-56, DOI: 10.1002/adma.201003963.
95. Neuman MG, Nanau RM, Oruña-Sanchez L, Coto G. *Hyaluronic acid and wound healing*. *J Pharm Pharm Sci* 2015;**18**(1):53–60, DOI: 10.18433/J3K89D.
96. Zhang Z, Christopher GF. *The nonlinear viscoelasticity of hyaluronic acid and its role in joint lubrication*. *Soft Matter* 2015;**11**(13):2596–603, DOI: 10.1039/C5SM00131E.
97. A. Maroudas. *Hyaluronic acid films: lubrication and wear in living and artificial human joints*. *Proc Inst Mech Eng* 1967;**181**:122, DOI: 10.1243/PIME_CONF_1966_181_214_02.
98. Tadmor R, Chen N, Israelachvili JN. *Thin film rheology and lubricity of hyaluronic acid solutions at a normal physiological concentration*. *J. Biomed. Mater. Res.* 2002;**61**(4):514–23, DOI: 10.1002/jbm.10215.
99. Nyman E, Henricson J, Ghafouri B, Anderson CD, Kratz G. *Hyaluronic Acid Accelerates Re-epithelialization and Alters Protein Expression in a Human Wound Model*. *Plast Reconstr Surg* 2019;**7**(5):e2221, DOI: 10.1097/GOX.0000000000002221.
100. Khunmanee S, Jeong Y, Park H. *Crosslinking method of hyaluronic-based hydrogel for biomedical applications*. *J Tissue Eng* 2017;**8**:2041731417726464, DOI: 10.1177/2041731417726464.

101.Klein J. *Polymers in living systems: from biological lubrication to tissue engineering and biomedical devices*. *Polym Adv Technol* 2012;**23**(4):729–35, DOI: 10.1002/pat.3038.
102.Tabares FL, Junkar I. *Cold Plasma Systems and their Application in Surface Treatments for Medicine*. *Molecules* 2021;**26**(7):1903, DOI: 10.3390/molecules26071903.
103.Bazaka K, Jacob MV, Crawford RJ, Ivanova EP. *Plasma-assisted surface modification of organic biopolymers to prevent bacterial attachment*. *Acta biomater* 2011;**7**(5):2015–28, DOI: 10.1016/j.actbio.2010.12.024.
104.Yang J, Cohen Stuart MA, Kamperman M. *Jack of all trades: versatile catechol crosslinking mechanisms*. *Chem Soc Rev* 2014;**43**(24):8271–98, DOI: 10.1039/C4CS00185K.
105.Kord Forooshani P, Lee BP. *Recent approaches in designing bioadhesive materials inspired by mussel adhesive protein*. *J Polym Sci Part A Polym Chem* 2017;**55**(1):9–33, DOI: 10.1002/pola.28368.
106.Ryu JH, Messersmith PB, Lee H. *Polydopamine Surface Chemistry: A Decade of Discovery*. *ACS Appl Mater Interfaces* 2018;**10**(9):7523–40, DOI: 10.1021/acsami.7b19865.
107.Qie R, Zajforoushan Moghaddam S, Thormann E. *Dopamine-Assisted Layer-by-Layer Deposition Providing Coatings with Controlled Thickness, Roughness, and Functional Properties*. *ACS omega* 2023;**8**(3):2965–72, DOI: 10.1021/acsomega.2c05620.
108.Hemmatpour H, Luca O de, Crestani D, Stuart MCA, Lasorsa A, van der Wel PCA et al. *New insights in polydopamine formation via surface adsorption*. *Nat Commun* 2023;**14**(1):664, DOI: 10.1038/s41467-023-36303-8.
109.Lynge ME, Schattling P, Städler B. *Recent developments in poly(dopamine)-based coatings for biomedical applications*. *Nanomedicine* 2015;**10**(17):2725–42, DOI: 10.2217/nnm.15.89.
110.Boettcher K, Grumbein S, Winkler U, Nachtsheim J, Lieleg O. *Adapting a commercial shear rheometer for applications in cartilage research*. *The Review of scientific instruments* 2014;**85**(9):93903, DOI: 10.1063/1.4894820.
111.Hertz H. *Ueber die Berührung fester elastischer Körper*. *crll* 1882;**1882**(92):156–71, DOI: 10.1515/crll.1882.92.156.
112.Winkeljann B, Bussmann AB, Bauer MG, Lieleg O. *Oscillatory Tribology Performed With a Commercial Shear Rheometer*. *Biotribology* 2018;**14**:11–8, DOI: 10.1016/j.biotri.2018.04.002.
113.C Isenberg. *The science of soap films and soap bubbles: Isenberg C (1992) The science of soap films and soap bubbles. Dover, New York*; 1992.
114.Pellicer J, Manzanares JA, Mafé S. *The physical description of elementary surface phenomena: Thermodynamics versus mechanics*. *Am J Phys* 1995;**63**(6):542–7, DOI: 10.1119/1.17866.
115.Hunter RJ. *Foundations of colloid science, 2nd edn. Oxford Univ Press, Oxford*; 2001.
116.Brown RC. *The fundamental concepts concerning surface tension and capillarity*. *Proc. Phys. Soc.* 1947;**59**(3):429–48, DOI: 10.1088/0959-5309/59/3/310.
117.Berry MV. *The molecular mechanism of surface tension*. *Phys. Educ.* 1971;**6**(2):79–84, DOI: 10.1088/0031-9120/6/2/001.
118.Temperley HNV, Trevena DH. *Liquids and their properties: A molecular and macroscopic treatise with applications*. Chichester: Ellis Horwood Limited; 1978.
119.Sophocleous M. *Understanding and explaining surface tension and capillarity: an introduction to fundamental physics for water professionals*. *Hydrogeol J* 2010;**18**(4):811–21, DOI: 10.1007/s10040-009-0565-5.
120.Shanahan MER, Possart W. Wetting of Solids. In: L. F. M. da Silva, A. Oechsner, R. Adams. *Handbook of Adhesion Technology*. Cham: Springer; 2019, p 1–31.
121.Young T. *III. An essay on the cohesion of fluids*. *Phil. Trans. R. Soc.* 1805;**95**:65–87, DOI: 10.1098/rstl.1805.0005.
122.Gilboa A, Bachmann J, Woche SK, Chen Y. *Applicability of Interfacial Theories of Surface Tension to Water-Repellent Soils*. *Soil Sci Soc Am J* 2006;**70**(5):1417–29, DOI: 10.2136/sssaj2005.0033.
123.Kwok DY, Neumann AW. *Contact angle measurement and contact angle interpretation*. *Adv Colloid Interf Sci* 1999;**81**(3):167–249, DOI: 10.1016/S0001-8686(98)00087-6.
124.Orowan E. *Surface energy and surface tension in solids and liquids*. *Proc. R. Soc. Lond. A* 1970;**316**(1527):473–91, DOI: 10.1098/rspa.1970.0091.
125.S. Ebnesajjad (ed.). *Adhesives Technology Handbook*. 2nd ed.: William Andrew Publishing Inc; 2009.
126.Introduction and Adhesion Theories. In: S. Ebnesajjad. *Adhesives Technology Handbook*, 2nd ed.: William Andrew Publishing Inc; 2009, p 1–19.
127.Gennes PG de. The Dynamics of Wetting. In: Lee L-H. *Fundamentals of Adhesion*. Boston, MA: Springer US; 1991, p 173–179.
128.Bruyne NA de. *The adhesive properties of epoxy resins*. *J. Appl. Chem.* 1956;**6**(7):303–10, DOI: 10.1002/jctb.5010060708.
129.Lee L-H. The Chemistry and Physics of Solid Adhesion. In: Lee L-H. *Fundamentals of Adhesion*. Boston, MA: Springer US; 1991, p 1–86.
130.Gennes P-G de. *Simple Views on Condensed Matter*: Sci World; 1998.
131.M Doi. *The theory of polymer dynamics: Doi M, Edwards SF (1986) The theory of polymer dynamics. Clarendon, Oxford*; 1986.
132.Brochard-Wyart F. Kinetics of Polymer—Polymer Interdiffusion. In: Lee L-H. *Fundamentals of Adhesion*. Boston, MA: Springer US; 1991, p 181–206.
133.Schultz J, Lavielle L, Carre A, Comien P. *Surface properties and adhesion mechanisms of graft polypropylenes*. *J Mater Sci* 1989;**24**(12):4363–9, DOI: 10.1007/BF00544513.
134.JJ Bikerman. *Physical surfaces: Bikerman JJ (1970) Physical surfaces. Academic, New York*; 1970.
135.JJ Bikerman, Or D, Tuller M. *The science of adhesive joints: Bikerman JJ (1961) The science of adhesive joints. Academic, London*: Elsevier; 2005.
136.Andelman D, Joanny J-F. *Polyelectrolyte adsorption*. *C R Acad IV Physics* 2000;**1**(9):1153–62, DOI: 10.1016/S1296-2147(00)01130-6.
137.Hill RL. *Hydrolysis of proteins*. *Adv Protein Chem* 1965;**20**:37–107, DOI: 10.1016/S0065-3233(08)60388-5.
138.Bjerrum J. *On the tendency of the metal ions toward complex formation*. *Chem Rev* 1950;**46**(2):381–401, DOI: 10.1021/cr60144a004.

139.Rocha F, Paula Rezende J de, Maciel Dos Santos Dias M, Rodrigues Arruda Pinto V, César Stringheta P, Clarissa Dos Santos Pires A et al. *Complexation of anthocyanins, betalains and carotenoids with biopolymers: An approach to complexation techniques and evaluation of binding parameters*. *Food Res Int* 2023;**163**:112277, DOI: 10.1016/j.foodres.2022.112277.
140.Kretschmer M, Lieleg O. *Chelate chemistry governs ion-specific stiffening of Bacillus subtilis B-1 and Azotobacter vinelandii biofilms*. *Biomater Sci* 2020;**8**(7):1923–33, DOI: 10.1039/C9BM01763A.
141.Bhushan B. *Introduction to Tribology*: Wiley; 2013.
142.Meng Y, Xu J, Jin Z, Prakash B, Hu Y. *A review of recent advances in tribology*. *Friction* 2020;**8**(2):221–300, DOI: 10.1007/s40544-020-0367-2.
143.Urbakh M, Klafter J, Gourdon D, Israelachvili J. *The nonlinear nature of friction*. *Nature* 2004;**430**(6999):525–8, DOI: 10.1038/nature02750.
144.Blau PJ. *The significance and use of the friction coefficient*. *Tribol Int* 2001;**34**(9):585–91, DOI: 10.1016/S0301-679X(01)00050-0.
145.Popova E, Popov VL. *The research works of Coulomb and Amontons and generalized laws of friction*. *Friction* 2015;**3**(2):183–90, DOI: 10.1007/s40544-015-0074-6.
146.Rickert CA, Wittmann B, Fromme R, Lieleg O. *Highly Transparent Covalent Mucin Coatings Improve the Wettability and Tribology of Hydrophobic Contact Lenses*. *ACS Appl Mater Interfaces* 2020;**12**(25):28024–33, DOI: 10.1021/acsami.0c06847.
147.Budynas RG. *Shigley's mechanical engineering design*. 9th ed. New York: McGraw-Hill; 2011.
148.Hersey MD. *The laws of lubrication of horizontal journal bearings*. *J Wash Acad Sci*:542–52; Available from: https://www.jstor.org/stable/24520857. [November 07, 2023].
149.Stribeck R. *Kugellager für beliebige Belastungen [Ball Bearings for Any Stress]*. *Zeitschrift des Vereins Deutscher Ingenieure*.
150.Stribeck R. *Die wesentlichen Eigenschaften der Gleit- und Rollenlager*: Springer Berlin Heidelberg; 1903.
151.Zhang J, Meng Y. *Boundary lubrication by adsorption film*. *Friction* 2015;**3**(2):115–47, DOI: 10.1007/s40544-015-0084-4.
152.Spikes HA. Boundary Lubrication and Boundary Films. In: D. Dowson, C. M. Taylor, T. H. C. Childs, M. Godet, G. Dalmaz. *Thin Films in Tribology*: Elsevier; 1993, p 331–346.
153.Spikes HA. *Mixed lubrication — an overview*. *Lubr Sci (Lubrication Science)* 1997;**9**(3):221–53, DOI: 10.1002/ls.3010090302.
154.Zakharov SM. *Hydrodynamic lubrication research: Current situation and future prospects*. *J Frict Wear (Journal of Friction and Wear)* 2010;**31**(1):56–67, DOI: 10.3103/S106836661001006X.
155.Etsion I. *Modeling of surface texturing in hydrodynamic lubrication*. *Friction* 2013;**1**(3):195–209, DOI: 10.1007/s40544-013-0018-y.
156.Zhang Z-M, Wang X-J, Sun M-L. *Turbulence models of hydrodynamic lubrication*. *J. of Shanghai Univ.* 2003;**7**(4):305–14, DOI: 10.1007/s11741-003-0001-3.
157.Siddaiah A, Menezes PL. *Advances in Bio-inspired Tribology for Engineering Applications*. *J Bio Tribo Corros* 2016;**2**(4), DOI: 10.1007/s40735-016-0053-0.
158.Gebeshuber IC. *Biotribology inspires new technologies*. *Nano Today* 2007;**2**(5):30–7, DOI: 10.1016/S1748-0132(07)70141-X.
159.Zhou ZR, Jin ZM. *Biotribology: Recent progresses and future perspectives*. *Biosurface Biotribology* 2015;**1**(1):3–24, DOI: 10.1016/j.bsbt.2015.03.001.
160.Dėdinaitė A. *Biomimetic lubrication*. *Soft Matter* 2012;**8**(2):273–84, DOI: 10.1039/C1SM06335A.
161.Klein J. *Hydration lubrication*. *Friction* 2013;**1**(1):1–23, DOI: 10.1007/s40544-013-0001-7.
162.Raviv U, Klein J. *Fluidity of bound hydration layers*. *Science* 2002;**297**(5586):1540–3, DOI: 10.1126/science.1074481.
163.Ma L, Gaisinskaya-Kipnis A, Kampf N, Klein J. *Origins of hydration lubrication*. *Nat Commun* 2015;**6**:6060, DOI: 10.1038/ncomms7060.
164.J N Israelachvili. *Intermolecular and Surface Forces*. 3rd ed.: Academic Press; 2011.
165.Israelachvili JN, Adams GE. *Measurement of forces between two mica surfaces in aqueous electrolyte solutions in the range 0–100 nm*. *J. Chem. Soc., Faraday Trans. 1* 1978;**74**(0):975, DOI: 10.1039/f19787400975.
166.Leneveu DM, Rand RP, Parsegian VA. *Measurement of forces between lecithin bilayers*. *Nature* 1976;**259**(5544):601–3, DOI: 10.1038/259601a0.
167.Pashley R. *Hydration forces between mica surfaces in aqueous electrolyte solutions*. *J Colloid Interface Sci* 1981;**80**(1):153–62, DOI: 10.1016/0021-9797(81)90171-5.
168.Pashley R. *DLVO and hydration forces between mica surfaces in Li+, Na+, K+, and Cs+ electrolyte solutions: A correlation of double-layer and hydration forces with surface cation exchange properties*. *J Colloid Interface Sci* 1981;**83**(2):531–46, DOI: 10.1016/0021-9797(81)90348-9.
169.Pashley RM. *Hydration forces between mica surfaces in electrolyte solutions*. *Adv Colloid Interface Sci* 1982;**16**(1):57–62, DOI: 10.1016/0001-8686(82)85006-9.
170.Espinosa-Marzal RM, Drobek T, Balmer T, Heuberger MP. *Hydrated-ion ordering in electrical double layers*. *Phys Chem Chem Phys* 2012;**14**(17):6085–93, DOI: 10.1039/c2cp40255f.
171.F A Cotton, G Wilkinson, C A Murillo, M Bochmann. *Advanced Inorganic Chemistry*. 6th ed.: Jon Wiley & Sons Inc; 1999.
172.J Burgess. *Metal Ions in Solution*: Ellis Horwood Limited; 1978.
173.Raviv U, Perkin S, Laurat P, Klein J. *Fluidity of water confined down to subnanometer films*. *Langmuir* 2004;**20**(13):5322–32, DOI: 10.1021/la030419d.
174.Israelachvili JN, McGuiggan PM, Homola AM. *Dynamic properties of molecularly thin liquid films*. *Science* 1988;**240**(4849):189–91, DOI: 10.1126/science.240.4849.189.
175.Klein J, Kumacheva E. *Confinement-induced phase transitions in simple liquids*. *Science* 1995;**269**(5225):816–9, DOI: 10.1126/science.269.5225.816.

176.Luo J, Wen S, Huang P. *Thin film lubrication. Part I. Study on the transition between EHL and thin film lubrication using a relative optical interference intensity technique*. *Wear* 1996;**194**(1-2):107–15, DOI: 10.1016/0043-1648(95)06799-X.
177.Jagla EA. *Boundary lubrication properties of materials with expansive freezing*. *Phys Rev Lett* 2002;**88**(24):245504, DOI: 10.1103/PhysRevLett.88.245504.
178.Chan SMT, Neu CP, DuRaine G, Komvopoulos K, Reddi AH. *Tribological altruism: A sacrificial layer mechanism of synovial joint lubrication in articular cartilage*. *J Biomech* 2012;**45**(14):2426–31, DOI: 10.1016/j.jbiomech.2012.06.036.
179.Neu CP, Komvopoulos K, Reddi AH. *The interface of functional biotribology and regenerative medicine in synovial joints. Tissue Eng Part B Rev* 2008;**14**(3):235–47, DOI: 10.1089/ten.teb.2008.0047.
180.Hsu SM. *Boundary lubrication: current understanding*. *Tribol Lett* 1997;**3**(1):1–11, DOI: 10.1023/A:1019152331970.
181.Salem M, Mauguen Y, Prangé T. *Revisiting glutaraldehyde cross-linking: the case of the Arg-Lys intermolecular doublet*. *Acta Crystallogr Sect F Struct Biol* 2010;**66**(Pt 3):225–8, DOI: 10.1107/S1744309109054037.
182.Migneault I, Dartiguenave C, Bertrand MJ, Waldron KC. *Glutaraldehyde: behavior in aqueous solution, reaction with proteins, and application to enzyme crosslinking*. *BioTechniques* 2004;**37**(5):790-6, 798-802, DOI: 10.2144/04375RV01.
183.Gadhave RV, Mahanwar PA, Gadekar PT. *Effect of glutaraldehyde on thermal and mechanical properties of starch and polyvinyl alcohol blends*. *Des Monomers Polym* 2019;**22**(1):164–70, DOI: 10.1080/15685551.2019.1678222.
184.Musa BH, Hameed NJ. *Effect of crosslinking agent (glutaraldehyde) on the mechanical properties of (PVA/Starch) blend and (PVA/PEG) binary blend films*. *J Phys: Conf Ser* 2021;**1795**(1):12064, DOI: 10.1088/1742-6596/1795/1/012064.
185.Hsu P-Y, Hu T-Y, Kumar SR, Wu KC-W, Lue SJ. *Swelling-Resistant, Crosslinked Polyvinyl Alcohol Membranes with High ZIF-8 Nanofiller Loadings as Effective Solid Electrolytes for Alkaline Fuel Cells*. *Nanomaterials* 2022;**12**(5), DOI: 10.3390/nano12050865.
186.Tomihata K, Ikada Y. *Crosslinking of hyaluronic acid with glutaraldehyde*. *J Polym Sci Part A Polym Chem* 1997;**35**(16):3553–9, DOI: 10.1002/(SICI)1099-0518(19971130)35:16<3553:AID-POLA22>3.0.CO;2-D.
187.Miller Naranjo B, Naicker S, Lieleg O. *Macromolecular Coatings for Endotracheal Tubes Probed on An Ex Vivo Extubation Setup*. *Adv Mater Inter* 2023;**10**(6), DOI: 10.1002/admi.202201757.
188.Rashid S, Nawaz MH, Rehman Iu, Hayat A, Marty JL. *Dopamine/mucin-1 functionalized electro-active carbon nanotubes as a probe for direct competitive electrochemical immunosensing of breast cancer biomarker*. *Sens Actuators B Chem* 2021;**330**:129351, DOI: 10.1016/j.snb.2020.129351.
189.Collins MN, Birkinshaw C. *Physical properties of crosslinked hyaluronic acid hydrogels*. *J Mater Sci: Mater Med* 2008;**19**(11):3335–43, DOI: 10.1007/s10856-008-3476-4.
190.Dmitriev I, Kuryndin I, Bobrova N, Smirnov M. *Swelling behavior and network characterization of hydrogels from linear polyacrylamide crosslinked with glutaraldehyde*. *Mater Today Commun* 2015;**4**:93–100, DOI: 10.1016/j.mtcomm.2015.06.005.
191.Cowman MK, Schmidt TA, Raghavan P, Stecco A. *Viscoelastic Properties of Hyaluronan in Physiological Conditions*. *F1000Res* 2015;**4**:622, DOI: 10.12688/f1000research.6885.1.
192.Han G-Y, Park JY, Lee T-H, Yi M-B, Kim H-J. *Highly Resilient Dual-Crosslinked Hydrogel Adhesives Based on a Dopamine-Modified Crosslinker*. *ACS Appl Mater Interfaces* 2022;**14**(32):36304–14, DOI: 10.1021/acsami.2c04791.
193.Han L, Wang M, Li P, Gan D, Yan L, Xu J et al. *Mussel-Inspired Tissue-Adhesive Hydrogel Based on the Polydopamine-Chondroitin Sulfate Complex for Growth-Factor-Free Cartilage Regeneration*. *ACS Appl Mater Interfaces* 2018;**10**(33):28015–26, DOI: 10.1021/acsami.8b05314.
194.Lieleg O, Lieleg C, Bloom J, Buck CB, Ribbeck K. *Mucin biopolymers as broad-spectrum antiviral agents*. *Biomacromolecules* 2012;**13**(6):1724–32, DOI: 10.1021/bm3001292.
195.Yan H, Hjorth M, Winkeljann B, Dobryden I, Lieleg O, Crouzier T. *Glyco-Modification of Mucin Hydrogels to Investigate Their Immune Activity*. *ACS Appl Mater Interfaces* 2020;**12**(17):19324–36, DOI: 10.1021/acsami.0c03645.
196.Cheung DT, Nimni ME. *Mechanism of crosslinking of proteins by glutaraldehyde II. Reaction with monomeric and polymeric collagen*. *Connect Tissue Rev* 1982;**10**(2):201–16, DOI: 10.3109/03008208209034419.
197.Eddington DT, Puccinelli JP, Beebe DJ. *Thermal aging and reduced hydrophobic recovery of polydimethylsiloxane*. *Sens Actuators B Chem*. 2006;**114**(1):170–2, DOI: 10.1016/j.snb.2005.04.037.
198.Mortazavi M, Nosonovsky M. *A model for diffusion-driven hydrophobic recovery in plasma treated polymers*. *Appl Surf Sci* 2012;**258**(18):6876–83, DOI: 10.1016/j.apsusc.2012.03.122.
199.Qiu W-Z, Yang H-C, Xu Z-K. *Dopamine-assisted co-deposition: An emerging and promising strategy for surface modification*. *Adv Colloid Interface Sci* 2018;**256**:111–25, DOI: 10.1016/j.cis.2018.04.011.
200.Antonucci JM, Dickens SH, Fowler BO, Xu HHK, McDonough WG. *Chemistry of Silanes: Interfaces in Dental Polymers and Composites*. *J Res Natl Inst Stand Technol* 2005;**110**(5):541–58, DOI: 10.6028/jres.110.081.
201.Naik VV, Crobu M, Venkataraman NV, Spencer ND. *Multiple Transmission-Reflection IR Spectroscopy Shows that Surface Hydroxyls Play Only a Minor Role in Alkylsilane Monolayer Formation on Silica*. *J. Phys. Chem. Lett.* 2013;**4**(16):2745–51, DOI: 10.1021/jz401440d.
202.Subramanian V, van Ooij WJ. *Silane based metal pretreatments as alternatives to chromating: Shortlisted*. *Surf Eng* 1999;**15**(2):168–72, DOI: 10.1179/026708499101516407.
203.Graeve I de, Tourwé E, Biesemans M, Willem R, Terryn H. *Silane solution stability and film morphology of water-based bis-1,2-(triethoxysilyl)ethane for thin-film deposition on aluminium*. *Prog Org Coat* 2008;**63**(1):38–42, DOI: 10.1016/j.porgcoat.2008.04.002.
204.Xiong L, Chen P, Zhou Q. *Adhesion promotion between PDMS and glass by oxygen plasma pre-treatment*. *J Adhes Sci Technol* 2014;**28**(11):1046–54, DOI: 10.1080/01694243.2014.883774.

205.Bhattacharya S, Datta A, Berg JM, Gangopadhyay S. *Studies on surface wettability of poly(dimethyl) siloxane (PDMS) and glass under oxygen-plasma treatment and correlation with bond strength. J. Microelectromech. Syst.* 2005;**14**(3):590–7, DOI: 10.1109/JMEMS.2005.844746.
206.Gonzalez-Gallardo CL, Díaz Díaz A, Casanova-Moreno JR. *Improving plasma bonding of PDMS to gold-patterned glass for electrochemical microfluidic applications. Microfluid Nanofluid* 2021;**25**(2), DOI: 10.1007/s10404-021-02420-3.
207.Eddings MA, Johnson MA, Gale BK. *Determining the optimal PDMS–PDMS bonding technique for microfluidic devices. J Micromech Microeng* 2008;**18**(6):67001, DOI: 10.1088/0960-1317/18/6/067001.
208.Tsao C-W, DeVoe DL. *Bonding of thermoplastic polymer microfluidics. Microfluid Nanofluid* 2009;**6**(1):1–16, DOI: 10.1007/s10404-008-0361-x.
209.Yang WJ, Neoh K-G, Kang E-T, Teo SL-M, Rittschof D. *Polymer brush coatings for combating marine biofouling. Prog Polym Sci* 2014;**39**(5):1017–42, DOI: 10.1016/j.progpolymsci.2014.02.002.
210.Feng C, Huang X. *Polymer Brushes: Efficient Synthesis and Applications. Acc Chem Res* 2018;**51**(9):2314–23, DOI: 10.1021/acs.accounts.8b00307.
211.Vries R de. *Flexible polymer-induced condensation and bundle formation of DNA and F-actin filaments. Biophys J* 2001;**80**(3):1186–94, DOI: 10.1016/S0006-3495(01)76095-X.
212.Chremos A, Douglas JF. *Impact of Monovalent Counter-ions on the Conformation of Flexible Polyelectrolytes Having Different Molecular Architectures. MRS Adv* 2016;**1**(25):1841–6, DOI: 10.1557/adv.2016.12.
213.Higgs PG, Ball RC. *Polydisperse polymer networks elasticity, orientational properties, and small angle neutron scattering. J. Phys. France* 1988;**49**(10):1785–811, DOI: 10.1051/jphys:0198800490100178500.
214.Raviv U, Giasson S, Kampf N, Gohy J-F, Jérôme R, Klein J. *Lubrication by charged polymers. Nature* 2003;**425**(6954):163–5, DOI: 10.1038/nature01970.
215.Ye S, Liu G, Li H, Chen F, Wang X. *Effect of dehydration on the interfacial water structure at a charged polymer surface: negligible χ(3) contribution to sum frequency generation signal. Langmuir* 2012;**28**(2):1374–80, DOI: 10.1021/la203690p.
216.Yoneda JS, Miles AJ, Araujo APU, Wallace BA. *Differential dehydration effects on globular proteins and intrinsically disordered proteins during film formation. Protein Sci* 2017;**26**(4):718–26, DOI: 10.1002/pro.3118.
217.Lopes JLS, Orcia D, Araujo APU, DeMarco R, Wallace BA. *Folding factors and partners for the intrinsically disordered protein micro-exon gene 14 (MEG-14). Biophys J* 2013;**104**(11):2512–20, DOI: 10.1016/j.bpj.2013.03.063.
218.Uversky VN, Dunker AK. *Understanding protein non-folding. Biochim Biophys Acta* 2010;**1804**(6):1231–64, DOI: 10.1016/j.bbapap.2010.01.017.
219.Klonos PA. *Crystallization, glass transition, and molecular dynamics in PDMS of low molecular weights: A calorimetric and dielectric study. Polymer* 2018;**159**:169–80, DOI: 10.1016/j.polymer.2018.11.028.
220.Dvornic PR. Thermal Properties of Polysiloxanes. In: Jones RG, Ando W, Chojnowski J. *Silicon-Containing Polymers: The Science and Technology of Their Synthesis and Applications*. Dordrecht, s.l.: Springer Netherlands; 2000, p 185–212.
221.Imamura K, Fukushima A, Sakaura K, Sugita T, Sakiyama T, Nakanishi K. *Water sorption and glass transition behaviors of freeze-dried sucrose-dextran mixtures. J Pharm Sci* 2002;**91**(10):2175–81, DOI: 10.1002/jps.10218.
222.Znamenskaya Y, Sotres J, Engblom J, Arnebrant T, Kocherbitov V. *Effect of hydration on structural and thermodynamic properties of pig gastric and bovine submaxillary gland mucins. J Phys Chem B* 2012;**116**(16):5047–55, DOI: 10.1021/jp212495t.
223.Momoh MA, Adikwu MU, Ibezim CE, Ofokansi KC, Attama AA. *Thermal characterisation of PEGylated mucin. Asian Pac J Trop Med* 2010;**3**(6):458–60, DOI: 10.1016/S1995-7645(10)60110-1.
224.Builders PF, Kunle OO, Adikwu MU. *Preparation and characterization of mucinated agarose: a mucin-agarose physical crosslink. Int J Pharm* 2008;**356**(1-2):174–80, DOI: 10.1016/j.ijpharm.2008.01.006.
225.Davies JM, Viney C. *Water–mucin phases: conditions for mucus liquid crystallinity. Thermochim Acta* 1998;**315**(1):39–49, DOI: 10.1016/S0040-6031(98)00275-5.
226.Waigh TA, Papagiannopoulos A, Voice A, Bansil R, Unwin AP, Dewhurst CD et al. *Entanglement Coupling in Porcine Stomach Mucin. Langmuir* 2002;**18**(19):7188–95, DOI: 10.1021/la025515d.
227.Pardieu E, Chau NTT, Dintzer T, Romero T, Favier D, Roland T et al. *Polydopamine-coated open cell polyurethane foams as an inexpensive, flexible yet robust catalyst support: a proof of concept. Chem Comm* 2016;**52**(25):4691–3, DOI: 10.1039/c6cc00847j.
228.Anand JN, Kabam HJ. *Interfacial Contact and Bonding in Autohesion I-Contact Theory. J Adhes* 1969;**1**(1):16–23, DOI: 10.1080/00218466908077369.
229.Anand JN, Balwinski RZ. *Interfacial Contact and Bonding in Autohesion II-Intermolecular Forces. J Adhes* 1969;**1**(1):24–30, DOI: 10.1080/00218466908077370.
230.Southall NT, Dill KA, Haymet ADJ. *A View of the Hydrophobic Effect. J Phys Chem B* 2002;**106**(3):521–33, DOI: 10.1021/jp015514e.
231.Laage D, Elsaesser T, Hynes JT. *Water Dynamics in the Hydration Shells of Biomolecules. Chem. Rev.* 2017;**117**(16):10694–725, DOI: 10.1021/acs.chemrev.6b00765.
232.Sun PD, Foster CE, Boyington JC. *Overview of protein structural and functional folds. Current protocols in protein science* 2004;**Chapter 17**(1):Unit 17.1, DOI: 10.1002/0471140864.ps1701s35.
233.Gomes CM, Faísca PF. *Protein Folding: An Introduction*. Cham: Springer International Publishing; 2019.
234.Xiong YL. Protein Denaturation and Functionality Losses. In: Erickson MC, Hung Y-C. *Quality in frozen food*. New York, NY: Chapman & Hall; 1997, p 111–140.
235.Ballauff M. *Denaturation of proteins: electrostatic effects vs. hydration. RSC Adv* 2022;**12**(16):10105–13, DOI: 10.1039/d2ra01167k.
236.Acharya VV, Chaudhuri P. *Modalities of Protein Denaturation and Nature of Denaturants. IJPSRR* 2021;**69**(2), DOI: 10.47583/ijpsrr.2021.v69i02.002.
237.Riesz P, White FH. *Determination of free radicals in gamma irradiated proteins. Nature* 1967;**216**(5121):1208–10, DOI: 10.1038/2161208b0.

238.Kornacka EM, Przybytniak G, Zimek Z. *Radicals initiated by gamma-rays in collagen and its main components. Radiat Phys Chem* 2018;**142**:4–8, DOI: 10.1016/j.radphyschem.2017.03.034.
239.Ngo PL, Udugama IA, Gernaey KV, Young BR, Baroutian S. *Mechanisms, status, and challenges of thermal hydrolysis and advanced thermal hydrolysis processes in sewage sludge treatment. Chemosphere* 2021;**281**:130890, DOI: 10.1016/j.chemosphere.2021.130890.
240.Cao Y, Zhang X, Tao L, Li K, Xue Z, Feng L et al. *Mussel-inspired chemistry and Michael addition reaction for efficient oil/water separation. ACS Appl Mater Interfaces* 2013;**5**(10):4438–42, DOI: 10.1021/am4008598.
241.Ren P-F, Yang H-C, Liang H-Q, Xu X-L, Wan L-S, Xu Z-K. *Highly Stable, Protein-Resistant Surfaces via the Layer-by-Layer Assembly of Poly(sulfobetaine methacrylate) and Tannic Acid. Langmuir* 2015;**31**(21):5851–8, DOI: 10.1021/acs.langmuir.5b00920.
242.Leng C, Liu Y, Jenkins C, Meredith H, Wilker JJ, Chen Z. *Interfacial structure of a DOPA-inspired adhesive polymer studied by sum frequency generation vibrational spectroscopy. Langmuir* 2013;**29**(22):6659–64, DOI: 10.1021/la4008729.
243.Reactions of Carbonyl Compounds. In: Carey FA, Sundberg RJ. *Advanced organic chemistry*, 4th ed. Boston, MA: Springer; 2000, p 449–508.
244.Sarkari S, Khajehmohammadi M, Davari N, Li D, Yu B. *The effects of process parameters on polydopamine coatings employed in tissue engineering applications. Front Bioeng Biotechnol* 2022;**10**:1005413, DOI: 10.3389/fbioe.2022.1005413.
245.Wu Y, He Q, Che X, Liu F, Lu J, Kong X. *Effect of number of lysine motifs on the bactericidal and hemolytic activity of short cationic antimicrobial peptides. Biochem Biophys Res Commun* 2023;**648**:66–71, DOI: 10.1016/j.bbrc.2023.01.094.
246.Deng W, Fu T, Zhang Z, Jiang X, Xie J, Sun H et al. *L-lysine potentiates aminoglycosides against Acinetobacter baumannii via regulation of proton motive force and antibiotics uptake. Emerg Microbs Infect* 2020;**9**(1):639–50, DOI: 10.1080/22221751.2020.1740611.
247.Alkekhia D, Shukla A. *Influence of poly-l-lysine molecular weight on antibacterial efficacy in polymer multilayer films. J Biomed Mater Res Part A* 2019;**107**(6):1324–39, DOI: 10.1002/jbm.a.36645.
248.Godoy-Gallardo M, Portolés-Gil N, López-Periago AM, Domingo C, Hosta-Rigau L. *Multi-layered polydopamine coatings for the immobilization of growth factors onto highly-interconnected and bimodal PCL/HA-based scaffolds. Mat Sci Eng C Mater Biol Appl* 2020;**117**:111245, DOI: 10.1016/j.msec.2020.111245.
249.Di Fan, Miller Naranjo B, Mansi S, Mela P, Lieleg O. *Dopamine-Mediated Biopolymer Multilayer Coatings for Modulating Cell Behavior, Lubrication, and Drug Release. ACS Appl Mater Interfaces* 2023;**15**(31):37986–96, DOI: 10.1021/acsami.3c05298.
250.Mazia D, Schatten G, Sale W. *Adhesion of cells to surfaces coated with polylysine. Applications to electron microscopy. J Cell Biol* 1975;**66**(1):198–200, DOI: 10.1083/jcb.66.1.198.

C Acknowledgements

An dieser Stelle möchte ich mich bei allen bedanken, die mich bei meiner Dissertation unterstützt und auf meinem Weg begleitet haben.
Zuallererst gilt mein besonderer Dank meinem Doktorvater Prof. Dr. rer. nat. Oliver Lieleg. Danke für die hilfreichen Diskussionen und den wertvollen, wissenschaftlichen Austausch. Ein besonderer Dank an dein Vertrauen in mich ein so umfangreiches Projekt wie das APRICOT, mit all seinen Fristen, Berichten, Meetings und Regularien, als „Projekt-Managerin" verlässlich zu betreuen und dafür, dass du mich auch immer wieder daran erinnert hast, dass nicht alles mindestens 120% perfekt sein muss. Und natürlich für deinen unermüdlichen Versuch mir Satzzeichensetzung beizubringen.

Natürlich möchte ich mich auch bei all meinen Kollegen des „Lielabs" für die gemeinsamen, unvergessliche Jahre bedanken. Danke für die Grillnachmittage, die Proseccoabende und die Unmengen an Kaffee aus aller Welt! Und nicht zuletzt, für all die interessanten fachlichen und kollegialen Unterhaltungen und Unterstützungen, die meine Doktorandenzeit mit euch einfach einzigartig gemacht haben.

And I would like to acknowledge the good cooperation with and the support from all the project partners associated with the APRICOT Project. Especially I would like to thank 'the Boss': Prof. Dr. Martin Browne, for his consolidated way of coordinating the project with all its minor and major mitigations and his henchman Charles 'Charlie' Burson-Thomas: thank you for taking care of all the tedious and unpleasant administrative details but also for appreciated the scientific exchange. And thank you to all the friendly people who welcomed me so warmly during my short research visit to the University of Southampton. And since it must never be forgotten in any APRICOT-related publication:

This project has received funding from the European Union's Horizon 2020 research and innovation programme under grant agreement No 863183. This publication represents the views of the author(s) only. The European Commission is not responsible for any use that may be made of the information it contains.

Des Weiteren möchte ich den Kollegen an den Lehrstühlen von Prof. Mela und Prof. Torgersen für die gute Zusammenarbeit an den gemeinsamen Publikationen danken.
Darüber hinaus möchte ich mich für die administrativen Hilfestellungen bei Iris König-Decker bedanken. Ein besonderer Dank geht Tobias Fuhrmann, der bei allerlei (labor-)technischen Angelegenheiten zur Unterstützung kam, aber auch als Co-Dauerbesetzer des Rheolabors immer willkommen war. Bei Rudolf Lehrhuber möchte ich mich für seine fachkundige und tatkräftige handwerkliche Unterstützung bedanken.

Und nicht zuletzt möchte ich mich bei meiner Familie und meinen Freunden für die unermüdliche Unterstützung, ständige Motivation und die willkommenen Ablenkungen während der letzten vier Jahre bedanken! Ohne euch hätte ich es nie so weit geschafft!

Papa, danke für dein unerschütterliches Vertrauen in mich, dass ich meinen Weg finden und gehen werde und dafür, dass ich, auch wenn es einmal schwierig wird, immer auf dich als unterstützender und vernünftiger Ruhepol zählen kann.
Opa und Heidi, ihr habt mich unschätzbar geprägt und ich durfte so viel von euch lernen, danke, dass ich jederzeit zu euch kommen konnte.
Lukas auf unerwartete Gruppen-Videocalls, durch diskutierte und -philosophierte Nächte und kleinere, geschwisterliche Rivalitäten (auch wenn du es mir nicht besonders schwer machst vor dir einzureichen), und darauf, dass wir, komme was wolle, füreinander da sind!
Alex, Isabella, und Susie, danke für eure Zeit und Unterstützung, dafür, dass ich mit persönlichen Angelegenheiten bei euch immer ein offenes Ohr gefunden habe und ihr mich daran erinnert habt, dass es neben Arbeit und Wissenschaft auch noch ein Leben gibt. Möge es immer einen neuen Prosecco, Spritz oder deliziösen Rotwein zu verkosten geben!
Meine Leidenskollegen seit dem ersten Semester: Manuel Kipp, Victor Zappek und Amadeus Gebauer, was haben wir die letzten 10 Jahre geschuftet, gehofft, geschimpft und wären in so manchen Moment fast verzweifelt, nur um uns danach noch mehr reinzuhängen! Unglaublich, dass wir diesen Weg so lange zusammen durchgezogen haben, das so entstandene, gegenseitige Verständnis, die Unterstützung und die langjährigen Freundschaften schätze ich wirklich sehr. (Und auf die Gefahr hin, dass ich großkotzig klinge: bald seid ihr auch so weit!)
Leon, ich glaub ich fange mal am Ende an: Danke, dass du mich die letzten sechs Wochen ertragen hast, meine Hochs und Tiefs mitgemacht hast, und mich so sehr unterstützt und motiviert hast und manchmal auch einfach nicht gefragt hast, wie es läuft!
Danke, dass du an mich glaubst und mich dazu bringst über mich hinauszuwachsen. Ich weiß es sehr zu schätzen in dir einen ehrgeizigen, vorwärtsgewandten, und eigenständigen Gleichgesinnten gefunden zu haben, der lange Arbeitstage mindestens so gut kennt wie ich und trotzdem immer vorne mit dabei ist, wenn es um die Unterstützung von Freunden und soziale Aktivitäten geht.